

School of Doctoral Studies in Biological Sciences
University of South Bohemia in České Budějovice
Faculty of Science



**F_0F_1 -ATP synthase/ATPase in the parasitic protist,
*Trypanosoma brucei***

Ph.D. Thesis

Mgr. Karolína Šubrtová

Supervisor: RNDr. Alena Zíková, Ph.D.

Institute of Parasitology
Biology Centre of the Czech Academy of Sciences



České Budějovice, 2015

This thesis should be cited as:

Šubrtová, K., 2015: **F₀F₁-ATP synthase/ATPase in the parasitic protist, *Trypanosoma brucei***. Ph.D. thesis. University of South Bohemia, Faculty of Science, School of Doctoral Studies in Biological Sciences, České Budějovice, Czech Republic, 160 p.

ANNOTATION

This thesis primarily focuses on the F₀F₁-ATP synthase/ATPase complex in the parasitic protist, *Trypanosoma brucei*. Instead of its normal aerobic function to synthesize ATP, it is required to hydrolyze ATP to maintain the $\Delta\psi_m$ in the infective bloodstream stage of *T. brucei* and the related parasite, *T. b. evansi*. To better understand the composition, structure and function of this druggable target, my work focused on deciphering the function of three of the unique Euglenozoa specific subunits that comprise this complex molecular machine. Furthermore, the ADP/ATP carrier, which provides substrates for the F₀F₁-ATP synthase/ATPase, was functionally characterized and evaluated if it is physically associated with the complexes of the oxidative phosphorylation pathway.

FINANCIAL SUPPORT

This work was funded by Ministry of Education ERC CZ grant LL1205, the Czech Grant Agency grant 204/09/P563 and P302/12/2513, the EMBO Installation grant 1965 and the Grant Agency of University of South Bohemia grants 140/2010/P, 04/092/2011/P, and 092/2011/P. We acknowledge the use of research infrastructure that has received funding from the European Union Seventh Framework Programme (FP7/2007-2013) under grant agreement no.316304.

DECLARATION

I hereby declare that I did all the work presented in this thesis by myself or in collaboration with co-authors of the presented papers and only using the cited literature.

České Budějovice, 19 April 2014



Karolína Šubrtová

DECLARATION [IN CZECH]

Prohlašuji, že svoji disertační práci jsem vypracovala samostatně pouze s použitím pramenů a literatury uvedených v seznamu citované literatury.

Prohlašuji, že v souladu s § 47b zákona č.111/1998 Sb. v platném znění souhlasím se zveřejněním své disertační práce, a to v nezkrácené podobě elektronickou cestou ve veřejně přístupné části databáze STAG provozované Jihočeskou univerzitou v Českých Budějovicích na jejích internetových stránkách, a to se zachováním mého autorského práva k odevzdanému textu této kvalifikační práce. Souhlasím dále s tím, aby toutéž elektronickou cestou byly v souladu s uvedeným ustanovením zákona č. 111/1998 Sb. zveřejněny posudky školitele a oponentů práce i záznam o průběhu a výsledku obhajoby kvalifikační práce. Rovněž souhlasím s porovnáním textu mé kvalifikační práce s databází kvalifikačních prací Theses.cz provozovanou Národním registrem vysokoškolských kvalifikačních prací a systémem na odhalování plagiátů.

V Českých Budějovicích, 19. dubna 2015



Karolína Šubrtová

This thesis originated from a partnership of Faculty of Science, University of South Bohemia, and Institute of Parasitology, Biology Centre CAS, supporting doctoral studies in the Molecular and cell biology and Genetics study programme.



Přírodovědecká
fakulta
Faculty
of Science



Statement regarding author's contribution

Author of this thesis significantly contributed to the following papers (listed chronologically):

1. **Šubrtová K**, Panicucci B, Zíková A (2015) ATPaseTb2, a Unique Membrane-bound F_oF₁-ATPase Component, Is Essential in Bloodstream and Dyskinetoplastic Trypanosomes. PLoS Pathogens. (IF=8,06)

The study was designed by AZ, KS and BP. Moreover, KS performed all the experiments, analyzed data and significantly contributed to the writing process.

Experimental contribution: 100 %

Contribution to the writing: 40 %

2. Gnipová A, **Šubrtová K**, Panicucci B, Horváth A, Lukeš J, Zíková A. (2015) The ADP/ATP carrier and its relationship to OXPHOS in an ancestral protist, *Trypanosoma brucei*. Eukaryot Cell. (IF=3,18)


This study was designed by mainly by AZ and BP. The experiments were performed by AG and KS (e.g. KS did all the experiments for Figures 2 and 5). KS also prepared final version of all figures and helped write the first draft of the manuscript. Moreover KS significantly contributed to this paper during the resubmission period (repeating some experiments, rewriting the paper, recreating some figures) as the first author already left the lab.

Experimental contribution: 30 %

Contribution to the writing: 30 %

RNDr. Alena Zíková, Ph.D. as the corresponding author of these papers approves this statement.

České Budějovice, 17.4.2015


.....
RNDr. Alena Zíková, Ph.D.

Acknowledgements:

First of all, I would like to express my big appreciation to my supervisor, Alena, and my co-supervisor, Brian. Thank you very much for your advice, guidance, and all the time, effort and patience you invested in me through all these years. I have learnt a great deal from you and I wish you all the best in a future! Then, I feel a huge gratitude for support from all past and current members of our team: Dave, Míša (blonde :-P), Evča, Ondra, Hanka, Zuzka, Honzík, Míša (ginger), and Geri. Thank you for creating a pleasant work atmosphere and willingness to help me every time. Thank you Dave, for helping me with my clumsy english (you are amazing :-). I also want to acknowledge members of Lukeš lab which were very supportive. Big thank you belongs to Hassan for his helpful input, and to Jula, for explaining me how to see the bigger picture in a research project. My special thanks belongs to *Umbrella Corp.* © for pushing me forward - Priscila, Corinna, Dave - I would never get so far without you, I hope we will all meet again. Thank you Evička (*cmuk*) and Priscila (*Carmen :-P*) for amazing coffee breaks and your friendship, I would not make it without your support. I would also like to acknowledge (former) members of Anton Horvath lab for their helpful advice - Anton, Inka and small Zdeněk. One more very special thanks belongs to Anička for sharing her never ending enviable optimism with me. Thank you for your friendship (<3) and (*děláš to pořádně?*).

Finally, I would like to acknowledge my family for their great patience and amazing endless support during these tough years(ö). This thesis would never be completed without Jiřík, thank you for your love and understanding, and constant support, even during the most stressful sleepless nights. You are the one who gives me strength to face all the dark clouds (:-*)! In the end, I would like to dedicate this thesis to the amazing personalities that are no longer here, it was an honour for me to have you in my life.

Table of contents:

List of abbreviations	i
Chapter 1- Introduction	1
1.1. Introduction and aims of the thesis	2
Chapter 2 - Overview	4
2.1. <i>Trypanosoma brucei</i> and related kinetoplastids	5
2.2. Human and animal trypanosomiasis	6
2.3. <i>T. brucei</i> cell biology	7
2.4. Trypanosomes as a model organism	9
2.5. <i>T. brucei</i> life cycle	10
2.6. Energy metabolism of Trypanosomes	12
2.6.1. Glycolytic pathway	12
2.6.2. Amino acid catabolism	16
2.6.3. Tricarboxylic acid cycle	19
2.6.4. Oxidative phosphorylation pathway	20
2.6.4.1. Respiratory chain of bloodstream and dyskinetoplastic trypanosomes	21
2.6.4.2. Respiratory chain of procyclic trypanosomes	22
2.7. F ₀ F ₁ -ATP synthase (Complex V)	25
2.7.1. F ₀ F ₁ -ATP synthase architecture	25
2.7.2. Mechanism of ATP synthesis and ATP hydrolysis	28
2.7.3. Regulation of mitochondrial F ₀ F ₁ -ATP synthase by IF1	30
2.7.4. Supramolecular organisation of the mitochondrial F ₀ F ₁ -ATP synthase	31
2.7.4.1. Dimeric F ₀ F ₁ -ATP synthase	31
2.7.4.2. ATP synthasome	32
2.7.4.3. The ADP/ATP carrier	32
2.7.5. Composition of the mitochondrial F ₀ F ₁ -ATP synthase	33
2.7.5.1. F ₁ moiety, central and peripheral stalks	33
2.7.5.2. F ₀ moiety	34
2.7.5.3. Divergent F ₀ F ₁ -ATP synthases	35
2.8. <i>Trypanosoma</i> F ₀ F ₁ -ATP synthase	36
2.8.1. Function of F ₀ F ₁ -ATP synthase in bloodstream and dyskinetoplastic Trypanosomes	38
Chapter 3 - Results	49
3.1. Published results	
3.1.1. ATPaseTb2, a unique membrane-bound F ₀ F ₁ -ATPase component, is essential in bloodstream and dyskinetoplastic trypanosomes	50
3.1.2. The ADP/ATP carrier and its relationship to oxidative phosphorylation in ancestral protist <i>Trypanosoma brucei</i>	81
3.2. Unpublished results	
3.2.1. The functionality of <i>Trypanosoma brucei</i> F ₁ -ATPase requires the additional subunit p18... ..	97
3.2.2. Functional analysis of ATPaseTb1, a novel and essential subunit of the F ₀ F ₁ -ATP synthase in <i>T. brucei</i>	130
Chapter 4 - Conclusions	155
4.1. Conclusions and future perspectives	156

List of abbreviations:

1,3-BPGA	1,3-bisphosphoglycerate
3-PGA	3-phosphoglycerate
AA	Amino acid
AAC	ATP/ADP carrier
Ab	Antibody
ACA	Aminocaproic acid
acetyl-CoA /AcCoA	Acetyl Co-enzyme A
ADP	Adenosine diphosphate
AMP-PNP	Adenylyl-imidodiphosphate
AOX	Alternative oxidase
APEX	Ascorbate peroxidase
apo	Apocytochrome
ASA	ATP synthase associated protein
ASCT	Acetate: succinate-co-enzyme-A transferase
ATP	Adenosine triphosphate
AZ	Azide
BF	Bloodstream form
BLAST	Basic Local Alignment Search Tool
BNE/ BN-PAGE	Blue native PAGE
BSA	Bovine serum albumin
C	Cytochrome C
ci-cV	Complexes I-V
CNS	Central nervous system
CoA	Co-enzyme-A
cox	Cytochrome c oxidase
cryo-EM	Cryo-electron microscopy
cryo-ET	Cryo-electron tomography
cyt	Cytochrome
CYT/CYTO	Cytosolic fraction
$\Delta\psi_m$	Mitochondrial membrane potential
Da	Dalton
DAPI	4',6-diamidino-2-phenylindole
DAPIT	Diabetes associated protein in insulin-sensitive tissue
DDT	Dichlorodiphenyltrichloroethane
DHAP	Dihydroxyacetone-phosphate
Dk	Dyskinetoplastic
DNA	Deoxyribonucleic acid
EDTA	Ethylenediamine tetraacetic acid
EM	Electron microscopy

FACS	Fluorescence-activated cell sorting
FAD	Flavin adenine dinucleotide
FADH ₂	Flavin adenine dinucleotide (hydroquinone form)
FBS	Fetal bovine serum
FCCP	Carbonilcyanide <i>p</i> -triflouromethoxyphenylhydrazone
Fe-S cluster	Iron-sulphur cluster
FRET	Förster resonance energy transfer
G-3-P	Glyceraldehyde 3-phosphate
G3P	Glycerol 3-phosphate
gDNA	Genomic DNA
GG	Glycerol gradient
Gly-3-P	Glycerol-3-phosphate
Gly-3-P DH	Glycerol-3-phosphate dehydrogenase
gRNA	Guide RNA
GST	Glutathione S-transferase
GTP	Guanosine-5'-triphosphate
HAT	Human African trypanosomiasis
HMI-9	Hirumi's modified Iscove's medium 9
HMM	Hidden markov model
hrCNE	High resolution clear native PAGE
HRP	Horse radish reroxidase
IC ₅₀	50% Inhibitory Concentration
IF1	Inhibitory factor 1
IFA	Immunofluorescent analysis
IgG	Immunoglobulin G
IM	Inner mitochondrial membrane
IMS	Mitochondrial inner mebrane space
IND	RNAi Induced
kb	Kilobase
KD	Knock-down
kDa	Kilodalton
kDNA	Kinetoplast DNA
LC-MS/MS	Liquid chromatography tandem mass spectrometry
LETM1	Leucine zipper EF-hand-containing transmembrane 1
M	Membrane fraction
mAb	Monoclonal antibody
MALDI	Matrix-assisted laser desorption/ionization
MCF	Mitochondrial carrier family
MCP	Mitochondrial carrier protein
MCU	Mitochondrial calcium uniporter
Mdm	Mitochondrial distribution and morphology

mg1	Mitochondrial genome integrity
MIX	Mitochondrial protein X
MPP	Mitochondrial processing peptidase
mRNA	Messenger RNA
MRP	Mitochondrial RNA-binding protein
MS	Mass spectrometry
mt	Mitochondrial
mtDNA	Mitochondrial DNA
MTS	Mitochondrial targeting signal
MURF	Maxicircle unidentified reading frame
MX	Matrix fraction
NAD ⁺	Nicotinamide adenine dinucleotide oxidized
NADH	Nicotinamide adenine dinucleotide reduced
NADPH	Nicotinamide adenine dinucleotide phosphate (reduced form)
NCBI	National Centre for Biotechnology Information
NDH ₂	NADH dehydrogenase
NECT	Nifurtimox-eflornithine combination therapy
NMR	Nuclear magnetic resonance
NON	RNAi Non-induced
om	Oligomycin
OM	Mitochondrial outer membrane
ORG	Organellar
OSCP	Oligomycin sensitivity conferring protein
Oxac	Oxaloacetate
OxPhos	Oxidative phosphorylation
pAb	Polyclonal antibody
PAGE	Polyacrylamide gel electrophoresis
PBS	Phosphate buffer saline
PCR	Polymerase chain reaction
PEP	Phosphoenolpyruvate
PF	Procyclic form
Pi	Inorganic phosphate
PiC	Phosphate carrier
PTM	Posttranslational modification
RECC	RNA Editing Core Complex
rDNA	Ribosomal DNA
RNA	Ribonucleic acid
RNAi	Ribonucleic acid Interference
ROS	Reactive oxygen species
rpm	Revolutions per minute
rRNA	Ribosomal RNA

RT	Room temperature
RT-qPCR	Quantitative reverse transcription PCR
SAM	S-adenosyl methionine
SCS	Succinyl-CoA synthetase
SD	Standard deviation
SDM-79	Semi-defined medium 79
SDS-PAGE	Polyacrylamide Gel Electrophoresis in Sodium Dodecyl Sulphate
SEM	Standard error of mean
SHAM	Salicylhydroxamic acid
SL-RNA	Spliced leader RNA
SM	Single marker
SoTE	Sorbitol Tris EDTA buffer
SRA	Serum resistance-associated protein
T7RNAP	T7 RNA polymerase
TAO	Trypanosome alternative oxidase
TAP	Tandem affinity purification
TCA	Tricarboxylic acid
tet	Tetracycline
TetR	Tetracycline repressor
TIM	Translocating inner membrane protein
TLF	Trypanosome lytic factor
TM	Transmembrane
TMRE	Tetramethylrhodamine
TOF	Time-of-flight mass spectrometer
tRNA	Transfer RNA
Ub	Ubiquinone
USD	United States dollar
UV	Ultraviolet
VDAC	Voltage dependent anion channel
VSG	Variant surface glycoprotein
WHO	World Health Organization
WT	Wild Type

CHAPTER 1

INTRODUCTION

1.1. Introduction and aims of the thesis

The eukaryotic F_0F_1 -ATP synthase (also referred to as complex V) is a large multisubunit complex composed of the proton pumping F_0 moiety and the catalytic F_1 part. These two subcomplexes are connected via the central and peripheral stalks. In almost every aerobic eukaryotic cell, the mitochondrial (mt) F_0F_1 -ATP synthase utilizes the mt membrane potential ($\Delta\psi_m$) to synthesize ATP from ADP and inorganic phosphate (Pi) (Devenish et al. 2008; Walker 2013). Interestingly, the complex can also work in reverse as an ATP hydrolase. This activity is usually only observed under rare environmental conditions (e.g. low oxygen levels, lack of respiratory chain substrates), that prevent the conventional respiratory chain from sustaining the essential $\Delta\psi_m$. During this mitochondrial dysfunction, the F_0F_1 -ATP synthase/ATPase hydrolyzes ATP and pumps protons across the mt inner membrane to maintain the $\Delta\psi_m$ (von Ballmoos et al. 2008; Campanella et al. 2009; Walker 2013). Activity of the F_0F_1 -ATP synthase/ATPase also depends on the availability of its substrates (ATP, ADP, and Pi), which are transported across the mt inner membrane by the ATP/ADP carrier and the phosphate carrier (Klingenberg 2008). In mammalian cells, these carriers are associated with F_0F_1 -ATP synthase, forming a supercomplex called the ATP synthasome (Ko et al. 2003; Chen et al. 2004), which is suggested to increase the efficiency of the oxidative phosphorylation pathway (Pedersen 2007).

In the parasitic protist, *Trypanosoma brucei*, the composition and structure of the F_0F_1 -ATP synthase complex is exceptional because it contains 14 novel subunits with no homology outside Euglenozoa (Zikova et al. 2009; Perez et al. 2014). Moreover, the absence of the traditional respiratory chain in the infective bloodstream stage of this parasite requires this molecular machine to continuously operate in reverse to generate the essential $\Delta\psi_m$ (Nolan & Voorheis 1992; Schnauffer et al. 2005; Brown et al. 2006).

The mechanism of maintaining the $\Delta\psi_m$ is even more unique in a closely related flagellate, *T. b. evansi*. This parasite lacks the mtDNA that encodes the F_0 subunit a, an essential component of the proton pore. Thus, this trypanosome maintains the $\Delta\psi_m$ using the hydrolytic activity of the F_1 -ATPase coupled to the electrogenic exchange of ATP^{4-}/ADP^{3-} by the ATP/ADP carrier (Schnauffer et al. 2005; Dean et al. 2013).

In order to gain insight into the composition, activity, and function of the *T. brucei* F_0F_1 -ATP synthase/ATPase, the following aims were investigated:

Aims:

- i) Elucidate the specific function of several unique F_0F_1 -ATPase subunits in the bloodstream trypanosomes.
- ii) Characterize a novel F_1 -ATPase subunit, p18, in both life stages of *T. brucei*.
- iii) Investigate the functional and structural association of F_0F_1 -ATP synthase with the ATP/ADP carrier.

References:

- Von Ballmoos, C., Cook, G.M. & Dimroth, P., 2008. Unique rotary ATP synthase and its biological diversity. *Annual review of biophysics*, 37, pp.43–64.
- Brown, S. V et al., 2006. ATP synthase is responsible for maintaining mitochondrial membrane potential in bloodstream form *Trypanosoma brucei*. *Eukaryotic cell*, 5(1), pp.45–53.
- Campanella, M. et al., 2009. IF(1): setting the pace of the F(1)F(o)-ATP synthase. *Trends in biochemical sciences*, 34(7), pp.343–50.
- Dean, S. et al., 2013. Single point mutations in ATP synthase compensate for mitochondrial genome loss in trypanosomes. *Proceedings of the National Academy of Sciences of the United States of America*, 110(36), pp.14741–6.
- Devenish, R.J., Prescott, M. & Rodgers, A.J.W., 2008. The structure and function of mitochondrial F1F0-ATP synthases. *International review of cell and molecular biology*, 267(08), pp.1–58.
- Chen, C. et al., 2004. Mitochondrial ATP synthasome: three-dimensional structure by electron microscopy of the ATP synthase in complex formation with carriers for Pi and ADP/ATP. *The Journal of biological chemistry*, 279(30), pp.31761–8.
- Klingenberg, M., 2008. The ADP and ATP transport in mitochondria and its carrier. *Biochimica et biophysica acta*, 1778(10), pp.1978–2021.
- Ko, Y.H. et al., 2003. Mitochondrial ATP synthasome. Cristae-enriched membranes and a multiwell detergent screening assay yield dispersed single complexes containing the ATP synthase and carriers for Pi and ADP/ATP. *The Journal of biological chemistry*, 278(14), pp.12305–9.
- Nolan, D.P. & Voorheis, H.P., 1992. The mitochondrion in bloodstream forms of *Trypanosoma brucei* is energized by the electrogenic pumping of protons catalysed by the F1F0-ATPase. *European journal of biochemistry / FEBS*, 209(1), pp.207–16.
- Pedersen, P.L., 2007. Transport ATPases into the year 2008: a brief overview related to types, structures, functions and roles in health and disease. *Journal of bioenergetics and biomembranes*, 39(5-6), pp.349–55.
- Perez, E. et al., 2014. The mitochondrial respiratory chain of the secondary green alga *Euglena gracilis* shares many additional subunits with parasitic Trypanosomatidae. *Mitochondrion*, pp.1–12.
- Schnauffer, A. et al., 2005. The F1-ATP synthase complex in bloodstream stage trypanosomes has an unusual and essential function. *The EMBO journal*, 24(23), pp.4029–40.
- Walker, J.E., 2013. The ATP synthase: the understood, the uncertain and the unknown. *Biochemical Society transactions*, 41(1), pp.1–16.
- Zikova, A. et al., 2009. The F(0)F(1)-ATP synthase complex contains novel subunits and is essential for procyclic *Trypanosoma brucei*. *PLoS pathogens*, 5(5), p.e1000436.

CHAPTER 2

OVERVIEW

2.1. *Trypanosoma brucei* and related kinetoplastids

The order Kinetoplastida includes a number of unicellular flagellates that cause some of the most serious parasitic diseases of vertebrates, resulting in devastating health and economic effects (Stuart et al. 2008). In sub-Saharan Africa, infection from the extracellular protozoan *Trypanosoma brucei* causes Human African trypanosomiasis (HAT), also referred to as sleeping sickness, and nagana, an important veterinary disease of livestock. The genus *Leishmania* is distributed worldwide and is the etiological agent of various leishmaniases (visceral, cutaneous, mucocutaneous). Finally, the intracellular parasite *Trypanosoma cruzi* is responsible for Chagas disease in South America (Stuart et al. 2008).

There are various subspecies of *T. brucei* that infect a wide range of mammals through distinct modes of transmission. *Trypanosoma brucei gambiense* and *Trypanosoma brucei rhodiense* have gained the most interest, as they are able to establish infections in humans by evading the innate immune complexes – primate-specific trypanosome lytic factors (TLF) (Vanhollebeke & Pays 2010; DeJesus et al. 2013). *T. b. gambiense* is resistant to TLF due to the reduced expression of a receptor mediating TLF transport (Kieft et al. 2010). This parasite is endemic in West and Central Africa, and causes a chronic form of sleeping sickness (Stuart et al. 2008). *T. b. rhodesiense* evolved the serum resistance-associated protein (SRA) that binds and neutralizes TLF, thereby providing protection from the human immune response (Xong et al. 1998). This subspecies causes an acute form of sleeping sickness in the eastern and southern regions of Africa (Stuart et al. 2008). The third *Trypanosoma brucei* subspecies, *T. b. brucei* stands alone from its two relatives as it is sensitive to the TLF killing mechanism and is therefore not pathogenic to humans. However, together with other animal trypanosomes, it infects livestock and therefore it threatens a major economic resource in African rural areas (Steverding 2008).

These three *T. brucei* subspecies are all transmitted by the blood-feeding tsetse fly (genus *Glossina*); however, rare instances of transmission can also occur via congenital contact or blood transfusion (Hira & Husein 1979; Stuart et al. 2008; Lindner & Priotto 2010). *T. brucei* parasites undergo a highly complex digenetic life cycle alternating between the bloodstream form in the mammalian host and the procyclic stage in the tsetse fly midgut; therefore their occurrence is restricted to the sub-Saharan area called the African tsetse belt. In contrast, related flagellates, *T. b. evansi* and *T. b. equiperdum*, became independent from the insect vector by locking themselves in the bloodstream form of the parasite, enabling them to spread into Asia, Europe and South America (Brun et al. 1998; Lai et al. 2008; Dean et al. 2013).

Both subspecies strictly rely on physical modes of transmission between mammalian hosts, resulting in no observable cyclical developmental stages. *T. b. equiperdum* is sexually transmitted between horses and causes a disease called dourine. In comparison, the mechanical transmission of *T. b. evansi* is predominantly achieved by blood-sucking insects such as the horsefly (*Tabanus*) and stablefly (*Stomoxys*), resulting in the economically important disease named surra that affects various mammals (horses, mules, camels,

buffalo, cattle and deer). This mode of transmission requires a short time interval between blood meals, as the parasites that remain on the surface or inside the insect's rostrum or proboscis are short lived. In South and Central America, *T. b. evansi* is also transmitted by the vampire bat (*Desmodus*), which then plays the dual role of vector and reservoir host (Brun et al. 1998; Desquesnes et al. 2013).

The taxonomical classification of *T. b. evansi* and *T. b. equiperdum* remains controversial. The characterization of *T. b. equiperdum* is most complex, because it is hypothesized that some reported *T. b. equiperdum* strains are actually *T. b. evansi* or *T. b. brucei* (Claes et al. 2005; Carnes et al. 2015). Furthermore, *T. b. equiperdum* as well as *T. b. evansi* have been classified as independent species (Brun et al. 1998). Most recent reports suggest that both these trypanosomes are actually a subspecies of *T. brucei* (Lai et al. 2008; Carnes et al. 2015).

2.2. Human and animal trypanosomiasis

As HAT mostly occurs in rural and remote sub-Saharan communities, which are constantly under-surveyed, it is almost impossible to evaluate the real prevalence of this severe endemic disease. Nevertheless, the World Health Organization (WHO) estimates that 70 million people were at risk of the infection in 1995, and 20 000 individuals were infected (Stuart et al. 2008; Sutherland et al. 2015). Over 95% of the diagnosed cases of sleeping sickness are caused by *T. brucei gambiense*. This subspecies causes chronic trypanosomiasis, which can last for months or years before any symptoms emerge, while *T. b. rhodesiense* causes acute HAT with rapid disease progression (within weeks to months) (Stuart et al. 2008; WHO 2013; Sutherland et al. 2015). Both forms of sleeping sickness are almost always fatal if left untreated (Jamonneau et al. 2012).

The acute form of the disease manifests during the early haemolymphatic stage, when the parasites are replicating by binary fission to high densities in the blood and lymph system. Initial symptoms include bouts of fever, headaches, joint pains and itching. More severe and typical symptoms of HAT appear in the later stage of the disease as the trypanosomes cross the blood-brain barrier and invade the central nervous system (CNS). In the neurological phase, parasites reside in the cerebrospinal fluid and intercellular spaces. An infected individual undergoes sensory disturbances, confusion, poor coordination, and a disturbance of the circadian rhythm (Stuart et al. 2008; Steverding 2008; Jamonneau et al. 2012).

Animal trypanosomiasis (nagana disease) affects millions of domestic and wild animals every year. In wild animals, trypanosomes cause relatively mild infections, while in domestic animals they cause a severe, often fatal disease. Domestic cattle with nagana disease exhibit symptoms such as fever, muscle wasting, anemia, edema and paralysis. As the illness progresses, the animal weakens and eventually becomes too weak for farming, hence the name "N'gana" - a Zulu word that means "powerless" (Steverding 2008). The major causative agents of animal trypanosomiasis are *T. b. brucei*, *T. congolense* and *T. vivax*. It is estimated

that together they cause economic losses in cattle production that amount to 1.3 billion USD annually; this accounts for livestock morbidity, mortality, diagnostic and treatment costs and losses in milk and meat production (Courtin et al. 2008).

Despite being the object of intense research for many years, there are no vaccines against human or animal trypanosomiasis. Furthermore, the development of a vaccine is highly unlikely due to the expression of the variant surface glycoprotein (VSG) coat in the bloodstream form that can rapidly change to evade the host's immune system. To combat *T. brucei* infection, there are currently five drugs that can be administered depending on the disease progression (Barrett et al. 2007; Simarro et al. 2012). The first stage of *T. b. rhodesiense* and *T. b. gambiense* infections are treated with Suramin and Pentamidine, respectively (Kennedy 2006). Melarsoprol is used to treat later stages of both infections. However, all these drugs were developed in the early 20th century and have many undesirable adverse effects, especially Melarsoprol, which can cause tachycardia, convulsions, coma, heart failure and severe post-treatment encephalopathy. Melarsoprol treatment results in death in up to 5% of patients (Kennedy 2006; Barrett et al. 2007). Only Eflornithine, the most recent drug released (1981) for the late CNS stage of *T. b. gambiense* infection, causes side effects that are usually reversible (Barrett et al. 2007; Rodgers 2009). Besides toxicity concerns, all four licensed compounds require parenteral administration of highly concentrated drugs, which is difficult to achieve in a rural environment. Moreover, it has been shown that the parasite is becoming increasingly resistant to these compounds. To combat these issues, several new trials of combination therapies have been performed that resulted in some success (Barrett et al. 2007; Simarro et al. 2012). For example, the treatment with Nifurtimox (originally medication for Chagas disease) in combination with Eflornithine (the NECT combination) has become the standard treatment for late CNS stage of *T. b. gambiense* infection since 2009 as it reduced both the previously required drug dosage and treatment time. However, the rapid rise in the preferred NECT therapy has increased the average cost to treat patients with the CNS stage disease as it has replaced melarsoprol, which is considerably cheaper to produce (Simarro et al. 2012). Despite the implementation of NECT, the current treatment of HAT is still insufficient and therefore a cheaper and less toxic alternative is urgently needed (Barrett et al. 2007; Stuart et al. 2008; Simarro et al. 2012).

2.3. *T. brucei* cell biology

The medical aspect is not the only reason why *T. brucei* is a fascinating research subject. Kinetoplastida diverged early in evolution from other eukaryotic lineages, which allowed them to develop a number of peculiarities. The best known examples are listed below.

- a) *Antigenic variation via programmed DNA rearrangement.* The surface of metacyclic and bloodstream trypanosomes is covered by tightly packed VSGs that change periodically

and thus help protect the parasite from the host immune system. There are approximately 2500 transcriptionally silent VSG genes and pseudogenes encoded by the *T. brucei* genome. A single VSG gene is expressed only when it is moved into one of subtelomeric expression sites by homologous recombination (McCulloch 2004; Günzl et al. 2015).

- b) *Transcription of nuclear genes as polycistronic RNA molecules, which are then processed to mRNAs by trans-splicing.* Most of protein coding genes is transcribed into long mRNA precursors (polycistrons); the exception being VSGs, which are expressed monocistronically. The pre-mRNAs are then processed into individual mature mRNAs via trans-splicing and polyadenylation. In *T. brucei*, trans-splicing is a process through which the 39 bp long sequence of the spliced leader RNA (SL-RNA) is transferred as a cap to the 5' end of all mRNAs (Parsons et al. 1984; Günzl 2010).
- c) *The unique compartmentalization of the glycolytic pathway into glycosomes.* The peroxisome-derived organelles contain the first seven glycolytic enzymes, which in other eukaryotes, are localized in the cytosol. This sequestering helps to overcome the lack of regulation of the first glycolytic steps and prevents the accumulation of toxic glycolytic intermediates (Hannaert et al. 2003; Michels et al. 2006; Haanstra et al. 2014). Moreover, glycosomes contain enzymes for other metabolic pathways such as the pentose-phosphate pathway, β -oxidation of fatty acids, purine salvage pathway, and biosynthetic pathways for pyrimidines, ether-lipids and squalenes. It is speculated that rapid change of peroxisome enzymatic content enables trypanosomes to adapt rapidly to new nutritional conditions during their complex life cycle (Hannaert et al. 2003; Michels et al. 2006; Bauer et al. 2013; Colasante et al. 2013).
- d) *The presence of the kinetoplast, a special section of the single mitochondrion that contains an atypical mitochondrial DNA structure.* In kinetoplastids, the mitochondrial DNA (mtDNA) is known as kinetoplast DNA (kDNA), and it is organized into a massive network of thousands of topologically interlocked DNA circles. This unique, electron dense structure was what led to the name of the order of Kinetoplastida. In contrast to other eukaryotes, it is only replicated once per cell cycle and is synchronized with nuclear replication and division. The kDNA is composed of two types of DNA molecules - maxi and minicircles (Ryan et al. 1988; Shapiro & Englund 1995; Lukeš et al. 2002; Liu et al. 2005). The maxicircles are largely homologous to the mtDNA of other eukaryotes. They encode both the 12S and 9S rRNAs; subunits of respiratory complexes I, III, IV and cV; ribosomal protein S12 and also several genes with unknown function. Interestingly, maxicircles do not encode any tRNAs, which must be imported from the cytosol. The minicircles encode guide RNAs (gRNAs), which are essential for the mt RNA editing process (Stuart & Panigrahi 2002; Aphasizhev & Aphasizheva 2011; Aphasizheva et al. 2013).

e) *An unusual, often highly complex form of extensive editing of the mitochondrial RNA.* Out of a total of 18 maxicircle transcripts, 12 pre-mRNAs are post-transcriptionally modified by the insertion or deletion of uridine residues (U) to produce functional mRNAs that serve as a template for translation. The mature mRNA sequence is specified by gRNAs and the process is carried out by large multiprotein RNA Editing Core Complex (RECC), also referred to as the 20S editosome (Stuart & Panigrahi 2002; Aphasizhev & Aphasizheva 2011). The range of required editing varies from the incorporation of a few uridylates (partially edited mRNAs) to a massive insertion/deletion of hundreds of uridylates (pan-edited mRNAs) (Stuart & Panigrahi 2002; Aphasizhev & Aphasizheva 2011; Aphasizheva et al. 2013) The alternative editing of several subunits of oxidative phosphorylation pathway that can increase transcript diversity was also reported (Ochsenreiter et al. 2008).

2.4. Trypanosomes as a model organism

The animal parasite *T. b. brucei* has an advantage over most other kinetoplastids because two of the life cycle stages (insect procyclic and bloodstream form) can be easily and safely cultivated *in vitro*. Importantly, the genome was completely sequenced, and it is freely accessible via TriTrypDB (Berriman et al. 2005; Aslett et al. 2005; Aslett et al. 2010). This provides an essential tool for genetic manipulations of the protist, which is amenable to methods of both forward and reverse genetics. The parasite also provides a good system for studying many aspects of cell biology, including: cell structure and morphology, organelle positioning, cell division, and protein trafficking. Therefore, it is employed not only as a model organism for the order Kinetoplastida, but is often useful for addressing more fundamental research topics in all eukaryotes (Matthews 2005). One example involves the discovery of acidocalcisomes (Vercesi et al. 1994), single membrane organelles participating in osmoregulation, intracellular pH homeostasis, calcium homeostasis and metabolism modulation. Since their discovery in trypanosomes, acidocalcisomes have been found in a wide range of organisms from bacteria to humans (Docampo & Moreno 2011).

The examples of forward genetic methods used in the field of trypanosomes are rare. Genetic crosses are possible but technically difficult to achieve as they require mixing strains through the insect vector, *Glossina spp.* (Hide 2008). Chemical mutagenesis brought a significant contribution to the field, when trypanosomes lacking their kinetoplast DNA (dyskinetoplastic) were generated using high concentrations of DNA intercalators, such as ethidium bromide and acriflavine (Riou et al. 1980; Stuart 1971). In contrast, the reverse genetic tools that are available for *T. brucei* are abundant. Widely used approaches include the generation of knock-out cells via homologous recombination, constitutive or inducible over-expression of variously tagged or mutated genes, and gene silencing via the RNA interference (RNAi) pathway, which was lost in *T. cruzi* and Leishmania parasites (Balaña-Fouce & Reguera 2007). The latter two methods have been facilitated by the generation of transgenic trypanosome cell lines that constitutively express the tetracycline repressor

(TetR) and the T7 RNA polymerase (T7RNAP). Therefore, most genetic experiments are performed in the Lister 427 single marker (SM) bloodstream cell line and the procyclic PF 29-13 cell line (Wirtz et al. 1999). The transgenic dyskinetoplastic *T. b. evansi* is also available (Schnauffer et al. 2005) and the *T. b. evansi* genome was recently sequenced (Carnes et al. 2015). With this powerful methodological toolkit, trypanosomes represent a suitable system for the characterization of novel proteins with unknown function.

2.5. *T. brucei* life cycle

Digenetic trypanosomes have a complex life cycle during which the parasite's morphology, expression of major surface markers and its biochemistry undergo rapid and substantial changes (Matthews et al. 2004; Matthews 2005; Stuart et al. 2008). These are known to be triggered by external stimuli like temperature and pH changes, as well as by the addition of the Krebs cycle intermediates, citrate or cis-aconitate (Czichos et al. 1986).

When a tsetse fly (*Glossina* spp.) takes a blood meal, it injects non-dividing metacyclic trypomastigotes into the host's skin (Figure 1). The parasites then pass via the lymphatic system into the mammalian bloodstream where they transform into proliferating bloodstream trypomastigotes. The bloodstream forms of *T. brucei* are able to evade the host's immune system very effectively through the elaborate variation of antigenically distinct variable surface glycoproteins (VSGs). Slender bloodform trypanosomes multiply by binary fission and settle into body fluids (for example blood, lymph, spinal fluid) (Matthews et al. 2004; Stuart et al. 2008). When the parasitemia becomes elevated in the host, a sub-population of slender bloodform stage cells differentiate into stumpy bloodforms that await to be taken up in the blood meal of the next tsetse fly. Stumpy form cells are relatively resistant to lysis by the proteolytic environment of the tsetse midgut and are uniformly arrested in the G1 phase of the cell cycle, rendering them non-proliferative. This cell cycle arrest limits the density of the bloodform parasites, which serves to both prolong host survival (and hence the probability of disease transmission) and ensure that the morphological changes occurring upon transmission to the tsetse fly can be coordinated with the re-entry into the cell cycle (Matthews et al. 2004; Matthews 2005).

Only stumpy bloodforms are competent to progress to the next stage. Upon uptake by the tsetse fly, they attach to the vector midgut and continue their life cycle as dividing procyclic trypomastigotes. These procyclic cells express a surface coat composed of procyclins (two forms - GP and GPEET) instead of the VSG coat of the bloodstream cells. After proliferation in the insect alimentary tract, the parasites migrate to the salivary gland and transform into the epimastigote forms, which are attached to the gland wall through elaborations of the flagellar membrane. After further multiplication, the epimastigotes undergo division arrest, reacquire the VSG coat and again become infective metacyclic trypomastigotes that are able to enter a new mammalian host (Matthews et al. 2004; Matthews 2005; Stuart et al. 2008; Batram et al. 2014).

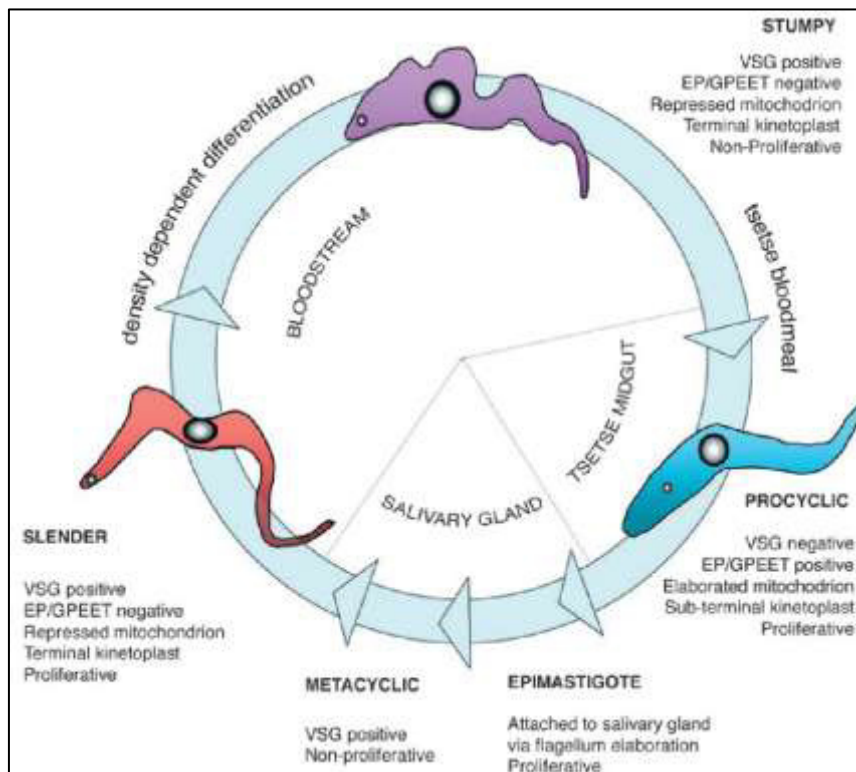


Figure 1: The life cycle of *Trypanosoma brucei*. Adapted from (Matthews 2005). Slender BF trypanosomes multiply in the blood of a mammalian host, express a VSG coat, and their mitochondrial activity is reduced. When the parasitemia levels reaches a threshold, differentiation into BF stumpy forms begins. BF stumpy cells are division-arrested forms preadapted for uptake by *Glossina spp.* In a tsetse fly midgut, procyclic proliferative forms are generated. PF cells express a surface coat composed of EP and GPEET procyclins and they have fully active mitochondria. After their establishment in the *Glossina* midgut, PF forms are arrested in division and migrate to the salivary glands, where epimastigotes attach. Later, some parasites detach and differentiate into infective metacyclic trypomastigotes.

2.6. Energy metabolism of Trypanosomes

The complex trypanosome energy metabolism has been studied for many years and has constantly been redefined (Besteiro et al. 2005; van Hellemond, Opperdoes, et al. 2005; Bringaud et al. 2006; Bringaud et al. 2012; van Weelden et al. 2005; Mazet et al. 2013). A comprehensive database that includes generic and condition specific metabolic networks was implemented in 2014 (Shameer et al. 2014). The most intensely studied cells are the procyclic trypanosomes, which are versatile and quickly adapt to different carbon sources. In a glucose-rich environment (culture medium, bloodmeal in tsetse fly midgut), PF preferentially consume glucose and ATP is produced primarily by substrate level phosphorylation. In a sugar-poor environment (tsetse fly fluids), PF cells are able to catabolize amino acids and ATP is generated via the oxidative phosphorylation pathway (Lamour et al. 2005; Coustou et al. 2008). Consequently, the procyclic mitochondrion is well developed with abundant cristae, tricarboxylic acid (TCA) cycle enzymes, and cytochrome containing respiratory complexes (Besteiro et al. 2005; Bringaud et al. 2012). An accurate metabolic PF model is difficult to create due to a combination of factors that include growth in glucose-rich conditions, differences between trypanosome strains, and methodologies. Recent research has focused on the cultivation of procyclic cells in glucose-depleted conditions, which is more representative of the rich amino-acid environment in the tsetse fly midgut (Lamour et al. 2005; van Weelden et al. 2005; Bringaud et al. 2012).

The investigation of energy metabolism is less controversial in bloodstream *T. brucei* because these cells reside in the glucose-rich environment of vertebrate host fluids, and therefore their energy demand is covered sufficiently by glycolysis (Bringaud et al. 2006). This mechanism of ATP production is also used by the dyskinetoplastic parasites, *T. b. evansi* and *T. b. equiperdum* (Schnauffer et al. 2002; Dean et al. 2013). The simplification of the carbohydrate metabolism in these parasites resulted in a structural and molecular reduction of the single mitochondrion which lacks cristae, key TCA cycle enzymes, and a functional respiratory chain (Schnauffer et al. 2005; Bringaud et al. 2006; Dean et al. 2013).

2.6.1. Glycolytic pathway

Glycolysis is a ubiquitously present metabolic pathway, through which glucose is oxidised for ATP generation. The chemistry of this reaction sequence is completely conserved across the entire tree of life and in most eukaryotic cells all 10 glycolytic steps are localised in the cytosol (Nelson & Cox 2008). However, the glycolytic pathway of *T. brucei* (Figures 2, 3) is organised in such a way that the first enzymes converting glucose into 3-phosphoglycerate (3-PGA) or 1,3-bisphosphoglycerate (1,3-BPGA) are compartmentalized within the glycosome, a unique peroxisome-like organelle found in Kinetoplastids. In the glycosome, the NAD⁺/NADH equilibrium as well as the total consumption and production of ATP are balanced. The net ATP production occurs in the cytosol, where the remainder of the glycolytic enzymes reside.

It is notable, that there are several important differences between the glycolytic pathway contained within the glycosome of bloodform and procyclic trypanosomes (Hannaert et al. 2003; Michels et al. 2006; Haanstra et al. 2014). In the BF *T. brucei* (Figure 2), phosphoglycerate kinase (step 7) has glycosomal localization, therefore 3-phosphoglycerate (3-PGA) is produced in the glycosome and exported into the cytosol, where ATP and pyruvate are generated. It was accepted that pyruvate was the excreted end product of BF trypanosomes under aerobic conditions (Hannaert et al. 2003; Michels et al. 2006; Tielens & van Hellemond 2009); however, recent data demonstrate that a minor fraction of pyruvate is further metabolized in a fatty acid biosynthetic pathway (Mazet et al. 2013). Furthermore, the NAD⁺/NADH balance of the BF *T. brucei* glycosome is maintained via a glycerol-3-phosphate (Gly-3-P)/dihydroxyacetone-phosphate (DHAP) shuttle. The shuttle is composed of the glycosomal NADH-dependent Gly-3-P dehydrogenase (step 8), a putative glycosomal exchanger, which exchanges Gly-3-P for DHAP, and the mitochondrial Gly-3-P oxidase (step 13), which regenerates DHAP from Gly-3-P. The Gly-3-P oxidase system is comprised of FAD-dependent Gly-3-P dehydrogenase, ubiquinone and the Trypanosome alternative oxidase (TAO); the latter passing electrons from Gly-3-P to molecular oxygen, producing water (Hannaert et al. 2003; Michels et al. 2006; Chaudhuri et al. 2006; Haanstra et al. 2014). In procyclic cells (Figure 3), the phosphoglycerate kinase (step 7) has a cytosolic localization, and thus ATP and 3-phosphoglycerate (3-PGA) are not produced in the glycosome, but in the cytosol (Figure 3). 1,3-biphosphoglycerate leaves the glycosome and it is sequentially converted to phosphoenolpyruvate (PEP). The PEP is either converted into pyruvate in the cytosol (step 12) or it re-enters the glycosome. The PEP re-entry leads to the production of glycosomal pyruvate (step 18) and glycosomal succinate (steps 14-17), of which the latter is the major excreted end product of this branch. The glycosomal and cytosolic pools of pyruvate are further metabolized either in the mitochondria to produce acetate or in the cytosol where lactate and alanine are the end products (Hannaert et al. 2003; Michels et al. 2006). The succinate producing branch is only active in procyclic cells, where it acts to balance the glycosomal ATP (steps 14,18) and NAD⁺/NADH levels (Hannaert et al. 2003; Michels et al. 2006; Haanstra et al. 2014). The glycosomal redox balance is maintained by two NADH-dependent oxidoreductases, malate dehydrogenase (step 15) and fumarate reductase (step 17), which re-oxidize the NADH produced by Gly-3-P dehydrogenase (step 6) (Hannaert et al. 2003; Michels et al. 2006; Haanstra et al. 2014; Bringaud et al. 2015). The Gly-3-P/DHAP shuttle that is employed by bloodstream forms to maintain the redox balance is most likely not used in procyclic cells unless the succinate production is abolished (Ebikeme et al. 2010). Indeed, the mt TAO steady state and activity in the PF form are significantly decreased compared to BF (Michels et al. 2006; Chaudhuri et al. 2006).

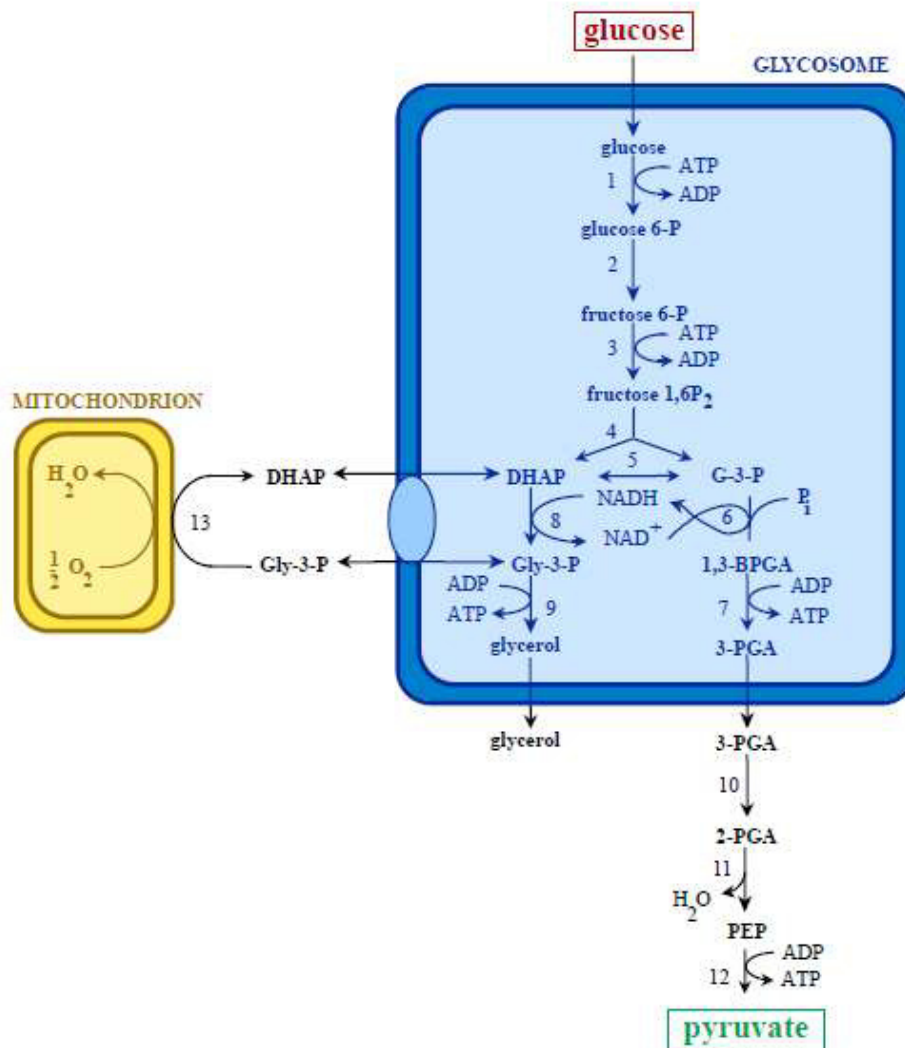


Figure 2: Glycolytic pathway of bloodstream stage. Adapted from (Hannaert et al. 2003). Enzymes: 1, hexokinase; 2, glucose-6-phosphate isomerase; 3, phosphofructokinase; 4, aldolase; 5, triosephosphate isomerase; 6, glyceraldehyde-3-phosphate dehydrogenase; 7, phosphoglycerate kinase; 8, glycerol-3-phosphate dehydrogenase; 9, glycerol kinase; 10, phosphoglycerate mutase; 11, enolase; 12, pyruvate kinase; 13, glycerol-3-phosphate oxidase. Abbreviations: G-3-P, glyceraldehyde 3-phosphate; 1,3-BPGA, 1,3-bisphosphoglycerate; 3/2-PGA, 3/2-phosphoglycerate; PEP, phosphoenolpyruvate; DHAP, dihydroxyacetone phosphate; Gly-3-P, glycerol 3-phosphate. Substrates and secreted end-products are indicated in green and red, respectively.

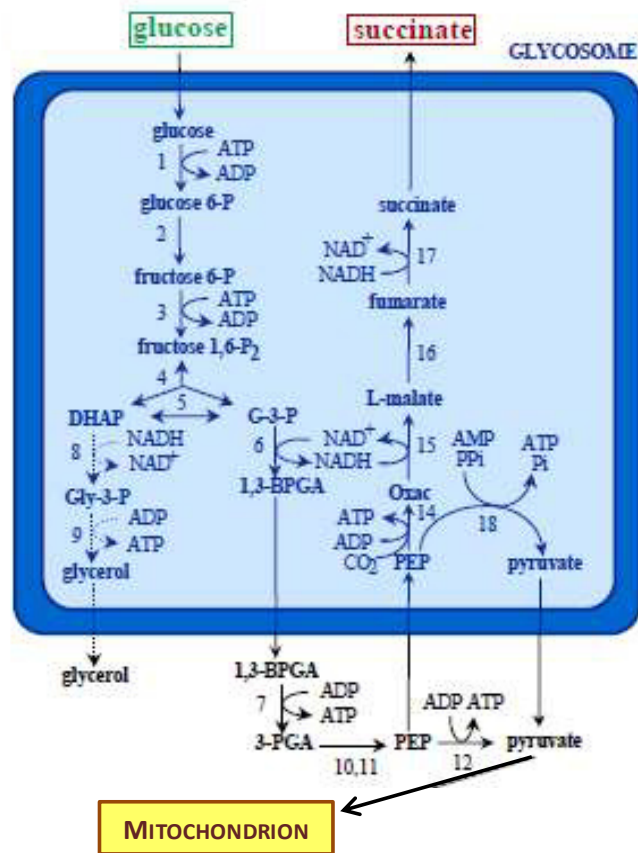


Figure 3: Glycolytic pathway of procylic stage. Adapted from (Hannaert et al. 2003). Enzymes: 1, hexokinase; 2, glucose-6-phosphate isomerase; 3, phosphofruktokinase; 4, aldolase; 5, triosephosphate isomerase; 6, glyceraldehyde-3-phosphate dehydrogenase; 7, phosphoglycerate kinase; 8, glycerol-3-phosphate dehydrogenase; 9, glycerol kinase; 10, phosphoglycerate mutase; 11, enolase; 12, pyruvate kinase; 14, phosphoenolpyruvate carboxykinase; 15, malate dehydrogenase; 16, fumarase; 17, fumarate reductase; 18, pyruvate phosphate dikinase. Abbreviations: G-3-P, glyceraldehyde 3-phosphate; 1,3-BPGA, 1,3-bisphosphoglycerate; DHAP, dihydroxyacetone phosphate; Gly-3-P, glycerol 3-phosphate; 3-PGA, 3-phosphoglycerate; PEP, phosphoenolpyruvate; Oxac, oxaloacetate. Substrates and secreted end-products are indicated in green and red, respectively. Enzymes involved in reactions represented by dashed lines are present, but experiments indicated that no significant fluxes occurred through these steps (Besteiro et al. 2002; van Weelden et al. 2003).

2.6.2. Amino acid catabolism

In a glucose depleted environment, the procyclic form cells rely upon the catabolism of amino acids and oxidative phosphorylation for energy production. Proline, an abundant metabolite in the tsetse fly midgut, is actively transported by the parasite and metabolized in the mitochondrion (Figure 4). During this catabolic process, ATP is produced by the conversion of succinyl-CoA to succinate (steps 6 and 21), and also by oxidative phosphorylation as the proline catabolism is directly linked to the respiratory chain via complex II (step 26) (Bringaud et al. 2012). The end products of proline catabolism are either utilized in biosynthetic pathways or excreted. Glutamate, alanine, and CO₂ are the predominant excreted end products, while acetate and succinate constitute minor products (Lamour et al. 2005; Bringaud et al. 2012).

At first, proline is converted to glutamate (steps 13, 14), which can be subsequently converted into alanine (step 16) and 2-oxoglutarate, but this step also requires the presence of pyruvate. 2-oxoglutarate then enters the TCA cycle and is further metabolized to succinate (steps 5,6), then to fumarate (step 26) by respiratory chain complex II, and finally to malate (step 8). Malate is either exported from the mitochondrion and used for gluconeogenesis or converted into pyruvate and CO₂ by the mt malic enzyme (step 9). Pyruvate is converted to acetyl-CoA (step 23) by pyruvate dehydrogenase and then metabolized into acetate by acetate: succinate-CoA transferase (ASCT) (step 22) (Bringaud et al. 2006; Coustou et al. 2008; Bringaud et al. 2012). Acetate was shown to be essential for the biosynthesis of fatty acids, although the primary contribution to this pathway comes from the degradation of threonine (steps 19-22) (Riviere et al. 2009; Millerioux et al. 2013).

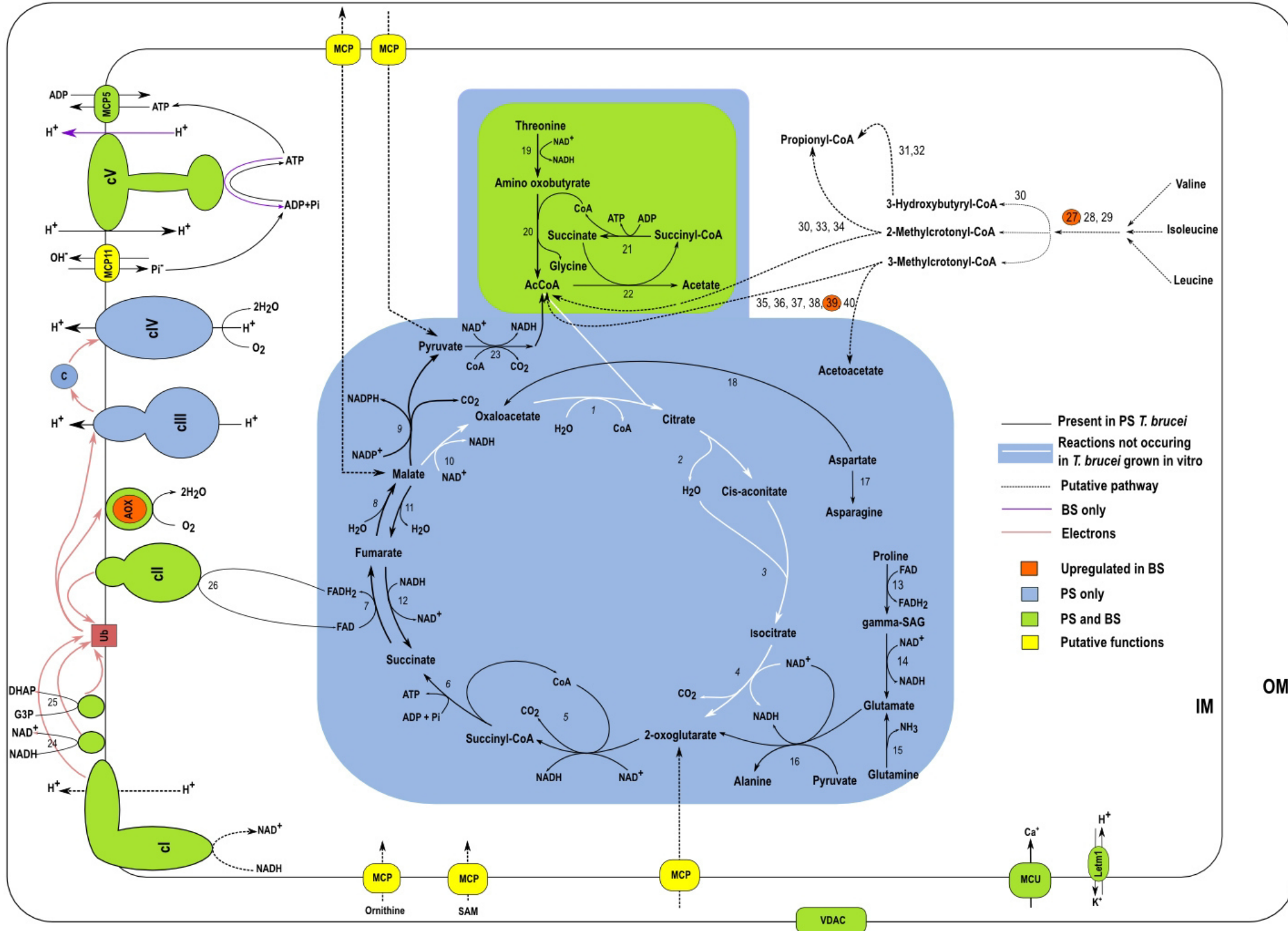


Figure 4: Mitochondrial energy metabolism in *T. brucei*. Adopted from (Verner et al. 2015). Black lines depict pathways found in *T. brucei*; white lines depict pathways found in mammalian cells; purple lines depict reactions present only in the bloodstream form stage (BSF) of *T. brucei*; pink lines depict transit of electrons in the respiratory chain. Pathways with a green background represent those present in both procyclic form stage (PCF) and BSF trypanosomes. Pathways with blue background are present in BSF only; orange represents pathways up-regulated in BSF; yellow background and dotted lines indicate putative proteins whose activity has not been experimentally verified, but their homologs are annotated in the *T. brucei* genome or have been found by proteomic analyses.

Enzymes: 1) citrate synthase; 2) and 3) aconitase; 4) isocitrate dehydrogenase; 5) α -ketoglutarate dehydrogenase (2-oxoglutarate); 6) succinyl-CoA synthetase; 7) succinate dehydrogenase/complex II; 8) fumarase; 9) malic enzyme; 10) malate dehydrogenase; 11) fumarase; 12) fumarate reductase; 13) L-proline dehydrogenase; 14) pyrroline-5-carboxylase; 15) L-glutamine deaminase; 16) glutamate dehydrogenase; 17) asparagine synthetase; 18) aspartate aminotransferase; 19) L-threonine dehydrogenase; 20) AcCoA:glycine C-acetyltransferase; 21) succinyl CoA synthetase; 22) acetate:succinate CoA transferase; 23) pyruvate dehydrogenase; 24) alternative NADH dehydrogenase; 25) glycerol-3-phosphate dehydrogenase; 26) succinate dehydrogenase; 27) branched-chain aminotransferase; 28) branched-chain keto acid dehydrogenase; 29) acyl-CoA dehydrogenase; 30) enoyl CoA hydratase; 31) hydroxyisobutyryl CoA hydrolase; 32) 3-hydroxybutyrate dehydrogenase; 33) 3-hydroxyacyl CoA dehydrogenase; 34) acetyl CoA acyltransferase; 35) 2-oxovalerate dehydrogenase; 36) isovaleryl CoA dehydrogenase; 37) methylcrotonyl CoA carboxylase; 38) methylglutaconyl CoA hydratase; 39) hydroxymethyl glutaryl CoA synthase; 40) hydroxymethyl glutaryl CoA lyase.

Abbreviations: AcCoA, acetyl Co enzyme A; AOX, alternative oxidase; C, cytochrome C; cI, cII, cIII, cIV and cV, respiratory chain complexes; DHAP, dihydroxyacetone phosphate; G3P, glycerol 3-phosphate; Letm1, leucine zipper EF-hand containing transmembrane protein 1; MCP, mitochondrial carrier protein; MCU, mitochondrial calcium uniporter; Pi, inorganic phosphate; OM, mitochondrial outer membrane; SAM, s-adenosyl methionine; Ub, ubiquinone; VDAC, voltage-dependent anion channel.

2.6.3. Tricarboxylic acid cycle

The conventional tricarboxylic acid cycle, also called the citric acid cycle or the Krebs cycle, is a hub in the energy metabolism of the cell. Under aerobic conditions, pyruvate is the end product of glycolysis, and it is imported into the mitochondrion where it is converted to acetyl-CoA by the pyruvate dehydrogenase complex. Acetyl-CoA enters the TCA cycle as it condenses with oxaloacetate to form citrate. The TCA cycle enzymes then convert citrate to oxaloacetate and releases two molecules of CO₂ through seven sequential reactions that include three NAD- and one FAD-mediated dehydrogenations, two decarboxylations, and a substrate phosphorylation. For every acetyl-CoA oxidized, the net energy yield is three molecules of NADH, one FADH₂, and one nucleoside triphosphate (ATP or GTP) (Nelson & Cox 2008). In most eukaryotic cells, the TCA cycle is linked to the electron transport chain to produce more ATP molecules as part of the oxidative phosphorylation (OxPhos) pathway.

The TCA cycle enzymes and the cytochrome-containing respiratory chain complexes appear to be absent from the reduced mitochondrion of bloodstream stage *T. brucei* (Hannaert et al. 2003; Tielens & van Hellemond 2009). In contrast to BF, procyclic cells possess detectable activities of all the TCA cycle enzymes (Figure 4) (van Hellemond, Opperdoes, et al. 2005; Urbaniak et al. 2012). However, their contribution towards energy generation is disputable as experimental data suggest that the TCA cycle does not operate as a true cycle in procyclic trypanosomes (van Weelden et al. 2005; Tielens & van Hellemond 2009). Several lines of evidence support this conclusion:

- a) *In vitro* cultivated PF cells mainly excrete partially oxidized end products (acetate, succinate, alanin) rather than CO₂ (van Weelden et al. 2003; Coustou et al. 2008).
- b) Even in low-carbohydrate conditions, PF cells do not shift towards a complete oxidation of TCA intermediates to form CO₂ (van Weelden et al. 2005).
- c) Gene disruption of aconitase (the second TCA enzyme) does not affect the viability or proliferation of PF cells grown *in vitro* (van Weelden et al. 2003). Moreover, the aconitase knock-out produces the same metabolic end products as the wild type cell line (van Weelden et al. 2003).
- d) Acetyl-CoA is diverted from the TCA cycle towards acetate production (most likely due to the kinetics of some enzymes) (van Hellemond, Opperdoes, et al. 2005).
- e) Instead of acetyl-CoA, the TCA cycle is fed with 2-oxoglutarate and malate, thus only parts of the cycle are required for their catabolism (Tielens & van Hellemond 2009; Bringaud et al. 2010).

Initially, pyruvate is imported into PF mitochondrion and metabolized to acetyl-CoA by pyruvate dehydrogenase (step 23). Interestingly, acetyl-CoA does not seem to enter the TCA cycle but it is converted into acetate predominantly through a two-enzyme cycle: I) acetate: succinate-CoA transferase (ASCT) (step 22) transfers the CoA to succinate, yielding acetate and succinyl-CoA; II) succinyl CoA synthetase (SCS) (step 21), which is also a part of the TCA

cycle (step 6), converts succinyl-CoA to succinate and produces ATP (Van Hellemond et al. 1998; Rivière et al. 2004; van Hellemond, Bakker, et al. 2005).

Instead of acetyl-CoA, the TCA cycle is mainly fed by 2-oxoglutarate derived from mitochondrial proline and glutamine catabolism (steps 13-16). 2-oxoglutarate is then metabolized to succinate by 2-oxoglutarate dehydrogenase (step 5) and succinyl-CoA synthetase (step 6). Alternatively, the TCA cycle can be fed by glucose derived malate that is also gradually converted to succinate by a fumarase (step 11) and soluble fumarate reductase (step 12) (Coustou et al. 2008; Tielens & van Hellemond 2009; Bringaud et al. 2010). As both of these substrates are metabolized by only a part of the classical TCA cycle, the question arises as to why all TCA enzymes are expressed in the procyclic stage. One possible explanation is that these enzymes are used in alternative metabolic pathways. For example:

- a) SCS (steps 6, 21) is used to produce acetate, which is essential for the *de novo* synthesis of fatty acids (Van Hellemond et al. 1998; Riviere et al. 2009).
- b) It has been proposed that part of the TCA cycle is used for the conversion of acetyl-CoA into citrate, which could then be exported from the mitochondrion and used for fatty acid biosynthesis (van Weelden et al. 2005).
- c) Both the mt catabolism of proline and glutamine (steps 16-6) and the production of succinate from malate (which concomitantly reoxidizes NADH) require TCA cycle enzymes (steps 11,12) (van Hellemond, Bakker, et al. 2005; Tielens & van Hellemond 2009).
- d) Part of the TCA cycle is also required for production of malate from succinate (steps 7 and 8). Malate can be exported from mitochondrion and used for gluconeogenesis pathway inside glycosome. This is especially important when the parasite is cultured in the absence of glucose (van Weelden et al. 2005; Tielens & van Hellemond 2009; Bringaud et al. 2012).
- e) Moreover, it can not be excluded that the flux through the TCA cycle is changing during the complex development of *T. brucei* as it progresses through various environments within the tsetse fly. Thus, all TCA cycle enzymes may be employed by other *T. brucei* stages during another portion of the life cycle (Bringaud et al. 2010).

2.6.4. Oxidative phosphorylation pathway

During oxidative phosphorylation (Figure 4), electrons are transferred from an electron donor (NADH or succinate) to an electron acceptor (O_2) through a series of redox reactions, that are linked to the phosphorylation of ADP. In eukaryotic cells, the redox reactions are carried out by a series of mitochondrial cytochrome-containing respiratory complexes that comprise the electron transport chain. This interconnected chain of the transmembrane respiratory proteins is formed by complexes I-IV (cI-IV). Complex I (NADH:ubiquinone oxidoreductase) and cII (succinate:ubiquinone oxidoreductase) catalyze the electron transfer

from NADH or FADH, respectively, to the hydrophobic membrane carrier ubiquinone. Complex III (ubiquinol:cytochrome *c* oxidoreductase, cytochrome *bc*₁ complex) then passes the electrons from the ubiquinol to a soluble heme-containing protein, cytochrome *c* (cyt *c*). Complex IV (cytochrome *c*:oxygen oxidoreductase, cytochrome *c* oxidase), completes the chain by transferring electrons from cyt *c* to O₂. The electron flow is coupled with the transfer of protons across the inner mitochondrial membrane (IM), which is impermeable to H⁺. This results in differences in the chemical concentration (ΔpH) and charge distribution ($\Delta\psi$) across the IM. The electrochemical energy is termed the proton-motive force (mt membrane potential, $\Delta\psi_m$) and is utilized by complex V (F_oF₁-ATP synthase) to synthesize ATP molecules from ADP and inorganic phosphate (Pi). These two substrates are transported into the mt matrix by two carriers: the ADP/ATP carrier (AAC) and the phosphate carrier (PiC) (Nelson & Cox 2008; Sun et al. 2013; Chaban et al. 2014).

Oxidative phosphorylation complexes in different eukaryotes form higher-order assemblies or supercomplexes. Supercomplexes consisting of various proportions of cI, cIII and cIV (i.e. I+III₂, III₂+IV₂, I+III₂+IV₁₋₄) were termed respirasomes as they generate large amounts of $\Delta\psi_m$. The functional role of these assemblies is debated; however, it is proposed that respirasomes may be important for efficient oxidation of multiple substrates, and for improvement of electron transfer between individual components, thereby reducing the generation of reactive oxygen species (Winge 2012; Chaban et al. 2014). Another example of higher-order assemblies affecting the morphology and function of the mitochondrion is evident in the dimerization of F_oF₁-ATP synthases, which cause the mt membrane to bend and form cristae (Chaban et al. 2014). Moreover, the rat, bovine, and *L. mexicana* F_oF₁-ATP synthases were identified as a component of a supercomplex comprised of the AAC and PiC carriers, forming the so called "ATP synthasome" (Ko et al. 2003; Chen et al. 2004; Wittig & Schägger 2008; Detke & Elsabrouty 2008).

The components of the OxPhos pathway have a dual genetic origin. Most of mt proteins are encoded by the nuclear genome, synthesized in the cytosol, and then imported into mitochondrion. However, a small number of proteins are encoded by the mtDNA and translated by mt ribosomes. In most eukaryotes, including *T. brucei*, mtDNA genes usually encode highly hydrophobic core subunits of the OxPhos pathway and components of the mt ribosomes (Gray et al. 1999; Ott & Herrmann 2010).

2.6.4.1. Respiratory chain of bloodstream and dyskinetoplasic trypanosomes

The respiratory chain of the bloodstream form *T. brucei* is reduced to the Gly-3-P/DHAP shuttle coupled with the cytochrome-independent Trypanosome alternative oxidase. This pathway reoxidizes glycolytic Gly-3-P (Figure 2, step 13) and thus maintains the glycosomal redox balance (Bringaud et al. 2006; Chaudhuri et al. 2006; Shiba et al. 2013). Alternative oxidases, also found in some higher plants, fungi and unicellular eukaryotes, are diiron proteins that transfer four electrons from ubiquinol to molecular oxygen, producing water. This cyanide-insensitive activity is not coupled to proton translocation and hence

neither generates $\Delta\psi_m$ nor contributes to ATP production via OxPhos (Chaudhuri et al. 2006; Shiba et al. 2013; Young et al. 2013).

In BF trypanosomes, the glycolysis alone is able to meet the energy demands of the cell, however, the $\Delta\psi_m$ is essential for several mitochondrial processes (Schnauffer et al. 2005; Tielens & van Hellemond 2009). This indispensable $\Delta\psi_m$ in the bloodstream stage is therefore sustained mainly by the hydrolytic activity of the F_0F_1 -ATPase, which translocates protons across the IM (Nolan & Voorheis 1992; Schnauffer et al. 2005; Brown et al. 2006).

As previously discussed (chapter 2.3), trypanosoma mt gene transcripts are encoded by the uniquely structured kDNA and most require pre-mRNA editing to generate functional mRNAs (Benne et al. 1986; Stuart & Panigrahi 2002; Aphasizhev & Aphasizheva 2011; Aphasizheva et al. 2013). The replication and expression of kDNA is an elaborate process requiring large multiprotein enzymatic complexes that are essential for PF as well as for BF *T. brucei* (Schnauffer et al. 2001; Hashimi et al. 2008). This enormous expenditure of energy in BF cells is fascinating because it appears that only one mt protein, the F_0F_1 -ATP synthase subunit a, is essential in this life stage. Interestingly, dyskinetoplastic trypanosomes completely bypass the requirement for functional kDNA expression through compensatory mutations in various F_0F_1 -ATP synthase subunits (Schnauffer et al. 2005)(Dean et al. 2013; Carnes et al. 2015). However, TAO, the Gly-3-P/ DHAP shuttle, and possibly other $\Delta\psi_m$ dependent mt functions are expected to be essential in Dk trypanosomes (Carnes et al. 2015), but this will require additional experimental confirmation. It has been shown indirectly that Dk cells lack a functional F_0 proton pumping activity, because they are not sensitive to oligomycin, a specific inhibitor of the F_0F_1 complex (Opperdoes et al. 1976; Schnauffer et al. 2005). Thus, Dk trypanosomes rely on the electrogenic generation of the $\Delta\psi_m$, a process independent of proton translocation (Schnauffer et al. 2005; Dean et al. 2013).

2.6.4.2. Respiratory chain of procyclic trypanosomes

In *T. brucei* procyclic cells, the presence of classic respiratory complexes, similar to that of other eukaryotes, is well established (Tielens & van Hellemond 2009; Acestor et al. 2011; Bringaud et al. 2012). In addition, there are another three enzymes that are capable of passing electrons to and from ubiquinone (Figure 4) (Tielens & van Hellemond 2009; Verner et al. 2015). Mitochondrial glycerol-3-phosphate dehydrogenase (Gly-3-P DH) (step 25) and an alternative rotenone-insensitive NADH dehydrogenase (NDH_2) (step 24) transfer electrons from Gly-3-P and NADH to ubiquinone, respectively (Fang & Beattie 2003; Guerra et al. 2006). The reduced ubiquinol can then be reoxidized by TAO, which passes the electrons to molecular oxygen. None of these three enzymes are directly contributing to the $\Delta\psi_m$; however, Gly-3-P DH and NDH_2 can participate via an increase in the electron flow through ubiquinol and complex III (Tielens & van Hellemond 2009; Verner et al. 2015).

While the procyclic respiratory complexes I- IV perform the same functions as in higher eukaryotes, their composition is substantially different. Complex I is the largest of these

multiprotein complexes and it catalyzes the transfer of two electrons from NADH to ubiquinone while simultaneously transferring four protons from the matrix to the intermembrane space. In bacteria, this complex consists of 13-15 subunits, whereas the eukaryotic mitochondrial enzyme has 45 subunits, seven of which are encoded by mtDNA. Both complexes contain the same redox components: a flavine mononucleotide and 8-9 iron-sulphur (Fe-S) clusters (Janssen et al. 2006; Sazanov 2007; Efremov & Sazanov 2011). Trypanosoma cl appears to have no less than 46 subunits, eight are kDNA encoded. However, at least 31 proteins have no homology outside Euglenozoa, suggesting that this complex may perform other diverse functions, as it has been suggested in the metabolism of fatty acids (Acestor et al. 2011; Duarte & Tomás 2014). The relevance of cl and its contribution to the OxPhos pathway in *T. brucei* is confounding for following reasons:

- a) Specific rotenone-sensitive NADH-dehydrogenase activity that was initially contributed to cl was later questioned because of the very high concentrations of inhibitor used in the experiments (Beattie et al. 1994; Hernandez & Turrens 1998).
- b) It was shown that the NDH2 enzyme is fundamentally a single-protein counterpart of cl, which may be able to offset most of cl activity (Fang & Beattie 2003; Verner et al. 2013).
- c) RNAi depletion of cl subunits has no effect on cell viability (Verner et al. 2011; Surve et al. 2012).
- d) The loss of cl was observed upon prolonged *in vitro* cultivation of *Crithidia fasciculata*, a related insect trypanosomatid (Speijer et al. 1997).

Complex I and NDH₂ both appear to also be expressed in BF mitochondrion, although their functions are unknown (Surve et al. 2011; Urbaniak et al. 2012).

Complex II is the smallest complex of the respiratory chain. As an integral part of the TCA cycle, it oxidizes succinate to fumarate and transfers electrons to ubiquinone. However, the energy accumulated from these passing electrons is not sufficient to translocate any protons, hence this complex does not directly contribute to $\Delta\psi_m$. The representative prokaryotic and eukaryotic enzyme has only four nuclear encoded subunits, a flavin adenine dinucleotide (FAD) cofactor, heme *b* and three different Fe-S clusters (Rutter et al. 2010; Maklashina & Cecchini 2010). In contrast, *T. brucei* cII is composed of up to nine subunits that were identified on the protein level (Acestor et al. 2011). Complex II was shown to be essential for PF only under glucose depleted conditions (Coustou et al. 2008).

Complex III re-oxidizes ubiquinone, which was reduced to ubiquinol by the complexes I and II. This oxidation event allows the transfer of electrons from ubiquinol to the soluble cytochrome *c*. For every transferred electron there are two protons translocated across the inner mt membrane; a mechanism known as the Q-cycle. Bacterial complex III has only three subunits, while the mammalian mitochondrial enzyme is composed of eleven proteins. All complexes have three subunits with redox cofactors: the iron-sulphur protein (Rieske), cytochrome *c1* and cytochrome *b*, which is the only mtDNA encoded subunit (Cramer et al. 2011; Xia et al. 2013).

T. brucei cIII is comprised of a total of seven subunits, three of which have redox centers. Rieske and cyt c_1 (apo c_1) subunits are nuclear encoded, while the cytochrome *b* protein is encoded by kDNA. Two subunits were also identified as homologues of the mt processing peptidase (MPP) protein family (α - and β - MPP) (Acestor et al. 2011; Mach et al. 2013), which recognizes and removes a mt targeting sequences of imported proteins (Iwata et al. 1998; Xia et al. 2013). Complex III was shown to be important for PF *T. brucei* viability as RNAi silencing of Rieske and apo c_1 inhibited cell growth (Horváth et al. 2005).

The final component of the respiratory chain, complex IV, transfers electrons from the reduced cyt *c* to molecular oxygen, the final electron acceptor. This reaction is also coupled to the translocation of two protons to the mt inner membrane space. The bacterial cytochrome *c* oxidase (cox) is composed of four subunits. Three subunits coxI-III bear four redox cofactors: two hemes (heme *a* and a_3) and two copper centres (Cu_A and Cu_B). The mammalian complex contains homologous catalytic subunits cox I-III, which are mt-encoded, as well as an additional ten nuclear encoded subunits (Richter & Ludwig 2009; Soto et al. 2012). In *T. brucei*, cIV was shown to be divergent from other organisms as it contains at least 19 subunits, only two of which are homologous to mammalian proteins. In addition, cIV associates with up to 18 other proteins, most of them with unidentified function. This suggests that cIV might have a secondary role, besides transferring electrons (Zikova et al. 2008).

For example, two cIV proteins, together with cIII and cV subunits, were found to associate within a multiprotein complex that imports tRNAs into the mitochondrion of a related protist, *L. tropica* (Chatterjee et al. 2006; Mukherjee et al. 2007). Moreover, the cIV associated mt protein X (MIX) has a role in mt segregation and cell division in *T. brucei* and *L. major*, and its depletion leads to a loss of *L. major* virulence (Uboldi et al. 2006; Zikova et al. 2008). The importance of cIV for PF *T. brucei* was investigated by the RNAi silencing of four kinetoplastid specific subunits. These proteins appear to have a different specific function within cIV; however, the RNAi knock-down of each of them decreased the $\Delta\psi_m$ and inhibited cell growth, indicating that cIV is essential for PF *T. brucei* viability (Horváth et al. 2005; Gnipová et al. 2012). The $\Delta\psi_m$ generated by respiratory complexes III and IV is used by the last component of the OxPhos pathway, the F_0F_1 -ATP synthase. The unique function, composition and possible involvement of this *T. brucei* complex within supercomplexes will be further discussed.

The organization of respiratory complexes I, III and IV into respirasomes was also investigated in PF cells. A possible hetero-multimeric supercomplex of cIII and cIV was detected *in vitro* by histochemical in-gel staining. Moreover, the mass spectrometry analysis of affinity purified cIII revealed the presence of five cIV proteins (Acestor et al. 2011). However, silencing of cIII subunits did not affect the structure of cIV, and vice versa. In addition, RNAi of neither cIII nor cIV subunits altered the already questionable cI activity (Horváth et al. 2005). These results together with our published data (Gnipová et al. 2015) suggest that supercomplexes appear to be absent in *T. brucei*.

2.7. F₀F₁-ATP synthase (Complex V)

The F₀F₁-ATP synthase complex plays a central role in the synthesis of ATP in all living organisms. This complex, also known as F-type ATPase belongs to a larger protein family, comprised of F-, V- and A-type ATPases. These enzymes have similar structures and mechanisms of operation; however, they differ in their biological function and taxonomic origin. Generally, F-type ATPases synthesize ATP, although they can operate in reverse and hydrolyze ATP under specific conditions. V-type ATPases (vacuolar) use the energy from ATP hydrolysis to pump ions across intracellular or plasma membranes. A-ATPases/A-synthases are structurally simple and versatile enzymes found in archaea (Jonckheere et al. 2012; Walker 2013).

The F₀F₁-ATP synthase is found in the plasma membrane of bacteria, in the thylakoid membrane of chloroplasts, and in the inner membrane of mitochondria. In each of these locations, this enzyme synthesizes ATP in a manner that is coupled to the translocation of protons (or Na⁺ ions) across the respective membranes (von Ballmoos et al. 2008; Nakamoto et al. 2008; Walker 2013). This principal mechanism was postulated by Peter Mitchell in his chemiosmotic theory (Mitchell 1961), which was rewarded the Nobel Prize in 1978. The elucidation of the mechanism of F₀F₁-ATP synthase operation was also awarded a Nobel Prize in Chemistry (1997), that is shared between Jens C. Skou, who discovered the Na⁺/K⁺ ATPase pump, Paul D. Boyer, and John E. Walker. While Paul Boyer and colleagues proposed the catalytic mechanism for ATP synthesis, Walker's group resolved the crystal structure of the bovine enzyme, which experimentally supported Boyer's theory (Boyer 1993) (Abrahams et al. 1994; Boyer 2002). Direct visual evidence of the F₀F₁-ATP synthase operation was provided by Yoshida's laboratory in 1997 (Noji et al. 1997). In recent decades, the F₀F₁-ATP synthase has been extensively studied using genetic, biochemical, crystallographic and microscopic techniques. Consequently, the general organisation, architecture and catalytic mechanism of this complex is well established in model organisms.

2.7.1. F₀F₁-ATP synthase architecture

This ubiquitous multisubunit enzyme (Figure 5), with a molecular mass of nearly 600 kDa, is composed of numerous nuclear and a few mtDNA encoded subunits (summarized in Table 1). Despite this complexity, the basic F₀F₁-ATP synthase structure is conserved throughout the biological kingdom, and is comprised of two functionally distinct parts. The hydrophilic F₁ moiety performs the enzymatic reaction, while the membrane bound F₀ moiety mediates H⁺ transport. These two subcomplexes are connected by the central and peripheral stalks (von Ballmoos et al. 2008; Walker 2013).

The prokaryotic F₀F₁-ATP synthase, which represents the simplest form of the complex, is a monomeric enzyme. Prokaryotic F₁ subcomplex is composed of five subunits α , β , γ , δ and ϵ with the stoichiometry: $\alpha_3\beta_3\gamma_1\delta_1\epsilon_1$. The three α and β subunits are alternately arranged around subunit γ , which protrudes below the $\alpha_3\beta_3$ hexamer and attaches this F₁ catalytic part

to the F_o moiety. This attachment is further strengthened by subunit ϵ . The membrane-bound F_o moiety is comprised of a single subunit a that interacts with a ring formed by oligomers of subunit c (in a stoichiometry of c_{8-15} , dependent on the species); this interaction between these two proteins forms the H^+ channel. Additionally, the bacterial peripheral stalk contains two b subunits that are attached to subunit a , and a single subunit δ (von Ballmoos et al. 2008; Walker 2013).

The eukaryotic mt F_oF_1 -ATP synthase has homologous components to the prokaryotic form, but it also incorporates additional subunits involved in the structure, oligomerization, and regulation of the complex. Detailed structural studies of the mitochondrial enzyme established that dimeric and even higher-oligomeric organization of the complex exists in different organisms ranging from unicellular eukaryotes to mammals. For example, in *S. cerevisiae*, the F_oF_1 -ATP synthase consists of at least 17 different subunits, some of which are specific only for the 1200 kDa dimer. Dimeric F_oF_1 -ATP synthase was also found in *Bos taurus*, where the complex is constructed from at least 16 different subunits (Walker 2013; Habersetzer et al. 2013).

The mammalian F_1 is composed of subunits α_3 , β_3 , γ_1 , δ_1 , ϵ_1 . Although it is confusing, the eukaryotic protein δ is the functional counterpart of the prokaryotic subunit ϵ and this designation is used for historical reasons. The eukaryotic subunit ϵ however, has no homolog in the bacterial complex. The F_o moiety also has a greater complexity in eukaryotes. Besides the conserved proton channel consisting of subunits a_1 and c_{8-15} , it incorporates single copies of subunits $A6L$, b , d , $F6$, e , f and g . None of these subunits have a prokaryotic homolog. Another two F_o ATP synthase associated proteins were identified in mammals: DAPIT (Diabetes associated protein in insulin-sensitive tissue) and a 6.8-kDa mitochondrial proteolipid (MLQ protein). Their function and association with the complex has yet to be determined (Jonckheere et al. 2012; Walker 2013). The yeast F_oF_1 -ATP synthase is mostly homologous to the mammalian complex with the exception of two yeast specific proteins, the F_o subunit i/j and the dimer specific subunit k (Jonckheere et al. 2012; Habersetzer et al. 2013).

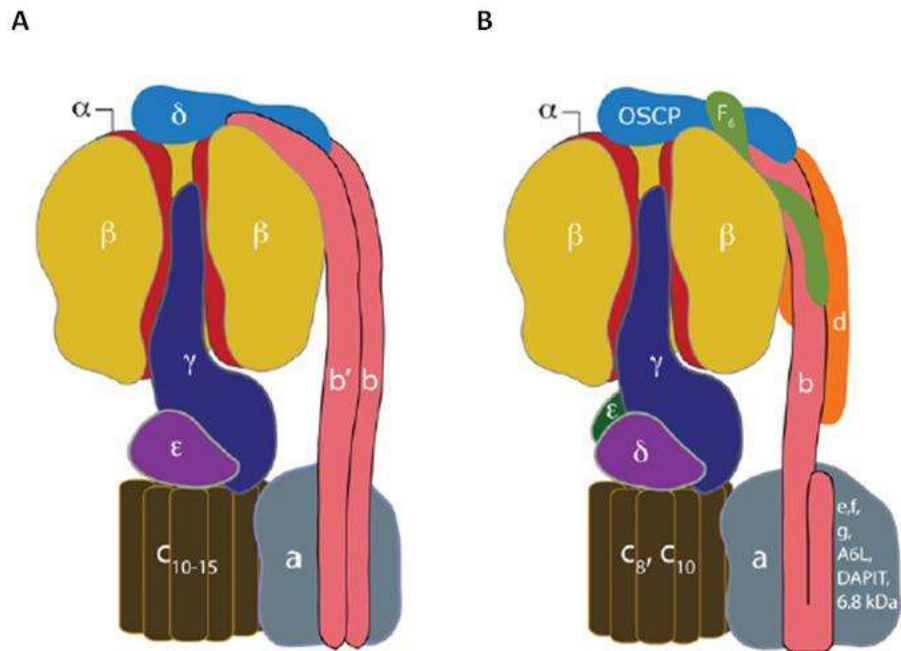


Figure 5: Organization of protein subunits in F_0F_1 -ATP synthases. Adapted from (Walker 2013). The prokaryotic (bacterial and chloroplast) F_0F_1 -ATP synthase (A) and the eukaryotic mt F_0F_1 -ATP synthase (B) are shown. The upper part of each model contains the subunits in the F_1 catalytic domain. One of the three α -subunits (red) has been removed to expose the elongated α -helical structure in the γ -subunit (dark blue), which lies approximately along the central axis of the spherical $\alpha_3\beta_3$ domain. The γ -subunit (and associated subunits) is in contact with the F_0 membrane domain, which contains the c-ring (brown) and the associated a-subunit (grey). The number of c-subunits in the c-ring differs between species. The rotor of the enzyme consists of the ensemble of the c-ring and the γ -subunit (and associated subunits). The pathway for protons through the F_0 domain is in the vicinity of the interface between the c-ring and a-subunit. The peripheral stalk is on the right of each model. In some bacterial enzymes, it consists of the δ -subunit (light blue) and two identical b-subunits (pink). In other bacterial enzymes, and in the chloroplast enzyme, the two b-subunits are replaced by single copies of homologous, but non-identical, subunits b and b'. In the mt complex, the peripheral stalk consists of single copies of subunits OSCP, b, d and F6. The membrane domains of the mt F_0F_1 -ATP synthase contain a number of membrane subunits that are not found in bacteria and chloroplasts. These supernumerary subunits have no known roles in the generation of ATP; subunits e, f, g, A6L, DAPIT and the 6.8 kDa proteolipid.

Table 1. Composition and subunit nomenclature of the F₁F_o-ATP synthase complex in different species. Adapted from (Devenish et al. 2008; Jonckheere et al. 2012; Habersetzer et al. 2013). Dashes indicate no equivalent subunit. Subunits marked with an asterisk are mtDNA encoded. Genes encoding individual yeast proteins are in parentheses.

Sector	<i>E. coli</i>	<i>S. cerevisiae</i>	<i>B. taurus</i>
F ₁	α	α (ATP1p)	α
F ₁	β	β (ATP2p)	β
Central stalk	γ	γ (ATP3p)	γ
Peripheral stalk	δ	OSCP(ATP5p)	OSCP
Central stalk	ε	δ (Atp16p)	δ
Central stalk	-	ε (Atp15p)	ε
F _o	a	a/6 (Atp6p)*	a*
Peripheral stalk	b	b (Atp4p)	b
F _o	c	c (Atp9p)*	c
F _o	-	8/aap1 (Atp8p)*	A6L*
Peripheral stalk	-	d (Atp7p)	d
Peripheral stalk	-	h (Atp14p)	F6
F _o	-	e (Tim11p)	e
F _o	-	f (Atp17p)	f
F _o	-	g (Atp20p)	g
F _o	-	i/j (Atp18p)	-
F _o	-	k (Atp19p)	-
F _o	-	-	DAPIT
F _o	-	-	6.8 kDa proteolipid

2.7.2. Mechanism of ATP synthesis and ATP hydrolysis

The F_oF₁-ATP synthase complex can operate in either the ATP synthesis or ATP hydrolysis (F_oF₁-ATPase) mode. In both scenarios, the F_o and F₁ units operate as a coordinated, reversible rotary motors by exchanging energy through the mechanical rotation of a central stalk.

From a mechanistic point of view, the F_oF₁-ATP synthase can be divided into rotor (c-ring, γ, δ, ε) and stator (α₃β₃ hexamer, a, b, d, F6, OSCP) components (bovine nomenclature is used) (Devenish et al. 2008). During ATP synthesis, the rotor converts the electrochemical gradient into torque, thus enabling the stator to act as an ATP generator. The energy provided for this generator results from the movement of H⁺ through the F_o channel, creating a clockwise rotation (as viewed from the membrane side) of the c-ring,

which in turn causes the central stalk to rotate. This torque is counterbalanced by the peripheral stalk, which fixes the $\alpha_3\beta_3$ hexamer relative to the F_o subunit a. The rotation of the F_1 central stalk subunit γ creates a conformational change in the F_1 catalytic $\alpha_3\beta_3$ hexamer, leading to the synthesis of ATP from bound ADP and inorganic phosphate (von Ballmoos et al. 2008; Devenish et al. 2008; Walker 2013).

The model for ATP synthesis (Figure 6) is well described and is commonly referred to as the binding change mechanism (Boyer 2002; von Ballmoos et al. 2008; Sielaff & Börsch 2013). The F_1 catalytic nucleotide-binding sites are located on each of the three β -subunits at the interface with the α -subunits. While all three α -subunits adopt similar conformations, the β -subunits are in three different nucleotide bound states:

- i) Subunit β_{DP} binds MgADP (the “tight” state of the binding change mechanism).
- ii) Subunit β_{TP} binds MgATP (the “loose” state).
- iii) Subunit β_E has a very low affinity for either nucleotide (the “empty” or “open” state).

The asymmetric geometry of the internal γ subunit forces a specific conformational change in each of the β subunits as it rotates through the $\alpha_3\beta_3$ headpiece. Thus, during one γ rotational cycle, each β subunit successively adopts a conformation of varying affinity for binding nucleotides (open, loose and tight state) (von Ballmoos et al. 2008; Sielaff & Börsch 2013). In the open state, ADP and phosphate enter the binding pocket, causing a conformational change in the catalytic site to bind the molecules loosely (the loose state). As the catalytic site continues to rotate, it creates the intermediary state of the enzymatic reaction by further undergoing a conformational change that brings the ADP and phosphate molecules closer together, effectively lowering the activation energy necessary to create the ATP molecules spontaneously (the tight state). Finally, the active site returns to the open state, releasing the newly-produced ATP. In summary, each 360° rotation of the F_o moiety provides the energy to generate three molecules of ATP by F_1 (Weber & Senior 2000; Capaldi & Aggeler 2002; von Ballmoos et al. 2008; Sielaff & Börsch 2013; Walker 2013).

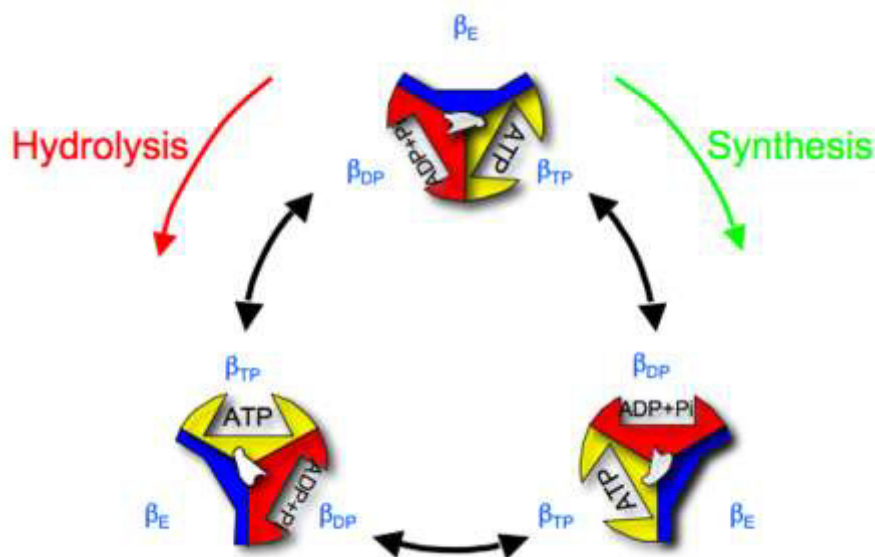


Figure 6: The binding change mechanism of the ATP synthesis/ hydrolysis. Adopted from (Nakamoto et al. 2008). The asymmetrical subunit γ (white) and three conformational states of subunit β (β_E - blue, β_{DP} - red, β_{TP} - yellow) are shown. The order of β conformations during ATP synthesis is $\beta_E \rightarrow \beta_{DP} \rightarrow \beta_{TP}$. ATP hydrolysis proceeds $\beta_E \rightarrow \beta_{TP} \rightarrow \beta_{DP}$.

In ATP hydrolysis mode, the F_1 motor converts the chemical energy of ATP into torque, causing the F_0 moiety to act as a proton pump. Rotation of the central stalk subunits and the F_0 c-ring is now driven by the F_1 -ATPase, and this rotation forces H^+ to pass through the F_0 proton pore to the outer side of the inner mitochondrial membrane (Nakamoto et al. 2008; Walker 2013). One complete 360° rotation in the counterclockwise direction (as viewed from the membrane side) takes subunit β through three different conformations, hydrolyzing three ATP molecules in the process (Nakamoto et al. 2008; Nakanishi-Matsui et al. 2010; Walker 2013).

The reverse F_0F_1 -ATPase activity represents a powerful mechanism to generate or restore the indispensable H^+ (or Na^+) gradient. Some anaerobic bacteria that lack membrane embedded respiratory complexes utilize this mechanism to generate an ion gradient to drive vital bioenergetic processes such as chemotaxis and membrane transport (von Ballmoos et al. 2008; Walker 2013). The bacterial F_0F_1 -ATPase activity is also coupled with maintaining intracellular pH or Na^+ homeostasis (von Ballmoos et al. 2008; Mesbah & Wiegel 2011). In contrast, the hydrolytic activity of other bacterial, chloroplast and mitochondrial F_0F_1 -ATPases is not desirable and has to be strictly regulated in order to prevent ATP depletion. Various mechanisms to inhibit ATP hydrolysis have evolved in different organisms (von Ballmoos et al. 2008; Campanella et al. 2009; Walker 2013).

2.7.3. Regulation of mitochondrial F_0F_1 -ATP synthase by IF1

In respiring mitochondria, the $\Delta\psi_m$ is high (approximately between 150 and 180 mV) and ATP synthesis is favored over ATP hydrolysis. However, when mitochondrial respiration

is compromised and the $\Delta\psi_m$ falls below a critical threshold, the F_0F_1 -ATP synthase activity reverses and the complex hydrolyzes ATP to pump H^+ across the IM (Campanella et al. 2009; Walker 2013). This process is triggered by various mechanisms; for example, when a cell is deprived of oxygen (during ischaemia or heart attack), or when the activities of the respiratory complexes are defective (Campanella et al. 2009). The F_0F_1 -ATPase represents a powerful mechanism to restore the $\Delta\psi_m$; however, the rapid depletion of ATP precipitates cell death and must be prevented (Campanella et al. 2009; Walker 2013).

For this reason, mitochondria employ a small (~10kDa) endogenous inhibitor protein. The inhibitory factor 1 (IF1) is highly conserved among eukaryotes and inhibits F_1 -ATPase in a pH-dependent manner (Campanella et al. 2008; Walker 2013). The inhibition of mitochondrial respiration that induces the hydrolytic activity of F_1 -ATPase is accompanied by the acidification of the mitochondrial matrix, as protons are no longer pumped into IMS. It has been shown in *B. taurus*, that when the pH drops below ~6.7, the IF1 acts as an α -helical homodimer with the N-terminal inhibitory sequences binding to two F_1 -ATPases (mostly interacting with subunit β), thereby blocking ATP hydrolysis. If the mitochondria re-energize in the presence of oxygen, the pH of the matrix increases and causes the IF1 peptides to form tetramers and higher oligomers that prevent the inhibitory sequences from interacting with F_1 -ATPase. This process restores F_0F_1 -ATP synthase activity (Cabezón et al. 2003; Gledhill et al. 2007; Walker 2013). The natural IF1 has been widely studied in mammals for its role in preventing cell death under hypoxic conditions. Moreover, the F_1 -ATPase binding properties of species specific inhibitory factors have been used to purify F_0F_1 -ATP synthases from various organisms (Campanella et al. 2009; Walker 2013).

2.7.4. Supramolecular organisation of the mitochondrial F_0F_1 -ATP synthase

2.7.4.1. Dimeric F_0F_1 -ATP synthase

The F_0F_1 -ATP synthase is commonly isolated as a functional monomer, although this does not appear to be the physiological state in a wide range of eukaryotes (Wittig & Schagger 2009; Habersetzer et al. 2013; Chaban et al. 2014). Biochemical and electron microscopy studies have revealed the presence of a dimeric F_0F_1 -ATP synthase in phylogenetically distant organisms that include protozoans, algae, yeast, plants, and mammals. In nearly all eukaryotes, two complex monomers associate through F_0 moieties, with the peripheral stalks opposing one another. In most of the species studied to date, the dimers display angles of 35-90° between the two F_1 headpieces; however, these differences in reported angles might have arisen due to different concentrations of detergent used during material preparation (Dudkina et al. 2010; Chaban et al. 2014). In the mitochondria, the F_0F_1 -ATP synthase dimers form long rows of oligomers along the ridges of cristae. It is now widely accepted that these dimers and oligomers have an active role in shaping the cristae (Habersetzer et al. 2013; Chaban et al. 2014). Indeed, *S. cerevisiae* mutants lacking F_0F_1 -ATP synthase dimer specific subunits e and g, exhibit an abnormal IM morphology

(Giraud et al. 2002; Davies et al. 2012). It was proposed that the F_0F_1 -ATP synthase dimerization and cristae formation in eukaryotes expanded the mt membrane surface to accommodate an increase in OxPhos components and improve the local H^+ concentration. Moreover, the dimerization may be counterbalancing the torque produced from two opposing monomeric F_0 c-rings (Chaban et al. 2014).

2.7.4.2. ATP synthasome

As mentioned previously, the F_0F_1 -ATP synthase was reported to be part of an even larger complex referred to as the ATP synthasome. In this mitochondrial supercomplex, the F_0F_1 -ATP synthase interacts with the phosphate and ADP/ATP carriers. The physiological function of this arrangement appears plausible, as both the phosphate and ADP molecules must be transported into the mitochondria to provide the substrates for ATP synthesis, whereas the newly synthesized ATP must be transported into the cytosol to meet other cellular energy demands. Therefore, this supercomplex may act as a substrate channel to promote a faster supply of the F_0F_1 -ATP synthase substrate molecules, thereby increasing OxPhos efficiency (Pedersen 2007). ATP synthasome has been detected in rat and bovine mitochondrion (Ko et al. 2003; Chen et al. 2004; Wittig & Schägger 2008). Moreover, this supercomplex was also reported from the kinetoplastid parasite, *L. mexicana*, an early branching eukaryote (Detke & Elsabrouty 2008). The presence of an ATP synthasome in the closely related parasite, *T. brucei*, was investigated in this study (Gnipová et al. 2015).

2.7.4.3. The ADP/ATP carrier

The ADP/ATP carrier is the most abundant protein in the IM and one of the best-studied members of the large mitochondrial carrier protein family (MCF) (Klingenberg 2008; Trézéguet et al. 2008). These carriers have been extensively characterized in a wide range of eukaryotic organisms, including *T. brucei* (Trézéguet et al. 2008; Palmieri et al. 2011; Peña-Diaz et al. 2012; Gnipová et al. 2015). The structures of yeast and bovine AAC were resolved by X-ray crystallography (Kunji & Harding 2003; Pebay-Peyroula et al. 2003), which demonstrated that the AAC structure is highly conserved with a six transmembrane α -helix bundle and three short α -helices that are parallel to the membrane plane on the matrix side. All ADP/ATP carriers contain a canonical hexapeptide motif (RRRMMM) that is essential for ADP-binding and ADP/ATP exchange (Cléménçon et al. 2011). Moreover, the AAC contains three distinctly conserved sites involved in the selective binding and transport of substrates (Kunji & Robinson 2006). The AAC is encoded by the nuclear genome and the number of gene isoforms is known to vary between organisms. For example, *S. cerevisiae* possesses three isoforms, although only one (AAC2) is essential for growth on nonfermentable carbon sources. Four isoforms were also identified in *H. sapiens* and their expression levels are tissue dependent (Dahout-Gonzalez et al. 2006). The *T. brucei* genome encodes two proteins with high homology to other eukaryotic AACs. However, it was experimentally shown that

only one, TbAAC (TbMCP5), functions as the main ADP/ATP carrier in the PF mitochondrion. This protein is encoded by three identical, consecutively arranged genes and its biochemical and kinetic properties are similar to the yeast AAC2. Moreover, RNAi studies demonstrated that TbAAC is essential for the growth of PF cells (Peña-Diaz et al. 2012; Gnipová et al. 2015).

The details of proposed mechanism of the ADP/ATP exchange activity have been discussed for decades (Krämer & Klingenberg 1982; Klingenberg 2008; Ruprecht et al. 2014). It is accepted that the carrier utilizes a single-binding centre-gated pore mechanism in which the substrates bind sequentially to the same site in a "ping-pong"-type mode. Thus, during oxidative phosphorylation, the AAC alternates between a cytoplasmic and matrix state, where free forms of a single molecule of either cytosolic ADP³⁻ or matrix ATP⁴⁻ bind their respective AAC state (Ruprecht et al. 2014). Because this electrogenic transport of a negative charge across the membrane is not charge compensated, it is driven by the $\Delta\psi_m$ (Krämer & Klingenberg 1980; Dahout-Gonzalez et al. 2006; Chinopoulos 2011). In the absence of the $\Delta\psi_m$, the AAC reverses and exchanges matrix ADP³⁻ for cytosolic ATP⁴⁻ molecules at a rate that strictly depends on their respective concentration gradients. This electrogenic ADP³⁻/ATP⁴⁻ exchange by AAC coupled with F₁-ATPase hydrolytic activity is considered to be the major contributor to the $\Delta\psi_m$ in cells that lack mtDNA encoded F_o subunits and thus the functional proton pore. Such a model of $\Delta\psi_m$ generation has been described in petite mutants of yeasts (Dupont et al. 1985; Clark-Walker 2003), ρ^0 -mammalian cells (Buchet & Godinot 1998; Appleby et al. 1999), and Dk *T. brucei* (Schnauffer et al. 2005).

Though it has been shown that the yeast AAC2 is fully functional as a monomer (Bamber et al. 2007), this yeast carrier has also been identified as a homodimer (Nury et al. 2005) or as a component of a supercomplex composed of cIII, cIV and the TIM23 translocase (Dienhart & Stuart 2008). Furthermore, the mammalian AAC was identified as a component of the ATP synthasome (Ko et al. 2003; Chen et al. 2004; Wittig & Schagger 2008). It has been found that cardiolipin, a unique lipid found in eukaryotes exclusively in IM, promotes the interactions of these supercomplexes as well as AAC homodimers (Claypool et al. 2008; Klingenberg 2009). Cardiolipin has also been reported to promote the activities of both AAC and Tim23 (Heimpel et al. 2001; Claypool et al. 2008), further advocating for a close association of these individual proteins within a supercomplex.

2.7.5. Composition of the mitochondrial F_oF₁-ATP synthase

2.7.5.1. F₁ moiety, central and peripheral stalks

As illustrated by the crystal structures of the bovine and yeast complexes, the structure of the F₁- moiety appears to be extremely conserved, at least in the eukaryotic super-group Opisthokonta. Several high-resolution crystal structures have been solved binding various inhibitors in the presence of MgADP, MgATP, or a non-hydrolyzable ATP analogue, MgAMP-PNP, providing greater insight into the mechanism of this complex rotary machine (Abrahams et al. 1994; van Raaij et al. 1996; Cabezon et al. 2003; Kabaleeswaran et

al. 2006; Rees et al. 2009; Robinson et al. 2013). Furthermore, cross-linking experiments combined with numerous NMR and cryo-EM studies have revealed secondary structures and protein-protein interactions of individual subunits.

The globular hexamer of alternating subunits α and β is situated on a central stalk consisting of subunit γ and small subunits δ and ϵ . The α and β subunits are very similar; each consisting of an N-terminal β -barrel domain, a central nucleotide-binding domain formed by α -helices and β -strands, and a C-terminal domain containing several α -helices. While the nucleotide binding sites in the β subunits undergo conformational changes throughout the catalytic cycle, the same domains in the α subunits continuously bind a Mg^{2+} ion and the same nucleotide (AMP-PNP). Subunit γ is largely a helical protein with N-terminal α -helix, middle α/β domain, and the long C-terminal α -helix extending to the bottom of $\alpha_3\beta_3$ hexamer (Devenish et al. 2008; Walker 2013).

The $\alpha_3\beta_3\gamma$ assembly represents the minimal catalytic core capable of ATP hydrolysis, although it was shown that even the $\alpha_3\beta_3$ hexamer alone retains residual ATPase activity (Devenish et al. 2008; La et al. 2013). Subunit δ has a N-terminal β -sandwich and a C-terminal α -helical hairpin, while subunit ϵ is folded into α -helix-loop- α -helix structure (Stock et al. 2000; Devenish et al. 2008). Subunits γ , δ and ϵ interact together at the foot of the central stalk, which is closely associated with the F_o c-ring (Stock et al. 1999; Stock et al. 2000).

The peripheral stalk is composed of four subunits. Subunit OSCP (oligomycin sensitivity conferring protein) is homologous to the prokaryotic protein δ . A single subunit OSCP is positioned in the "crown region" at the top of F_1 -ATP synthase, extending along the surface of F_1 to interact with other subunits of the peripheral stalk. The N-terminal region of OSCP forms an α -helical structure that binds the N-terminal region of the F_1 subunit α . In *E. coli*, it has been suggested that the high affinity binding between subunit δ and subunit α is responsible for the proposed role of the peripheral stalk (resisting the rotational torque of the rotor) (Walker & Dickson 2006; Dickson et al. 2006; Carbajo et al. 2007). Subunit b forms a long, mostly α -helical structure that protrudes from mt inner membrane towards the F_1 moiety and interacts with the rest of peripheral stalk subunits. Largely helical subunits d and F6 (h in yeast nomenclature) support and augment most of the length of the α -helical matrix part of the b subunit (Walker & Dickson 2006; Dickson et al. 2006).

2.7.5.2. F_o moiety

As previously mentioned, the F_oF_1 -ATP synthase proton pore is formed between a cylindrical ring of c subunits and a single subunit a. The highly hydrophobic subunit c consists of two transmembrane helical segments connected by a short loop. The C-terminal α -helix contains a strictly conserved aspartate or glutamate residue, whose carboxyl group is exposed on the external circumference of the c-ring (Collinson et al. 1994; Walker 2013). The short loop contains a conserved trimethyl-lysine residue that has been proposed to bind cardiolipin (Walpole et al. 2015). While there is no high resolution structure of the

eukaryotic subunit a available, a model has been established for the prokaryotic homolog, predicting the membrane topography. Bacterial subunit a is folded into five transmembrane α -helices, forming an aqueous channel (or two half-channels) for H^+ translocation. This subunit was shown to contain a conserved arginine residue that faces the essential carboxyl group on the c-ring (Martin et al. 2015).

A model for the generation of a H^+ -driven rotation of the F_o moiety has been proposed (Fillingame et al. 2003; Walker 2013). This model involves the formation of a channel at the interface of both subunits, and the sequential protonation and deprotonation of the conserved residue on subunit c. Consequently, the number of H^+ required to generate a single 360° rotation of the F_o c-ring corresponds to the number of c subunits present in the c-ring, which differs between species. Thus, the bioenergetic cost of generating one ATP molecule can be calculated as the number of c subunits divided by three (the number of ATP molecules generated per one 360° rotation). The smallest c_8 -ring was observed in mammals, resulting in a very efficient 2,7 H^+ /ATP ratio), while a c_{15} -ring with a 5 H^+ /ATP ratio was described for chloroplast F_oF_1 -ATP synthases (Watt et al. 2010; Walker 2013).

Besides the proton pore subunits, the F_o moiety of the mitochondrial complex contains several supernumerary subunits (e,f,g, i/j, k, A6L, DAPIT and 6.8 kDa proteolipid) that do not directly participate in the translocation of H^+ . These subunits vary between species, have low molecular weights (under 15 kDa), and contain transmembrane helices. The function of these proteins might be to stabilize F_oF_1 -ATP synthase dimers, to reinforce the peripheral stalk stator, or to regulate cellular energy metabolism (Dickson et al. 2006; Wittig & Schägger 2008; Jonckheere et al. 2012; Habersetzer et al. 2013).

2.7.5.3. Divergent F_oF_1 -ATP synthases

F_oF_1 -ATP synthase complexes with unusual composition were purified from chlorophycean algae, *Chlamydomonas reinhardtii* and *Polytomella* sp. (Vázquez-Acevedo et al. 2006; van Lis et al. 2007; Cano-Estrada et al. 2010). It was shown that these complexes contain the conserved subunits $\alpha, \beta, \gamma, \delta, a, c$, and OSCP; however, in contrast to other mt F_oF_1 -ATP synthases, the peripheral stalk subunits A6L, b, d, f, F6, and dimer specific subunits e and g are absent. Instead, the algal complexes are comprised of nine subunits with molecular masses ranging from ~ 8 to 60 kDa, that are known as ATP synthase associated proteins (ASA1-ASA9) (Cano-Estrada et al. 2010). Homologues of the ASA proteins have been detected in other members of Chlorophyceae (Lapaille et al. 2010). The ASA1-9 either form an atypical bulky peripheral stalk, or are responsible for complex dimerization (Chaban et al. 2014).

Other examples of unique F_oF_1 -ATP synthases can be found in the Alveolata clade, specifically from the apicomplexan parasite *Plasmodium* and the free-living ciliate *Tetrahymena thermopila* (Balabaskaran Nina et al. 2010; Balabaskaran Nina et al. 2011). These organisms exhibit ATP synthase activity, despite the lack of subunits a, b, d, and F6. However, there is a strong possibility that the missing subunits were replaced by highly

divergent novel proteins that retain the same function. Indeed, proteomic analysis identified at least 13 novel *T. thermopila* F₀F₁-ATP synthase subunits specific for ciliates. These include the mt encoded hydrophobic protein Ymf66, which was proposed to be the functional equivalent to subunit a (Balabaskaran Nina et al. 2010). Another peculiarity involves the atypical structure of the dimeric F₀F₁-ATP synthase of Tetrahymena. Rather than the angled configuration described in other organisms, the two *T. thermopila* monomers are arranged in parallel. Moreover, the c-rings of each monomer are not in close proximity, but instead they are connected via an additional protein densities in the lower part of the peripheral stalks (Balabaskaran Nina et al. 2010; Chaban et al. 2014). Finally, other divergent F₀F₁-ATP synthases were discovered in the phylum Euglenozoa (Zikova et al. 2009; Perez et al. 2014). Bioinformatic and proteomic studies of the green alga *Euglena gracilis* and the parasitic flagellate *T. brucei* established that many homologs of the typical eukaryotic F₀F₁-ATP synthase subunits are missing from these organisms. Nevertheless, their complexes are comprised of several unique proteins that may either represent counterparts of the absent subunits or have other functions specific for Euglenozoa (Zikova et al. 2009; Perez et al. 2014).

2.8. Trypanosoma F₀F₁-ATP synthase

The F₀F₁-ATP synthase was purified from PF *T. brucei* (Williams & Frank 1990; Williams et al. 1991; Zikova et al. 2009), and related trypanosomatids: *T. cruzi* (Cataldi de Flombaum et al. 1980), *L. donovani* (Rassam & Robert 1988), *L. tarentolae* (Nelson et al. 2004), and *Crithidia fasciculata* (Higa & Cazzulo 1981; Speijer et al. 1997). These studies employed different biochemical methods and reported the isolation of incomplete complexes that varied in their subunit composition. The most complete F₀F₁-ATP synthase complex was purified from the *T. brucei* PF stage by tandem affinity purification (TAP) using four different TAP-tagged subunits (β , p18, ATPaseTb1, ATPaseTb2). The purified tagged complexes were analyzed by liquid chromatography tandem mass spectrometry (LC-MS/MS). Out of the 22 identified proteins (summarized in Table 2), five are homologous to F₁ and three to F₀ subunits. The remaining 14 subunits appear to be unique as they share no apparent motifs or similarities with any proteins outside of the class Kinetoplastida or phylum Euglenozoa (Zikova et al. 2009; Perez et al. 2014). The novel subunits were suggested to be involved in i) complex assembly, ii) complex stability, iii) F₀F₁-ATP synthase/ase activity iv) F₀F₁-ATP synthase/ase activity regulation (Zikova et al. 2009).

Table 2. Composition the *T. brucei* F₁F_o-ATP synthase complex. Adapted from (Zikova et al. 2009; Gulde et al. 2013; Gahura et al. manuscript in preparation; Gahura et al. unpublished study). Subunit α and subunit c are encoded by two and three gene isoforms, respectively. Subunits depicted in italics were investigated in this work.

Sector	Subunit	Gene ID	predicted Mw [kDa]
<i>F₁</i>	α	<i>Tb927.7.7420/7430</i>	63.5
F ₁	β	Tb927.3.1380	55.7
Central stalk	γ	Tb427.10.180	34.3
Central stalk	δ	Tb927.6.4990	20.1
Central stalk	ϵ	Tb427.10.5050	8.6
Peripheral stalk	OSCP	Tb427.10.8030	28.8
<i>F₁</i>	<i>p18</i>	<i>Tb927.5.1710</i>	21.2
F _o	a	mt encoded (NCBI: AAA97428)	28.0
F _o	c	Tb927.7.1470,Tb927.10.1570,Tb927.11.5280	12.3
<i>F_o</i>	<i>ATPaseTb1</i>	<i>Tb927.10.520</i>	46.7
<i>F_o</i> (Peripheral stalk)	<i>ATPaseTb2</i>	<i>Tb927.5.2930</i>	43.3
Not assigned		Tb927.11.6250	27.5
Not assigned		Tb927.10.9830	17.1
Not assigned		Tb927.3.1690	17.1
Not assigned		Tb927.11.1270	20.2
Not assigned		Tb927.7.840	14.5
Not assigned		Tb927.11.600	12.0
Not assigned		Tb927.2.3610	16.0
Not assigned		Tb927.3.2880	12.6
Not assigned		Tb927.3.2180	17.9
Not assigned		Tb927.5.3090	11.6
Not assigned		Tb927.4.3450	13.7

Beside the unique proteins, *T. brucei* F_oF₁-ATP synthase possesses other atypical features:

- i) It was reported that *T. brucei* expresses three isoforms of the F_o subunit c, and that the mature proteins differ in their N-terminal regions (Gulde et al. 2013). This is in contrast to other organisms, where multiple gene copies of subunit c are translated into identical mature proteins (Andersson et al. 1997; De Grassi et al. 2006). All three identified isoforms were expressed in PF and BF *T. brucei* and incorporated into the PF F_oF₁-ATP synthase (Gulde et al. 2013).
- ii) *T. brucei* F_o subunit a is most likely encoded by the kDNA transcript MURF4, and it was reported that the MURF4 pre-mRNA requires extensive RNA editing in order to produce a mature protein (Bhat et al. 1990). The MURF4 assignment was based on an in silico analysis of the predicted translated product, which produced a similar

hydropathy profile and a low sequence similarity to subunit a orthologues from other organisms (Bhat et al. 1990). Subunit a has not been detected in any of the isolations of *T. brucei* F₀F₁-ATP synthase (Zikova et al. 2009). Nevertheless, the assembly of F₀F₁-ATP synthase monomers and oligomers was disrupted after RNAi silencing of two proteins involved in mt RNA metabolism, providing indirect evidence that the product of the MURF4 gene is the genuine F₀ subunit (Hashimi et al. 2010). It is assumed that subunit a is the only kDNA encoded subunit of *T. brucei* F₀F₁-ATP synthase.

- iii) The F₁ subunit α is cleaved *in vivo* into two fragments (Brown B et al. 2001; Zikova et al. 2009; Dean et al. 2013). This proteolytic cleavage was described in other Kinetoplastid species (Speijer et al. 1997; Nelson et al. 2004) and in *E. gracilis* (Perez et al. 2014), however the biological function of this cleavage is unknown.

2.8.1. Function of F₀F₁-ATP synthase in bloodstream and dyskinetoplastic Trypanosomes

As previously mentioned, BF cells lack the cytochrome mediated electron transport and therefore the $\Delta\psi_m$ is maintained by the hydrolytic activity of the F₀F₁-ATP synthase complex (Nolan & Voorheis 1992; Schnauffer et al. 2005; Brown et al. 2006). The $\Delta\psi_m$ is indispensable for the expression of kDNA genes and the import of nuclear-encoded proteins that perform vital mt functions (Neupert 1997; Schnauffer et al. 2001). Such processes may include maintaining the glycosomal redox balance through TAO (Bringaud et al. 2006; Chaudhuri et al. 2006; Shiba et al. 2013), lipid metabolism (Guler et al. 2008), ion homeostasis (Nolan & Voorheis 1992), calcium signalling (Vercesi et al. 1992; Huang et al. 2013), FeS cluster assembly (Kovárová et al. 2014), acetate production for *de novo* lipid biosynthesis (Mazet et al. 2013), and mitochondrial biogenesis (Neupert 1997; Schnauffer et al. 2005).

The hydrolytic activity of the F₀F₁-ATP synthase is observed in mammalian cells only under anoxic conditions and it needs to be tightly regulated or it will accelerate cell death (Campanella et al. 2009; Walker 2013). In contrast, BF *T. brucei* depend on this activity (Nolan & Voorheis 1992; Brown et al. 2006; Schnauffer et al. 2005), which suggests that the *T. brucei* F₀F₁-ATPase might be a promising drug target. Specific F₀F₁-ATPase inhibitors, developed to prevent human tissue damage caused by ischemic conditions, could potentially be exploited to treat HAT because they should be unharmed to the mammalian host (Schnauffer et al. 2005; Zikova et al. 2009). Another way to inhibit the BF F₀F₁-ATPase is to utilize the naturally occurring inhibitory peptide, IF1 (Zikova et al. 2009). Indeed, the genome of *T. brucei* encodes the inhibitory factor 1 (TbIF1), which is expressed about threefold less in BF than in PF cells (Urbaniak et al. 2012). Even weak ectopic expression of TbIF1 in BF cells leads to a significant decrease in the $\Delta\psi_m$ and a rapid inhibition of cell growth (Paniccuci et al.; Gahura et al. unpublished studies).

Nevertheless, the detailed mechanism by which the TbIF1 inhibits BF F₀F₁-ATPase, and how the PF F₀F₁-ATP synthase switches from ATP synthesis to ATP hydrolysis in the BF is not

understood. It is possible that some of the novel 14 subunits unique to Kinetoplastida are responsible for the regulation of the F_0F_1 -ATPase/synthase. Currently, it is essential to further characterize the composition and function of this druggable enzyme, determine how the activity of this complex is regulated between the life stages of *T. brucei*, and specify interactions between IF1 and the *T. brucei* F_1 -ATPase (Zikova et al. 2009).

As previously mentioned, the F_0F_1 -ATPase also has a unique function in dyskinetoplastic trypanosomes (Schnauffer et al. 2005; Dean et al. 2013), which are unable to express the F_0 subunit a, as they lack the gene itself or gRNAs essential for RNA editing (Lai et al. 2008). It was shown that Dk trypanosomes employ the TbAAC and the F_1 -ATPase hydrolytic activity to generate their $\Delta\psi_m$ by the electrogenic exchange of ADP^{3-}/ATP^{4-} . This mechanism is not dependent on F_0 proton pumping, and involves a key compensatory mutation in the nuclearly encoded F_1 subunit γ (Schnauffer et al. 2005; Dean et al. 2013). A similar scenario occurs in yeast, where mitochondrial genome integrity (*mgi*) mutations in α , β , and γ subunits help the cells to survive the loss of mtDNA (Clark-Walker et al. 2000; Wang et al. 2007; Arsenieva et al. 2010). Although the exact biochemical effect of *mgi* mutations is still a matter of debate, they have been shown to uncouple the F_0 and F_1 moieties of the complex (Wang et al. 2007; Arsenieva et al. 2010). Moreover, a reduced K_m value for ATP was also reported, which allows the F_1 -ATPase to hydrolyze ATP at lower concentrations (Clark-Walker 2003).

The laboratory induced Dk *T. b. brucei* (Stuart 1971) bears the L262P mutation in subunit γ (Schnauffer et al. 2005). The introduction of the γ L262P mutation into *T. b. brucei* resulted in F_0F_1 -ATP synthase uncoupling, an increased dependency of the $\Delta\psi_m$ on TbAAC, and allowed the cells to survive kDNA loss (Dean et al. 2013). Different mutations in the γ , α , and β subunits were also identified in naturally occurring Dk trypanosomes (Dean et al. 2013; Carnes et al. 2015). Additional studies are needed to determine the biochemical effects of these mutations and to investigate the kinetics of the F_1 -ATPase in Dk trypanosomes (Schnauffer et al. 2005; Carnes et al. 2015).

References:

- Abrahams, J.P. et al., 1994. Structure at 2.8 Å resolution of F1-ATPase from bovine heart mitochondria. *Nature*, 370(6491), pp.621–8.
- Acestor, N. et al., 2011. *Trypanosoma brucei* mitochondrial respiratome: composition and organization in procyclic form. *Molecular & cellular proteomics : MCP*, 10(9), p.M110.006908.
- Andersson, U., Houstek, J. & Cannon, B., 1997. ATP synthase subunit c expression: physiological regulation of the P1 and P2 genes. *The Biochemical journal*, 323 (Pt 2, pp.379–85.
- Aphasizhev, R. & Aphasizheva, I., 2011. Uridine insertion/deletion editing in trypanosomes: a playground for RNA-guided information transfer. *Wiley interdisciplinary reviews. RNA*, 2(5), pp.669–85.
- Aphasizheva, I., Maslov, D. a & Aphasizhev, R., 2013. Kinetoplast DNA-encoded ribosomal protein S12: A possible functional link between mitochondrial RNA editing and translation in *Trypanosoma brucei*. *RNA biology*, 10(11), pp.1679–88.
- Appleby, R.D. et al., 1999. Quantitation and origin of the mitochondrial membrane potential in human cells lacking mitochondrial DNA. *European journal of biochemistry / FEBS*, 262(1), pp.108–16.
- Arsenieva, D. et al., 2010. Crystal structures of mutant forms of the yeast F1 ATPase reveal two modes of uncoupling. *The Journal of biological chemistry*, 285(47), pp.36561–9.
- Aslett, M. et al., 2005. Integration of tools and resources for display and analysis of genomic data for protozoan parasites. *International journal for parasitology*, 35(5), pp.481–93.
- Aslett, M. et al., 2010. TriTrypDB: a functional genomic resource for the Trypanosomatidae. *Nucleic acids research*, 38(Database issue), pp.D457–62.
- Balabaskaran Nina, P. et al., 2011. ATP synthase complex of *Plasmodium falciparum*: dimeric assembly in mitochondrial membranes and resistance to genetic disruption. *The Journal of biological chemistry*, 286(48), pp.41312–22.
- Balabaskaran Nina, P. et al., 2010. Highly divergent mitochondrial ATP synthase complexes in *Tetrahymena thermophila*. *PLoS biology*, 8(7), p.e1000418.
- Balaña-Fouce, R. & Reguera, R.M., 2007. RNA interference in *Trypanosoma brucei*: a high-throughput engine for functional genomics in trypanosomatids? *Trends in parasitology*, 23(8), pp.348–51.
- Von Ballmoos, C., Cook, G.M. & Dimroth, P., 2008. Unique rotary ATP synthase and its biological diversity. *Annual review of biophysics*, 37, pp.43–64.
- Bamber, L. et al., 2007. The yeast mitochondrial ADP/ATP carrier functions as a monomer in mitochondrial membranes. *Proceedings of the National Academy of Sciences of the United States of America*, 104(26), pp.10830–4.
- Barrett, M.P. et al., 2007. Human African trypanosomiasis: pharmacological re-engagement with a neglected disease. *British journal of pharmacology*, 152(8), pp.1155–71.
- Batram, C. et al., 2014. Expression site attenuation mechanistically links antigenic variation and development in *Trypanosoma brucei*. *eLife*, 3, p.e02324.
- Bauer, S., Morris, J.C. & Morris, M.T., 2013. Environmentally regulated glycosome protein composition in the African trypanosome. *Eukaryotic cell*, 12(8), pp.1072–9.
- Beattie, D.S., Obungu, V.H. & Kiara, J.K., 1994. Oxidation of NADH by a rotenone and antimycin-sensitive pathway in the mitochondrion of procyclic *Trypanosoma brucei brucei*. *Molecular and biochemical parasitology*, 64(1), pp.87–94.
- Benne, R. et al., 1986. Major transcript of the frameshifted coxII gene from trypanosome mitochondria contains four nucleotides that are not encoded in the DNA. *Cell*, 46(6), pp.819–26.
- Berriman, M. et al., 2005. The Genome of the African trypanosome *Trypanosoma brucei*. *Science*, 309(5733), pp.416–22.
- Besteiro, S. et al., 2005. Energy generation in insect stages of *Trypanosoma brucei*: metabolism in flux. *Trends in parasitology*, 21(4), pp.185–91.
- Besteiro, S. et al., 2002. Succinate secreted by *Trypanosoma brucei* is produced by a novel and unique glycosomal enzyme, NADH-dependent fumarate reductase. *The Journal of biological chemistry*, 277(41), pp.38001–12.
- Bhat, G.J. et al., 1990. An extensively edited mitochondrial transcript in kinetoplastids encodes a protein homologous to ATPase subunit 6. *Cell*, 61(5), pp.885–94.
- Boyer, P.D., 2002. A research journey with ATP synthase. *The Journal of biological chemistry*, 277(42), pp.39045–61.
- Boyer, P.D., 1993. The binding change mechanism for ATP synthase--some probabilities and possibilities. *Biochimica et biophysica acta*, 1140(3), pp.215–50.

- Bringaud, F. et al., 2015. Combining reverse genetics and NMR-based metabolomics unravels trypanosome-specific metabolic pathways. *Molecular Microbiology*, p.n/a–n/a.
- Bringaud, F., Barrett, M.P. & Zilberstein, D., 2012. Multiple roles of proline transport and metabolism in trypanosomatids. *Frontiers in Bioscience*, 17, pp.349–374.
- Bringaud, F., Ebikeme, C. & Boshart, M., 2010. Acetate and succinate production in amoebae, helminths, diplomonads, trichomonads and trypanosomatids: common and diverse metabolic strategies used by parasitic lower eukaryotes. *Parasitology*, 137(9), pp.1315–31.
- Bringaud, F., Rivièrè, L. & Coustou, V., 2006. Energy metabolism of trypanosomatids: adaptation to available carbon sources. *Molecular and biochemical parasitology*, 149(1), pp.1–9.
- Brown B, S. V et al., 2001. Cloning and characterization of the subunits comprising the catalytic core of the *Trypanosoma brucei* mitochondrial ATP synthase. *Molecular and biochemical parasitology*, 113(2), pp.289–301.
- Brown, S. V et al., 2006. ATP synthase is responsible for maintaining mitochondrial membrane potential in bloodstream form *Trypanosoma brucei*. *Eukaryotic cell*, 5(1), pp.45–53.
- Brun, R., Hecker, H. & Lun, Z.R., 1998. *Trypanosoma evansi* and *T. equiperdum*: distribution, biology, treatment and phylogenetic relationship (a review). *Veterinary parasitology*, 79(2), pp.95–107.
- Buchet, K. & Godinot, C., 1998. Functional F1-ATPase essential in maintaining growth and membrane potential of human mitochondrial DNA-depleted ρ^0 cells. *Journal of Biological Chemistry*, 273(36), pp.22983–22989.
- Cabezón, E. et al., 2003. The structure of bovine F1-ATPase in complex with its regulatory protein IF1. *Nature Structural Biology*, 10(9), pp.744–750.
- Campanella, M. et al., 2009. IF1: setting the pace of the F(1)F(0)-ATP synthase. *Trends in biochemical sciences*, 34(7), pp.343–50.
- Campanella, M. et al., 2008. Regulation of mitochondrial structure and function by the F1Fo-ATPase inhibitor protein, IF1. *Cell Metabolism*, 8(1), pp.13–25.
- Cano-Estrada, A. et al., 2010. Subunit-subunit interactions and overall topology of the dimeric mitochondrial ATP synthase of *Polytomella* sp. *Biochimica et biophysica acta*, 1797(8), pp.1439–48.
- Capaldi, R.A. & Aggeler, R., 2002. Mechanism of the F(1)F(0)-type ATP synthase, a biological rotary motor. *Trends in biochemical sciences*, 27(3), pp.154–60.
- Carbajo, R.J. et al., 2007. How the N-terminal domain of the OSCP subunit of bovine F1Fo-ATP synthase interacts with the N-terminal region of an alpha subunit. *Journal of molecular biology*, 368(2), pp.310–8.
- Carnes, J. et al., 2015. genome and phylogenetic analyses of *Trypanosoma evansi* reveal extensive similarity to *T. brucei* and multiple independent origins for dyskinetoplasty. C. Tschudi, ed. *PLoS neglected tropical diseases*, 9(1), p.e3404.
- Cataldi de Flombaum, M. a., Frasch, a. C.C. & Stoppani, a. O.M., 1980. Adenosine triphosphatase from *Trypanosoma cruzi*: Purification and properties. *Comparative Biochemistry and Physiology Part B: Comparative Biochemistry*, 65(1), pp.103–109.
- Claes, F. et al., 2005. *Trypanosoma equiperdum*: master of disguise or historical mistake? *Trends in parasitology*, 21(7), pp.316–21.
- Clark-Walker, G.D., 2003. Kinetic properties of F1-ATPase influence the ability of yeasts to grow in anoxia or absence of mtDNA. *Mitochondrion*, 2(4), pp.257–65.
- Clark-Walker, G.D. et al., 2000. Mutant residues suppressing ρ^0 -lethality in *Kluyveromyces lactis* occur at contact sites between subunits of F1-ATPase. *Biochimica et Biophysica Acta (BBA) - Protein Structure and Molecular Enzymology*, 1478(1), pp.125–137.
- Claypool, S.M. et al., 2008. Cardiolipin defines the interactome of the major ADP/ATP carrier protein of the mitochondrial inner membrane. *The Journal of Cell Biology*, 182(5), pp.937–950.
- Cléménçon, B. et al., 2011. Yeast ADP/ATP carrier isoform 2: conformational dynamics and role of the RRRMMM signature sequence methionines. *The Journal of biological chemistry*, 286(41), pp.36119–31.
- Colasante, C. et al., 2013. Proteins and lipids of glycosomal membranes from *Leishmania tarentolae* and *Trypanosoma brucei*. *F1000Research*, 2, p.27.
- Collinson, I.R. et al., 1994. F0 membrane domain of ATP synthase from bovine heart mitochondria: Purification, subunit composition, and reconstitution with F1-ATPase. *Biochemistry*, 33(25), pp.7971–7978.
- Courtin, D. et al., 2008. Host genetics in African trypanosomiasis. *Infection, genetics and evolution : journal of molecular epidemiology and evolutionary genetics in infectious diseases*, 8(3), pp.229–38.
- Coustou, V. et al., 2008. Glucose-induced remodeling of intermediary and energy metabolism in procyclic *Trypanosoma brucei*. *The Journal of biological chemistry*, 283(24), pp.16342–54.
- Cramer, W.A., Hasan, S.S. & Yamashita, E., 2011. The Q cycle of cytochrome bc complexes: a structure perspective. *Biochimica et biophysica acta*, 1807(7), pp.788–802.

- Czichos, J., Nonnengaesser, C. & Overath, P., 1986. *Trypanosoma brucei*: cis-Aconitate and temperature reduction as triggers of synchronous transformation of bloodstream to procyclic trypomastigotes in vitro. *Experimental Parasitology*, 62(2), pp.283–291.
- Dahout-Gonzalez, C. et al., 2006. Molecular, functional, and pathological aspects of the mitochondrial ADP/ATP carrier. *Physiology (Bethesda, Md.)*, 21, pp.242–9.
- Davies, K.M. et al., 2012. Structure of the yeast F1Fo-ATP synthase dimer and its role in shaping the mitochondrial cristae. *Proceedings of the National Academy of Sciences of the United States of America*, 109(34), pp.13602–7.
- Dean, S. et al., 2013. Single point mutations in ATP synthase compensate for mitochondrial genome loss in trypanosomes. *Proceedings of the National Academy of Sciences of the United States of America*, 110(36), pp.14741–6.
- DeJesus, E. et al., 2013. A single amino acid substitution in the group 1 *Trypanosoma brucei* gambiense haptoglobin-hemoglobin receptor abolishes TLF-1 binding. K. L. Hill, ed. *PLoS pathogens*, 9(4), p.e1003317.
- Desquesnes, M. et al., 2013. *Trypanosoma evansi* and surra: a review and perspectives on transmission, epidemiology and control, impact, and zoonotic aspects. *BioMed research international*, 2013, p.321237.
- Detke, S. & Elsabrouty, R., 2008. Identification of a mitochondrial ATP synthase-adenine nucleotide translocator complex in Leishmania. *Acta tropica*, 105(1), pp.16–20.
- Devenish, R.J., Prescott, M. & Rodgers, A.J.W., 2008. The structure and function of mitochondrial F1Fo-ATP synthases. *International review of cell and molecular biology*, 267(08), pp.1–58.
- Dickson, V.K. et al., 2006. On the structure of the stator of the mitochondrial ATP synthase. *The EMBO journal*, 25(12), pp.2911–8.
- Dienhart, M.K. & Stuart, R.A., 2008. The yeast AAC2 protein exists in physical association with the cytochrome bc1-COX supercomplex and the TIM23 machinery. *Molecular biology of the cell*, 19(9), pp.3934–43.
- Docampo, R. & Moreno, S.N.J., 2011. Acidocalcisomes. *Cell calcium*, 50(2), pp.113–9.
- Duarte, M. & Tomás, A.M., 2014. The mitochondrial complex I of trypanosomatids--an overview of current knowledge. *Journal of bioenergetics and biomembranes*, 46(4), pp.299–311.
- Dudkina, N. V et al., 2010. Structure and function of mitochondrial supercomplexes. *Biochimica et biophysica acta*, 1797(6-7), pp.664–70.
- Dupont, C.H., Mazat, J.P. & Guerin, B., 1985. The role of adenine nucleotide translocation in the energization of the inner membrane of mitochondria isolated from rho + and rho degree strains of *Saccharomyces cerevisiae*. *Biochemical and biophysical research communications*, 132(3), pp.1116–23.
- Ebikeme, C. et al., 2010. Ablation of succinate production from glucose metabolism in the procyclic trypanosomes induces metabolic switches to the glycerol 3-phosphate/dihydroxyacetone phosphate shuttle and to proline metabolism. *The Journal of biological chemistry*, 285(42), pp.32312–24.
- Efremov, R.G. & Sazanov, L.A., 2011. Respiratory complex I: “steam engine” of the cell? *Current opinion in structural biology*, 21(4), pp.532–40.
- Fang, J. & Beattie, D.S., 2003. Identification of a gene encoding a 54 kDa alternative NADH dehydrogenase in *Trypanosoma brucei*. *Molecular and Biochemical Parasitology*, 127(1), pp.73–77.
- Fillingame, R.H., Angevine, C.M. & Dmitriev, O.Y., 2003. Mechanics of coupling proton movements to c-ring rotation in ATP synthase. *FEBS Letters*, 555(1), pp.29–34.
- Giraud, M.-F. et al., 2002. Is there a relationship between the supramolecular organization of the mitochondrial ATP synthase and the formation of cristae? *Biochimica et Biophysica Acta (BBA) - Bioenergetics*, 1555(1-3), pp.174–180.
- Gledhill, J.R. et al., 2007. How the regulatory protein, IF1, inhibits F1-ATPase from bovine mitochondria. *PNAS*, 104(40), pp.15671–15676.
- Gnipová, A. et al., 2012. Disparate phenotypic effects from the knockdown of various *Trypanosoma brucei* cytochrome c oxidase subunits. *Molecular and biochemical parasitology*, 184(2), pp.90–8.
- Gnipová, A. et al., 2015. The ADP/ATP carrier and its relationship to OXPHOS in an ancestral protist, *Trypanosoma brucei*. *Eukaryotic cell*, 14(3), pp.297–310.
- De Grassi, A., Lanave, C. & Saccone, C., 2006. Evolution of ATP synthase subunit c and cytochrome c gene families in selected Metazoan classes. *Gene*, 371(2), pp.224–33.
- Gray, M.W., Burger, G. & Lang, B.F., 1999. Mitochondrial evolution. *Science (New York, N.Y.)*, 283(5407), pp.1476–81.
- Guerra, D.G. et al., 2006. The mitochondrial FAD-dependent glycerol-3-phosphate dehydrogenase of Trypanosomatidae and the glycosomal redox balance of insect stages of *Trypanosoma brucei* and *Leishmania* spp. *Molecular and biochemical parasitology*, 149(2), pp.155–69.

- Gulde, P.E. et al., 2013. Three distinct isoforms of ATP synthase subunit c are expressed in *T. brucei* and assembled into the mitochondrial ATP synthase complex. *PLoS one*, 8(1), p.e54039.
- Guler, J.L. et al., 2008. Mitochondrial fatty acid synthesis is required for normal mitochondrial morphology and function in *Trypanosoma brucei*. *Molecular microbiology*, 67(5), pp.1125–42.
- Günzl, A. et al., 2015. Mono-allelic VSG expression by RNA polymerase I in *Trypanosoma brucei*: Expression site control from both ends? *Gene*, 556(1), pp.68–73.
- Günzl, A., 2010. The pre-mRNA splicing machinery of trypanosomes: complex or simplified? *Eukaryotic cell*, 9(8), pp.1159–70.
- Haanstra, J.R., Bakker, B.M. & Michels, P.A.M., 2014. In or out? On the tightness of glycosomal compartmentalization of metabolites and enzymes in *Trypanosoma brucei*. *Molecular and biochemical parasitology*, 198(1), pp.18–28.
- Habersetzer, J. et al., 2013. ATP synthase oligomerization: from the enzyme models to the mitochondrial morphology. *The international journal of biochemistry & cell biology*, 45(1), pp.99–105.
- Hannaert, V. et al., 2003. Evolution of energy metabolism and its compartmentation in Kinetoplastida. *Kinetoplastid Biology and Disease*, 2(11), pp.1–30.
- Hashimi, H. et al., 2008. TbRGG1, an essential protein involved in kinetoplastid RNA metabolism that is associated with a novel multiprotein complex. *RNA (New York, N.Y.)*, 14(5), pp.970–80.
- Hashimi, H. et al., 2010. The assembly of F(1)F(O)-ATP synthase is disrupted upon interference of RNA editing in *Trypanosoma brucei*. *International journal for parasitology*, 40(1), pp.45–54.
- Heimpel, S. et al., 2001. Expression of the mitochondrial ADP/ATP carrier in *Escherichia coli*. Renaturation, reconstitution, and the effect of mutations on 10 positive residues. *The Journal of biological chemistry*, 276(15), pp.11499–506.
- Van Hellemond, J.J., Bakker, B.M. & Tielens, A.M., 2005. Energy metabolism and its compartmentation in *Trypanosoma brucei*. *Advances in microbial physiology*, 50, pp.199–226.
- Van Hellemond, J.J., Opperdoes, F.R. & Tielens, a G., 1998. Trypanosomatidae produce acetate via a mitochondrial acetate:succinate CoA transferase. *Proceedings of the National Academy of Sciences of the United States of America*, 95(6), pp.3036–41.
- Van Hellemond, J.J., Opperdoes, F.R. & Tielens, A.G.M., 2005. The extraordinary mitochondrion and unusual citric acid cycle in *Trypanosoma brucei*. *Biochemical Society transactions*, 33(Pt 5), pp.967–71.
- Hernandez, F.R. & Turrens, J.F., 1998. Rotenone at high concentrations inhibits NADH-fumarate reductase and the mitochondrial respiratory chain of *Trypanosoma brucei* and *T. cruzi*. *Molecular and biochemical parasitology*, 93(1), pp.135–7.
- Hide, G., 2008. Visualizing trypanosome sex. *Trends in parasitology*, 24(10), pp.425–8.
- Higa, A.I. & Cazzulo, J.J., 1981. Mg²⁺-activated adenosine triphosphatase from *Crithidia fasciculata*: purification and inhibition by suramin and efrapeptin. *Molecular and biochemical parasitology*, 3(6), pp.357–67.
- Hira, P.R. & Husein, S.F., 1979. Some transfusion-induced parasitic infections in Zambia. *Journal of hygiene, epidemiology, microbiology, and immunology*, 23(4), pp.436–44.
- Horváth, A. et al., 2005. Downregulation of the nuclear-encoded subunits of the complexes III and IV disrupts their respective complexes but not complex I in procyclic *Trypanosoma brucei*. *Molecular microbiology*, 58(1), pp.116–30.
- Huang, G., Vercesi, A.E. & Docampo, R., 2013. Essential regulation of cell bioenergetics in *Trypanosoma brucei* by the mitochondrial calcium uniporter. *Nature communications*, 4, p.2865.
- Chaban, Y., Boekema, E.J. & Dudkina, N. V., 2014. Structures of mitochondrial oxidative phosphorylation supercomplexes and mechanisms for their stabilisation. *Biochimica et biophysica acta*, 1837(4), pp.418–26.
- Chatterjee, S. et al., 2006. An RNA-binding respiratory component mediates import of type II tRNAs into Leishmania mitochondria. *The Journal of biological chemistry*, 281(35), pp.25270–7.
- Chaudhuri, M., Ott, R.D. & Hill, G.C., 2006. Trypanosome alternative oxidase: from molecule to function. *Trends in parasitology*, 22(10), pp.484–91.
- Chen, C. et al., 2004. Mitochondrial ATP synthasome: three-dimensional structure by electron microscopy of the ATP synthase in complex formation with carriers for Pi and ADP/ATP. *The Journal of biological chemistry*, 279(30), pp.31761–8.
- Chinopoulos, C., 2011. Mitochondrial consumption of cytosolic ATP: not so fast. *FEBS letters*, 585(9), pp.1255–9.
- Iwata, S. et al., 1998. Complete structure of the 11-subunit bovine mitochondrial cytochrome bc1 complex. *Science (New York, N.Y.)*, 281(5373), pp.64–71.

- Jamonneau, V. et al., 2012. Untreated human infections by *Trypanosoma brucei gambiense* are not 100% fatal. *PLoS neglected tropical diseases*, 6(6), p.e1691.
- Janssen, R.J.R.J. et al., 2006. Mitochondrial complex I: structure, function and pathology. *Journal of inherited metabolic disease*, 29(4), pp.499–515.
- Jonckheere, A.I., Smeitink, J.A.M. & Rodenburg, R.J.T., 2012. Mitochondrial ATP synthase: architecture, function and pathology. *Journal of inherited metabolic disease*, 35(2), pp.211–25.
- Kabaleeswaran, V. et al., 2006. Novel features of the rotary catalytic mechanism revealed in the structure of yeast F1 ATPase. *The EMBO journal*, 25(22), pp.5433–42.
- Kennedy, P.G.E., 2006. Human African trypanosomiasis: in and out of Africa. *Neurology*, 66(7), pp.962–3.
- Kieft, R. et al., 2010. Mechanism of *Trypanosoma brucei gambiense* (group 1) resistance to human trypanosome lytic factor. *Proceedings of the National Academy of Sciences of the United States of America*, 107(37), pp.16137–41.
- Klingenberg, M., 2009. Cardiolipin and mitochondrial carriers. *Biochimica et biophysica acta*, 1788(10), pp.2048–58.
- Klingenberg, M., 2008. The ADP and ATP transport in mitochondria and its carrier. *Biochimica et biophysica acta*, 1778(10), pp.1978–2021.
- Ko, Y.H. et al., 2003. Mitochondrial ATP synthasome. Cristae-enriched membranes and a multiwell detergent screening assay yield dispersed single complexes containing the ATP synthase and carriers for Pi and ADP/ATP. *The Journal of biological chemistry*, 278(14), pp.12305–9.
- Kovárová, J. et al., 2014. mitochondrial and nucleolar localization of cysteine desulfurase Nfs and the scaffold protein Isu in *Trypanosoma brucei*. *Eukaryotic cell*, 13(3), pp.353–362.
- Krämer, R. & Klingenberg, M., 1982. Electrophoretic control of reconstituted adenine nucleotide translocation. *Biochemistry*, 21(5), pp.1082–9.
- Krämer, R. & Klingenberg, M., 1980. Modulation of the reconstituted adenine nucleotide exchange by membrane potential. *Biochemistry*, 19(3), pp.556–60.
- Kunji, E.R.S. & Harding, M., 2003. Projection structure of the atractyloside-inhibited mitochondrial ADP/ATP carrier of *Saccharomyces cerevisiae*. *Journal of Biological Chemistry*, 278(39), pp.36985–36988.
- Kunji, E.R.S. & Robinson, A.J., 2006. The conserved substrate binding site of mitochondrial carriers. *Biochimica et biophysica acta*, 1757(9-10), pp.1237–48.
- La, T. et al., 2013. Mutations on the N-terminal edge of the DELSEED loop in either the α or β subunit of the mitochondrial F1-ATPase enhance ATP hydrolysis in the absence of the central γ rotor. *Eukaryotic cell*, 12(11), pp.1451–61.
- Lai, D.-H. et al., 2008. Adaptations of *Trypanosoma brucei* to gradual loss of kinetoplast DNA: *Trypanosoma equiperdum* and *Trypanosoma evansi* are petite mutants of *T. brucei*. *Proceedings of the National Academy of Sciences of the United States of America*, 105(6), pp.1999–2004.
- Lamour, N. et al., 2005. Proline metabolism in procyclic *Trypanosoma brucei* is down-regulated in the presence of glucose. *The Journal of biological chemistry*, 280(12), pp.11902–10.
- Lapaille, M. et al., 2010. Atypical subunit composition of the chlorophycean mitochondrial F1FO-ATP synthase and role of Asa7 protein in stability and oligomycin resistance of the enzyme. *Molecular biology and evolution*, 27(7), pp.1630–44.
- Lindner, A.K. & Priotto, G., 2010. The unknown risk of vertical transmission in sleeping sickness--a literature review. *PLoS neglected tropical diseases*, 4(12), p.e783.
- Van Lis, R. et al., 2007. New insights into the unique structure of the FOF1-ATP synthase from the chlamydomonad algae *Polytomella* sp. and *Chlamydomonas reinhardtii*. *Plant physiology*, 144(2), pp.1190–9.
- Liu, B. et al., 2005. Fellowship of the rings: the replication of kinetoplast DNA. *Trends in parasitology*, 21(8), pp.363–9.
- Lukeš, J. et al., 2002. Kinetoplast DNA network: evolution of an improbable structure. *Eukaryotic cell*, 1(4), pp.495–502.
- Mach, J. et al., 2013. an advanced system of the mitochondrial processing peptidase and core protein family in *Trypanosoma brucei* and multiple origins of the core I subunit in Eukaryotes. *Genome biology and evolution*, 5(5), pp.860–75.
- Maklashina, E. & Cecchini, G., 2010. The quinone-binding and catalytic site of complex II. *Biochimica et biophysica acta*, 1797(12), pp.1877–82.
- Martin, J. et al., 2015. Fo₁-driven rotation in the ATP synthase direction against the force of F1 ATPase in the FoF1 ATP synthase. *Journal of Biological Chemistry*, p.jbc.M115.646430.

- Matthews, K.R., 2005. The developmental cell biology of *Trypanosoma brucei*. *Journal of cell science*, 118(Pt 2), pp.283–90.
- Matthews, K.R., Ellis, J.R. & Paterou, A., 2004. Molecular regulation of the life cycle of African trypanosomes. *Trends in Parasitology*, 20(1), pp.40–47.
- Mazet, M. et al., 2013. Revisiting the central metabolism of the bloodstream forms of *Trypanosoma brucei*: production of acetate in the mitochondrion is essential for parasite viability. *PLoS neglected tropical diseases*, 7(12), p.e2587.
- McCulloch, R., 2004. Antigenic variation in African trypanosomes: monitoring progress. *Trends in parasitology*, 20(3), pp.117–21.
- Mesbah, N.M. & Wiegel, J., 2011. The Na(+)-translocating F₁F_o-ATPase from the halophilic, alkalithermophile *Natronaerobius thermophilus*. *Biochimica et biophysica acta*, 1807(9), pp.1133–42.
- Michels, P. a M. et al., 2006. Metabolic functions of glycosomes in trypanosomatids. *Biochimica et biophysica acta*, 1763(12), pp.1463–77.
- Millerioux, Y. et al., 2013. The threonine degradation pathway of the *Trypanosoma brucei* procyclic form: the main carbon source for lipid biosynthesis is under metabolic control. *Molecular microbiology*.
- Mitchell, P., 1961. Coupling of phosphorylation to electron and hydrogen transfer by a chemi-osmotic type of mechanism. *Nature*, 191, pp.144–8.
- Mukherjee, S. et al., 2007. Necessary and sufficient factors for the import of transfer RNA into the kinetoplast mitochondrion. *EMBO reports*, 8(6), pp.589–95.
- Nakamoto, R.K., Baylis Scanlon, J.A. & Al-Shawi, M.K., 2008. The rotary mechanism of the ATP synthase. *Archives of biochemistry and biophysics*, 476(1), pp.43–50.
- Nakanishi-Matsui, M. et al., 2010. The mechanism of rotating proton pumping ATPases. *Biochimica et biophysica acta*, 1797(8), pp.1343–52.
- Nelson, D.L. & Cox, M.M., 2008. *Lehninger principles of biochemistry* 5th ed., New York: W.H. Freeman and Company.
- Nelson, R.E. et al., 2004. The I-complex in *Leishmania tarentolae* is an uniquely-structured F-1-ATPase. *Molecular and Biochemical Parasitology*, 135(2), pp.219–222.
- Neupert, W., 1997. Protein import into mitochondria. *Annual review of biochemistry*, 66, pp.863–917.
- Noji, H. et al., 1997. Direct observation of the rotation of F₁-ATPase. *Nature*, 386(6622), pp.299–302.
- Nolan, D.P. & Voorheis, H.P., 1992. The mitochondrion in bloodstream forms of *Trypanosoma brucei* is energized by the electrogenic pumping of protons catalysed by the F₁F_o-ATPase. *European journal of biochemistry / FEBS*, 209(1), pp.207–16.
- Nury, H. et al., 2005. Structural basis for lipid-mediated interactions between mitochondrial ADP/ATP carrier monomers. *FEBS letters*, 579(27), pp.6031–6.
- Ochsenreiter, T., Cipriano, M. & Hajduk, S.L., 2008. Alternative mRNA editing in trypanosomes is extensive and may contribute to mitochondrial protein diversity. *PloS one*, 3(2), p.e1566.
- Opperdoes, F.R., Borst, P. & de Rijke, D., 1976. Oligomycin sensitivity of the mitochondrial ATPase as a marker for fly transmissibility and the presence of functional kinetoplast DNA in African trypanosomes. *Comparative biochemistry and physiology. B, Comparative biochemistry*, 55(1), pp.25–30.
- Ott, M. & Herrmann, J.M., 2010. Co-translational membrane insertion of mitochondrially encoded proteins. *Biochimica et biophysica acta*, 1803(6), pp.767–75.
- Palmieri, F. et al., 2011. Evolution, structure and function of mitochondrial carriers: a review with new insights. *The Plant journal : for cell and molecular biology*, 66(1), pp.161–81.
- Parsons, M. et al., 1984. Trypanosome mRNAs share a common 5' spliced leader sequence. *Cell*, 38(1), pp.309–316.
- Pebay-Peyroula, E. et al., 2003. Structure of mitochondrial ADP/ATP carrier in complex with carboxyatractyloside. *Nature*, 426(6962), pp.39–44.
- Pedersen, P.L., 2007. Transport ATPases into the year 2008: a brief overview related to types, structures, functions and roles in health and disease. *Journal of bioenergetics and biomembranes*, 39(5-6), pp.349–55.
- Peña-Díaz, P. et al., 2012. Functional characterization of TbMCP5, a conserved and essential ADP/ATP carrier present in the mitochondrion of the human pathogen *Trypanosoma brucei*. *The Journal of biological chemistry*, 287(50), pp.41861–74.
- Perez, E. et al., 2014. The mitochondrial respiratory chain of the secondary green alga *Euglena gracilis* shares many additional subunits with parasitic Trypanosomatidae. *Mitochondrion*, pp.1–12.
- Van Raaij, M.J. et al., 1996. The structure of bovine F₁-ATPase complexed with the antibiotic inhibitor aurovertin B. *Proceedings of the National Academy of Sciences of the United States of America*, 93(14), pp.6913–7.

- Rassam, M.B. & Robert, Z.J., 1988. Solubilization and kinetic characterization of mitochondrial adenosine triphosphatase from *Leishmania donovani* promastigotes. *Molecular and biochemical parasitology*, 29(2-3), pp.153–8.
- Rees, D.M., Leslie, A.G.W. & Walker, J.E., 2009. The structure of the membrane extrinsic region of bovine ATP synthase. *Proceedings of the National Academy of Sciences of the United States of America*, 106(51), pp.21597–601.
- Richter, O.-M.H. & Ludwig, B., 2009. Electron transfer and energy transduction in the terminal part of the respiratory chain - lessons from bacterial model systems. *Biochimica et biophysica acta*, 1787(6), pp.626–34.
- Riou, G.F., Belnat, P. & Benard, J., 1980. Complete loss of kinetoplast DNA sequences induced by ethidium bromide or by acriflavine in *Trypanosoma equiperdum*. *The Journal of biological chemistry*, 255(11), pp.5141–4.
- Riviere, L. et al., 2009. Acetate produced in the mitochondrion is the essential precursor for lipid biosynthesis in procyclic trypanosomes. *Proceedings of the National Academy of Sciences of the United States of America*, 106(31), pp.12694–9.
- Rivière, L. et al., 2004. Acetyl:succinate CoA-transferase in procyclic *Trypanosoma brucei*. Gene identification and role in carbohydrate metabolism. *The Journal of biological chemistry*, 279(44), pp.45337–46.
- Robinson, G.C. et al., 2013. The structure of F1 -ATPase from *Saccharomyces cerevisiae* inhibited by its regulatory protein IF1. *Open Biology*, 3(2).
- Rodgers, J., 2009. Human African trypanosomiasis, chemotherapy and CNS disease. *Journal of neuroimmunology*, 211(1-2), pp.16–22.
- Ruprecht, J.J. et al., 2014. Structures of yeast mitochondrial ADP/ATP carriers support a domain-based alternating-access transport mechanism. *Proceedings of the National Academy of Sciences of the United States of America*, 111(4), pp.E426–34.
- Rutter, J., Winge, D.R. & Schiffman, J.D., 2010. Succinate dehydrogenase - Assembly, regulation and role in human disease. *Mitochondrion*, 10(4), pp.393–401.
- Ryan, K.A. et al., 1988. Replication of kinetoplast DNA in trypanosomes. *Annual review of microbiology*, 42, pp.339–58.
- Sazanov, L.A., 2007. Respiratory complex I: mechanistic and structural insights provided by the crystal structure of the hydrophilic domain. *Biochemistry*, 46(9), pp.2275–88.
- Shameer, S. et al., 2014. TrypanoCyc: a community-led biochemical pathways database for *Trypanosoma brucei*. *Nucleic acids research*.
- Shapiro, T. a & Englund, P.T., 1995. The structure and replication of kinetoplast DNA. *Annual review of microbiology*, 49, pp.117–43.
- Shiba, T. et al., 2013. Structure of the trypanosome cyanide-insensitive alternative oxidase. *Proceedings of the National Academy of Sciences of the United States of America*, 110(12), pp.4580–5.
- Schnauffer, A. et al., 2001. An RNA ligase essential for RNA editing and survival of the bloodstream form of *Trypanosoma brucei*. *Science (New York, N.Y.)*, 291(5511), pp.2159–62.
- Schnauffer, A. et al., 2005. The F1-ATP synthase complex in bloodstream stage trypanosomes has an unusual and essential function. *The EMBO journal*, 24(23), pp.4029–40.
- Schnauffer, A., Domingo, G.J. & Stuart, K.D., 2002. Natural and induced dyskinetoplastic trypanosomatids: how to live without mitochondrial DNA. *International Journal for Parasitology*, 32, pp.1071–1084.
- Sielaff, H. & Börsch, M., 2013. Twisting and subunit rotation in single F(O)(F1)-ATP synthase. *Philosophical transactions of the Royal Society of London. Series B, Biological sciences*, 368(1611), p.20120024.
- Simarro, P.P. et al., 2012. Update on field use of the available drugs for the chemotherapy of human African trypanosomiasis. *Parasitology*, 139(7), pp.842–6.
- Soto, I.C. et al., 2012. Biogenesis and assembly of eukaryotic cytochrome c oxidase catalytic core. *Biochimica et biophysica acta*, 1817(6), pp.883–97.
- Speijer, D. et al., 1997. Characterization of the respiratory chain from cultured *Crithidia fasciculata*. *Molecular and Biochemical Parasitology*, 85, pp.171–186.
- Steverding, D., 2008. The history of African trypanosomiasis. *Parasites & vectors*, 1(1), p.3.
- Stock, D. et al., 2000. The rotary mechanism of ATP synthase. *Current opinion in structural biology*, 10(6), pp.672–9.
- Stock, D., Leslie, A.G.W. & Walker, J.E., 1999. Molecular Architecture of the Rotary Motor in ATP Synthase. *Science*, 286(5445), pp.1700–1705.
- Stuart, K. et al., 2008. Kinetoplastids: related protozoan pathogens, different diseases. *The Journal of clinical investigation*, 118(4), pp.1301–10.

- Stuart, K. & Panigrahi, A.K., 2002. RNA editing: complexity and complications. *Molecular microbiology*, 45(3), pp.591–6.
- Stuart, K.D., 1971. Evidence for the retention of kinetoplast DNA in an acriflavine-induced dyskinetoplastic strain of *Trypanosoma brucei* which replicates the altered central element of the kinetoplast. *The Journal of cell biology*, 49(1), pp.189–95.
- Sun, F. et al., 2013. Revealing various coupling of electron transfer and proton pumping in mitochondrial respiratory chain. *Current opinion in structural biology*, 23(4), pp.526–38.
- Surve, S. et al., 2012. Enigmatic presence of mitochondrial complex I in *Trypanosoma brucei* bloodstream forms. *Eukaryotic cell*, 11(2), pp.183–93.
- Surve, S. et al., 2011. Enigmatic presence of mitochondrial complex I in *Trypanosoma brucei* bloodstream forms. *Eukaryotic cell*, 44(December), pp.183–93.
- Sutherland, C.S. et al., 2015. a literature review of economic evaluations for a neglected tropical disease: Human African trypanosomiasis (“Sleeping Sickness”). *PLoS neglected tropical diseases*, 9(2), p.e0003397.
- Tielens, A.G.M. & van Hellemond, J.J., 2009. Surprising variety in energy metabolism within Trypanosomatidae. *Trends in parasitology*, 25(10), pp.482–90.
- Trézéguet, V. et al., 2008. The mitochondrial ADP/ATP carrier: functional and structural studies in the route of elucidating pathophysiological aspects. *Journal of bioenergetics and biomembranes*, 40(5), pp.435–43.
- Uboldi, A.D. et al., 2006. A mitochondrial protein affects cell morphology, mitochondrial segregation and virulence in Leishmania. *International journal for parasitology*, 36(14), pp.1499–514.
- Urbaniak, M.D., Guther, M.L.S. & Ferguson, M.A.J., 2012. Comparative SILAC proteomic analysis of *Trypanosoma brucei* bloodstream and procyclic lifecycle stages. *PLoS one*, 7(5), p.e36619.
- Vanhollebeke, B. & Pays, E., 2010. The trypanolytic factor of human serum: many ways to enter the parasite, a single way to kill. *Molecular microbiology*, 76(4), pp.806–14.
- Vázquez-Acevedo, M. et al., 2006. The mitochondrial ATP synthase of chlorophycean algae contains eight subunits of unknown origin involved in the formation of an atypical stator-stalk and in the dimerization of the complex. *Journal of bioenergetics and biomembranes*, 38(5-6), pp.271–82.
- Vercesi, A.E., Docampo, R. & Moreno, S.N., 1992. Energization-dependent Ca²⁺ accumulation in *Trypanosoma brucei* bloodstream and procyclic trypomastigotes mitochondria. *Molecular and biochemical parasitology*, 56(2), pp.251–7.
- Vercesi, A.E., Moreno, S.N. & Docampo, R., 1994. Ca²⁺/H⁺ exchange in acidic vacuoles of *Trypanosoma brucei*. *The Biochemical journal*, 304 (Pt 1, pp.227–33.
- Verner, Z. et al., 2013. Alternative NADH dehydrogenase (NDH2): intermembrane-space-facing counterpart of mitochondrial complex I in the procyclic *Trypanosoma brucei*. *Parasitology*, 140(3), pp.328–37.
- Verner, Z. et al., 2011. Complex I (NADH:ubiquinone oxidoreductase) is active in but non-essential for procyclic *Trypanosoma brucei*. *Molecular and biochemical parasitology*, 175(2), pp.196–200.
- Verner, Z. et al., 2015. Malleable Mitochondrion of *Trypanosoma brucei*. *International review of cell and molecular biology*, 315, pp.73–151.
- Walker, J.E., 2013. The ATP synthase: the understood, the uncertain and the unknown. *Biochemical Society transactions*, 41(1), pp.1–16.
- Walker, J.E. & Dickson, V.K., 2006. The peripheral stalk of the mitochondrial ATP synthase. *Biochimica et biophysica acta*, 1757(5-6), pp.286–96.
- Walpole, T.B. et al., 2015. Conservation of complete trimethylation of lysine 43 in the rotor ring of c-subunits of metazoan ATP synthase. *Molecular & cellular proteomics : MCP*.
- Wang, Y., Singh, U. & Mueller, D.M., 2007. Mitochondrial genome integrity mutations uncouple the yeast *Saccharomyces cerevisiae* ATP synthase. *The Journal of biological chemistry*, 282(11), pp.8228–36.
- Watt, I.N. et al., 2010. Bioenergetic cost of making an adenosine triphosphate molecule in animal mitochondria. *Proceedings of the National Academy of Sciences of the United States of America*, 107(39), pp.16823–7.
- Weber, J. & Senior, A.E., 2000. ATP synthase: what we know about ATP hydrolysis and what we do not know about ATP synthesis. *Biochimica et biophysica acta*, 1458(2-3), pp.300–9.
- Van Weelden, S.W.H. et al., 2005. New functions for parts of the Krebs cycle in procyclic *Trypanosoma brucei*, a cycle not operating as a cycle. *The Journal of biological chemistry*, 280(13), pp.12451–60.
- Van Weelden, S.W.H. et al., 2003. Procyclic *Trypanosoma brucei* do not use Krebs cycle activity for energy generation. *The Journal of biological chemistry*, 278(15), pp.12854–63.
- WHO, 2013. *Control and surveillance of human African trypanosomiasis.*
- Williams, N. et al., 1991. The mitochondrial ATP synthase of *Trypanosoma brucei*: developmental regulation through the life cycle. *Archives of biochemistry and biophysics*, 288(2), pp.509–15.

- Williams, N. & Frank, P.H., 1990. The mitochondrial ATP synthase of *Trypanosoma brucei*: isolation and characterization of the intact F1 moiety. *Molecular and biochemical parasitology*, 43(1), pp.125–32.
- Winge, D.R., 2012. Sealing the mitochondrial respirasome. *Molecular and cellular biology*, 32(14), pp.2647–52.
- Wirtz, E. et al., 1999. A tightly regulated inducible expression system for conditional gene knock-outs and dominant-negative genetics in *Trypanosoma brucei*. *Molecular and biochemical parasitology*, 99(1), pp.89–101.
- Wittig, I. & Schägger, H., 2008. Structural organization of mitochondrial ATP synthase. *Biochimica et biophysica acta*, 1777(7-8), pp.592–8.
- Wittig, I. & Schägger, H., 2009. Supramolecular organization of ATP synthase and respiratory chain in mitochondrial membranes. *Biochimica et biophysica acta*, 1787(6), pp.672–80.
- Xia, D. et al., 2013. Structural analysis of cytochrome bc1 complexes: implications to the mechanism of function. *Biochimica et biophysica acta*, 1827(11-12), pp.1278–94.
- Xong, H. V et al., 1998. A VSG expression site-associated gene confers resistance to human serum in *Trypanosoma rhodesiense*. *Cell*, 95(6), pp.839–46.
- Young, L. et al., 2013. The alternative oxidases: simple oxidoreductase proteins with complex functions. *Biochemical Society transactions*, 41(5), pp.1305–11.
- Zikova, A. et al., 2008. Structural and functional association of *Trypanosoma brucei* MIX protein with cytochrome c oxidase complex. *Eukaryotic cell*, 7(11), pp.1994–2003.
- Zikova, A. et al., 2009. The F(0)F(1)-ATP synthase complex contains novel subunits and is essential for procyclic *Trypanosoma brucei*. *PLoS pathogens*, 5(5), p.e1000436.

CHAPTER 3

RESULTS

3.1. Published results

3.1.1. ATPaseTb2, a unique membrane-bound F_0F_1 -ATPase component, is essential in bloodstream and dyskinetoplastic trypanosomes

Reprint of: Šubrtová K, Panicucci B, Zíková A. 2015. PLoS Pathogens 11(2), e1004660.

RESEARCH ARTICLE

ATPaseTb2, a Unique Membrane-bound FoF1-ATPase Component, Is Essential in Bloodstream and Dyskinetoplastic Trypanosomes

Karolína Šubrtová^{1,2}, Brian Panicucci¹, Alena Zíková^{1,2*}

1 Institute of Parasitology, Biology Centre, CAS, České Budějovice, Czech Republic, **2** Faculty of Science, University of South Bohemia, České Budějovice, Czech Republic

* azikova@paru.cas.cz



 OPEN ACCESS

Citation: Šubrtová K, Panicucci B, Zíková A (2015) ATPaseTb2, a Unique Membrane-bound FoF1-ATPase Component, Is Essential in Bloodstream and Dyskinetoplastic Trypanosomes. *PLoS Pathog* 10(2): e1004660. doi:10.1371/journal.ppat.1004660

Editor: Achim Schnauffer, University of Edinburgh, UNITED KINGDOM

Received: June 13, 2014

Accepted: January 6, 2015

Published: February 25, 2015

Copyright: © 2015 Šubrtová et al. This is an open access article distributed under the terms of the [Creative Commons Attribution License](https://creativecommons.org/licenses/by/4.0/), which permits unrestricted use, distribution, and reproduction in any medium, provided the original author and source are credited.

Data Availability Statement: All relevant data are within the paper and its Supporting Information file.

Funding: This work was funded by Ministry of Education ERC CZ grant LL1205, the Czech Grant Agency grant P302/12/2513, the EMBO Installation grant 1965 (to AZ) and the Grant Agency of University of South Bohemia grants 140/2010/P and 04/092/2011/P (to KS). We acknowledge the use of research infrastructure that has received funding from the European Union Seventh Framework Programme (FP7/2007-2013) under grant agreement no.316304. The funders had no role in study design, data

Abstract

In the infectious stage of *Trypanosoma brucei*, an important parasite of humans and livestock, the mitochondrial (mt) membrane potential ($\Delta\psi_m$) is uniquely maintained by the ATP hydrolytic activity and subsequent proton pumping of the essential F_oF_1 -ATPase. Intriguingly, this multiprotein complex contains several trypanosome-specific subunits of unknown function. Here, we demonstrate that one of the largest novel subunits, ATPaseTb2, is membrane-bound and localizes with monomeric and multimeric assemblies of the F_oF_1 -ATPase. Moreover, RNAi silencing of ATPaseTb2 quickly leads to a significant decrease of the $\Delta\psi_m$ that manifests as a decreased growth phenotype, indicating that the F_oF_1 -ATPase is impaired. To further explore the function of this protein, we employed a trypanosoma strain that lacks mtDNA (dyskinetoplastic, Dk) and thus subunit a, an essential component of the proton pore in the membrane F_o -moiety. These Dk cells generate the $\Delta\psi_m$ by combining the hydrolytic activity of the matrix-facing F_1 -ATPase and the electrogenic exchange of ATP^{4-} for ADP^{3-} by the ATP/ADP carrier (AAC). Surprisingly, in addition to the expected presence of F_1 -ATPase, the monomeric and multimeric F_oF_1 -ATPase complexes were identified. In fact, the immunoprecipitation of a F_1 -ATPase subunit demonstrated that ATPaseTb2 was a component of these complexes. Furthermore, RNAi studies established that the membrane-bound ATPaseTb2 subunit is essential for maintaining normal growth and the $\Delta\psi_m$ of Dk cells. Thus, even in the absence of subunit a, a portion of the F_oF_1 -ATPase is assembled in Dk cells.

Author Summary

The presence of the F_oF_1 -ATP synthase in every aerobic organism suggests that evolution has settled on a basic blueprint for the complex rotary motor capable of synthesizing life's universal energy currency—ATP. However, compared to yeast and mammalian models of the F_oF_1 -ATP synthase, several recent studies have reported unique structural and functional features of this complex from organisms representing the clades of Chromalveolata,

collection and analysis, decision to publish, or preparation of the manuscript.

Competing Interests: The authors have declared that no competing interests exist.

Archaeplastida and Excavata. One of the most striking cases is observed in trypanosomes, important parasites of humans and animals. Notably, the F_0F_1 -ATP synthase/ATPase switches from synthesizing ATP in the insect vector life stage to hydrolyzing ATP in their mammalian hosts to generate the essential mitochondrial membrane potential ($\Delta\psi_m$). Moreover, this indispensable F_0F_1 -ATPase contains up to 14 trypanosome-specific subunits. Here we characterize one such novel subunit, ATPaseTb2. We demonstrate that this subunit is crucial for the survival of the infectious stage of trypanosomes, part of the fully assembled F_0F_1 -complex and it is essential for maintaining the $\Delta\psi_m$. Given the enzyme's irreplaceable function and extraordinary composition, we believe that the F_0F_1 -ATPase is an attractive drug target.

Introduction

Trypanosomes are unicellular flagellates from the order Kinetoplastida, which is comprised of some of the most devastating human pathogens in the world. For example, in sub-Saharan Africa, infection from *Trypanosoma brucei gambiense* and *T. b. rhodesiense* causes Human African Trypanosomiasis, which is almost always fatal if left untreated [1]. The latest WHO reports estimate that there are 10,000 new cases annually in endemic regions. Meanwhile, a third subspecies, *T. b. brucei*, infects livestock and therefore negatively affects the human population through malnutrition and economic hardships [2,3].

T. brucei parasites have a complex life cycle, alternating between the mammalian host and the insect vector, a tse-tse fly. During this environmental switch, the protist undergoes rapid and dramatic changes in cell morphology and metabolism [4–6]. In particular, the single mitochondrion undergoes extensive remodelling, which reflects the adaptability of the parasite to consume different carbon sources based on their availability [4]. The procyclic (insect) form (PF) of trypanosomes catabolizes amino acids and maintains a well-developed mitochondrion with abundant cristae, Krebs cycle enzymes and a complete oxidative phosphorylation pathway. This pathway includes enzymatic complexes that generate a mitochondrial (mt) membrane potential ($\Delta\psi_m$) that is coupled to ATP synthesis by the F_0F_1 -ATP synthase [5]. In contrast, the bloodstream form (BF) of this parasite populates the glucose-rich fluids (e.g. blood and spinal fluid) of its vertebrate host, allowing them to utilize just glycolysis for ATP production. This results in a drastically reduced mitochondrion that lacks significant cristae, key enzymes of the Krebs cycle and the cytochrome-containing respiratory complexes that pump protons into the inner mt membrane space [6,7]. Despite this reduction, the BF mitochondrion is still an active organelle, holding vital processes e.g. lipid metabolism [8], ion homeostasis [9], calcium signalling [10,11], FeS cluster assembly [12] and acetate production for *de novo* lipid biosynthesis [13]. Importantly, in the absence of proton-pumping respiratory complexes III and IV, the indispensable $\Delta\psi_m$ is sustained mainly by the hydrolytic activity of the F_0F_1 -ATPase. Thus, this complex possesses an essential, unique and irreplaceable function in BF mitochondria [14].

In other eukaryotes, this reverse activity of the F_0F_1 -ATP synthase is observed only rarely, for very brief moments of time and under very specific conditions (i.e. during oxygen deprivation or in response to damaged or mutated mt respiratory proteins). When the function of the respiratory complexes is compromised, the $\Delta\psi_m$ falls below a physiological threshold and is restored by the reverse proton pumping activity of the F_0F_1 -ATPase, which is powered by ATP hydrolysis. The hydrolytic activity of the catalytic F_1 -ATPase is also essential for exceptional cells that lack mtDNA (ρ^0 cells). These cells do not express several core subunits of the

membrane embedded F_o -moiety (subunits 6, 8 and 9 in yeast, subunits a and A6L in bovine) of the F_oF_1 -ATPase, notably those that are components of the proton pore. Thus, the matrix protruding F_1 -ATPase energizes the inner mt membrane by coupling ATP hydrolysis with the exchange of ADP^{3-} for ATP^{4-} by the ATP/ADP carrier (AAC) [15]. The same mechanism for producing the $\Delta\psi_m$ is utilized by trypanosomes that lack a mt genome, which is called a kinetoplast [16]. These naturally occurring dyskinetoplastic forms (Dk) of *T. brucei* (e.g. *T. b. evansi* or *T. b. equiperdum*) cause economically significant diseases in horses, camels, and water buffaloes. Remarkably, these parasites are not able to switch to the insect stage and are transmitted mechanically by bloodsucking insects or by coitus [17]. The mtDNA-lacking trypanosomes can also be chemically induced in the laboratory (e.g. Dk *T. brucei* EATRO164) [18]. Interestingly, each of the Dk cell lines characterized so far, bear one of several different compensatory mutations in the nuclear encoded subunit γ that enable the $\Delta\psi_m$ to be generated independently of the F_o -moiety [14,16,19].

In general, the F_oF_1 -ATP synthase complex consists of two functionally distinct enzymatic segments: the hydrophilic F_1 catalytic moiety and the membrane-bound F_o pore. Both of these subcomplexes are linked together by the central and peripheral stalks. The central stalk rotates with the c-ring when protons are allowed to pass through the F_o pore, located between the c-ring and subunit a. In contrast to the rotation of the central stalk, the stationary peripheral stalk plays a crucial role in keeping the catalytic F_1 headpiece static, thus resisting the rotational torque. The eubacterial F_1 -moiety consists of the catalytic domain and the central stalk, which are comprised of five subunits in a stoichiometry of $\alpha_3, \beta_3, \gamma_1, \delta_1, \epsilon_1$. The F_o -moiety is composed of the oligomeric c_{10-15} ring and a single subunit a joined together with two copies of subunit b, which extend from the membrane and form the base of the peripheral stalk. The composition of the eukaryotic enzyme has been determined mainly from detailed studies of F_oF_1 -ATP synthase purified from the mitochondria of *Bos taurus* and *Saccharomyces cerevisiae*, members of the clade Opisthokonta. These enzymes contain homologous prokaryotic-like core components, but also incorporate additional eukaryotic specific subunits involved in the structure, oligomerization and regulation of the complex [20]. These novel subunits have been assigned to various regions of the F_oF_1 -ATP synthase: i) subunit ϵ and inhibitory factor 1 (IF₁) bind to the F_1 -moiety; ii) the small hydrophobic subunit 8 (subunit A6L in bovine) is located in the membrane interacting with subunit a; iii) the soluble subunit h (subunit F_6 in bovine), oligomycin sensitivity-conferring protein (OSCP) and hydrophilic subunit d are assigned to the peripheral stalk; iv) subunits e, f, g, all containing one transmembrane helix, are regarded as accessory peripheral stalk proteins that predominantly reside in the inner membrane where they presumably stabilize the utmost hydrophobic subunit 6 (or subunit a in bovine), thereby assisting the peripheral stalk with its stator function [21–23].

Recently, however, several studies have reported unique structural and functional features of the F_oF_1 -ATP synthase from medically relevant parasites and other organisms that represent the clades of Chromalveolata [24], Archaeplastida [25] and Excavata [26]. In *Plasmodium falciparum*, a member of the phylum Apicomplexa, the genomic data indicates the likely presence of all eukaryotic F_1 subunits and some of the F_o and stator subunits [27]. Conspicuously absent are the subunits a and b, which are crucial to the function of all known F_oF_1 -ATP synthases. These subunits are also missing in the ATP synthase of *P. yoelii* and *Tetrahymena thermophila*, the latter a member of the sister phylum Ciliophora, both of which have been shown experimentally to possess ATP synthase activity [28–30]. This suggests that ciliates and apicomplexan species employ highly divergent or novel subunits to fulfil the functions of the classical subunits a and b. Another example of an unusual F_oF_1 -ATP synthase complex comes from studies of the chlorophycean alga *Chlamydomonas reinhardtii* and *Polytomella* sp. that determined the

complex contains up to 9 unique subunits (Asa1-Asa9) that either form an innovative peripheral stator or are responsible for complex dimerization [31].

Trypanosoma F_0F_1 -ATP synthase consists of the well conserved F_1 -moiety comprised of subunits α , β , γ , δ , ϵ and the trypanosome-specific subunit p18 [26,32], and the less characterized F_0 pore and peripheral stalk where only subunits c, a and OSCP were identified at the gene or protein level [26,33]. Additionally, the complex contains up to 14 Kinetoplastida-specific subunits that lack homology to any of the previously described subunits. Therefore, their position within the complex and their function is unknown. Interestingly, these recently identified F_0F_1 -ATP synthase subunits specific for *T. brucei* (ATPaseTb) may represent early evolutionary attempts to create the functional and structural components of the eukaryotic accessory subunits for this early divergent species. Previously, two of these novel subunits, ATPaseTb1 (Tb10.70.7760) and ATPaseTb2 (Tb927.5.2930), were shown to be essential for the proper function and structural integrity of F_0F_1 -ATP synthase in the procyclic form of this parasite [26].

Here, we have extended this study and functionally characterized ATPaseTb2 in the disease-relevant stage of *T. brucei* and Dk *T. b. evansi*. Our results demonstrate that the membrane-bound ATPaseTb2 protein is indispensable for the survival of BF and Dk trypanosomes because it is crucial for maintaining the $\Delta\psi_m$ in these cells. Furthermore, the unexpected observation of assembled F_0F_1 -ATPase complexes in two different strains of trypanosomes lacking mt DNA suggests that the composition of the Dk F_0F_1 -ATPase complex is more similar to the BF F_0F_1 -ATPase complex than previously thought.

Results

Bioinformatics reveals that ATPaseTb2 contains a putative transmembrane domain and a region homologous to the bovine subunit d

ATPaseTb2 is annotated as a hypothetical protein in the TriTrypDB database (www.tritrypdb.org) and its mt localization was predicted by the presence of an N-terminal mt targeting sequence assigned by Mitoprot II v1.101 [34] (probability 0.823). Strikingly, this subunit has no detectable homologs outside Kinetoplastida based on a similarity sequence search (e.g. BLAST). To uncover any homologous relationships for protein sequences that do not share high enough sequence identity, but might have similar secondary structure, we employed the HHpred toolkit (<http://toolkit.tuebingen.mpg.de>), which is based on an HMM-HMM comparison that reveals homologous relationships even if the sequences share less than 20% sequence identity [35]. All of the available Kinetoplastida ATPaseTb2 homologs obtained from the TriTrypDB (S1A Fig.) were analyzed using HHpred software. Among the first five structural homologs detected was the bovine F_0F_1 -ATP synthase subunit d, with a probability of 44.7 and a P-value of 0.0021. Then a consensus sequence generated from an alignment of this 92 amino acids (aa) region from all identified kinetoplastida homologs was resubmitted for HHpred analysis. This search returned a significant hit to the bovine subunit d with a probability of 78.1 and a P-value of 0.0002 (S1B Fig.). This bovine F_0F_1 -ATP synthase subunit is comprised of 160 aa and resides within the peripheral stalk where it interacts with all the other three components of the peripheral stalk (b, F_6 and OSCP). This subunit is predominantly hydrophilic, contains several long alpha-helices and is essential for the enzymatic function [23,36,37]. The region of similarity to subunit d falls in the middle of the ATPaseTb2 sequence and it is followed by a putative trans-membrane (TM) domain (aa 239–254) that was predicted by MEMSAT-SVM software (<http://bioinf.cs.ucl.ac.uk/psipred/>) [38] with a -0.738 prediction score (Fig. 1). This prediction is intriguing because a typical eukaryotic subunit d is not directly attached to the

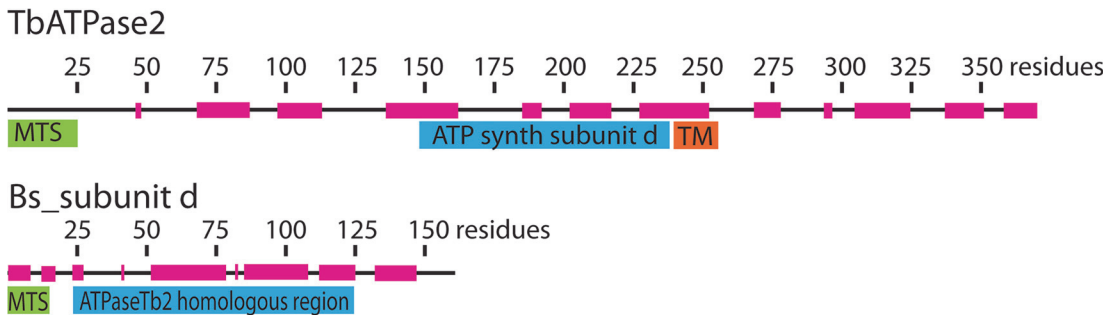


Fig 1. Bioinformatics reveal that ATPaseTb2 possesses a region of low homology to ATPase subunit d. A schematic representation depicting the ATPaseTb2 protein (370 aminoacids (AA)) and the *Bos taurus* subunit d (Bs_sub d, 161 AA) was created using Adobe Illustrator CS5.1. The mitochondrial targeting signals (MTS, green) were predicted by Mitoprot II v1.101. The transmembrane domain (TM, orange) within the ATPaseTb2 sequence was predicted by MEMSAT-SVM software. The homologous region (blue) to Bs_sub d was determined using HHpred toolkit. The regions of alpha-helices (magenta) depicted on the amino acid sequence line were predicted by software from EMBOSS garnier.

doi:10.1371/journal.ppat.1004660.g001

membrane, but rather it interacts with the soluble region of the membrane-bound subunit b via three coiled-coil interactions [23]. Thus, ATPaseTb2 may represent a novel subunit of the membrane-bound peripheral stalk that possibly depicts an early divergent functional alternative of the stator by creating a chimera of subunits b and d.

ATPaseTb2 is a mt membrane-bound protein expressed in various forms of *T. brucei*

The mitochondrial localization, as well as the structural and functional association of ATPaseTb2 with the F_0F_1 -ATP synthase in PF *T. brucei* cells was previously described [26]. Because the activity of this complex significantly differs between the insect and mammalian stage of the parasite, we were interested if the ATPaseTb2 protein is also expressed in trypanosomes residing in the bloodstream of their host. Therefore, we cultured PF427 (insect stage), BF427 (bloodstream forms) and the laboratory-induced dyskinetoplasic Dk164 *T. brucei* cells, in addition to the naturally occurring Dk *T.b.evansi*. Whole cell lysates from PF427, BF427, Dk164 and *T. b.evansi* cells were fractionated by SDS-PAGE and analyzed by western blot using a specific polyclonal antibody against ATPaseTb2 (Fig. 2A). Interestingly, ATPaseTb2 is expressed in all four cell types; however, its expression is significantly decreased in BF427 and even more reduced in Dk164 and *T.b.evansi* cells. A similar expression pattern for F_1 -ATPase subunit β and mt chaperone Hsp70 was also observed between PF, BF and Dk cells (Fig. 2A). These results are in agreement with the proposed reduction of the mitochondria size, function and activity in the various bloodstream forms of *T. brucei* [39].

To experimentally investigate the subcellular localization of ATPaseTb2 within the bloodstream *T. brucei* cell, the ATPaseTb2 gene product was C-terminally tagged with a v5-tag and inducibly expressed using tetracycline (tet). Cytosolic and mitochondrial fractions were isolated from a hypotonic lysate of cells over-expressing the ATPaseTb2_v5 protein. The mitochondrial fractions were then treated with digitonin to create mitoplasts that were further incubated with sodium carbonate (Na_2CO_3) to obtain mt membrane and mt matrix fractions. The subsequent western analyses established the purity of the extracted fractions as the cytosolic enolase, the mt inner membrane carrier protein (AAC) and the matrix-localized guide RNA binding protein (MRP1) were confined within their respective subcellular fractions. Notably, ATPaseTb2 was predominantly localized in the mt membrane fraction, while subunit β of the matrix-soluble F_1 -ATPase was released into the matrix fraction (Fig. 2B), demonstrating that ATPaseTb2 is firmly embedded in the inner mt membrane.

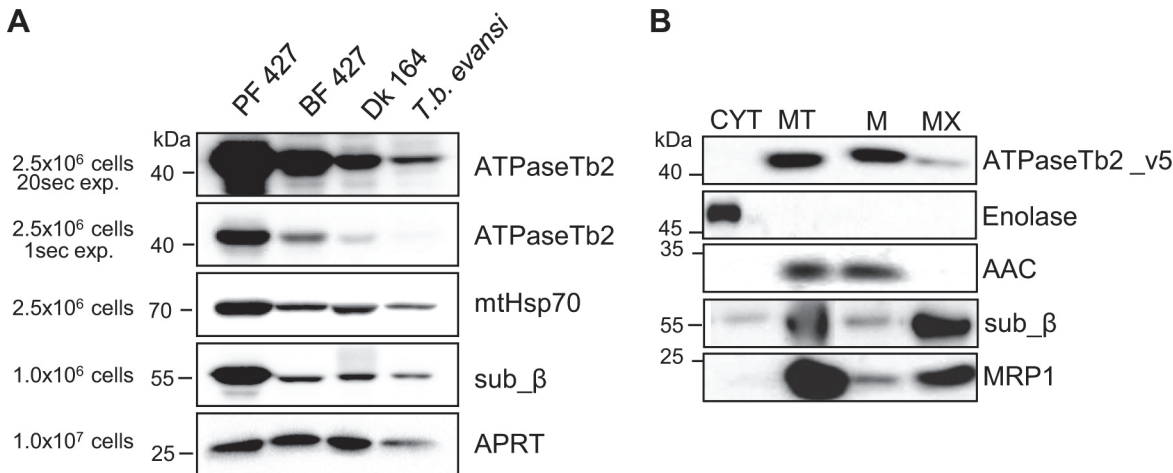


Fig 2. ATPaseTb2 is expressed in PF427, BF427, Dk164 *T. brucei* and *T. b. evansi* cells and it is a membrane-bound protein. A) The steady state abundance of ATPaseTb2 (two different exposure times), subunit β , mtHsp70 and cytosolic adenosine phosphoribosyl transferase (APRT) was determined in PF427, BF427, Dk164 and *T. b. evansi* cells by western blot analysis of whole cell lysates from 2.5×10^6 cells or 1×10^6 cells (for subunit β and APRT) resolved on SDS-PAGE gels. The pertinent sizes of the protein marker are indicated on the left. B) Subcellular localization of ATPaseTb2 was determined using BF cells expressing v5-tagged ATPaseTb2. Cytosolic (CYT) and mitochondrial (MT) fractions were obtained by hypotonic lysis. Mt pellets were further treated with Na_2CO_3 and spun at a high-speed to obtain mt membrane (M) and matrix (MX) fractions. Purified fractions were analyzed by western blot with the following antibodies: anti-v5 (ATPaseTb2_v5), anti-enolase (cytosol), anti-AAC (mt inner membrane), anti- β (F_1 -ATPase subunit) and anti-MRP1 (mt matrix). The relevant sizes of the protein marker are indicated on the left.

doi:10.1371/journal.ppat.1004660.g002

ATPaseTb2 is a bona fide subunit of F_0F_1 -ATPase monomers and higher oligomers

To confirm that ATPaseTb2 is a genuine subunit of both the BF and Dk F_0F_1 -ATPase, we employed the same strategy applied previously for PF cells [26]. Therefore, we first created BF cell lines in which either the ATPaseTb2 or the F_1 subunit p18 were inducibly expressed with a C-terminal tag. Complexes assembled with a tagged protein were then purified using a one-step IgG affinity purification, followed by treatment with TEV protease to release bound complexes from the IgG beads. The TEV eluates were further analyzed by western blot for the presence of the tagged proteins, known F_0F_1 -ATPase subunits, and AAC (Fig. 3A). Importantly, the presence of the tagged subunits ATPaseTb2 and p18 in the respective cell lines were confirmed using a specific antibody against the c-myc epitope that comprises part of the tag. In addition, the ATPaseTb2_TAP eluate contained F_0F_1 -ATPase subunits β , p18 and ATPaseTb1. Vice versa, the p18_TAP eluate contained subunits ATPaseTb2, ATPaseTb1 and subunit β . While AAC has been described to associate with mammalian F_0F_1 -ATPase under certain conditions [40], it is not a core component of the enzyme and the lack of its signal indicates the stringency of this technique. The TAP tag purification from non-induced cells was used as a negative control to verify that the detected proteins do not bind non-specifically to the charged beads. To analyze the composition of the Dk F_0F_1 -ATPase, p18 tagged complexes were purified and subjected to the same set of antibodies described for the BF complexes (Fig. 3B). These results also depicted the same interactions seen in Fig. 3A. Therefore, the co-purification of ATPaseTb2 with known ATPase subunits p18 and β validates that it is an authentic constituent of the F_0F_1 -ATPase complex in both BF and Dk cells.

The sedimentation profile of F_0F_1 -ATP synthase in 10–30% glycerol gradients (GG) was previously published and revealed two distinct regions representing the F_1 -moiety and the F_0F_1 -monomer and multimeric complexes [26]. In order to specify if ATPaseTb2 is a component of the F_1 -moiety or the F_0F_1 -complex, the glycerol gradient sedimentation profile was

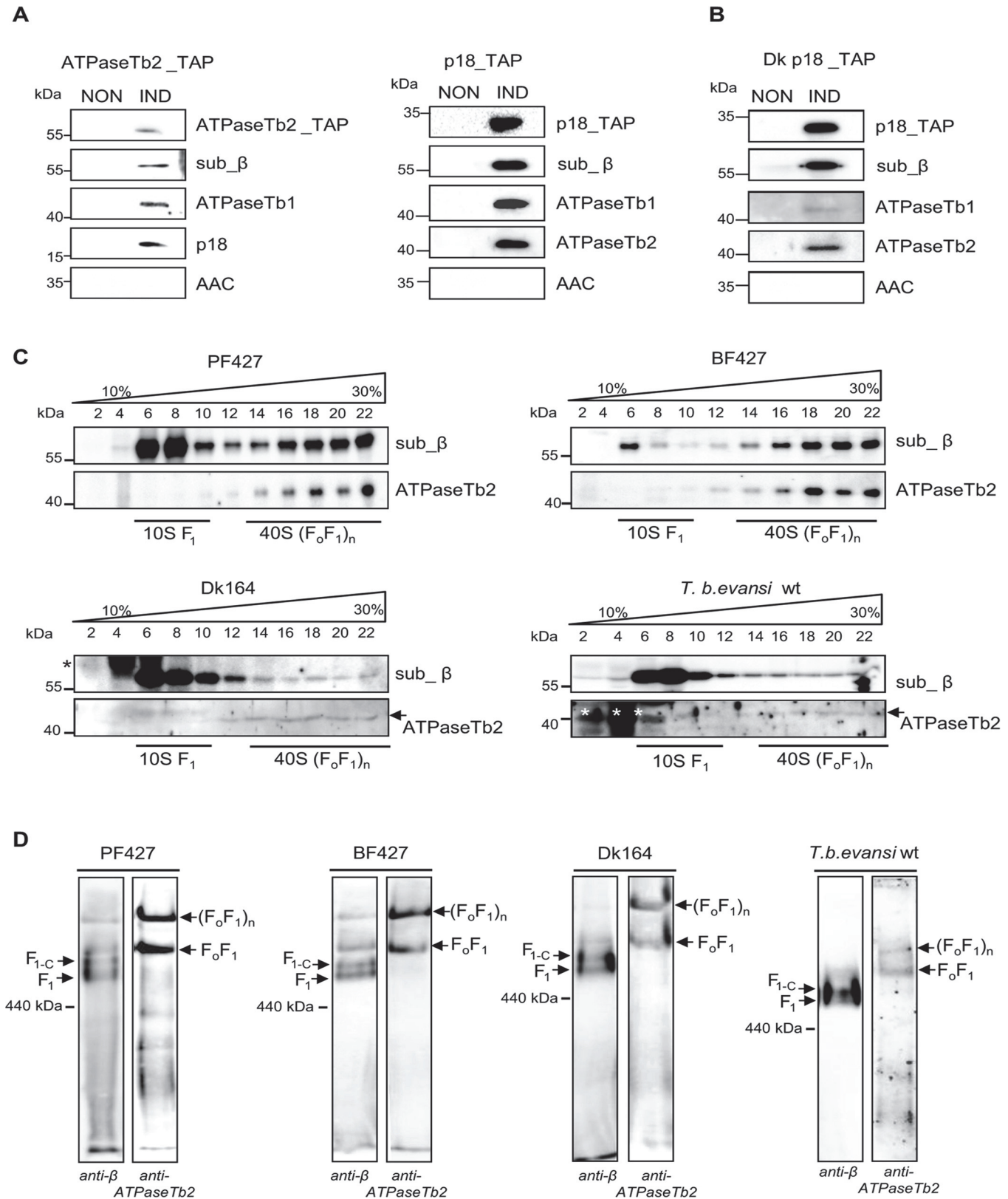


Fig 3. ATPaseTb2 is a bona fide subunit of the monomeric and multimeric F_oF₁-ATPases. A) ATPaseTb2_TAP and p18_TAP tagged complexes were purified from BF cells using one-step IgG affinity chromatography from non-induced (NON) and 2 days induced (IND) cells containing the regulatable ectopic

TAP tagged protein. The tagged protein complexes were eluted by TEV protease, fractionated on SDS-PAGE and examined by western blot analyzes. The presence of the tagged ATPaseTb2 and p18 subunits was verified using a c-myc antibody (top panels: ATPaseTb2_TAP and p18_TAP). The known F_0F_1 -ATPase subunits (sub β , p18 and ATPase_Tb1) were detected using specific antibodies. The lack of signal for AAC serves as a control for specificity of the used method. The applicable sizes of the protein marker are indicated on the left. B) p18_TAP tagged complexes were purified from dyskinetoplastic *T. b. evansi* as described above for BF cells and subjected to the same set of antibodies. C) The sedimentation profile of F_1 - and F_0F_1 -ATPase complexes was determined using glycerol gradient sedimentation. Hypotonically purified mitochondria from PF427, BF427, Dk164 and *T. b. evansi* cells were lysed with 1% Triton X-100 and fractionated on a 10–30% glycerol gradient. The glycerol gradient fractions were collected, fractionated by SDS-PAGE and analyzed by western blots. Western analyzes with an anti- β antibody depicted the sedimentation profile of the F_1 -ATPase and monomeric/multimeric F_0F_1 -ATP synthase complexes, whereas the anti-ATPaseTb2 antibody only immunodecorates this protein within the monomeric/multimeric F_0F_1 -ATPase complexes. The subdivision of the various structural forms of the F_0F_1 -ATPase complexes are underlined as determined in [26]. The glycerol gradient fractions and the sizes of the protein marker are indicated. Nonspecific bands visible in Dk164 and *T. b. evansi* gradients are indicated by asterisks. D) The native F_1 - and F_0F_1 -ATPase complexes were visualized using hrCNE. Purified mitochondria from PF427, BF427, Dk164 and *T. b. evansi* cells were lysed with digitonin (4 mg/mg), fractionated on a 3%-12% hrCNE and blotted onto a nitrocellulose membrane. The F_1 -ATPase (F_1), the F_1 -ATPase bound with the c-ring (F_{1+c}) and the monomeric F_0F_1 /multimeric (F_0F_1)_n complexes were all visualized using specific polyclonal antibodies against either subunit β or ATPaseTb2. The size of ferritin from the equine spleen (440 kDa) is indicated on the left.

doi:10.1371/journal.ppat.1004660.g003

determined using mt lysates from all four cell types: PF427, BF427, Dk164 and *T. b. evansi*. In correlation with the literature, a new specific antibody raised against the F_1 -subunit β depicted both regions, which are defined as $\sim 10S$ (fractions 6–10), and $\sim 40S$ (fractions 14–22) (Fig. 3C). A different sedimentation pattern was revealed when a specific antibody recognizing ATPaseTb2 detected only the 40S region (fractions 14–22), representing the F_0F_1 -monomer and -multimers. These findings suggest that the novel subunit is not a component of the F_1 -moiety, but rather a member of the fully assembled complex. Furthermore, compelling results hinting at the function of this hypothetical protein were also obtained when the mt lysates of Dk164 and *T. b. evansi* cells were fractionated on similar gradients. While the majority of the signal for subunit β was predictably detected in fractions 6–10, representing the F_1 -ATPase complex, there was also a weak signal detected in higher S values. These same $\sim 40S$ complexes were identified using the ATPaseTb2 antibody (Fig. 3C). This indicates that in the absence of subunit a, the F_1 -moiety is still attached to the mt membrane via a central stalk, a ring of subunit c and the peripheral stalk. Since the F_0 subunit a is missing in these cells, the attachment of this complex to the membrane is presumably not as strong as in BF cells. Therefore, upon treatment with detergent to lyse the mitochondria, a majority of F_1 -ATPase is released and detected in lower S values while a small portion of the F_0F_1 -complexes is preserved and sediments at higher S value fractions. Consequently, our data suggests that previously undetected membrane-bound F_0F_1 -complexes are present in the mitochondria of the Dk trypanosomes.

To verify our intriguing results, the F_0F_1 -ATP synthase/ATPase complex was examined by an alternative method involving high resolution clear native electrophoresis (hrCNE) followed by western blot analysis. Results obtained using the antibody against subunit β revealed four predominant bands in both the PF427 and BF427 samples, representing various forms of the F_1 -moiety and F_0F_1 -complexes (Fig. 3D). The lowest band likely corresponds to the F_1 -ATPase (subunits α , β , γ , δ , ϵ), while the one above it seemingly represents F_1 -ATPase with a ring of subunit c, as it has been described for the mammalian complex [41]. Noticeably, in each sample the antibody against ATPaseTb2 immunodetected only two major bands corresponding to the F_0F_1 -monomer and -multimers. When the mt lysates of Dk164 and *T. b. evansi* cells were fractionated on a hrCNE, subunit β was mainly detected in the lower bands representing the F_1 -moiety and the F_0F_1 -monomer, while only a weaker band was observed at the size depicting F_0F_1 -multimers. But western blot analysis with the ATPaseTb2 antibody clearly demonstrated the existence of higher assemblies of the F_0F_1 -ATPase complexes (Fig. 3D). Thus, ATPaseTb2 is a membrane-bound subunit of the monomeric and multimeric F_0F_1 -ATP synthase/ATPase complex in all four *T. brucei* cell types examined. Furthermore, no significant differences in size were observed between the F_0F_1 -monomeric and -multimeric complexes detected in

PF427, BF427 and Dk cells, indicating that subunit a might be the only missing component of the assembled F_0F_1 -ATPase complex in dyskinetoplastic cells.

Silencing of ATPaseTb2 inhibits cell growth by decreasing the $\Delta\psi_m$ in BF *T. brucei*

To assess the importance of ATPaseTb2 in the infective stage of *T. brucei* and to evaluate its functional association with F_0F_1 -ATPase, an ATPaseTb2 RNA interference (RNAi) cell line was created. The expression of dsRNA was triggered by the addition of tet to the culture medium and the *in vitro* growth of the ATPaseTb2 knock-down (KD) cells was inspected for seven days (Fig. 4A). Strikingly, a significant growth phenotype was already detected in RNAi induced cells on just the second day of tet addition. Presumably, the powerful selection forces acting on these cells missing a critical protein resulted in the emergence of a subpopulation that was no longer responsive to RNAi induction after only 120 hours, leading to the growth recovery of the culture (Fig. 4A). This phenomenon is often reported for RNAi experiments in BF *T. brucei* [42].

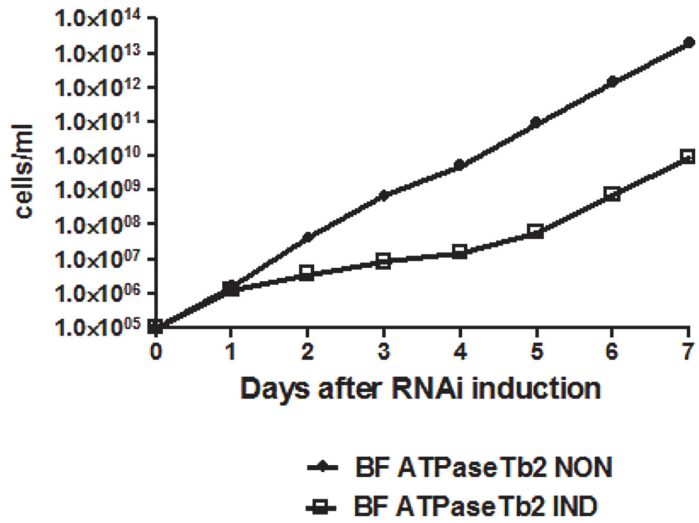
The targeted KD of ATPaseTb2 was confirmed by western blot analysis of whole cell lysates harvested from an equivalent number of cells for ATPaseTb2 RNAi non-induced and induced cells throughout the RNAi time course (Fig. 4B). Western blot analysis using the antibody against ATPaseTb2 exhibited a reduction of the targeted protein by 73% at day 2 of RNAi induction. A non-specific band detected on the same membrane was used to determine equal loading of the samples.

With the efficient knockdown of ATPaseTb2 verified, an *in vivo* assay was employed to measure the $\Delta\psi_m$ in the ATPaseTb2 KD cell population (Fig. 4C), since the $\Delta\psi_m$ is generated by the F_0F_1 -ATPase in BF *T. brucei* [9]. Flow cytometry analysis was used to determine the changes observed in these cells stained with Mitotracker Red CMX-Ros, whose fluorescent intensity is proportionally dependent on the strength of the $\Delta\psi_m$. A substantial decrease of the $\Delta\psi_m$ in the KD cell population was observed two days (IND2) after RNAi induction, coinciding with the first time point to display a significant growth inhibition. Importantly, this result confirms the vital function of ATPaseTb2 within the F_0F_1 -ATPase.

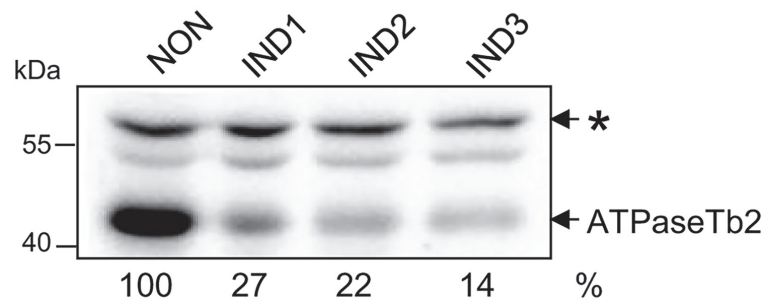
Depleting ATPaseTb2 does not significantly alter ATP hydrolysis capabilities

To assess if the decrease in the $\Delta\psi_m$ is the result of an impaired ATP hydrolytic activity of the enzyme, the total ATPase activity was measured in mt lysates with or without azide, an inhibitor of the catalytic F_1 -ATPase [43]. Typically, the specific F_1 -ATPase activity represents ~ 35–45% of total mt ATPase activity. Our results indicate that neither the total ATPase nor azide-sensitive activities were significantly altered between the non-induced and ATPaseTb2 RNAi-induced cells (Fig. 5A). ATPase activity can also be visualized by in-gel activity staining when mitochondria from these cells are solubilized with dodecyl maltoside and separated on a 2–12% blue native PAGE (BNE) [41]. The specific ATPase staining revealed two major bands in non-induced cells, the predominant lower one representing the activity produced from the F_1 -moiety and the less significant higher band representing the hydrolytic activity of the monomeric F_0F_1 -ATPase (Fig. 5B). It is important to note that solubilizing mitochondria with any detergent can result in unintended structural consequences not found under normal physiological conditions, especially for a large complex comprised of a matrix moiety and a membrane embedded region. Although detergents tend to dissociate the F_1 -moiety from F_0F_1 -ATPase complexes, it is intriguing that there is still a portion of ATP hydrolysis being produced from

A



B



C

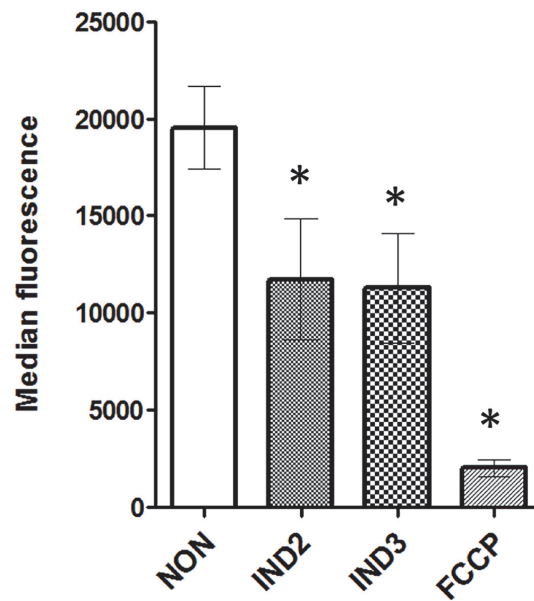


Fig 4. RNAi silencing of ATPaseTb2 inhibits the growth and mt membrane potential of BF *T. brucei*.
 A) Growth curves of the noninduced (NON) and RNAi induced (IND) ATPaseTb2 RNAi bloodstream *T. brucei* cell lines were measured for 7 days. Cells were maintained in the exponential growth phase (between 10^5 and 10^6 cells/ml) and the cumulative cell number was calculated from cell densities adjusted by the dilution factor needed to seed the cultures at 10^5 cells/ml each day. The figure is representative of three independent RNAi-inductions. B) The steady-state abundance of ATPaseTb2 in non-induced (NON) RNAi cells and in cells induced with tet for 1, 2 and 3 days (IND1, IND2, IND3) was determined by western blot analysis using a specific ATPaseTb2 antibody. The non-specific band (marked with an asterisk) detected on the same membrane served as a loading control. The numbers beneath the blots represent the abundance of immunodetected ATPaseTb2 expressed as a percentage of the non-induced samples after normalizing to the loading control. The relevant sizes of the protein marker are indicated on the left. The figure is a representative western blot from three independent RNAi-inductions. C) Using Mitotracker Red CMX-Ros, the mt membrane potential was measured by flow cytometry in non-induced (NON) ATPaseTb2 RNAi cells and cells induced for 2 or 3 days (IND2 and IND3). The median fluorescence for each sample is depicted on the y-axis of the column graph. The results are means \pm s.d. (n = 3). *P < 0.05, Student's t-test.

doi:10.1371/journal.ppat.1004660.g004

the complete F_0F_1 -ATPase in the non-induced BF cells. Conspicuously, this activity is absent when ATPaseTb2 RNAi is induced (Fig. 5B).

Loss of ATPaseTb2 disrupts the F_0F_1 -ATPase complexes in BF *T. brucei*

The absence of activity for the F_0F_1 -monomeric complex might be explained by complex instability. Thus, the structural integrity of the coupled F_0F_1 -complex was further analyzed using hrCNE, which were loaded with digitonin-lysed mitochondria from non-induced and ATPaseTb2 RNAi induced cells. After transferring the separated native protein complexes to a nitrocellulose membrane, a specific antibody against the p18 subunit detected the F_1 -moiety as well as both monomeric and oligomeric F_0F_1 -complexes (Fig. 5C). Interestingly, we repeatedly observed that the abundance of the monomeric and oligomeric complexes is decreased after RNAi induction and by day 3 these complexes are not detected at all. These results were complemented by the sedimentation profile of F_0F_1 -ATPase complexes on glycerol gradients. Mitochondria were isolated from non-induced RNAi cells and cells induced for two days (IND2). These were then lysed by 1% Triton X-100 and an equal amount of mt protein from each sample was fractionated on a 10–30% GG. The resolved fractions were then analyzed by western blot and the anti- β and anti-p18 antibodies demonstrated the effect of the ATPaseTb2 KD on the F_0F_1 -ATPase sedimentation profile. As indicated in Fig. 5D and the corresponding scanning densitometry results listed in S2 Fig., two days of RNAi induction resulted in a diminished amount of β and p18 signals from the higher S-values (IND2 panels), while the GG sedimentation pattern of RNAi non-induced cells was more similar to wild type BF427 (see Fig. 3C). These results are in agreement with the PF RNAi ATPaseTb2 cell lines, in which the stability of the monomeric and multimeric F_0F_1 -ATP synthases was significantly affected upon RNAi [26].

Using a variety of methods employing various detergent types, we have established that the ATPaseTb2 subunit is an essential component of the F_0F_1 -ATPase monomer and higher oligomers in the bloodstream stage of *T. brucei*. Furthermore, the depletion of ATPaseTb2 diminishes the abundance of membrane-bound F_0F_1 -ATPase complexes, which directly initiates a substantial decrease in the $\Delta\psi_m$ that manifests as a strong growth phenotype.

ATPaseTb2 depletion affects cell growth, the $\Delta\psi_m$ and F_0F_1 -ATPase integrity in Dk *T. b. evansi*

To further dissect the primary role of the membrane-bound ATPaseTb2 subunit, we investigated the effect of targeted gene silencing in transgenic Dk *T. b. evansi*, which facilitate the tet

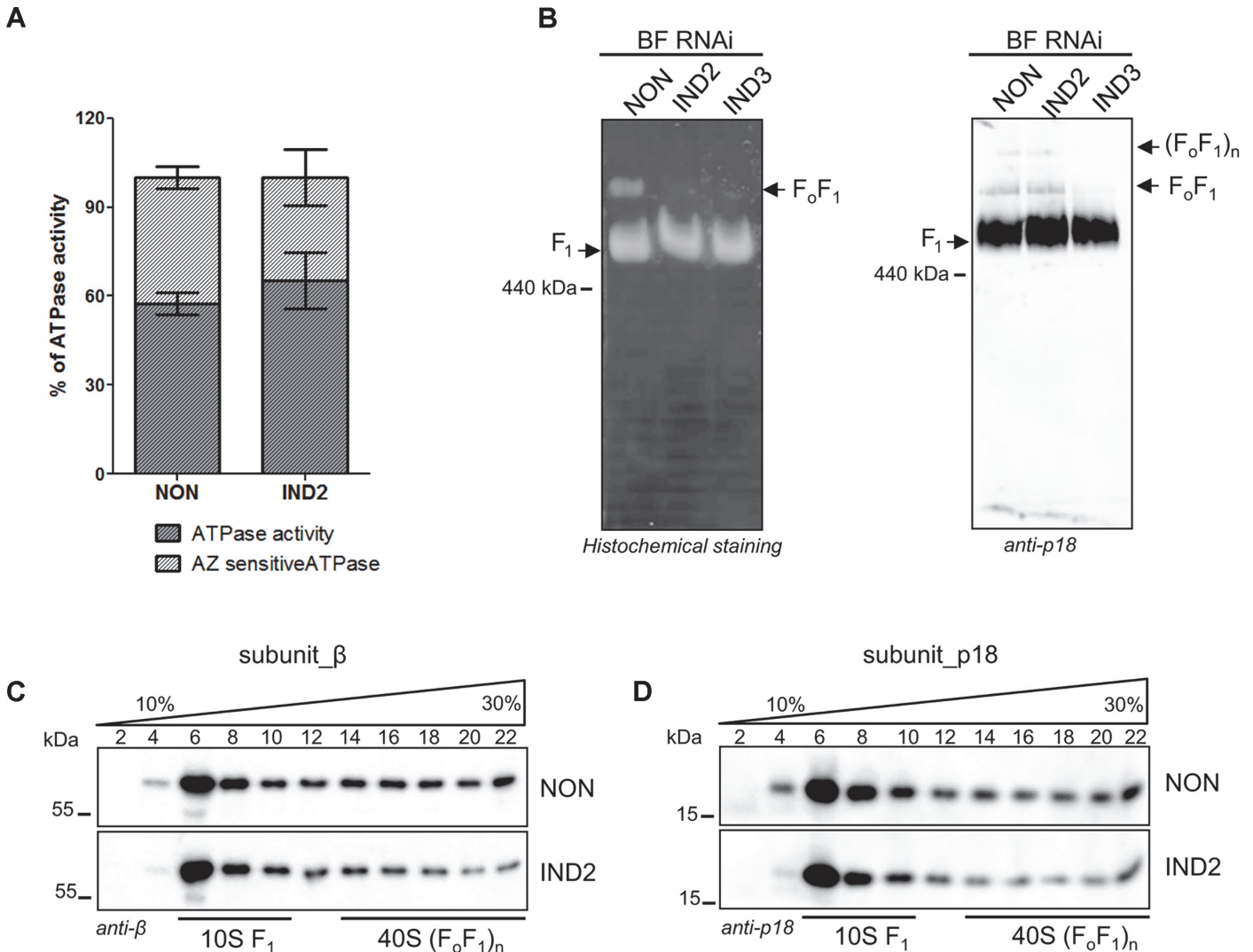


Fig 5. ATPaseTb2 depletion does not appreciably affect F₁-ATPase activity in BF *T. brucei* cells, but it does significantly diminish the stability of F_oF₁-ATPase complexes. A) Employing the Sumner ATPase assay, the F₁-ATPase hydrolytic activity was measured in ATPaseTb2 RNAi cells either not induced (NON) or induced for 2 days (IND2). Crude mt vesicles were obtained by digitonin extraction and the ATPase activity was assayed by measuring the release of free phosphates. The specific F₁-ATPase inhibitor, azide (AZ, 2 mM), was added as indicated. The total amount of free-phosphate created from all ATPase enzymes present in the sample was set at 100% (hatched column). The azide-sensitive activity representing the F₁-ATPase is depicted in dark grey. The results are means ± s.d. (n = 4). B) In-gel ATP hydrolysis activity of F_oF₁-ATPase was visualized after ATPaseTb2 reduction. Mitochondria from RNAi non-induced cells (NON) and cells induced for 2 (IND2) and 3 (IND3) days were lysed with 2% dodecyl maltoside. Equal amounts of lysed mitochondrial proteins (100 µg) were fractionated on a 2%-12% BNE and the F_oF₁-ATPase activity was visualized by in-gel histochemical staining resulting in a white lead phosphate precipitate. Positions of F₁-ATPase and monomeric F_oF₁-ATPase are depicted. The size of equine spleen ferritin (440 kDa) is indicated. C) The stability of F_oF₁-ATPase complexes upon ATPaseTb2 silencing was examined using hrCNE. Mitochondria from RNAi non-induced cells (NON) and cells induced for 2 (IND2) and 3 (IND3) days were lysed by digitonin (4 mg/mg). Equal amounts of lysed mitochondrial proteins (20 µg) were fractionated on a 3%-12% hrCNE, blotted onto a nitrocellulose membrane and probed with the anti-p18 antibody. Positions of F₁-ATPase and monomeric and dimeric F_oF₁-ATPases are depicted by arrows. The size of ferritin from equine spleen (440 kDa) is indicated. D) The sedimentation profile of F_oF₁-ATPase complexes was examined using western blot analysis of glycerol gradient fractions. Mitochondria from RNAi non-induced cells (NON) and cells induced for 2 days (IND2) were lysed with 1% Triton X-100. An equal amount of the cleared lysates (3,3 mg) were loaded on a manually poured 10–30% glycerol gradient. Western analyzes with anti-β and anti-p18 antibodies depicted the sedimentation profile of the F_oF₁-ATPase complexes. The manually fractionated glycerol gradient fractions are labelled and sizes of the protein marker are indicated.

doi:10.1371/journal.ppat.1004660.g005

inducible expression of dsRNA. These Dk cells were transfected with an ATPaseTb2 RNAi vector and several positive clones were screened for a growth phenotype. As shown in Fig. 6A, the surprising inhibition of cell growth in RNAi induced cells appeared two days after tet induction

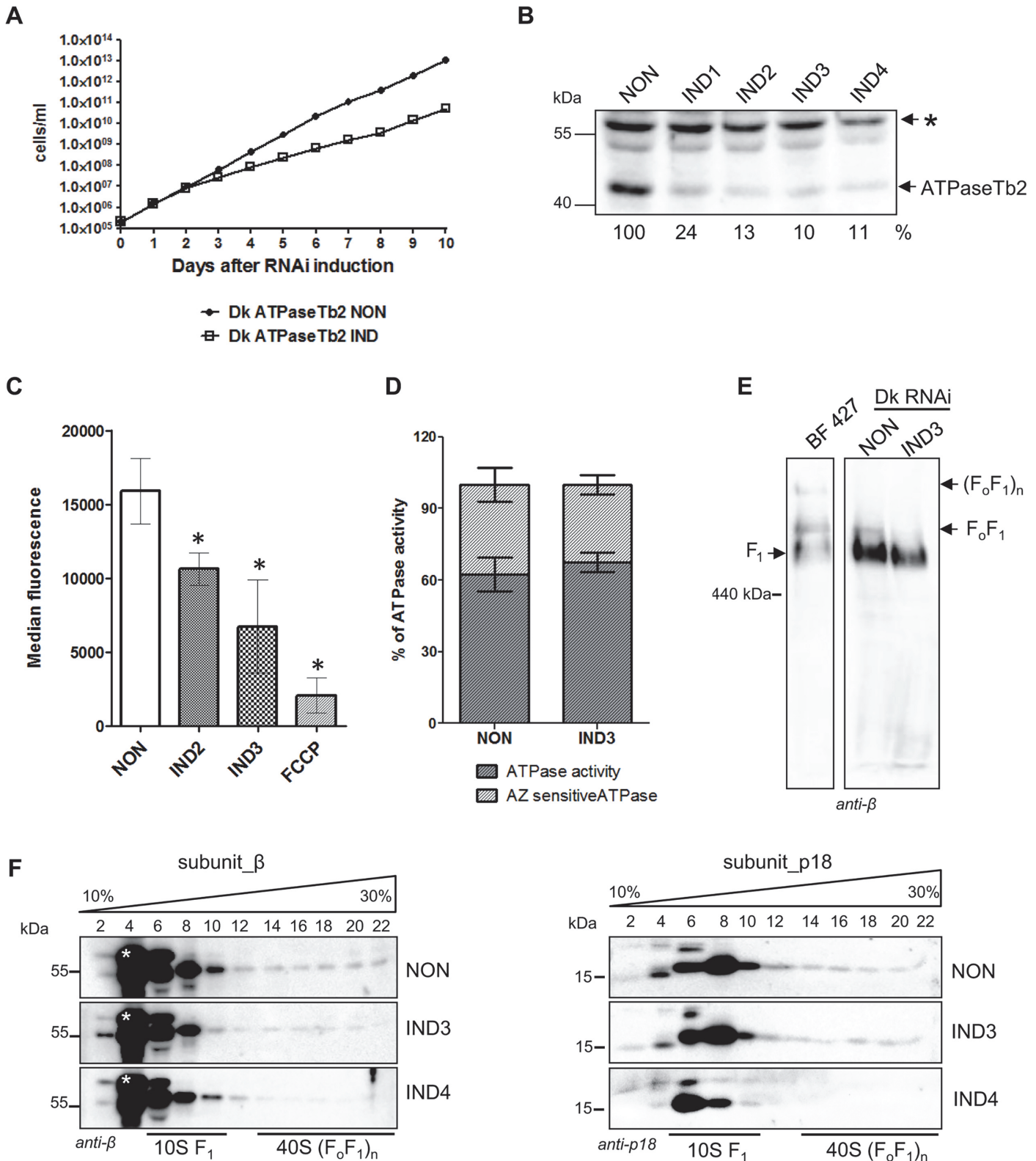


Fig 6. Cell growth, $\Delta\psi_m$ maintenance and the stability of FoF1-ATPase complexes are all affected by the loss of ATPaseTb2 in dyskinetoplactic *T. b. evansi*. A) Growth curves of the non-induced (NON) and induced (IND) ATPaseTb2 RNAi Dk *T. b. evansi* cell lines were measured for 10 days. Cells were maintained in the exponential growth phase (between 10^5 and 10^6 cells/ml) and the cumulative cell number represents the cell density adjusted by the daily dilution factor. The figure is representative of three independent RNAi-inductions. B) The steady-state abundance of ATPaseTb2 in non-induced (NON)

cells and cells harvested 1, 2, 3 and 4 days post RNAi induction (IND1, IND2, IND3, IND4) was determined by western blot analysis using a specific ATPaseTb2 antibody. Mt Hsp70 served as a loading control. The numbers underneath the ATPaseTb2 panel represent the abundance of immunodetected protein expressed as a percentage of the non-induced samples after normalizing to the loading control. The pertinent sizes of the protein marker are indicated on the left. The figure is a representative western blot from three independent RNAi-inductions. C) The $\Delta\psi_m$ was measured in non-induced (NON) ATPaseTb2 RNAi cells and cells induced for 2 and 3 days (IND2 and IND3) by flow cytometry using Mitotracker Red CMX-Ros. The results are means \pm s.d. ($n = 3$). * $P < 0.05$, Student's t -test. D) The F_1 -ATPase hydrolytic activity was measured for induced (IND3) or non-induced Dk ATPaseTb2 RNAi cells as described in Fig. 5A. The results are means \pm s.d. ($n = 4$). E) The stability of F_0F_1 -ATPase complexes upon ATPaseTb2 depletion was examined using hrCNE. Mitochondria from wild type BF427, ATPaseTb2 RNAi *T. b. evansi* non-induced cells (NON) and cells induced for 3 days (IND3) were lysed by digitonin (4 mg/mg). Equal amounts of lysed mitochondrial proteins (20 μ g) were fractionated on a 3%-12% hrCNE, blotted onto a nitrocellulose membrane and probed with an anti- β antibody. Positions of F_1 -ATPase and monomeric and multimeric F_0F_1 -ATPases are depicted by arrows. The size of the equine spleen ferritin (440 kDa) is indicated on the left. F) The sedimentation profile of F_0F_1 -ATPase complexes was examined using western blot analysis of glycerol gradient fractions. Mitochondria from RNAi non-induced cells (NON) and cells induced for 3 and 4 days (IND3 and IND4) were lysed by 1% Triton X-100 and an equal amount of the cleared samples (1.3 mg) were loaded on a 10–30% glycerol gradient. Western analyzes with anti- β and anti-p18 antibodies depicted the sedimentation profile of the F_0F_1 -ATPase complexes. The glycerol gradient fractions are labelled and the relevant sizes of the protein marker are indicated. A nonspecific band only visible in Dk164 gradients is indicated by an asterisk.

doi:10.1371/journal.ppat.1004660.g006

and the doubling time remained reduced throughout the whole ten day experiment. Furthermore, western analysis of whole cell lysates harvested over the RNAi time course exhibited a significant reduction of ATPaseTb2 in the RNAi induced cells beginning on day 1 (Fig. 6B), while the analysis of a non-specific band served as the loading control. Interestingly, if the only role of the subunit was to stabilize the proton pore, it presumably would not be essential in cells that lack mtDNA and have adapted to the loss of a functioning proton pore. However, these results suggest that ATPaseTb2 is important for F_0F_1 -ATPase complexes in these unique cells and thus this cell line was further exploited to characterize the function of ATPaseTb2.

Since the $\Delta\psi_m$ in Dk cells is generated using the hydrolytic activity of the F_1 -moiety coupled with ATP/ADP translocation, the $\Delta\psi_m$ was examined in ATPaseTb2 non-induced and RNAi induced cell populations. As shown in Fig. 6C, a reduction of the $\Delta\psi_m$ was detected in the RNAi induced cell population after 2 (IND2) and 3 days (IND3). Since the reduction of the $\Delta\psi_m$ already appears at day 2 of tet induction and the growth phenotype does not truly manifest until day 3, we postulate that the observed decrease of the $\Delta\psi_m$ is a direct effect of ATPaseTb2 silencing and not a consequence of decreased cell viability. Furthermore, to assess if this decreased $\Delta\psi_m$ is caused by an impairment of the F_1 -ATPase hydrolytic activity, the total ATPase activity was measured in mt lysates with or without azide. Similar to BF RNAi ATPaseTb2 cells (Fig. 5A), no changes in total or azide-sensitive activities were observed between the non-induced and ATPaseTb2 RNAi-induced cells (Fig. 6D).

The structural integrity of Dk F_0F_1 -ATPase complexes was then investigated using mild non-denaturing hrCNE to fractionate mitochondrial proteins purified from BF427 cells and Dk cells either induced for ATPaseTb2 RNAi or not. A western blot containing BF427 mitochondria as a reference sample was probed with an anti- β antibody and used as marker to visualize each state of the F_1 -moiety, either isolated by itself or being partnered with the monomeric and multimeric F_0F_1 -complexes. Strikingly, while a majority of the β subunit signal in Dk RNAi non-induced cells was observed in the region of isolated F_1 -ATPase, we also consistently detected an irrefutable signal corresponding to the F_0F_1 -monomeric complex, presumably assembled intact with the exception of subunit a (Fig. 6E). While there is evidence of mammalian rho cells containing a similar complex [44–46], this is the first time it has been demonstrated in the comparable Dk trypanosomatids. Furthermore, the induction of ATPaseTb2 RNAi in the Dk cells led to the disappearance of the monomeric complex, leaving only the F_1 -ATPase to be detected on the western blot (Fig. 6E). Once again, the evidence indicates that ATPaseTb2 is important for the structural integrity of the F_0F_1 -ATPase and its depletion in Dk *T. b. evansi* cells leads to the disruption of the unique membrane-bound F_0F_1 -ATPase complexes.

To corroborate this observation, we purified mitochondria from Dk *T. b. evansi* non-induced and ATPaseTb2 RNAi-induced cells and lysed them with Triton X-100. These gently disrupted lysates were then fractionated on glycerol gradients, which revealed that a majority of the signal from subunits β and p18 was located within fractions 6–10, representing the F_1 -moiety (Fig. 6F). Nevertheless, weaker bands representing the F_0F_1 -ATPase complexes (fractions 14–22) were again detected in the non-induced samples (Fig. 6F NON panels). Noticeably, these same protein markers in the mt fractionation of ATPaseTb2 RNAi induced cells displayed a significant reduction in fractions 14–22 (Fig. 6F IND4 panels), where the F_0F_1 -monomer/oligomer sediments. This observation is quite surprising since the main role of this enzyme is to create the $\Delta\psi_m$, presumably using only the hydrolytic activity of the matrix facing F_1 -moiety. In an attempt to determine if a portion of the F_1 -ATPase is membrane associated and that the disruption of this attachment is the reason for the observed decrease in the $\Delta\psi_m$ and the detected growth phenotype, we decided to visualize these complexes *in situ* using immunogold labelling followed by electron microscopy.

Loss of ATPaseTb2 leads to the dissociation of F_1 -ATPase from the mt membrane

Immunogold labeling with a primary anti- β antibody was performed on ultrasections of Dk *T. b. evansi* non-induced (NON) and ATPaseTb2 RNAi induced cells for 3 (IND3) and 5 (IND5) days. Electron micrographs illustrate that Dk trypanosomes have a simple and reduced mitochondrion (S3A Fig.), lacking both cristae and a typical kinetoplast structure, as previously reported for the dyskinetoplastic *T. b. evansi* [17]. Whenever these reduced double-membrane organelles could be unequivocally identified, we tallied the number of immunogold beads either in the close proximity of the mt membrane or in the matrix (S3A Fig.). Strikingly, 70% of the gold particles identified were found associated with the mt membrane in the NON images (S3B Fig.). From the 113 images captured from either NON, IND3 or IND5 samples, we performed a Chi-squared analysis on the immunogold beads associated with the mt membrane to determine if their distribution is random (S3C Fig.). With two degrees of freedom, the calculated $\chi^2 = 43.5$ ($p < 0.0001$), which signifies that the difference between the observed and expected particles was statistically significant. These values were then plotted to determine the relative labelling index ($RLI = N_{obs}/N_{exp}$) for the mt membrane associated gold particles (S3D Fig.). This analysis reveals that the observed number of gold particles found in close proximity to the mt membrane for the NON electron micrographs is significantly greater than if the particles were randomly distributed ($RLI = 1$), while the opposite is true for the IND5 samples. Since we understand the general subjectivity of this method, we performed this experiment in a blinded study and only considered a gold bead to be associated with the mt membrane if it was in the immediate proximity of the membrane. For the very few scored beads that could potentially fall in a membrane-bound grey zone, it should be noted that the physical distance from the subunit β antigen to the gold particle can be up to 15–20 nm, not to mention that subunit β itself is projected from the membrane by subunit γ by as much as 13 nm [47,48]. Furthermore, very few immunogold beads were detected outside of defined mt structures and each mt image only contained 1–8 immunogold beads (average of 2.4 beads/mt image), suggesting that the labelling was very specific for our abundant mt antigen. It is important to note, that utilizing an assay that does not require the use of any detergents, we demonstrated that a majority of the F_1 -ATPase is located within close proximity of the mt membrane and this association is disrupted when ATPaseTb2 is depleted.

Discussion

The *T. brucei* F_0F_1 -ATPase has obtained unique properties in comparison to its eukaryotic counterparts. The occurrence of novel subunits combined with the lack of typical eukaryotic subunits that compose the F_0 membrane-bound moiety and the peripheral stalk is intriguing from an evolutionary viewpoint. Because these atypical subunits lack significant homology to known proteins, questions arise concerning their authenticity as genuine subunits of the complex and what their function and localization within the complex might be. Here, we focused on the functional characterization of one of the trypanosomatid specific subunits, ATPaseTb2 in the bloodstream stages of *T. brucei*. Notably, we determined that its function is essential for maintaining the normal growth rate of the infectious stage of *T. brucei* and also for the important veterinary dyskinetoplastic parasite, *T. b. evansi*. Additional analyses demonstrated that the ATPaseTb2 is membrane embedded and a component of the F_0F_1 -ATPase that is present in both BF and Dk cells. Furthermore, the depletion of this F_0 -moiety subunit results in a decreased $\Delta\psi_m$ and a loss of F_0F_1 -ATPase complexes. Combined with bioinformatic tools that predict a transmembrane domain and identify a low homology to subunit d, we suggest that ATPaseTb2 might be a component of the peripheral stalk of the F_0F_1 -ATPase.

The peripheral stalk is indispensable for ATP synthesis as it serves to impede the movement of the catalytic $\alpha_3\beta_3$ headpiece while the proton motive force rotates the c-ring and the connected asymmetrical central stalk in a way that imposes conformational changes in the catalytic nucleotide binding sites of the β subunits. The peripheral stator is also essential when the complex harnesses the energy provided from ATP hydrolysis to drive the rotation of the enzyme in reverse, allowing protons to be pumped across the mt inner membrane to produce the $\Delta\psi_m$ when physiological conditions dictate.

The bovine and yeast peripheral stalk is composed of four subunits, OSCP, b, d, and F_6/h (bovine/yeast nomenclature). Subunit b (~20kDa protein) contains two trans-membrane segments at the N-terminus, while the rest of the protein is hydrophilic—protruding into the matrix and interacting with OSCP and subunit d [23,49–51]. The interaction between subunit b and OSCP is stabilized by subunit F_6 [22]. The predominantly hydrophilic subunit d interacts with all three mentioned subunits and it has been shown to be essential for the function of the F_0F_1 -complex. The yeast knock-out of subunit d was characterized by the de-attachment of the catalytic F_1 -ATPase from the protonophoric sector, the loss of detectable oligomycin sensitive ATPase activity and the absence of subunit a in the F_0 -moiety [36]. Notably, of these four subunits, the only homolog identified in the *T. brucei* genome is OSCP and its protein product was identified as a bona fide subunit of the purified F_0F_1 -ATP synthase [26]. Homologs for subunits b, d, and F_6 are missing and most likely have been replaced by the novel proteins that associate with the *T. brucei* F_0F_1 -ATP synthase. Here we demonstrated that the ATPaseTb2 subunit is a membrane-bound protein, containing one predicted transmembrane domain, with a large hydrophilic region extending into the matrix that possesses a low homology to the bovine subunit d. In accordance with other yeast or bovine subunits of the peripheral stalk, the down-regulation of ATPaseTb2 affects the stability of the F_0F_1 -complex and its oligomycin sensitivity (this study, [26]).

Considering the relatively large molecular mass of ATPaseTb2 (43 kDa), it is plausible to speculate that ATPaseTb2 functionally represents the membrane-bound subunit of the peripheral stalk fused with subunit d, offering an early attempt by eukaryotes to add layers of complexity that will allow for greater adaptability. It is noteworthy to mention that a species-specific architectural variant of the peripheral stalk was also proposed for colorless and green algae, where the novel subunits Asa2, Asa4 and Asa7 fulfil a structural role in forming the peripheral stalk [52,53]. Other discrepancies from the typical eukaryotic enzyme model can be

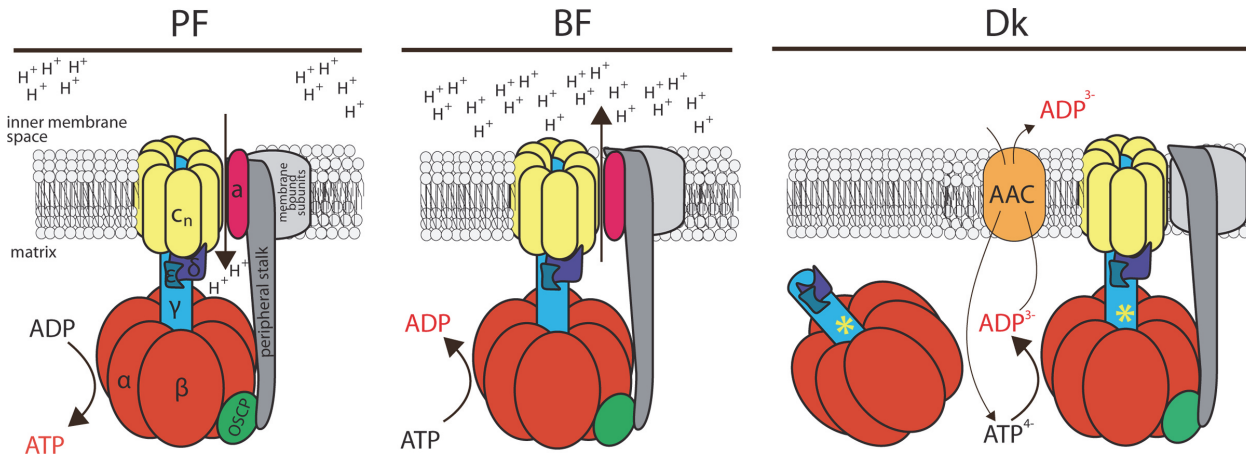


Fig 7. Schematic representation of the F_0F_1 -ATP synthase/ATPase complex in trypanosome mitochondria. The F_0F_1 -ATP synthase possesses the conventional function in the procyclic form (PF) of the parasite, coupling transmembrane proton transfer with ATP synthesis. In contrast, this enzymatic complex works in reverse in the bloodstream form (BF) of the parasite, hydrolyzing ATP to generate the $\Delta\psi_m$ in the absence of canonical cytochrome-containing respiratory complexes. This hydrolytic activity is also utilized in the dyskinetoplastid (Dk) form, which lacks mitochondrial DNA and thus a proton pore. Therefore, in Dk cells, enhanced ATP hydrolysis by a mutated F_1 -moiety (a necessary mutation in the γ subunit is marked with the asterisk) provides substrate for the ATP/ADP carrier (AAC) and the $\Delta\psi_m$ is produced by the electrogenic exchange of ADP^{3-} for ATP^{4-} . Furthermore, we present that a minor fraction of F_1 -ATPase still appears to be associated with F_0 and that association may be functionally important for maintaining the $\Delta\psi_m$. Orthologues of the colored subunits (α , β , γ , δ , ϵ , OSCP, a and c) have been annotated in trypanosomes. In addition to OSCP, the peripheral stalk (dark grey) is usually composed of subunits b, F_6 and d, but these homologs have not been identified in the *T. brucei* genome. Also, conspicuously absent are subunits A6L, e, f and g, which are all membrane-bound (light grey).

doi:10.1371/journal.ppat.1004660.g007

found in the ciliate *Tetrahymena thermophila*, representing the superphylum of Alveolates, where the homolog of the conserved subunit b has so far not been identified in the genome. Instead, three novel proteins detected in this ATP synthase complex have been proposed to substitute for subunit b [28]. Thus, it seems that the composition and overall structural appearance of the F_0F_1 -ATP synthase from organisms representing different lineages other than Opisthokonts, might be more diverse than previously thought and deserve more attention from basic researchers to elucidate alternate evolutionary solutions to a common thread of life.

T. brucei is a member of the Excavata clade and represents a desirable model to study the function and regulation of the F_0F_1 -ATP synthase/ase complex since it utilizes the proton motive force to produce ATP in the PF life stage, while in the BF stage it hydrolyzes ATP to pump the protons necessary to create the $\Delta\psi_m$. Moreover, dyskinetoplastic *T. b. evansi* employs the hydrolytic activity of the F_1 -ATPase and the electrogenic exchange of ADP^{3-} for ATP^{4-} by the AAC as yet another strategy to generate the $\Delta\psi_m$ (Fig. 7). Therefore, it was surprising that the ATPaseTb2 protein was detected in all four examined cell types (PF, BF, Dk 164 and *T. b. evansi*), albeit at a much lower abundance in BF and Dk cells, but that is in full agreement with the reduced mitochondria previously defined for these two forms [39]. Furthermore, when PF and BF mt lysates were resolved by GG and hrCNE, ATPaseTb2 was only detected when co-localized with the monomeric and oligomeric F_0F_1 -ATP synthase/ase complexes. Interestingly, similar results were obtained from the mt lysates of cells lacking mtDNA. Considering that only the F_1 -ATPase was previously assumed to be important for maintaining the $\Delta\psi_m$ in the Dk trypanosomes, the presence of these complexes is intriguing. Nevertheless, a proteomics study performed with osteosarcoma 143B ρ^0 cells revealed that in addition to the F_1 -ATPase subunits, subunit d of the peripheral stalk was also identified [54]. In a similar project involving fibroblast MRC5 ρ^0 cells, the oligomycin insensitive complex was purified and determined to contain several F_0 (b and c) subunits along with a couple of peripheral stalk subunits (OSCP, d). Notably, this complex was loosely associated with the mt membrane [45]. Furthermore,

several additional studies have shown that the F_1 -ATPase in yeast or mammalian cells lacking a mt genome (i.e. mammalian subunits a/ATP6, A6L; yeast subunits 6, 8 and 9) is membrane associated, with the attachment most likely occurring via the central and/or peripheral stalk [44,46,55,56]. Our data also suggest that since ATPaseTb2 membrane-bound complexes (monomeric and multimeric) do not display significant differences in their native size or sedimentation values, then the mt encoded subunit a might be the only missing subunit from these complexes. Such a uniquely structured complex can be explained by the current model for the assembly of the F_0F_1 -ATPase, in which the F_0 subunit a is the last protein incorporated into the enzyme to ensure that it is able to function properly before introducing a complete proton pore. Furthermore, this integration is dependent on the presence of subunit b of the peripheral stalk [57].

RNAi silencing of ATPaseTb2 in BF cells caused a strong growth phenotype concurring with a decreased $\Delta\psi_m$. Importantly, ATPaseTb2 also proved to be essential for maintaining the normal growth rate and the $\Delta\psi_m$ of Dk cells. Combined with the hrCNE and glycerol gradient sedimentation assays that revealed a decrease of the high molecular weight complexes, but not the F_1 -ATPase, our studies suggest that these membrane-bound enzymes might significantly contribute to the membrane potential in Dk cells. The biological significance of this localization of the F_1 -ATPase might be to efficiently coordinate the activity of this enzyme with its substrate transporter, both of which are responsible for producing the $\Delta\psi_m$ in Dk. By restricting the F_1 -ATPase to the mt membrane, it keeps it within the close vicinity of its biochemically functional partner, the AAC. In this way, it helps ensure that the hydrolysis of ATP results in a relatively concentrated region of substrate for the mt membrane embedded AAC, especially in a mitochondrion lacking defined cristae and the microenvironments they create. Indeed, there is precedence for such a close spatial collaboration to increase efficiency, as an actual physical interaction between these two enzymes has been reported as the ATP synthasome in mammals [40,58]. We are currently building a set of tools to perform additional functional assays and imaging techniques that we hope will further resolve the function of the F_0F_1 -ATPase complexes in these pathogenic trypanosomes.

Materials and Methods

Plasmid construction

The ATPaseTb2 (Tb927.5.2930) RNAi constructs targeted an 825 bp fragment of the gene that was PCR amplified from *T. brucei* strain 427 genomic DNA with the following oligonucleotides: FW—CACGGATCCATGCGCCGTGTATC, REV—CACCTCGAGTTCGGCCCCGATC. Utilizing the BamHI and XhoI restriction sites inherent in the primers (underlined), this fragment was cloned into the p2T7-TA blue plasmid [59] (used to create a BF RNAi cell line) and the p2T7-177 plasmid [60] (used to generate a Dk RNAi cell line). For the inducible expression of ATPaseTb2 fused with a C-terminal 3xv5 tag, the ATPaseTb2 coding sequence was PCR amplified (Fw: ACAAAGCTTATGC GCCGTGTATC, Rev: ATAGGATCCGTG ATGGGCCTTTTTC) and cloned into the pT7_v5 vector using HindIII and BamHI restriction enzymes [61]. The pLEW79MHTAP vectors for the tet inducible expression of ATPaseTb2 and Tb927.5.1710 (F_0F_1 -ATPase subunit p18) TAP-tagged proteins were previously described in [26].

Trypanosoma culture conditions and generation of cell lines

Bloodstream form *T. brucei brucei* Lister 427 strain, stable acriflavin-induced dyskinetoplastic *T. b. brucei* EATRO 164 [18] and dyskinetoplastic *T. b. evansi* Antat 3/3 [62] were all grown *in vitro* at 37°C and 5% CO₂ in HMI-9 media containing 10% FBS. The BF427 single marker cell

line [63] and a *T. b. evansi* cell line [14], both constitutively expressing the ectopic T7 RNA polymerase and tet repressor (TetR) were used for the tet inducible expression of dsRNA and the TAP- and v5-tagged proteins. Each plasmid was linearized with NotI enzyme and transfected into the appropriate cell line as described previously [63]. Linearized p2T7-177 was targeted to the minichromosome 177 basepair repeat region, while linear pTv5 and pLEW79MHTAP vectors were integrated into the rDNA intergenic spacer region [60,61,63]. The induction of RNAi and ectopically expressed tagged proteins was triggered by the addition of 1 µg/ml of tet into the media. Cell densities were measured using the Z2 Cell Counter (Beckman Coulter Inc.). Throughout the analyses, cells were maintained in the exponential mid-log growth phase (between 1×10^5 to 1×10^6 cells/ml).

Tandem affinity purification (TAP) of tagged complexes

The TAP protocol was generously provided by L. Jeacock and A. Schnauffer (personal communication) and optimized for BF cells. Briefly, 2×10^8 cells were harvested and lysed for 20 min on ice with 1% Triton X-100 in an IPP150 buffer (150 mM NaCl, 0.1% NP40, 10mM Tris-HCl pH 8.0) containing Complete protease inhibitors (Roche). The lysates were then cleared by centrifugation (16,000 g, 15 min, 4°C). Meanwhile, IgG antibodies were covalently bound to Dynabeads M-270 Epoxy (Invitrogen) using a protocol previously described [64]. Charged beads were blocked with 1% BSA and then incubated with the cleared cell lysates (4°C for 2 hours, constantly rotating). The beads were then washed three times with IPP150 and once with a TEVCB buffer (150 mM NaCl, 0.1% NP40, 0.5 mM EDTA, 1 mM DTT, 10 mM Tris-HCl, pH 8.0). Finally, the bound protein complexes were released by AcTEV protease (Invitrogen) cleavage and the eluate was analyzed by SDS-PAGE.

Isolation of mt vesicles

Crude mt vesicles were obtained by hypotonic lysis as described in detail earlier [65]. Briefly, cell pellets from $\sim 2 \times 10^9$ cells were washed with SBG (150 mM NaCl, 20 mM glucose, 20 mM NaHPO₄, pH 7.9), resuspended in DTE (1 mM Tris, 1 mM EDTA, pH 8.0) and homogenized in a Dounce homogenizer. Alternatively, for a smaller scale hypotonic isolation, cell pellets from $\sim 1 \times 10^9$ cells were washed in NET buffer (150 mM NaCl, 100 mM EDTA, 10 mM Tris, pH 8.0), resuspended in DTE and homogenized by passing through a 25G needle. To re-create the physiological isotonic environment, 60% sucrose was immediately added to the lysed cells to reach a final concentration of 250 mM. Samples were spun down at 15,000 g, 10 min, 4°C to clear the soluble cytoplasmic material from the lysates. The resulting pellets were resuspended in STM (250 mM sucrose, 20 mM Tris pH 8.0, 2 mM MgCl₂), supplemented with a final concentration of 3 mM MgCl₂ and 0.3 mM CaCl₂ before incubating with 5 µg/ml DNase I for 1hr on ice. Then an equal volume of STE buffer (250 mM sucrose, 20 mM Tris pH 8.0, 2 mM EDTA pH 8.0) was added and the material was centrifuged at 15,000 g, 10 min, 4°C. Pellets enriched with the mt membrane vesicles were washed in STE and kept at -70°C.

SDS-PAGE and Western blot

Protein samples were separated on SDS-PAGE, blotted onto a PVDF membrane (PALL) and probed with the appropriate monoclonal (mAb) or polyclonal (pAb) antibody. This was followed by incubation with a secondary HRP-conjugated anti-rabbit or anti-mouse antibody (1:2000, BioRad). Proteins were visualized using the Pierce ECL system (Genetica/Biorad) on a ChemiDoc instrument (BioRad). When needed, membranes were stripped at 50°C for 30 min in a stripping buffer (62.5 mM Tris pH 6.8, 100 mM mercapthoethanol, 2% SDS) and re-probed. The PageRuler prestained protein standard (Fermentas) was used to determine the size

of detected bands. Primary antibodies used in this study were: mAb anti-v5 epitope tag (1:2000, Invitrogen), mAb anti-mtHsp70 (1:2000) [66], pAb anti-AAC (1:2000) [67], pAb anti-MRP1 (1:1000) [68], pAb anti-APRT (1:1000) and pAb anti-enolase (1:1000) [69]. Antibodies against ATPaseTb2 (1:1000), ATPaseTb1 (1:1000), subunit β (1:2000) and subunit p18 (1:1000) were prepared for the purpose of this study. The open reading frames of the respective genes without their predicted mt localization signal were cloned into the *E. coli* expression plasmid, pSKB3. The proteins were overexpressed in BL21 *E. coli* cells and purified under native conditions (subunit β) or denatured conditions (ATPaseTb2, ATPaseTb1 and p18) using a 6 M guanidinium lysis buffer and 8 M urea binding buffer. The denatured proteins were then refolded with a step-wise dialysis procedure that included 0.5 M arginine in the refolding buffer. Native and refolded antigens were sent to Pineda (Antikörper-Service, Germany) or Davids Biotechnologie (Regensburg, Germany) for polyclonal antibody production.

Mt membrane potential ($\Delta\psi_m$) measurement

The $\Delta\psi_m$ was determined utilizing the red-fluorescent stain Mitotracker Red CMX-Ros (Invitrogen). Cells in the exponential growth phase were stained with 100 nM of the dye for 30 min at 37°C. Cells were pelleted (1,300 g, 10 min, RT), resuspended in 2 ml of PBS (pH 7.4) and immediately analyzed by flow cytometry (BD FACS Canto II Instrument). For each sample, 10,000 events were collected. Treatment with the protonophore FCCP (20 μ M) was used as a control for mt membrane depolarization. Data were evaluated using BD FACSDiva (BD Company) software.

F₁-ATPase assay

ATPase activity was measured with the Sumner assay, which is based on the release of free phosphate when ATP is hydrolyzed by the enzyme as described earlier [14,70]. Briefly, crude mt lysates were obtained from 2×10^8 cells by SoTe/digitonin extraction (0.015% digitonin, 0.6 M Sorbitol, 2 mM EDTA, 20 mM Tris-HCl pH 7.5). Mt pellets were resuspended in an assay buffer (200 mM KCl, 2 mM MgCl₂, Tris-HCl pH 8.0) and the 20 min reaction was initiated by the addition of ATP to a final concentration of 5 mM. Where indicated, samples were pre-treated with the F₁-ATPase specific inhibitor, sodium azide (2 mM) for 10 min at 37°C. The 100 μ l enzymatic reactions were deproteinated by the addition of 1.9 μ l of 70% perchloric acid. After a 30 min incubation on ice, the samples were spun down (16,000g, 10 min, 4°C) and 90 μ l of the supernatant was incubated for 10 min with 0.5 ml of Sumner reagent (8.8% FeSO₄·7H₂O, 375 mM H₂SO₄, 6.6% (NH₄)Mo₇O₂₄·4H₂O) [62]. 200 μ l was then transferred to a 96 well plate and the absorbance was measured at 610 nm using a Tecan Infinite plate reader (Infinite M200Pro, Tecan). To calibrate the assay, a standard curve was calculated from the absorbance values of linear inorganic phosphate samples (0–2 mM).

In-gel histochemical staining of F₁-ATPase activity

Blue native PAGE (BNE) of mt lysates, followed by in-gel activity staining was adapted from published protocols [26,32]. Briefly, mt vesicles from $\sim 2 \times 10^9$ cells were resuspended in a mt lysis buffer (0.75 M amino-n-caproic acid—ACA, 50 mM Bis-Tris, 0.5 mM EDTA, pH 7.0), lysed with 2% dodecylmaltoside (DDM) for 1 hr on ice and then cleared by centrifugation (16,000g for 30 min, 4°C). The protein concentration of each mt lysate was determined by a Bradford assay (BioRad), so that 100 μ g of total mt protein could be mixed with 1 M ACA and 5% Coomassie brilliant blue G-250 before being loaded on a 2–12% Bis-Tris BNE gel. Immediately after the run (3 hr, 100 V, 4°C), the gel was incubated overnight in an ATPase reaction buffer (35 mM Tris pH 8.0, 270 mM glycine, 19mM MgSO₄, 0.3% Pb(NO₃)₂, 11 mM ATP).

High resolution clear native PAGE (hrCNE)

The protocol for hrCNE was adapted from published studies [71,72]. In summary, crude mt vesicles from $\sim 5 \times 10^8$ cells were resuspended in a mt lysis buffer (2 mM ACA, 50 mM Imidazole-HCl, 1 mM EDTA, 50 mM NaCl, pH 7) and lysed for one hour on ice with 4 mg digitonin/1 mg protein. The samples were spun down at 16,000 g for 30 min and the cleared lysate protein concentrations were determined by a Bradford assay. Samples were mixed with a 5x loading dye (0.1% Ponceau-S, 50% glycerol) and loaded onto a 3%-12% native gradient gel. After electrophoresis (3 hr, 100 V, 4°C), the resolved mt lysates were transferred onto a nitrocellulose membrane (overnight, 20 V, 4°C) and probed with selected antibodies.

Na₂CO₃ submitochondrial fractionation

Na₂CO₃ extraction of mt membranes was adapted from a previously published protocol [73]. Mt vesicles from 1×10^9 cells were isolated by hypotonic lysis as described above. The resulting supernatant from the 25G needle homogenization step was kept as a cytosolic fraction (CYTO). The mt pellet was further treated with digitonin (80 µg/ml) for 15 min on ice to disrupt the mt outer membrane. The material was then cleared by centrifugation (12,000 g, 20 min, 4°C) and the pelleted mitoplasts were resuspended in 0.1 M Na₂CO₃ buffer (pH 11.5) and incubated for 30 min on ice. A final ultracentrifugation step (100,000 g, 4°C for 1 hr) performed in an SW50Ti rotor of a Beckman Instrument resulted in a supernatant comprised of proteins from the mt matrix (MX), including stripped peripheral membrane proteins, and a pellet containing integral proteins isolated from the mt membrane fraction (M).

Glycerol gradient (GG) sedimentation

Hypotonically purified mt vesicles from $\sim 2.5 \times 10^9$ cells were resuspended in a GG lysis buffer (10 mM Tris, pH 7.2, 10 mM MgCl₂, 200 mM KCl, 1mM DTT) and lysed with 1% Triton X-100 (30 min, on ice). The lysates were cleared by a centrifugation step (2x 16,000 g, 30 min, 4°C) and the protein concentration was determined by a Bradford assay. Mt cleared lysates were resolved by ultracentrifugation (Beckman Instrument, SW40 rotor) at 38,000 g for 5 hr on 11ml 10–30% GG, which was poured manually or using the Gradient Station (Biocomp) according to the manufacturer's protocol. The glycerol gradients were then fractionated either manually or with the Gradient station and 500µl fractions were stored at -70°C.

Immunogold staining of ultrathin sections and transmission electron microscopy

Cells ($\sim 5 \times 10^7$) were pelleted (1300 g, 10 min, RT), washed in PBS (pH 7.4) and immediately fixed in a 4% formaldehyde/ 0.1 M phosphate buffer. Samples were then dehydrated at -10°C through a series of seven steps that increased the concentration of ethanol from 30% to 100%, pausing at each step for 1 hour. Next, the samples were embedded in LR White Resin (Electron Microscopy Sciences) and polymerized (UV light, 48 hours at -10°C). Ultrathin sections were prepared by the Ultracut UCT ultramicrotome (Leica) and mounted on nickel grids. Prepared sections were blocked in 5% BSA, labelled with primary anti-β antibody (1:10 dilution), washed three times with PBS and incubated with protein A conjugated to 10 nm gold particles (1:100 dilution, Aurion). The immunogold labelled grids were contrasted, carbon coated and examined by the TEM (JEM-1010, Jeol). Grids, which were immunolabeled with only the protein A conjugated to 10nM gold particles, were used as a negative control.

Quantification and statistical analysis of immunogold labelling

The number of gold particles was statistically evaluated as described earlier [12,74]. Using ImageJ software (NIH, USA), a grid consisting of squares (test points, P) with constant size ($16,105 \mu\text{m}^2$) was superimposed randomly on the electron micrographs of identified mitochondria. All test squares and immunogold particles within the immediate proximity to the mt membrane were counted separately for each micrograph. In order to statistically evaluate the labelling, all observed gold particles (N_{obs}) and all test points (P) from 113 images captured from NON, IND3 and IND5 samples were tallied. Expected numbers of gold particles (N_{exp}) for each sample were calculated as (total sum $N_{\text{obs}} \times P$)/total sum P. To determine if the difference between the observed and expected particles was significant and not due to random fluctuations, a Chi-squared analysis $\chi^2 = (N_{\text{obs}} - N_{\text{exp}})^2 / N_{\text{exp}}$ was performed using GraphPad QuickCalcs calculator (www.graphpad.com/quickcalcs). In addition, the relative labeling index (RLI), where the predicted RLI = 1 for random labelling, was calculated as $\text{RLI} = N_{\text{obs}} / N_{\text{exp}}$.

Gene IDs for the genes and proteins mentioned in this study

ATPaseTb2 (Tb927.5.2930), ATPaseTb1 (Tb927.10.520), TbAAC (Tb927.10.14820/30/40), p18 (Tb927.5.1710), mtHsp70 (Tb927.6.3740), MRP1 (Tb927.11.1710), APRT (Tb927.7.1780), enolase (Tb427.10.2890), subunit β (Tb927.3.1380).

Supporting Information

S1 Fig. Bioinformatics analysis of ATPaseTb2. A) The multiple sequence alignment of ATPaseTb2 homologs from the order Kinetoplastida was performed by ClustalW on the following species (accession number, name): *Trypanosoma vivax* Y486 (TvY486_0502300, ATPaseTv2), *T. cruzi* Sylvio X10/1 (TCSYLVIO_010784, ATPaseTc2), *T. congolense* IL3000 (TcIL3000_5_3200, ATPaseTco2), *T. cruzi* CL Brener Non-Esmeraldo-like (TcCLB.506321.280, ATPaseTcB2), *T. cruzi* marinkellei strain B7 (Tc_MARK_9008, ATPaseTcm2), *T. brucei* TREU927 (Tb927.5.2930, ATPaseTb2), *L. tarentolae* Parrot-TarII (LtaP08.0840, ATPaseLt2), *L. mexicana* MHOM/GT/2001/U1103 (LmxM.08.1100, ATPaseLmx2), *L. major* strain Friedlin (LmjF.08.1100, ATPaseLm2), *L. infantum* JPCM5 (LinJ.08.1010, ATPaseLin2), *L. donovani* BPK282A1 (LdBPK_081010.1, ATPaseLd2), *L. braziliensis* MHOM/BR/75/M2904 (LbrM.08.0870, ATPaseLbr2), *Bodo saltans* (ATPaseBs2), *Strigomonas culicis* (STCU_02070, ATPaseSc2). Sequences were obtained from GeneDB database or from Welcome Trust Sanger centrum (*B. saltans* sequence). Numbers at the top indicate the amino acid positions in *T. vivax* ATPaseTv2. The mitochondrial targeting signal for ATPaseTb2 (MTS, green) was predicted by Mitoprot II v1.101. The homologous region (red) to Bs_sub d was determined using HHpred toolkit. B) The homology of ATPaseTb2 to subunit d (*B. taurus*) was based on HHpred, which utilizes the homology detection & structure prediction by HMM-HMM comparison. (<http://toolkit.tuebingen.mpg.de>) The alignments consist of one or more blocks with the following lines: ss_pred: query secondary structure as predicted by PSIPRED (upper case letters: high probability, lower case letters: low probability). Q query_name: query sequence Q Consensus: query alignment consensus sequence Quality of colum-column match: very bad =; bad—; neutral.; good +; very good |T Consensus: template alignment consensus sequence T templ_name: template sequence T ss_dssp: template secondary structure as determined by DSSP T ss_pred: template secondary structure as predicted by PSIPRED (upper case letters: high probability, lower case letters: low probability) The consensus sequence uses capital letters for amino acids that occur with $\geq 60\%$ probability and lower case letters for amino acids that have $\geq 40\%$ probability. For unconserved columns a tilde is used. The line in the middle shows the column score between the query and template amino

acid distributions. It gives a valuable indication for the alignment quality. (A unit of column score corresponds approximately to 0.6 bits.)

=: very bad match column score below -1.5

-: bad match column score between -1.5 and -0.5

.: neutral match column score between -0.5 and +0.5

+: good match column score between +0.5 and +1.5

|: very good match column score above +1.5

(PDF)

S2 Fig. Densitometric analysis of anti-sub β and anti-p18 immunoblots of the BF ATPaseTb2 RNAi glycerol gradients depicted in Fig. 5D. The glycerol gradient fractions analyzed by western blot using anti- β (A) and anti-p18 (B) antibodies (Fig. 5D) were also examined using densitometry analysis. The chemiluminescent blots were imaged with the LAS3000 Imaging System (FUJI). The specific bands for subunit β and p18 were selected using the band analysis tool from the ImageQuant TL software (Amersham Biosciences), which allowed their background-subtracted densities to be determined. The background-corrected volumes of the corresponding protein bands were normalized to the highest value of each blot, which was set to 100.

(PDF)

S3 Fig. ATPaseTb2 depletion alters the distribution of the F₁-ATPase subunit β in *T.b. evansi* mitochondria. A) Ultrathin sections of RNAi non-induced cells (NON) and cells induced for 3 (IND3) and 5 (IND5) days were immunostained with a primary anti- β antibody, followed by incubation with a 10 nM gold bead conjugated anti-protein A secondary antibody. Images of the electron micrographs were captured and the immunogold particles visualized within identified mitochondria. Particles located in the matrix are marked with dashed arrows, while gold beads located within the immediate proximity of the mt membrane are designated with a solid arrow. B) All immunogold beads identified from 113 images of NON, IND3 and IND5 electron micrographs were itemized according to their localization and plotted as either mt inner membrane associated (grey) or matrix (white). C) Counts of observed mt membrane associated gold particles (N_{obs}) and all test points (P) from NON, IND3 and IND5 images were recorded under their appropriate column. Expected numbers of gold particles (N_{exp}) were calculated as (total sum N_{obs} x P)/total sum P. D) The relative labeling index was calculated ($RLI = N_{obs}/N_{exp}$) for the mt membrane associated gold particles tabulated in S3B Fig. and is depicted on the y-axis of the column graph.

(PDF)

Acknowledgments

We thank Ken Stuart (Seattle Biomed) and Minu Chaudhuri (Meharri Medical College) for kindly providing antibodies, Achim Schnauer (University of Edinburgh) for providing the *T. b. evansi* strain used in this study. We would also like to express our gratitude to Marie Vancová from the Laboratory of Electron Microscopy (Biology Centre) for the sample preparation and an opportunity to use the JEM-1010 electron microscope.

Author Contributions

Conceived and designed the experiments: KS BP AZ. Performed the experiments: KS. Analyzed the data: KS BP AZ. Contributed reagents/materials/analysis tools: AZ KS BP. Wrote the paper: AZ BP KS.

References

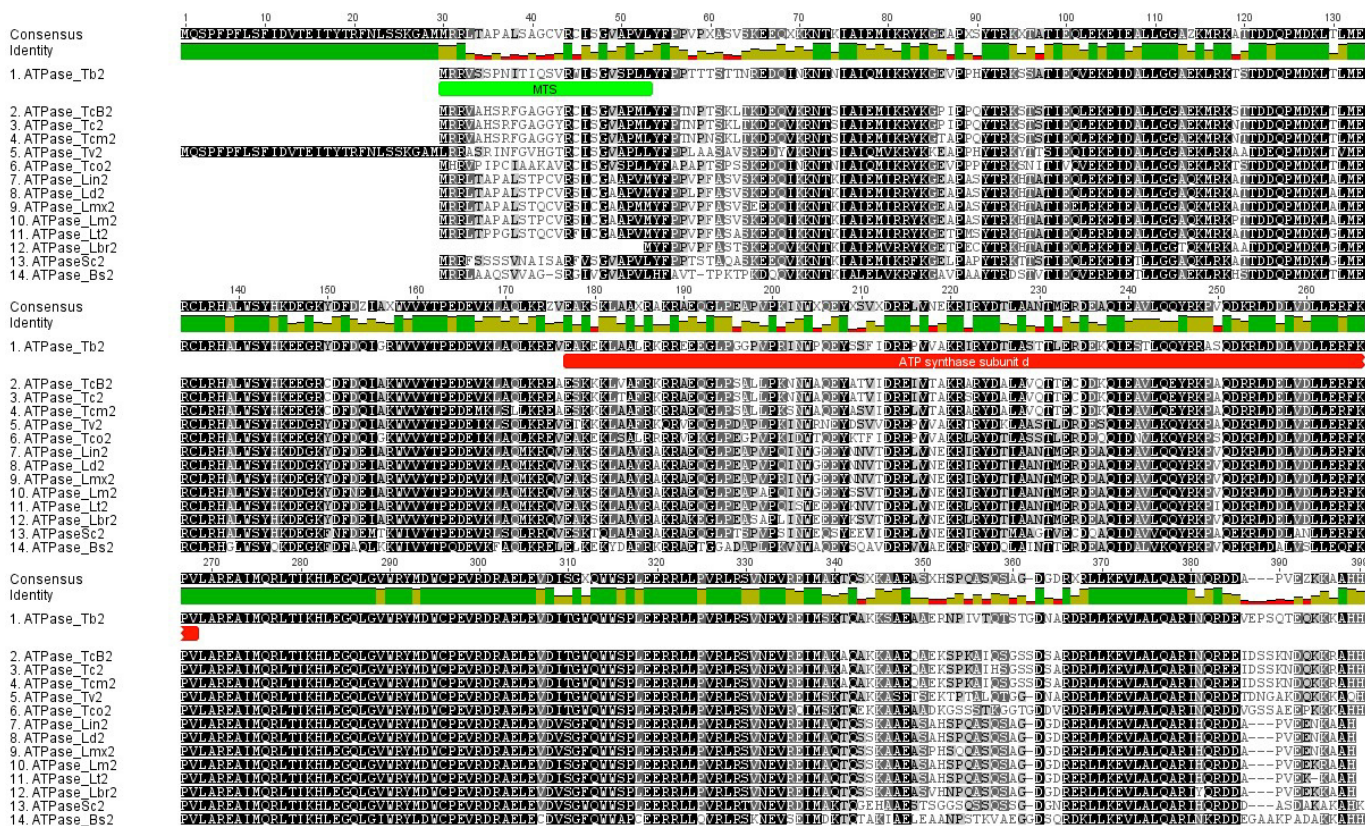
1. Jamonneau V, Ilboudo H, Kabore J, Kaba D, Koffi M, et al. (2012) Untreated human infections by *Trypanosoma brucei gambiense* are not 100% fatal. *PLoS Negl Trop Dis* 6: e1691. doi: [10.1371/journal.pntd.0001691](https://doi.org/10.1371/journal.pntd.0001691) PMID: [22720107](https://pubmed.ncbi.nlm.nih.gov/22720107/)
2. Stuart K, Brun R, Croft S, Fairlamb A, Gurtler RE, et al. (2008) Kinetoplastids: related protozoan pathogens, different diseases. *J Clin Invest* 118: 1301–1310. doi: [10.1172/JCI33945](https://doi.org/10.1172/JCI33945) PMID: [18382742](https://pubmed.ncbi.nlm.nih.gov/18382742/)
3. Steverding D (2008) The history of African trypanosomiasis. *Parasit Vectors* 1: 3. doi: [10.1186/1756-3305-1-3](https://doi.org/10.1186/1756-3305-1-3) PMID: [18275594](https://pubmed.ncbi.nlm.nih.gov/18275594/)
4. Bringaud F, Riviere L, Coustou V (2006) Energy metabolism of trypanosomatids: adaptation to available carbon sources. *Mol Biochem Parasitol* 149: 1–9. PMID: [16682088](https://pubmed.ncbi.nlm.nih.gov/16682088/)
5. Besteiro S, Barrett MP, Riviere L, Bringaud F (2005) Energy generation in insect stages of *Trypanosoma brucei*: metabolism in flux. *Trends Parasitol* 21: 185–191. PMID: [15780841](https://pubmed.ncbi.nlm.nih.gov/15780841/)
6. Hannaert V, Bringaud F, Opperdoes FR, Michels PA (2003) Evolution of energy metabolism and its compartmentation in Kinetoplastida. *Kinetoplastid Biol Dis* 2: 11. PMID: [14613499](https://pubmed.ncbi.nlm.nih.gov/14613499/)
7. Brown SV, Hosking P, Li J, Williams N (2006) ATP synthase is responsible for maintaining mitochondrial membrane potential in bloodstream form *Trypanosoma brucei*. *Eukaryot Cell* 5: 45–53. PMID: [16400167](https://pubmed.ncbi.nlm.nih.gov/16400167/)
8. Guler JL, Kriegova E, Smith TK, Lukes J, Englund PT (2008) Mitochondrial fatty acid synthesis is required for normal mitochondrial morphology and function in *Trypanosoma brucei*. *Mol Microbiol* 67: 1125–1142. doi: [10.1111/j.1365-2958.2008.06112.x](https://doi.org/10.1111/j.1365-2958.2008.06112.x) PMID: [18221265](https://pubmed.ncbi.nlm.nih.gov/18221265/)
9. Nolan DP, Voorheis HP (1992) The mitochondrion in bloodstream forms of *Trypanosoma brucei* is energized by the electrogenic pumping of protons catalysed by the F1F0-ATPase. *Eur J Biochem* 209: 207–216. PMID: [1327770](https://pubmed.ncbi.nlm.nih.gov/1327770/)
10. Huang G, Vercesi AE, Docampo R (2013) Essential regulation of cell bioenergetics in *Trypanosoma brucei* by the mitochondrial calcium uniporter. *Nat Commun* 4: 2865. doi: [10.1038/ncomms3865](https://doi.org/10.1038/ncomms3865) PMID: [24305511](https://pubmed.ncbi.nlm.nih.gov/24305511/)
11. Vercesi AE, Docampo R, Moreno SN (1992) Energization-dependent Ca²⁺ accumulation in *Trypanosoma brucei* bloodstream and procyclic trypomastigotes mitochondria. *Mol Biochem Parasitol* 56: 251–257. PMID: [1484549](https://pubmed.ncbi.nlm.nih.gov/1484549/)
12. Kovarova J, Horakova E, Changmai P, Vancova M, Lukes J (2014) Mitochondrial and nucleolar localization of cysteine desulfurase Nfs and the scaffold protein Isu in *Trypanosoma brucei*. *Eukaryot Cell* 13: 353–362. doi: [10.1128/EC.00235-13](https://doi.org/10.1128/EC.00235-13) PMID: [24243795](https://pubmed.ncbi.nlm.nih.gov/24243795/)
13. Mazet M, Morand P, Biran M, Bouyssou G, Courtois P, et al. (2013) Revisiting the central metabolism of the bloodstream forms of *Trypanosoma brucei*: production of acetate in the mitochondrion is essential for parasite viability. *PLoS Negl Trop Dis* 7: e2587. doi: [10.1371/journal.pntd.0002587](https://doi.org/10.1371/journal.pntd.0002587) PMID: [24367711](https://pubmed.ncbi.nlm.nih.gov/24367711/)
14. Schnauffer A, Clark-Walker GD, Steinberg AG, Stuart K (2005) The F1-ATP synthase complex in bloodstream stage trypanosomes has an unusual and essential function. *EMBO J* 24: 4029–4040. PMID: [16270030](https://pubmed.ncbi.nlm.nih.gov/16270030/)
15. Buchet K, Godinot C (1998) Functional F1-ATPase essential in maintaining growth and membrane potential of human mitochondrial DNA-depleted rho degrees cells. *J Biol Chem* 273: 22983–22989. PMID: [9722521](https://pubmed.ncbi.nlm.nih.gov/9722521/)
16. Dean S, Gould MK, Dewar CE, Schnauffer AC (2013) Single point mutations in ATP synthase compensate for mitochondrial genome loss in trypanosomes. *Proc Natl Acad Sci U S A* 110: 14741–14746. doi: [10.1073/pnas.1305404110](https://doi.org/10.1073/pnas.1305404110) PMID: [23959897](https://pubmed.ncbi.nlm.nih.gov/23959897/)
17. Brun R, Hecker H, Lun ZR (1998) *Trypanosoma evansi* and *T. equiperdum*: distribution, biology, treatment and phylogenetic relationship (a review). *Vet Parasitol* 79: 95–107. PMID: [9806490](https://pubmed.ncbi.nlm.nih.gov/9806490/)
18. Stuart KD (1971) Evidence for the retention of kinetoplast DNA in an acriflavine-induced dyskinetoplastic strain of *Trypanosoma brucei* which replicates the altered central element of the kinetoplast. *J Cell Biol* 49: 189–195. PMID: [4102002](https://pubmed.ncbi.nlm.nih.gov/4102002/)
19. Lai DH, Hashimi H, Lun ZR, Ayala FJ, Lukes J (2008) Adaptations of *Trypanosoma brucei* to gradual loss of kinetoplast DNA: *Trypanosoma equiperdum* and *Trypanosoma evansi* are petite mutants of *T. brucei*. *Proc Natl Acad Sci U S A* 105: 1999–2004. doi: [10.1073/pnas.0711799105](https://doi.org/10.1073/pnas.0711799105) PMID: [18245376](https://pubmed.ncbi.nlm.nih.gov/18245376/)
20. Walker JE (2013) The ATP synthase: the understood, the uncertain and the unknown. *Biochem Soc Trans* 41: 1–16. doi: [10.1042/BST20110773](https://doi.org/10.1042/BST20110773) PMID: [23356252](https://pubmed.ncbi.nlm.nih.gov/23356252/)
21. Devenish RJ, Prescott M, Rodgers AJ (2008) The structure and function of mitochondrial F1F0-ATP synthases. *Int Rev Cell Mol Biol* 267: 1–58. doi: [10.1016/S1937-6448\(08\)00601-1](https://doi.org/10.1016/S1937-6448(08)00601-1) PMID: [18544496](https://pubmed.ncbi.nlm.nih.gov/18544496/)

22. Walker JE, Dickson VK (2006) The peripheral stalk of the mitochondrial ATP synthase. *Biochim Biophys Acta* 1757: 286–296. PMID: [16697972](#)
23. Dickson VK, Silvester JA, Fearnley IM, Leslie AG, Walker JE (2006) On the structure of the stator of the mitochondrial ATP synthase. *EMBO J* 25: 2911–2918. PMID: [16791136](#)
24. Vaidya AB, Mather MW (2009) Mitochondrial evolution and functions in malaria parasites. *Annu Rev Microbiol* 63: 249–267. doi: [10.1146/annurev.micro.091208.073424](#) PMID: [19575561](#)
25. Lapaille M, Escobar-Ramirez A, Degand H, Baurain D, Rodriguez-Salinas E, et al. (2010) Atypical subunit composition of the chlorophycean mitochondrial F1FO-ATP synthase and role of Asa7 protein in stability and oligomycin resistance of the enzyme. *Mol Biol Evol* 27: 1630–1644. doi: [10.1093/molbev/msq049](#) PMID: [20156838](#)
26. Zikova A, Schnauffer A, Dalley RA, Panigrahi AK, Stuart KD (2009) The F(0)F(1)-ATP synthase complex contains novel subunits and is essential for procyclic *Trypanosoma brucei*. *PLoS Pathog* 5: e1000436. doi: [10.1371/journal.ppat.1000436](#) PMID: [19436713](#)
27. Mather MW, Henry KW, Vaidya AB (2007) Mitochondrial drug targets in apicomplexan parasites. *Curr Drug Targets* 8: 49–60. PMID: [17266530](#)
28. Balabaskaran Nina P, Dudkina NV, Kane LA, van Eyk JE, Boekema EJ, et al. (2010) Highly divergent mitochondrial ATP synthase complexes in *Tetrahymena thermophila*. *PLoS Biol* 8: e1000418. doi: [10.1371/journal.pbio.1000418](#) PMID: [20644710](#)
29. Nishi A, Scherbaum OH (1962) Oxidative phosphorylation in synchronized cultures of *Tetrahymena pyriformis*. *Biochim Biophys Acta* 65: 419–424. PMID: [13938753](#)
30. Uyemura SA, Luo S, Vieira M, Moreno SN, Docampo R (2004) Oxidative phosphorylation and rotenone-insensitive malate- and NADH-quinone oxidoreductases in *Plasmodium yoelii yoelii* mitochondria in situ. *J Biol Chem* 279: 385–393. PMID: [14561763](#)
31. Vazquez-Acevedo M, Cardol P, Cano-Estrada A, Lapaille M, Remacle C, et al. (2006) The mitochondrial ATP synthase of chlorophycean algae contains eight subunits of unknown origin involved in the formation of an atypical stator-stalk and in the dimerization of the complex. *J Bioenerg Biomembr* 38: 271–282. PMID: [17160464](#)
32. Hashimi H, Benkovicova V, Cermakova P, Lai DH, Horvath A, et al. (2010) The assembly of F(1)F(O)-ATP synthase is disrupted upon interference of RNA editing in *Trypanosoma brucei*. *Int J Parasitol* 40: 45–54. doi: [10.1016/j.ijpara.2009.07.005](#) PMID: [19654010](#)
33. Chi TB, Brown BS, Williams N (1998) Subunit 9 of the mitochondrial ATP synthase of *Trypanosoma brucei* is nuclearly encoded and developmentally regulated. *Mol Biochem Parasitol* 92: 29–38. PMID: [9574907](#)
34. Claros MG, Vincens P (1996) Computational method to predict mitochondrially imported proteins and their targeting sequences. *Eur J Biochem* 241: 779–786. PMID: [8944766](#)
35. Biegert A, Mayer C, Remmert M, Soding J, Lupas AN (2006) The MPI Bioinformatics Toolkit for protein sequence analysis. *Nucleic Acids Res* 34: W335–339. PMID: [16845021](#)
36. Norais N, Prome D, Velours J (1991) ATP synthase of yeast mitochondria. Characterization of subunit d and sequence analysis of the structural gene ATP7. *J Biol Chem* 266: 16541–16549. PMID: [1832157](#)
37. Walker JE, Runswick MJ, Poulter L (1987) ATP synthase from bovine mitochondria. The characterization and sequence analysis of two membrane-associated sub-units and of the corresponding cDNAs. *J Mol Biol* 197: 89–100. PMID: [2890767](#)
38. Nugent T, Jones DT (2009) Transmembrane protein topology prediction using support vector machines. *BMC Bioinformatics* 10: 159. doi: [10.1186/1471-2105-10-159](#) PMID: [19470175](#)
39. Vertommen D, Van Roy J, Szikora JP, Rider MH, Michels PA, et al. (2008) Differential expression of glycosomal and mitochondrial proteins in the two major life-cycle stages of *Trypanosoma brucei*. *Mol Biochem Parasitol* 158: 189–201. doi: [10.1016/j.molbiopara.2007.12.008](#) PMID: [18242729](#)
40. Ko YH, Delannoy M, Hullihen J, Chiu W, Pedersen PL (2003) Mitochondrial ATP synthasome. Cristae-enriched membranes and a multiwell detergent screening assay yield dispersed single complexes containing the ATP synthase and carriers for Pi and ADP/ATP. *J Biol Chem* 278: 12305–12309. PMID: [12560333](#)
41. Meyer B, Wittig I, Trifilieff E, Karas M, Schagger H (2007) Identification of two proteins associated with mammalian ATP synthase. *Mol Cell Proteomics* 6: 1690–1699. PMID: [17575325](#)
42. Chen Y, Hung CH, Burdener T, Lee GS (2003) Development of RNA interference revertants in *Trypanosoma brucei* cell lines generated with a double stranded RNA expression construct driven by two opposing promoters. *Mol Biochem Parasitol* 126: 275–279. PMID: [12615326](#)
43. Bowler MW, Montgomery MG, Leslie AG, Walker JE (2006) How azide inhibits ATP hydrolysis by the F-ATPases. *Proc Natl Acad Sci U S A* 103: 8646–8649. PMID: [16728506](#)

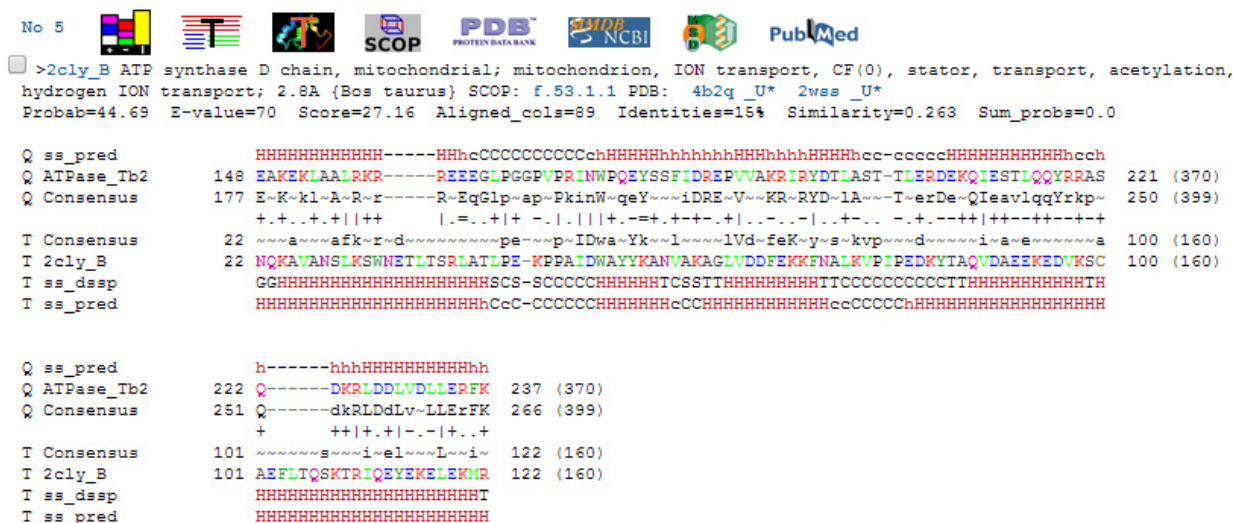
44. Appleby RD, Porteous WK, Hughes G, James AM, Shannon D, et al. (1999) Quantitation and origin of the mitochondrial membrane potential in human cells lacking mitochondrial DNA. *Eur J Biochem* 262: 108–116. PMID: [10231371](#)
45. Garcia JJ, Ogilvie I, Robinson BH, Capaldi RA (2000) Structure, functioning, and assembly of the ATP synthase in cells from patients with the T8993G mitochondrial DNA mutation—Comparison with the enzyme in Rho(0) cells completely lacking mtDNA. *Journal of Biological Chemistry* 275: 11075–11081. PMID: [10753912](#)
46. Wittig I, Meyer B, Heide H, Steger M, Bleier L, et al. (2010) Assembly and oligomerization of human ATP synthase lacking mitochondrial subunits a and A6L. *Biochim Biophys Acta* 1797: 1004–1011. doi: [10.1016/j.bbabi.2010.02.021](#) PMID: [20188060](#)
47. Stock D, Leslie AG, Walker JE (1999) Molecular architecture of the rotary motor in ATP synthase. *Science* 286: 1700–1705. PMID: [10576729](#)
48. Strauss M, Hofhaus G, Schroder RR, Kuhlbrandt W (2008) Dimer ribbons of ATP synthase shape the inner mitochondrial membrane. *EMBO J* 27: 1154–1160. doi: [10.1038/emboj.2008.35](#) PMID: [18323778](#)
49. Arnold I, Pfeiffer K, Neupert W, Stuart RA, Schagger H (1998) Yeast mitochondrial F1F0-ATP synthase exists as a dimer: identification of three dimer-specific subunits. *EMBO J* 17: 7170–7178. PMID: [9857174](#)
50. Burger G, Lang BF, Braun HP, Marx S (2003) The enigmatic mitochondrial ORF ymf39 codes for ATP synthase chain b. *Nucleic Acids Res* 31: 2353–2360. PMID: [12711680](#)
51. Heazlewood JL, Whelan J, Millar AH (2003) The products of the mitochondrial orf25 and orfB genes are FO components in the plant F1FO ATP synthase. *FEBS Lett* 540: 201–205. PMID: [12681508](#)
52. Miranda-Astudillo H, Cano-Estrada A, Vazquez-Acevedo M, Colina-Tenorio L, Downie-Velasco A, et al. (2014) Interactions of subunits Asa2, Asa4 and Asa7 in the peripheral stalk of the mitochondrial ATP synthase of the chlorophycean alga *Polytomella* sp. *Biochim Biophys Acta* 1837: 1–13. doi: [10.1016/j.bbabi.2013.08.001](#) PMID: [23933283](#)
53. van Lis R, Mendoza-Hernandez G, Groth G, Atteia A (2007) New insights into the unique structure of the F0F1-ATP synthase from the chlamydomonad algae *Polytomella* sp. and *Chlamydomonas reinhardtii*. *Plant Physiol* 144: 1190–1199. PMID: [17468226](#)
54. Chevallet M, Lescuyer P, Diemer H, van Dorsselaer A, Leize-Wagner E, et al. (2006) Alterations of the mitochondrial proteome caused by the absence of mitochondrial DNA: A proteomic view. *Electrophoresis* 27: 1574–1583. PMID: [16548050](#)
55. Orian JM, Hadikusumo RG, Marzuki S, Linnane AW (1984) Biogenesis of mitochondria: defective yeast H⁺-ATPase assembled in the absence of mitochondrial protein synthesis is membrane associated. *J Bioenerg Biomembr* 16: 561–581. PMID: [6242247](#)
56. Paul MF, Velours J, Arselin de Chateaubodeau G, Aigle M, Guerin B (1989) The role of subunit 4, a nuclear-encoded protein of the F0 sector of yeast mitochondrial ATP synthase, in the assembly of the whole complex. *Eur J Biochem* 185: 163–171. PMID: [2553400](#)
57. Rak M, Gokova S, Tzagoloff A (2011) Modular assembly of yeast mitochondrial ATP synthase. *EMBO J* 30: 920–930. doi: [10.1038/emboj.2010.364](#) PMID: [21266956](#)
58. Chen C, Ko Y, Delannoy M, Ludtke SJ, Chiu W, et al. (2004) Mitochondrial ATP synthasome: three-dimensional structure by electron microscopy of the ATP synthase in complex formation with carriers for Pi and ADP/ATP. *J Biol Chem* 279: 31761–31768. PMID: [15166242](#)
59. Alibu VP, Storm L, Haile S, Clayton C, Horn D (2005) A doubly inducible system for RNA interference and rapid RNAi plasmid construction in *Trypanosoma brucei*. *Mol Biochem Parasitol* 139: 75–82. PMID: [15610821](#)
60. Wickstead B, Ersfeld K, Gull K (2002) Targeting of a tetracycline-inducible expression system to the transcriptionally silent minichromosomes of *Trypanosoma brucei*. *Mol Biochem Parasitol* 125: 211–216. PMID: [12467990](#)
61. Surve S, Heestand M, Panicucci B, Schnauffer A, Parsons M (2012) Enigmatic presence of mitochondrial complex I in *Trypanosoma brucei* bloodstream forms. *Eukaryot Cell* 11: 183–193. doi: [10.1128/EC.05282-11](#) PMID: [22158713](#)
62. Borst P, Fase-Fowler F, Gibson WC (1987) Kinetoplast DNA of *Trypanosoma evansi*. *Mol Biochem Parasitol* 23: 31–38. PMID: [3033499](#)
63. Wirtz E, Leal S, Ochatt C, Cross GA (1999) A tightly regulated inducible expression system for conditional gene knock-outs and dominant-negative genetics in *Trypanosoma brucei*. *Mol Biochem Parasitol* 99: 89–101. PMID: [10215027](#)
64. Oeffinger M, Wei KE, Rogers R, DeGrasse JA, Chait BT, et al. (2007) Comprehensive analysis of diverse ribonucleoprotein complexes. *Nat Methods* 4: 951–956. PMID: [17922018](#)

65. Panigrahi AK, Ogata Y, Zikova A, Anupama A, Dalley RA, et al. (2009) A comprehensive analysis of *Trypanosoma brucei* mitochondrial proteome. *Proteomics* 9: 434–450. doi: [10.1002/pmic.200800477](https://doi.org/10.1002/pmic.200800477) PMID: [19105172](https://pubmed.ncbi.nlm.nih.gov/19105172/)
66. Panigrahi AK, Zikova A, Dalley RA, Acestor N, Ogata Y, et al. (2008) Mitochondrial complexes in *Trypanosoma brucei*: a novel complex and a unique oxidoreductase complex. *Mol Cell Proteomics* 7: 534–545. PMID: [18073385](https://pubmed.ncbi.nlm.nih.gov/18073385/)
67. Singha UK, Peprah E, Williams S, Walker R, Saha L, et al. (2008) Characterization of the mitochondrial inner membrane protein translocator Tim17 from *Trypanosoma brucei*. *Mol Biochem Parasitol* 159: 30–43. doi: [10.1016/j.molbiopara.2008.01.003](https://doi.org/10.1016/j.molbiopara.2008.01.003) PMID: [18325611](https://pubmed.ncbi.nlm.nih.gov/18325611/)
68. Vondruskova E, van den Burg J, Zikova A, Ernst NL, Stuart K, et al. (2005) RNA interference analyses suggest a transcript-specific regulatory role for mitochondrial RNA-binding proteins MRP1 and MRP2 in RNA editing and other RNA processing in *Trypanosoma brucei*. *J Biol Chem* 280: 2429–2438. PMID: [15504736](https://pubmed.ncbi.nlm.nih.gov/15504736/)
69. Hannaert V, Albert MA, Rigden DJ, da Silva Giotto MT, Thiemann O, et al. (2003) Kinetic characterization, structure modelling studies and crystallization of *Trypanosoma brucei* enolase. *Eur J Biochem* 270: 3205–3213. PMID: [12869196](https://pubmed.ncbi.nlm.nih.gov/12869196/)
70. Law RH, Manon S, Devenish RJ, Nagley P (1995) ATP synthase from *Saccharomyces cerevisiae*. *Methods Enzymol* 260: 133–163. PMID: [8592441](https://pubmed.ncbi.nlm.nih.gov/8592441/)
71. Wittig I, Karas M, Schagger H (2007) High resolution clear native electrophoresis for in-gel functional assays and fluorescence studies of membrane protein complexes. *Mol Cell Proteomics* 6: 1215–1225. PMID: [17426019](https://pubmed.ncbi.nlm.nih.gov/17426019/)
72. Acestor N, Zikova A, Dalley RA, Anupama A, Panigrahi AP, et al. (2011) *Trypanosoma brucei* Mitochondrial Respiratome: Composition and organization in procyclic form. *Molecular Cell Proteomics* resubmitted.
73. Acestor N, Panigrahi AK, Ogata Y, Anupama A, Stuart KD (2009) Protein composition of *Trypanosoma brucei* mitochondrial membranes. *Proteomics* 9: 5497–5508. doi: [10.1002/pmic.200900354](https://doi.org/10.1002/pmic.200900354) PMID: [19834910](https://pubmed.ncbi.nlm.nih.gov/19834910/)
74. Mayhew TM, Lucocq JM (2008) Quantifying immunogold labelling patterns of cellular compartments when they comprise mixtures of membranes (surface-occupying) and organelles (volume-occupying). *Histochem Cell Biol* 129: 367–378. doi: [10.1007/s00418-007-0375-6](https://doi.org/10.1007/s00418-007-0375-6) PMID: [18180944](https://pubmed.ncbi.nlm.nih.gov/18180944/)

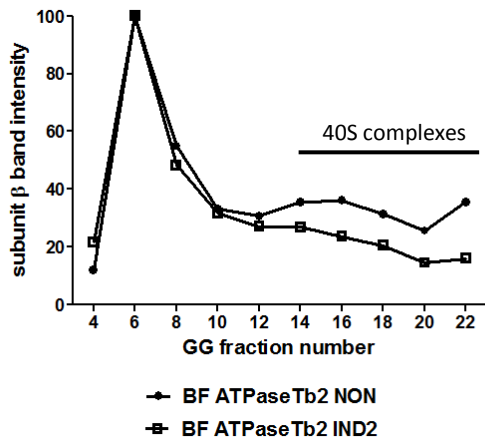
A



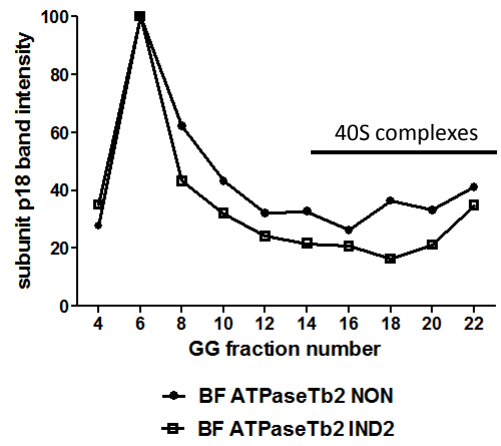
B



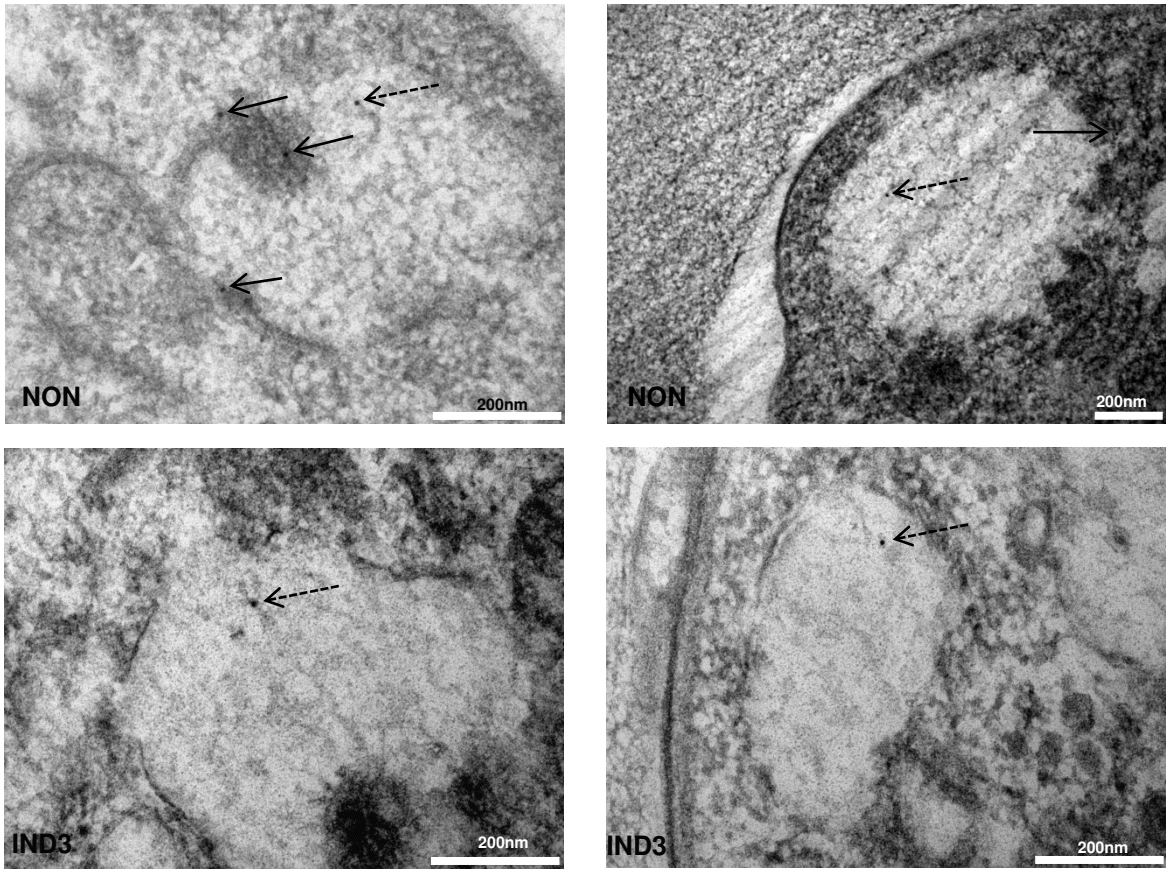
A



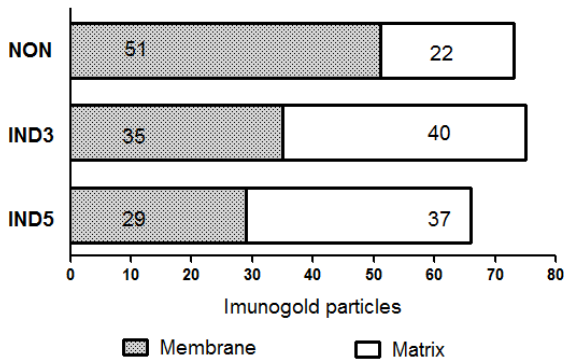
B



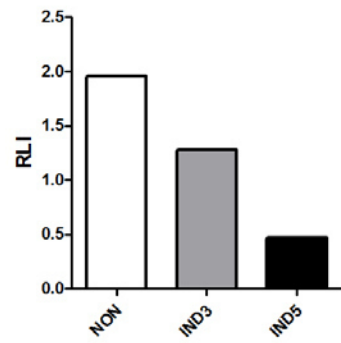
A



B



D



C

	Gold particles observed (N_{obs})	Test point number (P)	Gold particles expected (N_{exp})	χ^2 partial value
NON	51.0	1226.0	26.0	24.0
IND3	35.0	1287.0	27.3	2.2
IND5	29.0	2906.0	61.7	17.3
total	115.0	5419.0	115.0	43.5

3.1.2. The ADP/ATP carrier and its relationship to oxidative phosphorylation in ancestral protist *Trypanosoma brucei*

Reprint of: Gnipová A, Šubrtová K, Panicucci B, Horváth A, Lukeš J, Zíková A. 2015. Eukaryotic Cell 14(3), 297-310.

The ADP/ATP Carrier and Its Relationship to Oxidative Phosphorylation in Ancestral Protist *Trypanosoma brucei*

Anna Gnipová,^{a,b} Karolína Šubrtová,^{a,c} Brian Panicucci,^a Anton Horváth,^b Julius Lukeš,^{a,c,d} Alena Zíková^{a,c}

Biology Center, Institute of Parasitology, Czech Academy of Sciences, České Budějovice, Czech Republic^a; Department of Biochemistry, Faculty of Natural Sciences, Comenius University, Bratislava, Slovakia^b; Faculty of Science, University of South Bohemia, České Budějovice, Czech Republic^c; Canadian Institute for Advanced Research, Toronto, Ontario, Canada^d

The highly conserved ADP/ATP carrier (AAC) is a key energetic link between the mitochondrial (mt) and cytosolic compartments of all aerobic eukaryotic cells, as it exchanges the ATP generated inside the organelle for the cytosolic ADP. *Trypanosoma brucei*, a parasitic protist of medical and veterinary importance, possesses a single functional AAC protein (TbAAC) that is related to the human and yeast ADP/ATP carriers. However, unlike previous studies performed with these model organisms, this study showed that TbAAC is most likely not a stable component of either the respiratory supercomplex III+IV or the ATP synthasome but rather functions as a physically separate entity in this highly diverged eukaryote. Therefore, TbAAC RNA interference (RNAi) ablation in the insect stage of *T. brucei* does not impair the activity or arrangement of the respiratory chain complexes. Nevertheless, RNAi silencing of TbAAC caused a severe growth defect that coincides with a significant reduction of mt ATP synthesis by both substrate and oxidative phosphorylation. Furthermore, TbAAC downregulation resulted in a decreased level of cytosolic ATP, a higher mt membrane potential, an elevated amount of reactive oxygen species, and a reduced consumption of oxygen in the mitochondria. Interestingly, while TbAAC has previously been demonstrated to serve as the sole ADP/ATP carrier for ADP influx into the mitochondria, our data suggest that a second carrier for ATP influx may be present and active in the *T. brucei* mitochondrion. Overall, this study provides more insight into the delicate balance of the functional relationship between TbAAC and the oxidative phosphorylation (OXPHOS) pathway in an early diverged eukaryote.

The origination event of an ADP/ATP carrier (AAC) was crucial in the evolution of the present-day mitochondrion that enabled it to become the powerhouse of the eukaryotic cell. Due to the activity of AAC, the energy-producing mitochondria can supply the cytosol with ATP molecules, which fuel most cellular reactions. AAC belongs to the well-defined family of mitochondrial (mt) carrier proteins that are located in the inner mt membrane and are involved in the transport of a wide range of metabolites (1). Under physiological aerobic conditions, AAC is responsible for the 1:1 counterexchange of mt ATP for cytosolic ADP (2).

mt ATP is produced mainly by the evolutionarily conserved biochemical pathway of oxidative phosphorylation (OXPHOS), which employs respiratory complexes I through IV to convert the redox energy of various mt substrates into an electrochemical proton gradient ($\Delta\psi_m$) across the mt inner membrane. Respiratory complexes I (NADH-ubiquinone oxidoreductase) and II (succinate-ubiquinone oxidoreductase) are responsible for the oxidation of reduced NADH and FADH₂, respectively. The electrons derived from these biochemical processes continue along the electron transport chain as they are sequentially passed to coenzyme Q, complex III (ubiquinol-cytochrome *c* oxidoreductase), cytochrome *c*, complex IV (cytochrome *c*-O₂ oxidoreductase), and finally oxygen, the terminal electron acceptor. The electron movement up the redox potential is coupled with proton translocation into the intermembrane space, resulting in the $\Delta\psi_m$. The protons are then permitted to flow down their concentration gradient and return to the mt matrix via F₀F₁-ATP synthase, which harnesses this potential energy to rotate its macromolecular enzymatic machine to generate ATP from ADP and inorganic phosphate (P_i). These two substrates are transported into the mt matrix via their carrier proteins, AAC and the phosphate carrier (P_iC).

In some eukaryotes, OXPHOS complexes form higher-order

assemblies or supercomplexes to promote faster diffusion of the substrate molecules and increase respiration efficiency (3). Complexes I, III, and IV have been found to form different types of supercomplexes (i.e., I+III₂, III₂+IV₂, and I+III₂+IV₁₋₄) in a wide range of organisms (4). Moreover, F₀F₁-ATP synthase forms dimers that appear to be crucial for mt inner membrane folding and consequently crista morphology (5, 6). Though the translocase activity of AAC is self-contained within a single protein (7), in yeast, this transporter can be found also as a homodimer (8) or as a component of supercomplexes composed of complexes III and IV and the TIM23 translocase (9, 10). Moreover, in rat mitochondria, a minor population of AAC was also detected in a supercomplex comprised of the F₀F₁-ATP synthase and P_iC, forming the ATP synthasome (11, 12).

Organization of proton translocation OXPHOS components into supercomplexes seems to be absent in the early-branching protist *Trypanosoma brucei*, a member of the eukaryotic supergroup Excavata (13). *T. brucei* is a flagellated parasite of major medical and veterinary importance, causing sleeping sickness in

Received 22 October 2014 Accepted 16 January 2015

Accepted manuscript posted online 23 January 2015

Citation Gnipová A, Šubrtová K, Panicucci B, Horváth A, Lukeš J, Zíková A. 2015. The ADP/ATP carrier and its relationship to oxidative phosphorylation in ancestral protist *Trypanosoma brucei*. *Eukaryot Cell* 14:297–310. doi:10.1128/EC.00238-14.

Address correspondence to Alena Zíková, azikova@paru.cas.cz.

Supplemental material for this article may be found at <http://dx.doi.org/10.1128/EC.00238-14>.

Copyright © 2015, American Society for Microbiology. All Rights Reserved. doi:10.1128/EC.00238-14

humans and nagana in cattle (14, 15). The morphology and biochemical activity of its single mitochondrion differs dramatically between life stages as the parasite alternates between the insect vector and a mammalian host (16). Since amino acids (e.g., proline and threonine) in the midgut of the insect vector constitute the main energy source available to the procyclic form of trypanosomes (PF), they maintain a well-developed mitochondrion with abundant cristae, Krebs cycle enzymes, and a fully active cytochrome-mediated respiratory chain that is coupled to ATP production by F_0F_1 -ATP synthase (17, 18). In addition to OXPHOS, significant amounts of ATP are also produced by mt substrate phosphorylation (19). In this life stage, TbAAC works in its forward mode, importing ADP into the organelle while concurrently exporting ATP to the cytosol.

In contrast, the mammalian bloodstream stage (BS) relies solely on the host's abundant glucose, which is catabolized by the inefficient glycolysis pathway to meet its energy demands (20). The conventional respiratory pathway is absent, and the mt reducing equivalents are reoxidized by another route composed of an alternative oxidase and alternative dehydrogenase (21, 22). Importantly, this process is not coupled to proton translocation; thus, the $\Delta\psi_m$ is maintained by the reverse activity of F_0F_1 -ATPase, while AAC presumably supplies the enzyme with the requisite ATP substrate (23, 24).

The *T. brucei* genome encodes two different proteins, Tb927.8.1310 and TbAAC, with the latter being represented by three identical and consecutively arranged genes (Tb927.10.14820, -30, and -40) and showing significant amino acid sequence similarity to functionally characterized AACs from other eukaryotes (25). Importantly, TbAAC exhibits biochemical properties and ADP/ATP exchange kinetics similar to the main yeast carrier, AAC2, while Tb927.8.1310 lacks the canonical sequence features required for ADP/ATP exchange activity (26). Furthermore, RNA interference (RNAi) studies demonstrated that TbAAC is essential for the growth of PF cells and therefore must function as the main ADP/ATP carrier in PF mitochondria (26).

Since PF *T. brucei* represents an ancestral eukaryote possessing typical mt functions (27), we explored the relationship between TbAAC and the other OXPHOS components. Our analysis of the structural and functional interactome of TbAAC reveals that it exists as a physically separate entity that could not be detected as a stable component of either respiratory complex III or IV or F_0F_1 -ATP synthase. Furthermore, the activities of the OXPHOS complexes were not impaired upon TbAAC RNAi silencing. However, TbAAC depletion induced a cellular ADP/ATP imbalance followed by low levels of cytosolic ATP, higher $\Delta\psi_m$, elevated quantities of reactive oxygen species (ROS), and reduced mt oxygen consumption. In summary, the apparent lack of a tight physical interaction between TbAAC and the OXPHOS pathway hints at the unique functional relationships between these fundamental components of the PF *T. brucei* mt bioenergetics.

MATERIALS AND METHODS

Plasmid construction. To create the TbAAC (Tb927.10.14820, Tb927.10.14830, and Tb927.10.14840) RNAi construct, a 901-bp fragment that is identical for each of the TbAAC genes was PCR amplified from *T. brucei* strain 427 genomic DNA with the oligonucleotides CTC GAG CGG ATA AAA AGC GG (FW) and GGA TCC TCC ACA TAA ATG GGT (REV), utilizing the respective XhoI and BamHI restriction sites inherent in the primers (underlined). The digested amplicon was then cloned into the p2T7-177 plasmid (28). For the inducible expression of TbAAC fused with a C-terminal v5 tag, the TbAAC coding sequence was PCR amplified with the primers CAC

AAG CTT ATG ACG GAT AAA AAG and CAC GGA TCC ATT CGA TCT GCG CCA C and then cloned into the pT7_v5 (29) vector using the HindIII and BamHI restriction sites (underlined). The construction of the pLEW79MHTAP vectors for the tetracycline (Tet)-inducible expression of tandem affinity purification (TAP)-tagged F_0F_1 -ATPase subunits p18 (Tb927.5.1710) and β (Tb927.3.1380) was described previously (18). For the constitutive expression of firefly luciferase in the cytosol of PF *T. brucei*, the luciferase reporter gene was PCR amplified from pLEW79 vector using the primers GC AAG CTT ATG GAA GAC GCC AAA AAC (FW) and GCT GGA TCC TTA CTT CTT GGC CTT TAT G (REV). The PCR amplicon was subcloned to PGEM-T Easy vector (Promega) and cloned into pHD1344tub plasmid (a kind gift from Achim Schnauffer) using HindIII and BamHI restriction sites.

Cell growth, transfection, and RNAi induction. PF *T. brucei* strain 29-13 cells are transgenic for both the T7 RNA polymerase and the Tet repressor (30). Grown *in vitro* at 27°C in SDM-79 medium containing hemin (7.5 mg/ml), hygromycin (25 μ g/ml), G-418 (10 μ g/ml), and 10% fetal bovine serum, these cells were used as the parental cell line for p2T7-177 and pT7_v5 transfections. Both of these plasmids were linearized with NotI and stably transfected into the minichromosome 177-bp repeat region and the rDNA spacer, respectively (28, 31). Cell lines containing p2T7-177 were selected with phleomycin (2.5 μ g/ml), while cells transfected with the pT7_v5 plasmid were selected with puromycin (1 μ g/ml). The TbAAC RNAi cell line was used as a parental cell line for pHD1344tub transfection and selected with puromycin. The inducible expression of double-stranded RNA (dsRNA) or the TbAAC_v5-tagged protein was triggered by the addition of 1 μ g/ml Tet to the medium. Growth curves were generated by measuring the cell density of Tet-treated and untreated cultures using the Z2 cell counter (Beckman Coulter Inc.). Throughout the experiments, cells were split daily to ensure that they continuously maintained an exponential growth phase of 10^6 to 10^7 cells/ml.

Immunoprecipitation and affinity purification methods. Mitochondria from TbAAC_v5, β _TAP, and p18_TAP cell lines were hypotonically purified from 4×10^9 noninduced and Tet-induced cells (day 2) as described earlier (32). mt pellets were resuspended in the appropriate buffer (TbAAC_v5 mitochondria in IPP100 buffer consisting of 100 mM KCl, 10 mM $MgCl_2$, and 10 mM Tris-HCl, pH 7.2; TAP mt pellets in another IPP100 buffer comprised of 100 mM KCl, 0.1% NP-40 and 10 mM Tris-HCl, pH 8.0), which was also supplemented with Complete protease inhibitors (Roche). Next, the samples were lysed with digitonin (at a detergent/protein ratio of 1 mg/mg) for 1 h on ice and then spun down ($15,000 \times g$, 1 h, 4°C). The TbAAC_v5-tagged complexes were purified using magnetic beads (Dynabeads M-280, sheep anti-mouse IgG) charged with monoclonal anti-v5 antibody. The mt lysate was incubated with the charged beads for 2 h (4°C). The beads were washed three times in PBS-T (phosphate-buffered saline with 0.05% Tween 20) and twice with IPP100 buffer before the bound protein complexes were released by the addition of SDS-PAGE loading buffer and boiling (97°C, 10 min). The β _TAP and p18_TAP cleared lysates were incubated for 2 h with IgG Sepharose 6 Fast Flow beads (GE Healthcare), which bind to protein A, a part of the TAP tag. The beads were then washed three times with IPP100 and once with a TEVCB buffer (100 mM KCl, 0.1% NP-40, 0.5 mM EDTA, 1 mM dithiothreitol [DTT], 10 mM Tris-HCl [pH 8.0]). The bound protein complexes were released by AcTEV protease (Invitrogen) cleavage (3 h, 16°C). All eluates were fractionated by SDS-PAGE and analyzed by Western blotting.

Glycerol gradient sedimentation. As described in an earlier publication (33), mt vesicles from 1×10^9 cells were isolated by hypotonic cell lysis and then incubated in a glycerol gradient lysis buffer (10 mM Tris-HCl [pH 7.2], 10 mM $MgCl_2$, 200 mM KCl, 1 mM DTT) containing dodecyl maltoside at a ratio of 1 mg detergent to 1 mg protein. The lysates were cleared by centrifugation (twice at $16,000 \times g$ for 30 min at 4°C), loaded onto an 11-ml 10-to-30% glycerol gradient, and sedimented by ultracentrifugation (SW40 rotor; Beckman Instruments) at $38,000 \times g$ for 12 h. Fractions (500 μ l) were collected and stored at -70°C.

Electrophoresis and Western blot analysis. Two-dimensional (2-D) PAGE analysis was performed by fractionating 100 μg of mt lysate on a 3 to 8% high-resolution clear native (hrCN) PAGE gel, which was then further resolved on a 10% Tricine-SDS-PAGE gel (34). After electrophoresis, the proteins were transferred onto a nitrocellulose membrane and probed with specific antibodies.

Protein samples from whole-cell lysates, mt lysates, and glycerol gradient fractions were separated on SDS-PAGE gels, blotted onto nitrocellulose membrane, and probed with the appropriate monoclonal (MAB) or polyclonal (PAb) antibody. This was followed by incubation with a secondary horseradish peroxidase (HRP)-conjugated anti-rabbit or anti-mouse antibody (1:2,000; Bio-Rad). Proteins were visualized using the Clarity Western enhanced chemiluminescence (ECL) substrate (Bio-Rad) on a ChemiDoc instrument (Bio-Rad). When needed, membranes were stripped at 50°C for 30 min in a stripping buffer (62.5 mM Tris-HCl [pH 6.8], 100 mM mercaptoethanol, 2% SDS) and reprobed. The PageRuler prestained protein standard (Fermentas) was used to determine the sizes of detected bands. The following primary antibodies were used in this study: a MAB against the paramyxovirus v5 tag (Invitrogen) (1:1,000), a PAb against the human *c-myc* protein (Sigma) (1:1,000), a MAB against the North American firefly luciferase (Invitrogen) (1:1,000), and a PAb against the *Leishmania tarentolae* cytochrome *c* oxidase subunit IV (trCOIV) (1:1,000) (35). Furthermore, specific antibodies raised against *T. brucei* antigens were utilized: anti-enolase PAb (1:1,000) (36), anti-mt Hsp70 MAB (1:2,000) (37), anti-apocytochrome *c* PAb (1:1,000) (38), anti-COVI PAb (1:1,000) (33), anti-ATPaseTb2 PAb (1:1,000) (39), anti- β PAb (1:2,000), and p18 PAb (1:1,000). Additional *T. brucei* antibodies against TbVDAC (1:1,000), putative TbP₁C (Tb927.9.10310; 1:1,000) (25), TbAAC (1:1,000), and complex III subunit Rieske (1:1,000) were prepared commercially (Davids Biotechnology) by administering antigen-specific oligopeptides (TbVDAC, VDK SLK PGV LIT HS; TbP₁C, SHP ADM LVS ARG KAS NVG KS; TbAAC, VDA LKP IYV EWR RSN; and complex III subunit Rieske, LSA LKH PET DEA RFP DHR E) to rabbits following a standard immunization protocol.

In vitro and in-gel activity measurements of respiratory complexes. mt vesicles isolated from 5×10^8 trypanosomes were lysed with 2% dodecyl maltoside, and the cytochrome *c* oxidase activity was determined *in vitro* by measuring the change in absorbance of cytochrome *c* as it became oxidized after passing its electrons to cytochrome *c* oxidase (40). Cytochrome *c* reductase activity was determined in a similar way; this time, the reduction of cytochrome *c* was measured when reduced decylubiquinone (Sigma) was added as an electron donor and cytochrome *c* reductase transferred those electrons to cytochrome *c* (33). In parallel, the same dodecyl maltoside lysed mitochondrion samples were resolved (100 μg of protein per lane) on either a 6% blue native (BN) PAGE gel or a 2 to 12% BN PAGE gel to detect cytochrome *c* oxidase and F₀F₁-ATPase activities by following in-gel assays, as described in earlier work (41). The ATPase activity was measured in digitonin-extracted mitochondria as described elsewhere (18).

ATP production and ATPase assays. ATP production in digitonin-extracted mitochondria was measured following a protocol described previously (42). Briefly, crude mt fractions from the RNAi knockdown cell lines were obtained by digitonin extraction (43). ATP production in these samples was induced by the addition of 67 μM ADP and a 5 mM concentration of one of the following substrates: succinate, pyruvate, or α -ketoglutarate. The mt preparations were preincubated for 10 min on ice with the inhibitors malonate (6.7 mM) and atractyloside (33 $\mu\text{g}/\text{ml}$). The concentration of ATP was determined by a luminometer (Orion II; Berthold Detection Systems) using the CLS II ATP bioluminescence assay kit (Roche Applied Science). ATPase activity was measured with the Sumner assay (44), which is based on the release of free phosphate when ATP is hydrolyzed by the enzyme, as defined earlier (24).

In vivo ATP measurement. Cytosolic ATP was measured *in vivo* using ATP-dependent luciferase bioluminescence. The method was adapted for *T. brucei* cells from published protocols (45, 46). Briefly, equal numbers of

PF luciferase (LUC)-expressing LUC-TbAAC noninduced and RNAi-induced cells (5×10^6) were harvested ($1,300 \times g$, 10 min, room temperature), washed with PBS (pH 7.4), and resuspended in PBS-LUC buffer (PBS [pH 7.7], 1 mM CaCl₂, 20 mM MgCl₂). The emission of light was triggered by addition of D-luciferin (50 μM ; Sigma) and immediately measured on a microplate luminometer. The cells exhibited a maximum luminescence signal 1 min after D-luciferin addition. Then the signal remained stable for at least 20 min afterwards, and it decayed at very low rate.

In vivo analysis of oxygen consumption, mt membrane potential, and ROS. Oxygen consumption of logarithmically growing cells was determined with a Clark-type polarographic electrode (1302 microcathode oxygen electrode, model 782; Strathkelvin Instruments) as described previously (41). Tetramethylrhodamine ethyl ester (TMRE; 60 nM; Molecular Probes) uptake was used to measure the mt membrane potential, whereas 2',7'-dichlorofluorescein diacetate (DCFH-DA; 10 μM ; Sigma) was implemented to monitor ROS production. Both methods were performed as described earlier (41).

Nuclear and kinetoplast DNA staining. Logarithmically grown non-induced and RNAi-induced cells were pelleted by centrifugation, washed, fixed with 4% formaldehyde, and treated with DAPI (4',6-diamidino-2-phenylindole; Sigma) to visualize nuclear and mt DNA. The images of the stained cells and their fluorescence were captured on a Axioplan2 imaging fluorescence microscope (Zeiss) equipped with a charge-coupled device (CCD) camera and the appropriate filters.

RESULTS

2-D PAGE reveals that a minor proportion of TbAAC migrates at higher molecular weights. To investigate potential TbAAC interactions within the mt inner membrane, purified mt vesicles were solubilized using digitonin and dodecyl maltoside at different detergent/protein ratios and then resolved by 2-D electrophoresis. These detergents are mild, nonionic surfactants that are capable of releasing membrane embedded protein complexes without disrupting internal protein-protein interactions. Furthermore, these surfactants are commonly applied in 2-D PAGE analyses and were extensively used to determine the AAC interactome in mammalian and yeast cells (9, 47–49). Therefore, detergent-solubilized mt complexes were resolved in a two-step process: by high-resolution clear native (hrCN) PAGE in the first dimension, followed by a second dimension of denaturing Tricine-SDS-PAGE. After proteins had been transferred to a nitrocellulose membrane, the Western blot was probed with an anti-TbAAC antibody (Fig. 1A). Interestingly, while a significant majority of TbAAC was detected in the lower-molecular-weight region, which likely depicts the monomeric protein, a portion of the signal also extended into a range of much higher molecular masses, culminating in two distinct peaks (Fig. 1A, middle, arrowheads). This signal is most intense when digitonin is used at a ratio of 1 mg/1 mg mt proteins, although comparable results were obtained when the isolated mitochondria were solubilized with dodecyl maltoside (data not shown).

While it is possible that these large TbAAC complexes are just aggregates of AAC that have not been separated with these mild detergents, we aimed to address whether these higher-molecular-weight TbAAC complexes might colocalize with any of the previously identified OXPHOS components, specifically with the respiratory complex IV and/or the F₀F₁-ATP synthasome (complex V and P₁C). A Western blot containing mt proteins resolved by the same 2-D PAGE conditions (1 mg digitonin/1 mg mt proteins) was immunodecorated with specific antibodies that recognize subunit COVI of complex IV, subunit β of complex V, and TbP₁C

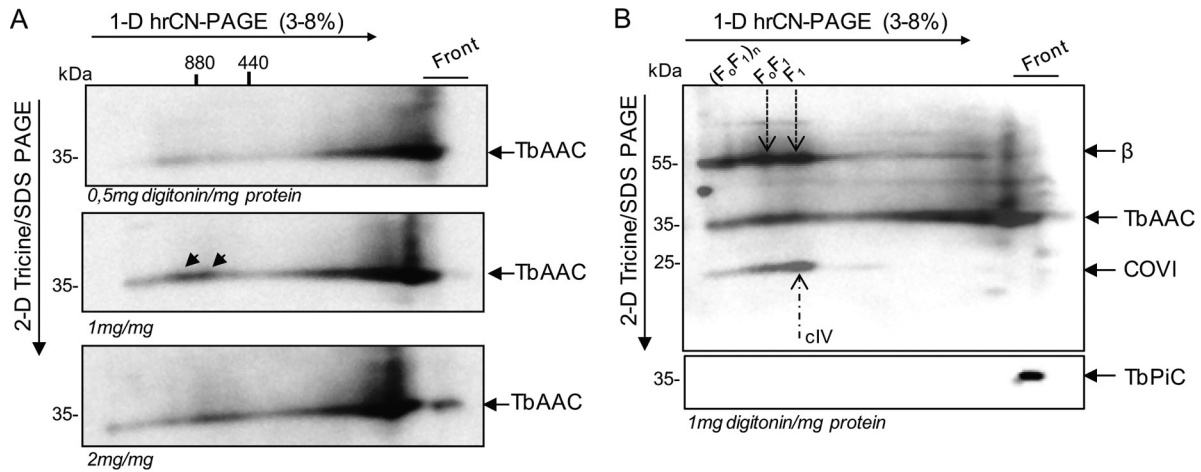


FIG 1 TbAAC colocalizes with higher-molecular-weight complexes. (A) The hypotonically purified mitochondria were solubilized using digitonin (0.5 mg, 1 mg, and 2 mg detergent/mg protein) and separated on a 3 to 8% hrCN PAGE. Isolated lanes from these native gels were further processed in the second dimension by denaturing Tricine-SDS-PAGE, and the gel was blotted on a nitrocellulose membrane for immunodetection using a polyclonal anti-TbAAC antibody. “Front” indicates the leading edge of the first-dimensional gel. The sizes of the native molecular mass markers are indicated on top of the first panel. The protein marker for the second dimension is indicated on the left. (B) The nitrocellulose membrane containing mitochondria lysed with 1 mg digitonin/mg mt protein was stripped and further probed individually with trypanosome-specific polyclonal antibodies against subunit COVI (complex IV), subunit β (F_0F_1 -ATP synthase), and P_iC . The positions of monomeric and oligomeric F_0F_1 -ATP synthase and complex IV are denoted by arrows. The resulting compilation of Western images was overlaid using Adobe Photoshop.

to identify the complexes listed above, respectively (Fig. 1B). Notably, the peak signals detected for complex IV and F_0F_1 -ATP synthase (Fig. 1B, dashed arrows) approximately colocalize with the higher-molecular-weight TbAAC bands, offering indirect proof that a minor fraction of TbAAC may interact with these protein complexes. Upon closer inspection, the main peak of complex IV and F_1 seems to lead the AAC peaks. While the trailing edge of the smear for cytochrome *c* oxidase does overlap the largest AAC peak, this portion of AAC better aligns with the distinct peak of F_0F_1 -ATP synthase. However, TbP_iC , a key component of the ATP synthasome, is clearly confined to the dye front of the hrCN PAGE. This observation weakens the possibility of the existence of a canonical ATP synthasome composed of complex V, AAC, and P_iC in trypanosomes.

TbAAC is not a stable component of respiratory complex III, IV, or V. While the observed colocalization of TbAAC with cytochrome *c* oxidase and F_0F_1 -ATP synthase in 2-D hrCN-Tricine-SDS-PAGE is intriguing, we wanted to further verify a direct and stable interaction between these components via immunoprecipitation experiments. Therefore, the ectopic expression of a C-terminally v5-tagged TbAAC protein was induced by Tet in the PF 29-13 cell line. The tagged TbAAC_v5 was immunoprecipitated using magnetic beads charged with anti-mouse IgG and a specific anti-v5 monoclonal antibody. Bound TbAAC_v5 proteins were then eluted from the beads by SDS treatment, and the specificity of the reaction was confirmed by TbAAC Western blot analysis of immunoprecipitated material from noninduced and Tet-induced cells. While no TbAAC signal was detected in the eluate from noninduced cells, a band of the expected size was visible in the sample from Tet-induced *T. brucei* cells (Fig. 2A). Therefore, the obtained eluates were further examined using specific antibodies to detect core subunits of complex III (Rieske), IV (trCOIV), and F_0F_1 -ATP synthase (β). No signal for Rieske or trCOIV was detected, indicating that there is no stable interaction between TbAAC and complex III or IV (Fig. 2A) under these conditions.

The initial analysis concerning a possible interaction with the F_0F_1 -ATP synthase was quite optimistic, as subunit β was enriched in the eluate from Tet-induced TbAAC_v5 cells, even though a basal level was also detected in the noninduced sample. Therefore, to determine if subunit β is just a spurious contaminant, we employed cell lines wherein either subunit β or p18 is TAP tagged to perform a reciprocal analysis involving the affinity purification of F_0F_1 -ATP synthase, as previously described (18) (Fig. 2B). Western blot analysis using specific antibodies against either the tag (anti-*c-myc*) or F_0F_1 -ATP synthase (F_1 moiety, subunit β and p18; F_0 moiety, ATPaseTb2) (39) validated a successful purification, while a specific antibody against TbAAC was implemented to detect if there is an interaction between this protein and F_0F_1 -ATP synthase. The absence of TbAAC in the eluates demonstrates that this protein does not stably associate with F_0F_1 -ATP synthase (Fig. 2B) when it is purified in this manner.

TbAAC is essential for the growth of PF *T. brucei* cells. Since we were not able to detect any stable structural interactions for TbAAC with *T. brucei* respiratory complexes IV and V, we next explored the possibility of functional associations between this protein and the same OXPHOS complexes. Therefore, we created a TbAAC RNAi cell line in PF 29-13 *T. brucei* cells that is capable of inducible dsRNA expression when triggered by the addition of Tet to the culture medium. A significant growth phenotype was detected in the TbAAC-depleted cells by the fourth day of RNAi induction (Fig. 3A). This result emphasizes the importance of TbAAC as the major ADP/ATP carrier in *T. brucei* mitochondria and its irreplaceable function in the PF stage of the parasite. The efficiency of the RNAi was verified by Northern blotting using a transcript-specific probe, demonstrating that the TbAAC mRNA was significantly reduced after only 2 days of RNAi induction (Fig. 3A, inset). The targeted knockdown of TbAAC was further confirmed by Western blotting of whole-cell lysates harvested from noninduced and RNAi-induced cells (Fig. 3B, top). Equivalent cell numbers were loaded for each sample, and then cells were

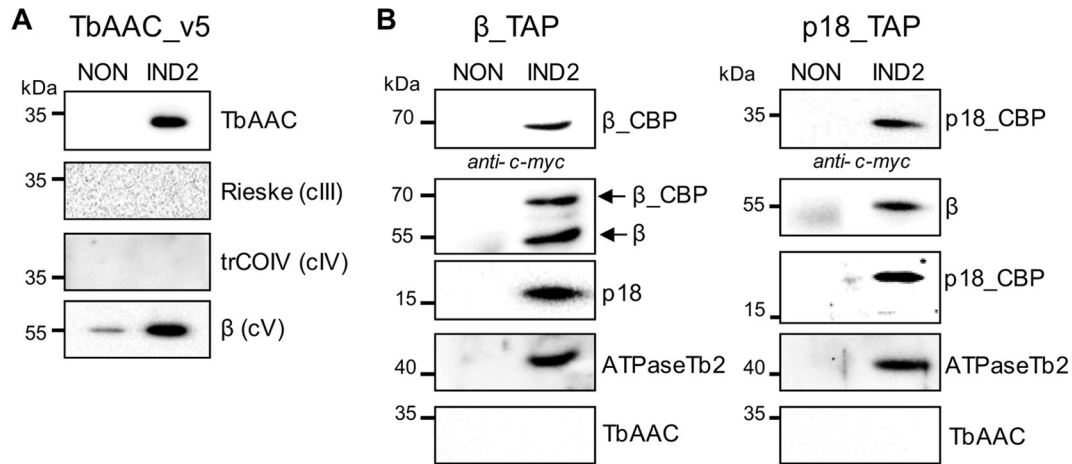


FIG 2 TbAAC does not copurify with complex IV or F_0F_1 -ATP synthase. (A) TbAAC_v5-tagged complexes were purified using magnetic beads (Dynabeads M-280, sheep anti-mouse IgG) charged with a monoclonal anti-v5 antibody. The tagged protein complexes were purified from noninduced (NON) cells and 2-day Tet-induced cells (IND2) containing the regulatable ectopic v5-tagged TbAAC protein. The tagged protein complexes were eluted with SDS-PAGE loading buffer, fractionated by SDS-PAGE, and examined by Western blotting. The presence of the tagged TbAAC_v5 was verified using an anti-TbAAC antibody (top). The association of TbAAC_v5 with core subunits of complex III (Rieske), IV (trCOIV), and F_0F_1 -ATPase (B) was determined using specific antibodies. The applicable sizes of the protein marker are indicated on the left. (B) F_0F_1 -ATP synthase complexes were purified by IgG affinity chromatography, eluted by TEV protease, resolved by SDS-PAGE, and examined by Western blotting. The presence of cleaved bait proteins now containing just the calmodulin-binding protein (CBP) and *c-myc* epitope tag, β _CBP and p18_CBP, was verified by an anti-*c-myc* antibody. Blots probed with antibodies specific to subunits β , p18, and ATPaseTb2 demonstrate that the TEV eluates contain common components of both the F_1 and F_0 moieties of the F_0F_1 -ATP synthase (endogenous and TAP tagged), while Western blots immunodecorated with an anti-TbAAC antibody demonstrate that the ADP/ATP transporter is not detectable in β - and p18-tagged complexes. Noninduced cells were used as a negative control for any nonspecific protein binding during the IgG affinity purification. The relevant sizes of the protein marker are indicated on the left.

analyzed with an anti-mt Hsp70 monoclonal antibody to normalize for equal loading. Finally, after being probed with an antibody against TbAAC, the Western blot exhibited reductions of the targeted protein by 40% and 71% at days 2 and 3 of RNAi induction, respectively (Fig. 3B, top).

Knockdown of TbAAC does not impair the steady state, structural integrity, and enzymatic activities of OXPHOS complexes. With the established TbAAC RNAi cell line, we examined if the steady-state abundance of specific core subunits of the OXPHOS complexes are affected upon efficient TbAAC depletion. Trypanosomatid-specific antibodies raised against subunits of complexes III (apoC and Rieske), IV (trCOIV and COVI), F_0F_1 -ATP synthase (β), and Tbp_iC were utilized to monitor the stability of these components over time in whole-cell lysates (Fig. 3B). No major changes were observed for any of the examined proteins except for Tbp_iC, which was detected as a double band running around 35 kDa (Fig. 3B, bottom). Since the lower band disappeared and an interaction between the AAC and P_iC proteins was reported in the mammalian system (11), it was important to elucidate which band is specific for Tbp_iC. Therefore, we created a Tbp_iC RNAi cell line, in which the upper band is abated during dsRNA induction, demonstrating that Tbp_iC (predicted mass, 34.3 kDa) migrates just above the 35-kDa protein marker (see Fig. S1A in the supplemental material) and thus is not affected by the knockdown of TbAAC (Fig. 3B, bottom). Hence, the Tbp_iC antibody cross-reacts with TbAAC, resulting in a doublet where the upper band is Tbp_iC and the lower band is TbAAC (see Fig. S1B in the supplemental material). This cross-reactivity was quite unexpected because the best match from a ClustalW alignment of the Tbp_iC peptide antigen with TbAAC (see Fig. S1C in the supplemental material) shares less than 22% identity.

While the steady-state abundance of a few individual subunits of complexes III, IV, and F_0F_1 -ATP synthase was unchanged upon the depletion of TbAAC, we wanted to verify that the integrity of these complexes was maintained by analyzing their sedimentation profiles on glycerol gradients. Mitochondria isolated from noninduced cells and RNAi cells induced for 5 days (IND5) were lysed by dodecyl maltoside (2 mg detergent/mg mt protein) and fractionated on a 10-to-30% glycerol gradient (Fig. 3C). The resolved fractions were then analyzed by Western blotting, utilizing the anti-TbAAC antibody to confirm a successful knockdown and the anti-apoC, anti-trCOIV, anti-subunit β , and anti-Tbp_iC antibodies to illustrate the sedimentation profile for complexes III and IV, F_0F_1 -ATP synthase, and the phosphate carrier. Notably, the sedimentation profiles of the examined complexes and Tbp_iC were unaltered between the noninduced and RNAi-induced samples (Fig. 3C). Thus, silencing of TbAAC does not interfere with the assembly and/or stability of the examined OXPHOS complexes.

The evolutionary benefit of the interaction between AAC and various components of OXPHOS is that it increases the efficiency of these machines. Indeed, when AAC was depleted in yeast cells, it was shown to affect the activity of complexes III and IV, which were decreased by 15% and 55%, respectively (9). Therefore, specific *in vitro* enzymatic activity assays were performed with mt extracts obtained from noninduced and TbAAC RNAi-induced cells and revealed no significant differences in the activities of respiratory complexes III and F_0F_1 -ATP synthase, while the activity of complex IV was slightly increased (i.e., cytochrome *c* reductase activity was 107% \pm 11%, cytochrome *c* oxidase activity was 126% \pm 11%, and ATP hydrolase activity was 118% \pm 5% in RNAi-induced cells relative to activities in noninduced cells). Furthermore, the enzymatic activities of complexes IV and V were

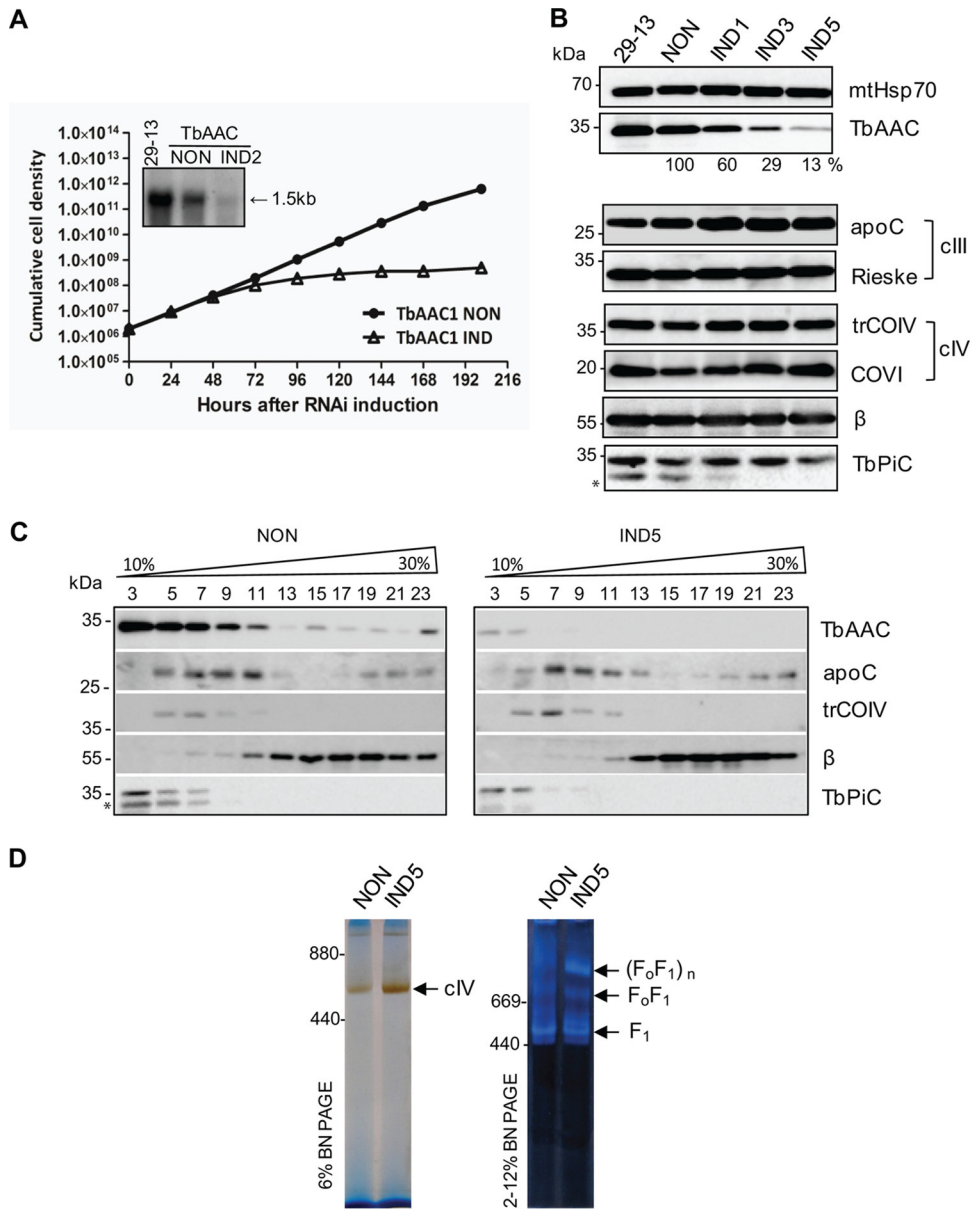


FIG 3 TbAAC is essential for *in vitro* growth but does not impair either the steady-state abundance or sedimentation profile of OXPHOS complexes or the in-gel activities of complex IV and F₀F₁-ATPase. (A) Growth curves of the noninduced (NON) and Tet-induced (IND) TbAAC RNAi procyclic *T. brucei* cell lines. Cells were maintained in the exponential growth phase (between 10⁶ and 10⁷ cells/ml), and cumulative cell numbers were calculated from daily counts that incorporated each subsequent dilution factor. The inset depicts a Northern blot analysis of TbAAC mRNA levels in the parental 29-13 cells, noninduced cells (NON), and cells induced for 2 days of RNAi (IND2). (B) The steady-state abundance of TbAAC, core subunits of complex III (apoC and Rieske), complex IV (trCOIV and COVI), F₀F₁-ATP synthase (β), and TbP₂C in noninduced (NON) TbAAC RNAi cells and those induced for 1, 3, and 5 days (IND1, IND3, and IND5) was determined by Western blotting using specific polyclonal antibodies. The numbers beneath the TbAAC blot represent the abundance of immunodetected TbAAC, expressed as a percentage of the noninduced samples after normalization to the loading control, mt Hsp70. The relevant sizes of the protein marker are on the left. The TbP₂C antiserum cross-reacts with TbAAC, and this band is indicated with an asterisk. (C) The sedimentation profiles of TbAAC, TbP₂C, complexes III and IV, and F₀F₁-ATP synthase were examined using Western blot analysis of glycerol gradient fractions. Mitochondria from non-RNAi-induced cells (NON) and cells induced for 5 days (IND5) were lysed with dodecyl maltoside. An equal amount of the cleared lysate from 1 × 10⁹ trypanosomes was loaded on each 10-to-30% glycerol gradient. Western analyses with trypanosomatid-specific antibodies raised against AAC, P₂C, apoC (complex III), trCOIV (complex IV), and subunit β (F₀F₁-ATP synthase) depict the sedimentation profile of the examined OXPHOS complexes. The glycerol gradient fractions are numbered, and the sizes of the protein marker are indicated. An asterisk designates the TbAAC band that cross-reacts with the TbP₂C antiserum. (D) In-gel complex IV and F₀F₁-ATP synthase activity staining after TbAAC repression. mt preparations from noninduced (NON) and RNAi cells Tet-induced for 5 days (IND5) were solubilized using dodecyl maltoside and separated either by 6% BN PAGE for complex IV staining or by 3-to-12% BN PAGE for F₀F₁-ATPase staining. The arrows denote bands visualized by the specific activity staining. The sizes of high-molecular-weight markers (ferritin and its dimer; Sigma) are on the left (in kilodaltons).

also examined using native 1-D BN PAGE followed by in-gel activity staining (Fig. 3C). Complex IV was visualized as a single band at ~700 kDa (13, 41), while F_0F_1 -ATP synthase was depicted by both the free F_1 moiety and multimeric F_0F_1 complexes (18). Though a slight increase of complex IV activity was detected, no major changes in the size and activity of the F_0F_1 -ATP synthase were revealed when TbAAC was abated (Fig. 3C).

In summary, an efficient knockdown of TbAAC did not trigger any visible changes in the steady-state abundance of TbP_iC and selected subunits of OXPHOS complexes. Furthermore, no major differences were found in the sedimentation profiles, and no reductions in *in vitro* enzymatic activities of the examined complexes were detected. Thus, it seems that TbAAC exists as a physically separate entity in the inner mt membrane with no effect on the structural arrangement of OXPHOS components.

TbAAC is responsible for the import of ATP and ADP into the mitochondrion. Under aerobic conditions, the most important role of the ADP/ATP carrier is to sustain the cellular ATP homeostasis by enabling the 1-to-1 exchange of cytosolic ADP for mt ATP produced by an active OXPHOS pathway. However, when the cell finds itself under anaerobic or microaerobic conditions, the OXPHOS activity is usually downregulated and the ADP/ATP carrier works in reverse, resulting in a 1:1 exchange of mt ADP for cytosolic ATP (50).

To test if TbAAC is fully or only partially responsible for the influx of ADP into the organelle, an mt ATP production assay was performed. The isolated mitochondria from noninduced and RNAi-induced cells were incubated with ADP, free phosphate, and a suitable respiratory substrate, such as succinate, to trigger oxidative phosphorylation, or either α -ketoglutarate or pyruvate/succinate, to trigger one of two specific substrate phosphorylation reactions. Upon the addition of all these substrates, the mitochondria are energized and produce ATP, which can be subsequently measured using a bioluminescent substrate. Comparison of the detected ATP levels between noninduced cells and RNAi-induced cells revealed a major reduction in mt ATP by ~75% and ~94% at days 3 and 5 after RNAi induction, respectively (Fig. 4A). Additional controls were included to demonstrate that the production of ATP by oxidative phosphorylation was sensitive to malonate, an inhibitor of succinate dehydrogenase, and that all three ATP production pathways were sensitive to atractyloside, a specific inhibitor of the ADP/ATP translocator. Samples with no ADP added served as a control to detect ATP produced from any of the remaining endogenous ADP molecules (Fig. 4A). Our results indicate that TbAAC is the only ADP/ATP carrier responsible for ADP influx into the mitochondrion of PF *T. brucei*.

Under specific conditions, AAC can also work in reverse, thereby importing ATP into the mitochondria. Therefore, we examined this ATP influx activity using digitonin-extracted mt vesicles that had been incubated with ATP. Through TbAAC activity, ATP is imported into the mitochondria, where it is immediately hydrolyzed to ADP and inorganic phosphate by ubiquitous ATPase activities. The amount of inorganic phosphate that is created is then assessed spectrophotometrically to determine its concentration, which can then be used to calculate the ATPase activity in the sample due to the linear relationship between the two variables. Importantly, in TbAAC RNAi samples induced for 3 or 5 days, the total ATPase activity was decreased by ~20% or ~50%, respectively (Fig. 4B). Moreover, the total ATPase activity measured in cleared mt lysates (mt fractions with disrupted mem-

branes) obtained from noninduced and RNAi-induced cells was unchanged (Fig. 4C). This result confirms that the decreased ATPase activity in the intact mt vesicles is not due to the general impairment of ATP hydrolytic protein complexes but rather is caused by the insufficient import of ATP into the mitochondria due to TbAAC ablation. However, it should be noted that the 50% reduction in ATP influx is not as high as one would expect, suggesting the presence of another carrier responsible for ATP influx into the mitochondria, possibly the ATP/ P_i carrier.

TbAAC is crucial for the export of mt ATP into the cytosol. One of the most significant evolutionary events that allowed an engulfed alphaproteobacterium to become the organellar powerhouse of a eukaryotic cell depended on its ability to export ATP to the rest of the cell. Therefore, to determine if TbAAC is the principal exporter of ATP, we generated a TbAAC RNAi cell line that constitutively expresses firefly luciferase and allows us to measure cytosolic ATP levels *in vivo*. The amount of luciferase expression and its cytosolic localization in the LUC-TbAAC RNAi cell line was verified by Western blotting of digitonin-treated fractions (Fig. 5A). A commercial anti-luciferase antibody and antibodies recognizing the cytosolic enolase and mt Hsp70 protein were used to immunodecorate cytosolic and mt fractions, respectively. Once these LUC-TbAAC RNAi cells, either noninduced or induced for 3 days, were exposed to luciferin, the *in vivo* cytosolic ATP levels were measured by a luminometer. RNAi-mediated depletion of TbAAC severely decreased the level of cytosolic ATP compared to that in noninduced cells (Fig. 5B). Since the cytosolic ATP is significantly reduced (by 67%) after just 3 days of RNAi induction, when the growth phenotype is not yet fully manifested, we propose that the drop in the cytosolic ATP level is the primary reason for the impending growth retardation.

An imbalance in the mt ADP/ATP pool leads to an increased $\Delta\psi_m$, an accumulation of ROS, and decreased respiration. The lack of ATP efflux activity from the organelle to the cytosol causes an aberrant mt ADP/ATP ratio, resulting from the limited availability of ADP and the accumulation of ATP in the mt matrix. This nucleotide imbalance likely impedes F_0F_1 -ATP synthase activity, causing an mt inner membrane hyperpolarization that in turn alters other mt processes, such as respiration and ROS production. Therefore, these conventional organellar functions were examined as TbAAC was depleted. As predicted, the $\Delta\psi_m$ was increased (up to 37% at day 5) in the RNAi-induced cells compared to noninduced controls (Fig. 6A; Table 1). Our previous *in vitro* assays demonstrated that the loss of TbAAC does not interfere with the ability of respiratory complexes III and IV to transmit electrons and presumably pump protons when they are provided the appropriate substrate. Therefore, this observed phenotype is likely due to the accumulation of protons in the intermembrane space, as the electrochemical potential of the proton motive force is never harnessed by the stagnant F_0F_1 -ATP synthase that is lacking its ADP substrate.

In time, the increased $\Delta\psi_m$ becomes so significant that respiration-coupled electron flow and proton pumping of complex III and IV become stalled. Consequently, we observed that the amount of ROS is dramatically elevated (210%) by day 5 of Tet-induced RNAi compared to noninduced samples (Fig. 6B; Table 1). This high level of oxidative stress likely contributes to the severe growth phenotype detected upon the knockdown of TbAAC. Furthermore, we determined that the total oxygen consumption is significantly decreased after 5 days of TbAAC depletion (Fig. 6C), most likely due to the hyperpolarization caused by the hindered

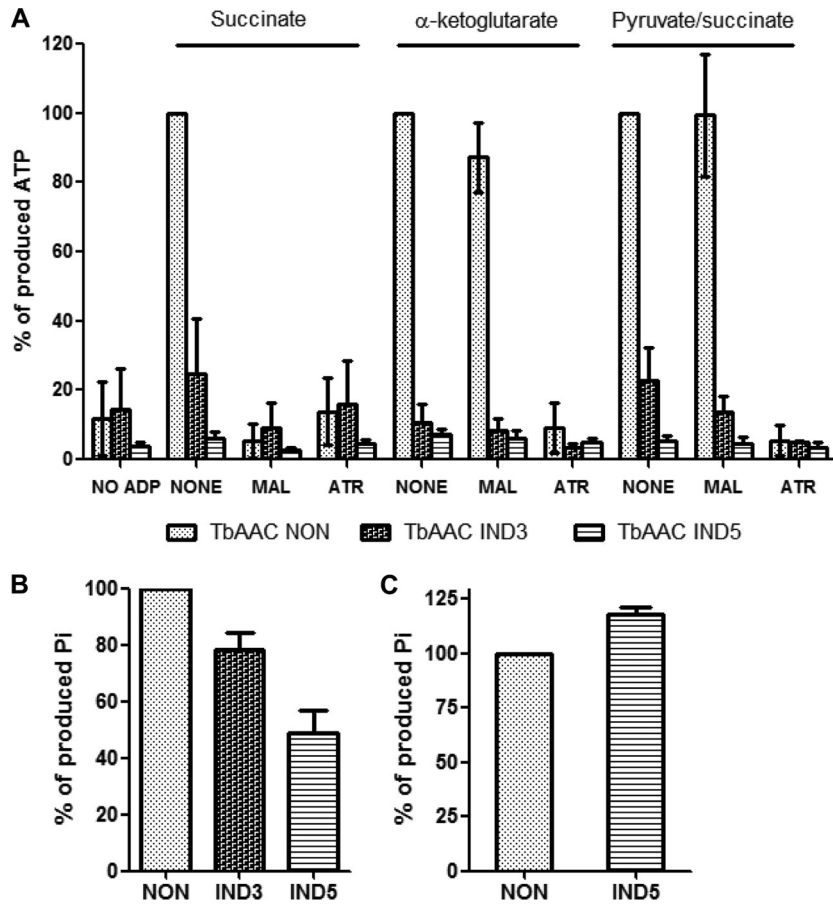


FIG 4 Both ADP and ATP influx into the mitochondrion are affected in cells silenced for TbAAC expression. (A) To determine levels of ADP influx into the mitochondrion, the *in vitro* production of ATP was measured in digitonin-extracted mitochondria from noninduced (NON) cells or cells with activated TbAAC RNAi for 3 (IND3) or 5 days (IND5). The phosphorylation pathways were triggered by the addition of ADP and one of the following substrates: succinate, α -ketoglutarate, and pyruvate/succinate. Malonate (MAL), a specific inhibitor of succinate dehydrogenase, was used to inhibit ATP production by oxidative phosphorylation, and atractyloside (ATR) was used to inhibit import of ADP into mitochondria. The level of ATP production in mitochondria isolated from noninduced RNAi cells stimulated with substrate, but in the absence of any specific inhibitors, was established as the reference and set to 100%. All other values for the same substrate are calculated arithmetic means expressed as percentages of this reference sample. The “No ADP” value serves as a control for the background production of ATP from endogenous mt ADP. The data are averages from at least three independent experiments and standard deviations. (B) To ascertain the extent of ATP import into active mitochondria, ATPase hydrolytic activities were measured in either noninduced (NON) TbAAC RNAi cells or cells induced with Tet for 3 (IND3) and 5 days (IND5). Crude mt vesicles were obtained by digitonin extraction. The ATPase activity was triggered by ATP addition (5 mM) and assayed by measuring the release of free phosphate. The total amount of free phosphate created from all ATPase enzymes present in the noninduced sample was set at 100%. The displayed results represent the average activities obtained from extracts prepared from four independent RNAi inductions. (C) Total ATPase activity measured in mitochondrial lysates from noninduced and RNAi cells induced for 5 days indicate that mt ATPases are still active when substrate is available. The total amount of free phosphates created from all ATPase enzymes present in the noninduced sample was set at 100%. The results are the average activities obtained from extracts prepared from four independent RNAi inductions.

activity of F_0F_1 -ATP synthase. Importantly, there are two terminal oxidases (complex IV and trypanosome alternative oxidase [TAO]) in *T. brucei*, both of which can catalyze the final reduction of an oxygen molecule and thus contribute to the total oxygen consumption. While it is still unknown how electron flow is regulated between these two pathways, utilizing TAO allows the electrons to bypass respiratory complexes III and IV, which should help alleviate the damaging effects of ROS generated from an elevated $\Delta\psi_m$. Nevertheless, we observed that complex IV contributed a majority of the respiration even in the presence of the excessive ROS created by day 5 in these TbAAC RNAi-induced cells (Fig. 6D). Strikingly, even the relative contribution of these two terminal oxidases to the overall cellular respiration was not significantly modified over time, suggesting that the activity of complex

IV is not specifically inhibited by a high ADP/ATP ratio, as observed in mammalian mitochondria (51, 52).

Silencing of TbAAC leads to defects in cell division. In humans, the lack of AAC activity triggers mt DNA rearrangements and deletions followed by a complete loss of mt DNA (53, 54). To ascertain if a loss of mt DNA also occurs in *T. brucei* with down-regulated TbAAC, the nuclear and mt DNA (termed kinetoplast DNA in these protists) were stained with DAPI and visualized by fluorescence microscopy (Fig. 7A). Trypanosomes in G₁ and S phase possess one nucleus and one kinetoplast (1N1K), while in the G₂/M transition phase, these flagellates have one nucleus and two kinetoplasts (1N2K), as the mitochondrion division precedes mitosis. Finally, before undergoing cytokinesis, these cells have two nuclei and two kinetoplasts (2N2K) (Fig. 7A, top). In the

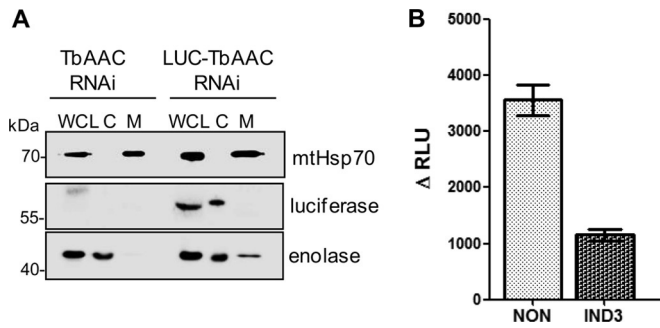


FIG 5 Cytosolic ATP levels are significantly decreased in TbAAC RNAi-induced cells. (A) The subcellular localization of luciferase was determined within TbAAC RNAi cells expressing luciferase (LUC-TbAAC RNAi). Parental TbAAC RNAi cells were used as a negative control. *T. brucei* cells (5×10^8) were harvested by centrifugation (WCL) and further separated into cytosolic (C) and mitochondrial (M) subcellular fractions upon digitonin extraction. Purified fractions were analyzed by Western blotting with anti-luciferase, anti-mt Hsp70 (mitochondria), and anti-enolase (cytosol) antibodies. The relevant sizes of the protein markers are on the left. (B) Total cytosolic ATP content was measured by a luminometer upon luciferin addition to living cells, either noninduced (NON) LUC-TbAAC RNAi cells or cells induced for 3 days (IND3). Values are in relative light units (RLU) and are averages from three independent RNAi inductions.

TABLE 1 $\Delta\psi_m$ and ROS measurements^a

Day	Fluorescence (%) of:	
	TMRE	DCFH-DA
3	119 ± 6	88 ± 25
5	137 ± 4	211 ± 20
7	125 ± 3	202 ± 21

^a $\Delta\psi_m$ and ROS were measured 3, 5, and 7 days after RNAi induction, using FACS analyses of the appropriate stain as described in Materials and Methods. Data were obtained from at least three independent RNAi inductions. Fluorescence intensity in the RNAi-induced cells is expressed as a percentage of that in noninduced cells. Values are means and standard deviations.

noninduced control, 76% of the cells were found to have a single nucleus of normal size and a single kinetoplast (1N1K), while the rest (24%) were either 1N2K or 2N2K (Fig. 7B), which is representative of a healthy population of these parasites grown in culture. Importantly, even after 5 days of TbAAC RNAi induction, we did not observe a loss of mt DNA, in contrast to reports concerning mammals (55), but rather, we detected a substantial accumulation of cells with an aberrant number of nuclei and kinetoplasts. Examples of these abnormalities include anuclear cells (1K), as well as cells with two nuclei and one kinetoplast (2N1K) and larger monster cells with multiple nuclei and kinetoplasts (xNxK) (Fig. 7A, bottom). These results, quantified in Fig. 7B, suggest a failure

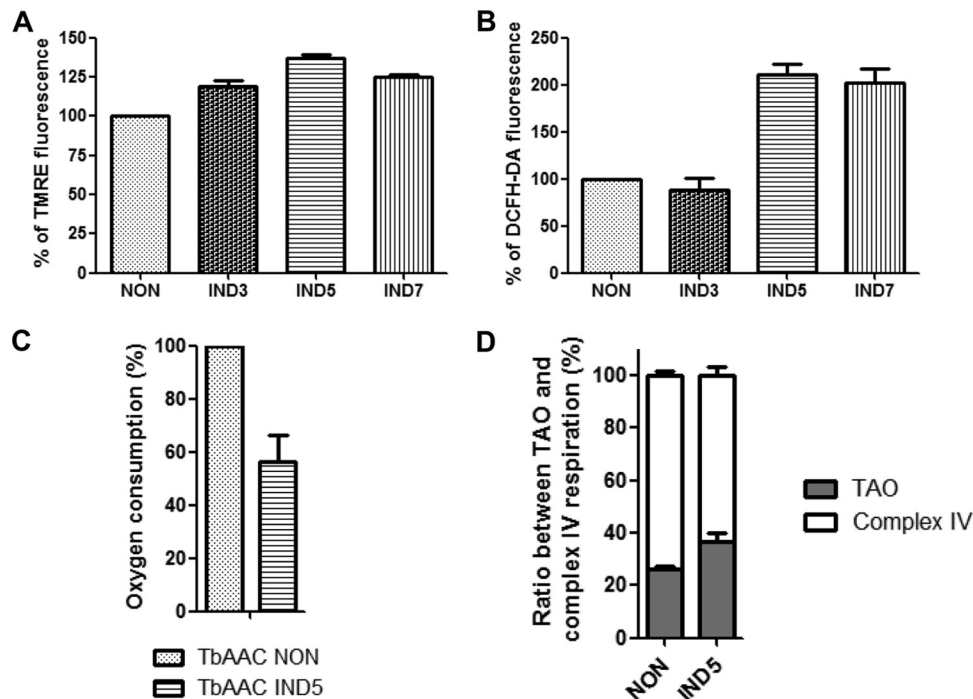


FIG 6 TbAAC silencing increases the $\Delta\psi_m$, resulting in decreased oxygen consumption and elevated ROS production. (A) After staining with 60 nM TMRE, the $\Delta\psi_m$ was measured by flow cytometry in both noninduced cells (NON) and TbAAC RNAi cells induced for 3 (IND3), 5 (IND5), and 7 (IND7) days. The median fluorescent intensity values are presented as percentages of the value for the noninduced sample, which was set to 100%. Data were obtained from at least three independent RNAi experiments, and the standard deviations are included. (B) The ROS detection reagent DCFH-DA was quantified by fluorescence-activated cell sorting (FACS) analysis in noninduced (NON) cells and TbAAC RNAi cells induced for 3 (IND3), 5 (IND5), and 7 (IND7) days. Increased fluorescence intensity corresponds to an accumulated ROS formation that was observed in three independent assays. (C) The oxygen consumption of noninduced (NON) and RNAi-induced (IND5) cells incubated in SDM-79 medium at 27°C was monitored with a Clark-type oxygen electrode. The total oxygen consumption in noninduced cells was set to 100%. Values are arithmetic means and standard deviations from three experiments. (D) The ratio of complex IV- and TAO-mediated respiration was measured in noninduced (NON) and TbAAC RNAi cells induced for 5 days (IND5). The total oxygen consumption in both cell lines was set to 100%. After the addition of salicylhydroxamic acid (SHAM) (0.03 mM), a potent TAO inhibitor, the remaining oxygen consumption represented respiration occurring via complex IV. Values are means and standard deviations from six independent experiments.

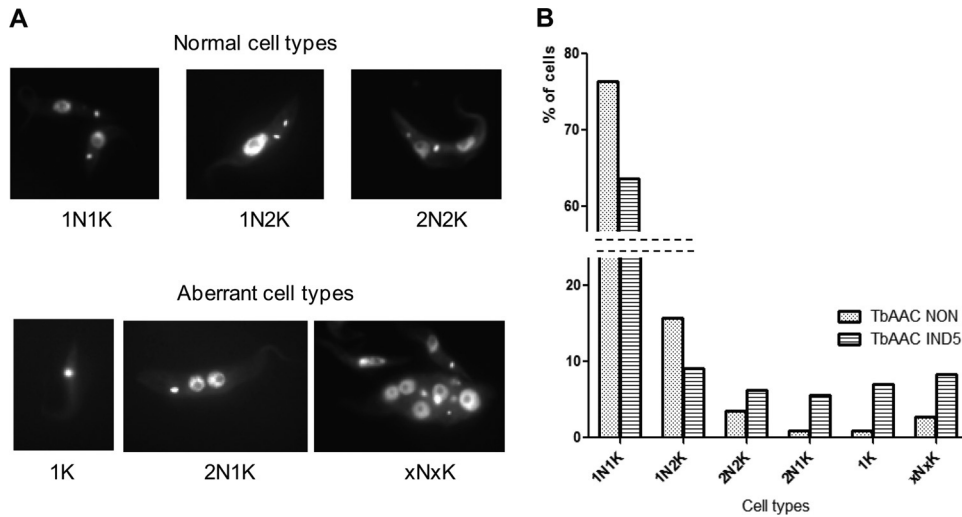


FIG 7 TbAAC depletion leads to defects in cell division. (A) DAPI staining was used to visualize various nucleus/kinetoplast (NK) phenotypes in noninduced TbAAC RNAi cells and cells induced with Tet for 5 days. (Top) Normal cell types either in G₁/S (1N1K) and G₂/M (1N2K) phases or undergoing cytokinesis (2N2K). (Bottom) Representative abnormal cell types (1K, 2N1K, and xNxK). N, nucleus; K, kinetoplast. (B) Quantification of the microscopy images based on the number of nuclei and kinetoplasts in more than 200 cells per time point. NON, noninduced cells; IND5, RNAi cells induced for 5 days.

in the overall cell division machinery, an effect likely to be caused by the shortage of cytosolic ATP.

DISCUSSION

In this study, we analyzed the functional and structural interactions of the mt ADP/ATP carrier in the insect stage of *T. brucei*, a highly diverged eukaryote. During this life stage, the parasite possesses an aerobically active mitochondrion that contains a fully developed respiratory chain coupled to ATP production by the F₀F₁-ATP synthase (17). Thus, in agreement with this mt function, silencing of TbAAC caused a decreased level of cytosolic ATP, a higher $\Delta\psi_m$, an elevated amount of ROS, and a reduced consumption of oxygen. We further established that TbAAC functions as a physically separate entity and its downregulation does not impair the activity or arrangement of the OXPHOS components. Our results suggest that the energy demands during this stage of the parasite do not necessitate the incorporation of AAC into the respiratory supercomplexes.

The majority of the literature describing respiratory supercomplexes focuses on two main assemblies, either the dimeric F₀F₁-ATP synthase or the union of proton translocating complexes I, III, and IV. The latter complexes are usually found to assemble into I+III₂, III₂+IV₁₋₂, and I+III₂+IV₂₋₄ supramolecular organizations, and their formation is well documented for only a few representatives of the supergroups Opisthokonta (*Saccharomyces cerevisiae*, *Yarrowia lipolytica*, *Bos taurus*, and *Homo sapiens*) and Archaeplastida (*Solanum tuberosum* and *Spinacia oleracea*) (56–59). It is believed that this physical association of the electron relay components creates patches within the mt inner membrane where the appropriate substrates can be concentrated, making the OXPHOS pathway more efficient to meet higher energy demands and decrease the potential for ROS formation. However, recent work with bovine mitochondria elegantly suggests that there is just one common pool of ubiquinone/ubiquinol and cytochrome *c*, which is free to interact with any OXPHOS components found in the protein-dense mt inner membrane (60). Whereas the interactions between respiratory supercomplexes ap-

pear to be quite delicate, the detection of the dimeric F₀F₁-ATP synthase has been more pervasive throughout the eukaryotic supergroups studied so far, including the protists of the supergroups Excavata and Alveolata (*T. brucei*, *Euglena gracilis*, *Plasmodium falciparum*, and *Tetrahymena thermophila*) (13, 61–64). This dimerization is proposed to be crucial for crista formation within the mt inner membrane (65), and the commonality of this structural organization in a wide variety of eukaryotes suggests that it was an early attempt to create microenvironments for components of the OXPHOS pathway.

To a lesser extent, the AAC has also been identified in special arrangements with some of these respiratory supercomplexes. In yeast, a large majority of the main ADP/ATP carrier, AAC2, physically interacts with a supercomplex comprised of III+IV and the TIM23 translocase, although this interaction is highly sensitive to the detergent type and its concentration (9). The mt ADP_{in}/ATP_{out} exchange under aerobic conditions is energetically costly because the efflux of ATP results in the expulsion of a net negative charge that partially collapses the $\Delta\psi_m$. Thus, positioning AAC in a microenvironment packed with supercomplexes that contribute to a heightened local $\Delta\psi_m$ may minimize this energetic cost, thus establishing a site that is conducive to maximum AAC transport activity. Furthermore, the OXPHOS pathway, specifically complex IV activity, is significantly downregulated in the absence of AAC2 (48), providing additional evidence for the energetic cost benefits of this supramolecular collaboration in yeast.

In *T. brucei* mitochondria, the migration of TbAAC also overlapped complex IV under low-detergent conditions in 2-D PAGE. However, this interaction was never detected in copurification assays that utilized lysis conditions nearly identical to those in the 2-D analysis. Furthermore, upon efficient TbAAC knockdown, we did not observe a decrease in the activity of complex IV, as seen in yeast (9). In fact, we consistently saw a slight increase in cytochrome *c* oxidase activity, as measured by in-gel staining or spectrophotometry assays, possibly due to a physiological response to an altered ADP/ATP ratio in the matrix. Importantly, the assem-

bly and integrity of the OXPHOS complexes and the steady-state abundance of their constituent subunits remained unchanged. These results significantly contrast those of studies performed in yeast, where, in the absence of AAC, the steady state of selected subunits of respiratory complex IV was diminished, and the assembly of the respiratory supercomplex (III₂+IV₂) was disrupted (9).

The association of AAC with the F_oF₁-ATP synthase and P_iC has been observed in highly enriched crista-like vesicles purified from rats (11, 12). In addition, it has been demonstrated that AAC and F_oF₁-ATP synthase in yeast cofractionate in CN or BN PAGE, implying that they also congregate into an ATP synthasome (49). Furthermore, cosedimentation and copurification studies of the F_oF₁-ATP synthase subunit p18 and AAC discerned a similar situation in *Leishmania mexicana*, a close relative of *T. brucei* (66). Contrary to these reports, our data do not support the existence of an ATP synthasome in *T. brucei*, as TbAAC did not copurify with tagged F_oF₁-ATP synthase subunit β or p18. Moreover, TbP_iC did not cosediment with the large molecular signals detected for TbAAC and subunit β in hrCN PAGE or with subunit β in glycerol gradients. While the authors of this study are quick to acknowledge that the absence of an interaction does not prove that it does not exist, we were careful to perform reciprocal copurification assays using a less harsh detergent and the low salt concentrations used in the *Leishmania* study.

Perhaps this intriguing difference between these two closely related parasites is the result of the environments they encounter during their distinctive life cycles. While *Leishmania* possesses a fully developed mitochondrion throughout its life cycle due to the persistent requirement for the OXPHOS pathway (67), the morphology of the *T. brucei* mitochondrion is more pleomorphic, as the parasite transitions between the tsetse fly vector and the mammalian host's bloodstream. It is during the infectious stage that the mitochondrion becomes greatly reduced, containing many fewer cristae, which is indicative of its independence of the OXPHOS pathway for energy production in this high-glucose environment. Therefore, a closer inspection of the energetic demands and mechanisms to cope with ROS in these two protists might help to uncover the evolutionary forces that necessitate the assembly of this more efficient respiratory complex. In fact, purification of the *Leishmania* F_oF₁-ATP synthase might identify components absent from the *T. brucei* complex that are important for the interaction with P_iC and AAC.

The *T. brucei* genome encodes a singly functional ADP/ATP carrier, whose function has been confirmed by a complementation assay of an AAC2-deficient yeast strain. Furthermore, TbAAC biochemical properties and ADP/ATP exchange kinetics are similar to those of the yeast AAC2 carrier (26). Similar to the study done by Pena-Diaz and coworkers (26), our *in vitro* data assaying ADP influx into the mitochondrion for oxidative and substrate phosphorylation support these data, as ADP import into the organelle ceases upon an efficient TbAAC knockdown. Interestingly, when we measured the reverse function of this transporter, mainly the ATP import into the mitochondrion, we observed only a 51% decrease in the ATP-induced ATPase activity, suggesting the existence of another mt import route for ATP. An obvious candidate for such an activity would be a homolog of the ATP-Mg/P_i transporter, a protein that is responsible for the electroneutral exchange between ATP-Mg²⁺ and HPO₄²⁻, which can supplement the mt ATP pool in cells using the hydrolytic activity of F_oF₁-

ATPase to maintain the Δψ_m (68). However, a putative *T. brucei* homolog of the ATP-Mg/P_i transporter (Tb927.4.1660, MCP6) was shown to be inactive for ATP and ADP transport (25, 69). Thus, besides TbAAC, any additional carrier(s) responsible for ATP influx into the mitochondria of this excavate protist remains to be elucidated.

The genome of *S. cerevisiae* contains three AAC genes: AAC1, AAC2, and AAC3 (70, 71). However, only the disruption of AAC2 triggers a growth phenotype when the yeast is grown on nonfermentable carbon sources (72). Notably, in the absence of AAC2, the downregulation of the ADP/ATP exchange across the mt inner membrane is followed by a reduction in oxygen consumption and a decrease in complex IV activity (9). A similar phenomenon has been described for human mitochondria, which also contain three isoforms of the adenine nucleotide translocase (ANT) (73). While the loss of the main ANT1 isoform is not lethal, it does induce mt myopathy, as the lack of ADP/ATP exchange activity depletes matrix ADP, which causes F_oF₁-ATP synthase stagnation (74, 75). Consequently, the flow of protons back to the matrix is blocked and the Δψ_m increases until it reaches a level that prohibits oxidative phosphorylation, resulting in increased ROS production and mt DNA damage (76). Furthermore, mutations in the human ANT1 gene cause autosomal dominant progressive external ophthalmoplegia (adPEO), an mt disorder characterized by reduced respiration, lowered mt cytochrome content, and mt DNA deletions (54, 77). Moreover, this loss of mt DNA can further exacerbate the adPEO disorder by compromising the synthesis of specific respiratory subunits (75).

Trypanosomes depleted of TbAAC1 also displayed an elevated Δψ_m, decreased oxygen consumption, and heightened levels of ROS. However, in contrast to the yeast and human data, we did not observe a reduction in the activity or integrity of cytochrome-containing complexes III and IV. Therefore, the diminished respiration measured in TbAAC RNAi cells is not caused by the destabilization of the OXPHOS complexes, suggesting that even though high levels of ROS are detected, they do not seem to have deleterious effects on the mt DNA. To verify this outcome, the DNA content was examined by fluorescence microscopy in TbAAC-depleted cells. Although mt DNA rearrangements, deletions, and total loss were identified in humans with adPEO ANT1 mutations (55), we did not observe a complete loss of mt DNA. Instead, we detected decreased populations of normal cells in the G₁ or S phase with a concurrent accumulation of cells with an aberrant number of nuclei and/or kinetoplasts or parasites apparently arrested in a state of incomplete cytokinesis. In their totality, these results indicate that the loss of TbAAC in *T. brucei* does not result in the targeted loss of mt genes but rather leads to general defects in cell cycle control or division due to an overall cellular depletion of ATP.

While identifying the often delicate interaction of AAC with components of the OXPHOS pathway is challenging, the totality of this work suggests that TbAAC does not interact with F_oF₁-ATP synthase in *T. brucei* as it does in its close relative, *L. mexicana*. It would be interesting to investigate if the association of TbAAC, TbP_iC, and F_oF₁-ATPase (F_oF₁-ATP hydrolasome) exists in the infectious bloodstream stage of *T. brucei*, where the Δψ_m depends on ATP hydrolysis by the F_oF₁-ATPase located in an environment lacking significant cristae and the microenvironments they create.

ACKNOWLEDGMENTS

We thank Ken Stuart (Seattle Biomed) for kindly providing anti-mt Hsp70 antibody. We express our gratitude to Zdeněk Paris and Zdeněk Verner for their contribution at the initial stage of this study.

This work was funded by Ministry of Education ERC CZ grant LL1205, Czech Grant Agency grant P302/12/2513, EMBO Installation grant 1965 to A.Z., and the Praemium Academiae award to J.L. and by the Slovak Research and Development Agency under contract APVV-0286-12 and the Scientific Grant Agency of the Slovak Ministry of Education and the Academy of Sciences 1/0664/13 to A.H. We acknowledge the use of research infrastructure that has received funding from the European Union Seventh Framework Programme (FP7/2007-2013) under grant agreement no. 316304.

REFERENCES

- Arco AD, Satrustegui J. 2005. New mitochondrial carriers: an overview. *Cell Mol Life Sci* 62:2204–2227. <http://dx.doi.org/10.1007/s00018-005-5197-x>.
- Klingenberg M. 2008. The ADP and ATP transport in mitochondria and its carrier. *Biochim Biophys Acta* 1778:1978–2021. <http://dx.doi.org/10.1016/j.bbame.2008.04.011>.
- Dudkina NV, Kouril R, Peters K, Braun HP, Boekema EJ. 2010. Structure and function of mitochondrial supercomplexes. *Biochim Biophys Acta* 1797:664–670. <http://dx.doi.org/10.1016/j.bbabi.2009.12.013>.
- Dudkina NV, Heinemeyer J, Sunderhaus S, Boekema EJ, Braun HP. 2006. Respiratory chain supercomplexes in the plant mitochondrial membrane. *Trends Plant Sci* 11:232–240. <http://dx.doi.org/10.1016/j.tplants.2006.03.007>.
- Minauro-Sanmiguel F, Wilkens S, Garcia JJ. 2005. Structure of dimeric mitochondrial ATP synthase: novel F0 bridging features and the structural basis of mitochondrial cristae biogenesis. *Proc Natl Acad Sci U S A* 102:12356–12358. <http://dx.doi.org/10.1073/pnas.0503893102>.
- Davies KM, Anselmi C, Wittig I, Faraldo-Gomez JD, Kuhlbrandt W. 2012. Structure of the yeast F1Fo-ATP synthase dimer and its role in shaping the mitochondrial cristae. *Proc Natl Acad Sci U S A* 109:13602–13607. <http://dx.doi.org/10.1073/pnas.1204593109>.
- Bamber L, Harding M, Monne B, Slotboom DJ, Kunji ER. 2007. The yeast mitochondrial ADP/ATP carrier functions as a monomer in mitochondrial membranes. *Proc Natl Acad Sci U S A* 104:10830–10834. <http://dx.doi.org/10.1073/pnas.0703969104>.
- Nury H, Dahout-Gonzalez C, Trezeguet V, Lauquin G, Brandolin G, Pebay-Peyroula E. 2005. Structural basis for lipid-mediated interactions between mitochondrial ADP/ATP carrier monomers. *FEBS Lett* 579:6031–6036. <http://dx.doi.org/10.1016/j.febslet.2005.09.061>.
- Dienhart MK, Stuart RA. 2008. The yeast Aac2 protein exists in physical association with the cytochrome bcl-COX supercomplex and the TIM23 machinery. *Mol Biol Cell* 19:3934–3943. <http://dx.doi.org/10.1091/mbc.E08-04-0402>.
- Mehnert CS, Rampelt H, Gebert M, Oeljeklaus S, Schrempp SG, Kochbeck L, Guiard B, Warscheid B, van der Laan M. 2014. The mitochondrial ADP/ATP carrier associates with the inner membrane presequence translocase in a stoichiometric manner. *J Biol Chem* 289:27352–27362. <http://dx.doi.org/10.1074/jbc.M114.556498>.
- Chen C, Ko Y, Delannoy M, Ludtke SJ, Chiu W, Pedersen PL. 2004. Mitochondrial ATP synthasome: three-dimensional structure by electron microscopy of the ATP synthase in complex formation with carriers for Pi and ADP/ATP. *J Biol Chem* 279:31761–31768. <http://dx.doi.org/10.1074/jbc.M401353200>.
- Ko YH, Delannoy M, Hüllihen J, Chiu W, Pedersen PL. 2003. Mitochondrial ATP synthasome. Cristae-enriched membranes and a multiwell detergent screening assay yield dispersed single complexes containing the ATP synthase and carriers for Pi and ADP/ATP. *J Biol Chem* 278:12305–12309. <http://dx.doi.org/10.1074/jbc.C200703200>.
- Acestor N, Zíková A, Dalley RA, Anupama A, Panigrahi AK, Stuart KD. 2011. Trypanosoma brucei mitochondrial respiratome: composition and organization in procyclic form. *Mol Cell Proteomics* 10:M110.006908. <http://dx.doi.org/10.1074/mcp.M110.006908>.
- Simarro PP, Jannin J, Cattand P. 2008. Eliminating human African trypanosomiasis: where do we stand and what comes next? *PLoS Med* 5:e55. <http://dx.doi.org/10.1371/journal.pmed.0050055>.
- Fevre EM, Wissmann BV, Welburn SC, Lutumba P. 2008. The burden of human African trypanosomiasis. *PLoS Negl Trop Dis* 2:e333. <http://dx.doi.org/10.1371/journal.pntd.0000333>.
- Tielens AG, van Hellemond JJ. 2009. Surprising variety in energy metabolism within Trypanosomatidae. *Trends Parasitol* 25:482–490. <http://dx.doi.org/10.1016/j.pt.2009.07.007>.
- Besteiro S, Barrett MP, Riviere L, Bringaud F. 2005. Energy generation in insect stages of Trypanosoma brucei: metabolism in flux. *Trends Parasitol* 21:185–191. <http://dx.doi.org/10.1016/j.pt.2005.02.008>.
- Zíková A, Schnauffer A, Dalley RA, Panigrahi AK, Stuart KD. 2009. The F(0)F(1)-ATP synthase complex contains novel subunits and is essential for procyclic Trypanosoma brucei. *PLoS Pathog* 5:e1000436. <http://dx.doi.org/10.1371/journal.ppat.1000436>.
- Bochud-Allemann N, Schneider A. 2002. Mitochondrial substrate level phosphorylation is essential for growth of procyclic Trypanosoma brucei. *J Biol Chem* 277:32849–32854. <http://dx.doi.org/10.1074/jbc.M205776200>.
- Hannaert V, Bringaud F, Opperdoes FR, Michels PA. 2003. Evolution of energy metabolism and its compartmentation in Kinetoplastida. *Kinetoplastid Biol Dis* 2:11. <http://dx.doi.org/10.1186/1475-9292-2-11>.
- Fang J, Beattie DS. 2003. Identification of a gene encoding a 54 kDa alternative NADH dehydrogenase in Trypanosoma brucei. *Mol Biochem Parasitol* 127:73–77. [http://dx.doi.org/10.1016/S0166-6851\(02\)00305-5](http://dx.doi.org/10.1016/S0166-6851(02)00305-5).
- Chaudhuri M, Ott RD, Hill GC. 2006. Trypanosome alternative oxidase: from molecule to function. *Trends Parasitol* 22:484–491. <http://dx.doi.org/10.1016/j.pt.2006.08.007>.
- Nolan DP, Voorheis HP. 1992. The mitochondrion in bloodstream forms of Trypanosoma brucei is energized by the electrogenic pumping of protons catalysed by the F1F0-ATPase. *Eur J Biochem* 209:207–216. <http://dx.doi.org/10.1111/j.1432-1033.1992.tb17278.x>.
- Schnauffer A, Clark-Walker GD, Steinberg AG, Stuart K. 2005. The F1-ATP synthase complex in bloodstream stage trypanosomes has an unusual and essential function. *EMBO J* 24:4029–4040. <http://dx.doi.org/10.1038/sj.emboj.7600862>.
- Colasante C, Pena Diaz P, Clayton C, Voncken F. 2009. Mitochondrial carrier family inventory of Trypanosoma brucei brucei: identification, expression and subcellular localisation. *Mol Biochem Parasitol* 167:104–117. <http://dx.doi.org/10.1016/j.molbiopara.2009.05.004>.
- Pena-Díaz P, Pelosi L, Ebikeme C, Colasante C, Gao F, Bringaud F, Voncken F. 2012. Functional characterization of TbMCP5, a conserved and essential ADP/ATP carrier present in the mitochondrion of the human pathogen Trypanosoma brucei. *J Biol Chem* 287:41861–41874. <http://dx.doi.org/10.1074/jbc.M112.404699>.
- Verner Z, Basu S, Benz C, Dixit S, Dobáková E, Faktorová D, Hashimi H, Horáková E, Huang Z, Paris Z, Peña-Díaz P, Ridlon L, Týč J, Wildridge D, Zíková A, Lukeš J. The malleable mitochondrion of Trypanosoma brucei. *Int Rev Cell Mol Biol*, in press.
- Wickstead B, Ersfeld K, Gull K. 2002. Targeting of a tetracycline-inducible expression system to the transcriptionally silent minichromosomes of Trypanosoma brucei. *Mol Biochem Parasitol* 125:211–216. [http://dx.doi.org/10.1016/S0166-6851\(02\)00238-4](http://dx.doi.org/10.1016/S0166-6851(02)00238-4).
- Flaspohler JA, Jensen BC, Saveria T, Kifer CT, Parsons M. 2010. A novel protein kinase localized to lipid droplets is required for droplet biogenesis in trypanosomes. *Eukaryot Cell* 9:1702–1710. <http://dx.doi.org/10.1128/EC.00106-10>.
- Wirtz E, Leal S, Ochatt C, Cross GA. 1999. A tightly regulated inducible expression system for conditional gene knock-outs and dominant-negative genetics in Trypanosoma brucei. *Mol Biochem Parasitol* 99:89–101. [http://dx.doi.org/10.1016/S0166-6851\(99\)00002-X](http://dx.doi.org/10.1016/S0166-6851(99)00002-X).
- Surve S, Heestand M, Panicucci B, Schnauffer A, Parsons M. 2012. Enigmatic presence of mitochondrial complex I in Trypanosoma brucei bloodstream forms. *Eukaryot Cell* 11:183–193. <http://dx.doi.org/10.1128/EC.05282-11>.
- Panigrahi AK, Ogata Y, Zíková A, Anupama A, Dalley RA, Acestor N, Myler PJ, Stuart KD. 2009. A comprehensive analysis of Trypanosoma brucei mitochondrial proteome. *Proteomics* 9:434–450. <http://dx.doi.org/10.1002/pmic.200800477>.
- Horváth A, Horáková E, Dunajčíková P, Verner Z, Pravdová E, Šlapetová I, Čuninková L, Lukeš J. 2005. Downregulation of the nuclear-encoded subunits of the complexes III and IV disrupts their respective complexes but not complex I in procyclic Trypanosoma brucei. *Mol Microbiol* 58:116–130. <http://dx.doi.org/10.1111/j.1365-2958.2005.04813.x>.
- Wittig I, Karas M, Schagger H. 2007. High resolution clear native electrophoresis for in-gel functional assays and fluorescence studies of mem-

- brane protein complexes. *Mol Cell Proteomics* 6:1215–1225. <http://dx.doi.org/10.1074/mcp.M700076-MCP200>.
35. Maslov DA, Ziková A, Kyselová I, Lukeš J. 2002. A putative novel nuclear-encoded subunit of the cytochrome c oxidase complex in trypanosomatids. *Mol Biochem Parasitol* 125:113–125. [http://dx.doi.org/10.1016/S0166-6851\(02\)00235-9](http://dx.doi.org/10.1016/S0166-6851(02)00235-9).
 36. Hannaert V, Albert MA, Rigden DJ, da Silva Giotto MT, Thiemann O, Garratt RC, Van Roy J, Opperdoes FR, Michels PA. 2003. Kinetic characterization, structure modelling studies and crystallization of *Trypanosoma brucei* enolase. *Eur J Biochem* 270:3205–3213. <http://dx.doi.org/10.1046/j.1432-1033.2003.03692.x>.
 37. Panigrahi AK, Ziková A, Dalley RA, Acestor N, Ogata Y, Anupama A, Myler PJ, Stuart KD. 2008. Mitochondrial complexes in *Trypanosoma brucei*: a novel complex and a unique oxidoreductase complex. *Mol Cell Proteomics* 7:534–545. <http://dx.doi.org/10.1074/mcp.M700430-MCP200>.
 38. Priest JW, Hajduk SL. 2003. *Trypanosoma brucei* cytochrome c1 is imported into mitochondria along an unusual pathway. *J Biol Chem* 278:15084–15094. <http://dx.doi.org/10.1074/jbc.M212956200>.
 39. Šubrtová K, Panicucci B, Ziková A. ATPaseTb2, a unique membrane-bound FoF1-ATPase component, is essential in bloodstream and dyskinetoplastic trypanosomes. *PLoS Pathog*, in press.
 40. Ziková A, Panigrahi AK, Uboldi AD, Dalley RA, Handman E, Stuart K. 2008. Structural and functional association of *Trypanosoma brucei* MIX protein with cytochrome c oxidase complex. *Eukaryot Cell* 7:1994–2003. <http://dx.doi.org/10.1128/EC.00204-08>.
 41. Gnipová A, Panicucci B, Paris Z, Verner Z, Horváth A, Lukeš J, Ziková A. 2012. Disparate phenotypic effects from the knockdown of various *Trypanosoma brucei* cytochrome c oxidase subunits. *Mol Biochem Parasitol* 184:90–98. <http://dx.doi.org/10.1016/j.molbiopara.2012.04.013>.
 42. Allemann N, Schneider A. 2000. ATP production in isolated mitochondria of procyclic *Trypanosoma brucei*. *Mol Biochem Parasitol* 111:87–94. [http://dx.doi.org/10.1016/S0166-6851\(00\)00303-0](http://dx.doi.org/10.1016/S0166-6851(00)00303-0).
 43. Tan TH, Bochud-Allemann N, Horn EK, Schneider A. 2002. Eukaryotic-type elongator tRNAMet of *Trypanosoma brucei* becomes formylated after import into mitochondria. *Proc Natl Acad Sci U S A* 99:1152–1157. <http://dx.doi.org/10.1073/pnas.022522299>.
 44. Law RH, Manon S, Devenish RJ, Nagley P. 1995. ATP synthase from *Saccharomyces cerevisiae*. *Methods Enzymol* 260:133–163. [http://dx.doi.org/10.1016/0076-6879\(95\)60135-X](http://dx.doi.org/10.1016/0076-6879(95)60135-X).
 45. de Wet JR, Wood KV, DeLuca M, Helinski DR, Subramani S. 1987. Firefly luciferase gene: structure and expression in mammalian cells. *Mol Cell Biol* 7:725–737.
 46. Maechler P, Wang H, Wollheim CB. 1998. Continuous monitoring of ATP levels in living insulin secreting cells expressing cytosolic firefly luciferase. *FEBS Lett* 422:328–332. [http://dx.doi.org/10.1016/S0014-5793\(97\)01618-9](http://dx.doi.org/10.1016/S0014-5793(97)01618-9).
 47. Saddar S, Dienhart MK, Stuart RA. 2008. The F1F0-ATP synthase complex influences the assembly state of the cytochrome bc1-cytochrome oxidase supercomplex and its association with the TIM23 machinery. *J Biol Chem* 283:6677–6686. <http://dx.doi.org/10.1074/jbc.M708440200>.
 48. Claypool SM, Oktay Y, Boonthueung P, Loo JA, Koehler CM. 2008. Cardiolipin defines the interactome of the major ADP/ATP carrier protein of the mitochondrial inner membrane. *J Cell Biol* 182:937–950. <http://dx.doi.org/10.1083/jcb.200801152>.
 49. Wittig I, Schagger H. 2008. Structural organization of mitochondrial ATP synthase. *Biochim Biophys Acta* 1777:592–598. <http://dx.doi.org/10.1016/j.bbabi.2008.04.027>.
 50. Kawamata H, Starkov AA, Manfredi G, Chinopoulos C. 2010. A kinetic assay of mitochondrial ADP-ATP exchange rate in permeabilized cells. *Anal Biochem* 407:52–57. <http://dx.doi.org/10.1016/j.ab.2010.07.031>.
 51. Helling S, Vogt S, Rhiel A, Ramzan R, Wen L, Marcus K, Kadenbach B. 2008. Phosphorylation and kinetics of mammalian cytochrome c oxidase. *Mol Cell Proteomics* 7:1714–1724. <http://dx.doi.org/10.1074/mcp.M800137-MCP200>.
 52. Ramzan R, Staniek K, Kadenbach B, Vogt S. 2010. Mitochondrial respiration and membrane potential are regulated by the allosteric ATP-inhibition of cytochrome c oxidase. *Biochim Biophys Acta* 1797:1672–1680. <http://dx.doi.org/10.1016/j.bbabi.2010.06.005>.
 53. Kucejova B, Li L, Wang X, Giannattasio S, Chen XJ. 2008. Pleiotropic effects of the yeast Sal1 and Aac2 carriers on mitochondrial function via an activity distinct from adenine nucleotide transport. *Mol Genet Genomics* 280:25–39. <http://dx.doi.org/10.1007/s00438-008-0342-5>.
 54. Wang X, Salinas K, Zuo X, Kucejova B, Chen XJ. 2008. Dominant membrane uncoupling by mutant adenine nucleotide translocase in mitochondrial diseases. *Hum Mol Genet* 17:4036–4044. <http://dx.doi.org/10.1093/hmg/ddn306>.
 55. Kaukonen J, Juselius JK, Tiranti V, Kyttala A, Zeviani M, Comi GP, Keranen S, Peltonen L, Suomalainen A. 2000. Role of adenine nucleotide translocator 1 in mtDNA maintenance. *Science* 289:782–785. <http://dx.doi.org/10.1126/science.289.5480.782>.
 56. Schagger H, Pfeiffer K. 2000. Supercomplexes in the respiratory chains of yeast and mammalian mitochondria. *EMBO J* 19:1777–1783. <http://dx.doi.org/10.1093/emboj/19.8.1777>.
 57. Nubel E, Wittig I, Kerscher S, Brandt U, Schagger H. 2009. Two-dimensional native electrophoretic analysis of respiratory supercomplexes from *Yarrowia lipolytica*. *Proteomics* 9:2408–2418. <http://dx.doi.org/10.1002/pmic.200800632>.
 58. Bultema JB, Braun HP, Boekema EJ, Kouril R. 2009. Megacomplex organization of the oxidative phosphorylation system by structural analysis of respiratory supercomplexes from potato. *Biochim Biophys Acta* 1787:60–67. <http://dx.doi.org/10.1016/j.bbabi.2008.10.010>.
 59. Krause F, Reifschneider NH, Vocke D, Seelert H, Rexroth S, Dencher NA. 2004. “Respirasome”-like supercomplexes in green leaf mitochondria of spinach. *J Biol Chem* 279:48369–48375. <http://dx.doi.org/10.1074/jbc.M406085200>.
 60. Blaza JN, Serreli R, Jones AJ, Mohammed K, Hirst J. 2014. Kinetic evidence against partitioning of the ubiquinone pool and the catalytic relevance of respiratory-chain supercomplexes. *Proc Natl Acad Sci U S A* 111:15735–15740. <http://dx.doi.org/10.1073/pnas.1413855111>.
 61. Chaban Y, Boekema EJ, Dudkina NV. 2014. Structures of mitochondrial oxidative phosphorylation supercomplexes and mechanisms for their stabilisation. *Biochim Biophys Acta* 1837:418–426. <http://dx.doi.org/10.1016/j.bbabi.2013.10.004>.
 62. Balabaskaran Nina P, Dudkina NV, Kane LA, van Eyk JE, Boekema EJ, Mather MW, Vaidya AB. 2010. Highly divergent mitochondrial ATP synthase complexes in *Tetrahymena thermophila*. *PLoS Biol* 8:e1000418. <http://dx.doi.org/10.1371/journal.pbio.1000418>.
 63. Balabaskaran Nina P, Morrissey JM, Ganesan SM, Ke H, Pershing AM, Mather MW, Vaidya AB. 2011. ATP synthase complex of *Plasmodium falciparum*: dimeric assembly in mitochondrial membranes and resistance to genetic disruption. *J Biol Chem* 286:41312–41322. <http://dx.doi.org/10.1074/jbc.M111.290973>.
 64. Perez E, Lapaille M, Degand H, Cilibrasi L, Villavicencio-Queijeiro A, Morsomme P, Gonzalez-Halphen D, Field MC, Remacle C, Baurain D, Cardol P. 2014. The mitochondrial respiratory chain of the secondary green alga *Euglena gracilis* shares many additional subunits with parasitic *Trypanosomatidae*. *Mitochondrion* 19:338–349. <http://dx.doi.org/10.1016/j.mito.2014.02.001>.
 65. Paumard P, Vaillier J, Couly B, Schaeffer J, Soubannier V, Mueller DM, Brethes D, di Rago JP, Velours J. 2002. The ATP synthase is involved in generating mitochondrial cristae morphology. *EMBO J* 21:221–230. <http://dx.doi.org/10.1093/emboj/21.3.221>.
 66. Detke S, Elsabrouty R. 2008. Identification of a mitochondrial ATP synthase-adenine nucleotide translocator complex in *Leishmania*. *Acta Trop* 105:16–20. <http://dx.doi.org/10.1016/j.actatropica.2007.08.008>.
 67. Opperdoes FR, Coombs GH. 2007. Metabolism of *Leishmania*: proven and predicted. *Trends Parasitol* 23:149–158. <http://dx.doi.org/10.1016/j.pt.2007.02.004>.
 68. Traba J, Froschauer EM, Wiesenberger G, Satrustegui J, Del Arco A. 2008. Yeast mitochondria import ATP through the calcium-dependent ATP-Mg/Pi carrier Sal1p, and are ATP consumers during aerobic growth in glucose. *Mol Microbiol* 69:570–585. <http://dx.doi.org/10.1111/j.1365-2958.2008.06300.x>.
 69. Colasante C, Alibu VP, Kirchberger S, Tjaden J, Clayton C, Voncken F. 2006. Characterization and developmentally regulated localization of the mitochondrial carrier protein homologue MCP6 from *Trypanosoma brucei*. *Eukaryot Cell* 5:1194–1205. <http://dx.doi.org/10.1128/EC.00096-06>.
 70. Lawson JE, Douglas MG. 1988. Separate genes encode functionally equivalent ADP/ATP carrier proteins in *Saccharomyces cerevisiae*. Isolation and analysis of AAC2. *J Biol Chem* 263:14812–14818.
 71. Kolarov J, Kolarova N, Nelson N. 1990. A third ADP/ATP translocator gene in yeast. *J Biol Chem* 265:12711–12716.
 72. Drgon T, Sabova L, Gavurnikova G, Kolarov J. 1992. Yeast ADP/ATP carrier (AAC) proteins exhibit similar enzymatic properties but their deletion produces different phenotypes. *FEBS Lett* 304:277–280. [http://dx.doi.org/10.1016/0014-5793\(92\)80637-V](http://dx.doi.org/10.1016/0014-5793(92)80637-V).

73. Stepien G, Torroni A, Chung AB, Hodge JA, Wallace DC. 1992. Differential expression of adenine nucleotide translocator isoforms in mammalian tissues and during muscle cell differentiation. *J Biol Chem* 267: 14592–14597.
74. Echaniz-Laguna A, Chassagne M, Ceresuela J, Rouvet I, Padet S, Acquaviva C, Nataf S, Vinzio S, Bozon D, Mousson de Camaret B. 2012. Complete loss of expression of the ANT1 gene causing cardiomyopathy and myopathy. *J Med Genet* 49:146–150. <http://dx.doi.org/10.1136/jmedgenet-2011-100504>.
75. Palmieri L, Alberio S, Pisano I, Lodi T, Meznaric-Petrusa M, Zidar J, Santoro A, Scarcia P, Fontanesi F, Lamantea E, Ferrero I, Zeviani M. 2005. Complete loss-of-function of the heart/muscle-specific adenine nucleotide translocator is associated with mitochondrial myopathy and cardiomyopathy. *Hum Mol Genet* 14:3079–3088. <http://dx.doi.org/10.1093/hmg/ddi341>.
76. Esposito LA, Melov S, Panov A, Cottrell BA, Wallace DC. 1999. Mitochondrial disease in mouse results in increased oxidative stress. *Proc Natl Acad Sci U S A* 96:4820–4825. <http://dx.doi.org/10.1073/pnas.96.9.4820>.
77. Fontanesi F, Palmieri L, Scarcia P, Lodi T, Donnini C, Limongelli A, Tiranti V, Zeviani M, Ferrero I, Viola AM. 2004. Mutations in AAC2, equivalent to human adPEO-associated ANT1 mutations, lead to defective oxidative phosphorylation in *Saccharomyces cerevisiae* and affect mitochondrial DNA stability. *Hum Mol Genet* 13:923–934. <http://dx.doi.org/10.1093/hmg/ddh108>.

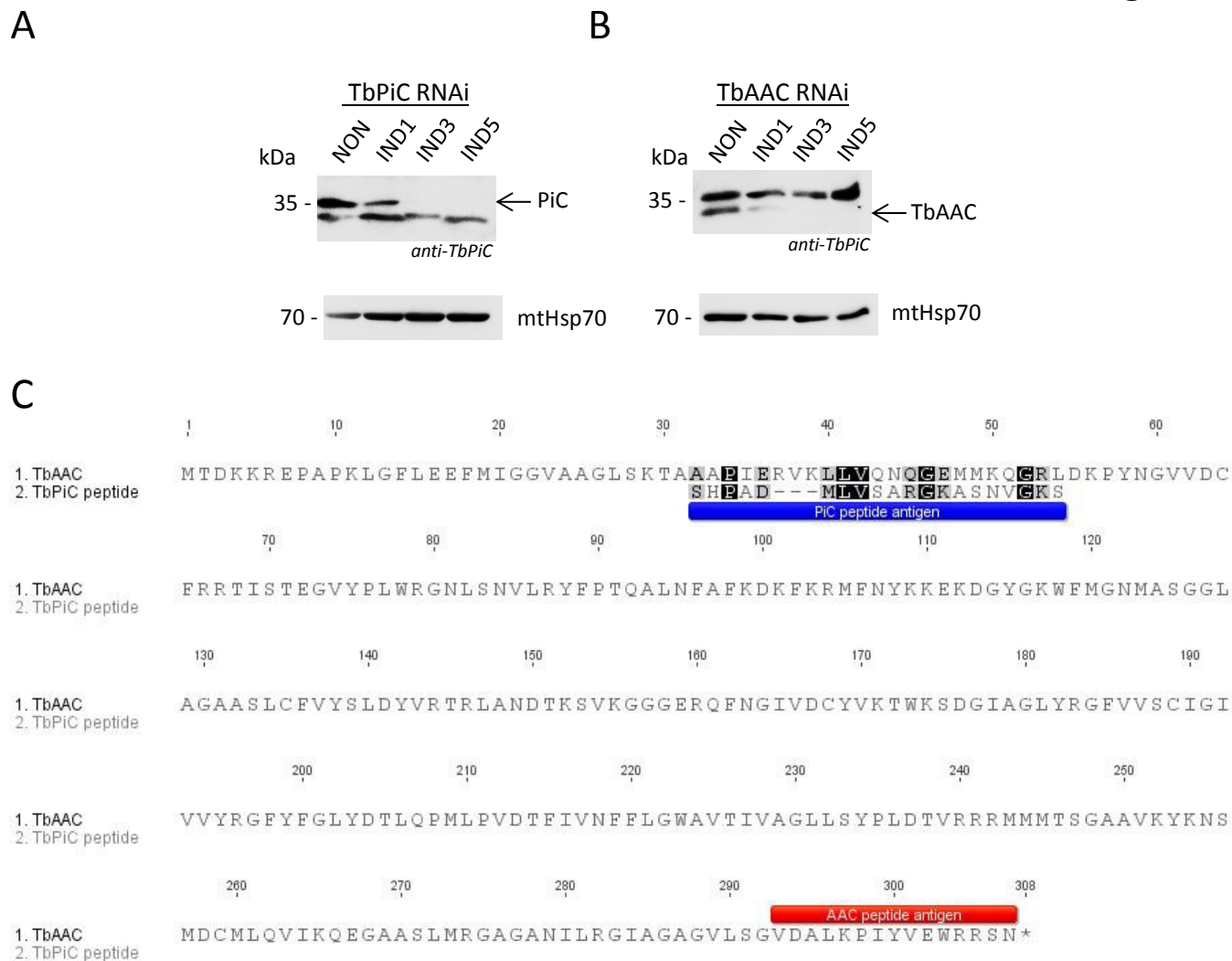


Fig. S1. A polyclonal antibody generated using a TbPiC peptide recognizes both TbPiC and TbAAC.

- A) A western blot containing whole cell lysates from TbPiC RNAi cells that were either non-induced (NON) or induced for 1 (IND1), 3 (IND3) and 5 (IND5) days was probed with a TbPiC peptide antibody generated in rabbits (upper panel). Upon RNAi induction, the upper signal of a doublet band centered around 35 kDa disappears by day 3, indicating that the TbPiC antibody specifically recognizes its antigen. A mtHSP70 monoclonal antibody serves as a loading control (bottom panel) and the sizes of relevant molecular weight markers are depicted on the left.
- B) Same as in A), except the western blot contains whole cell lysates from the TbAAC RNAi cell line. Here, the same TbPiC polyclonal antibody also detects a doublet band, but now the lower signal is abated upon TbAAC RNAi induction. Hence, the TbPiC antibody cross reacts with TbAAC.
- C) The TbPiC peptide (SHPADMLVSARGKASNVGKS, blue annotation) used to generate a rabbit polyclonal antibody was aligned with the TbAAC preprocessed protein sequence using ClustalW. The best pairwise sequence alignment resulted in less than 22% identity between the two peptides. For reference, the TbAAC peptide antigen (VDALKPIYVEWRRSN, red annotation) is depicted.

3.2. Unpublished results

3.2.1. The functionality of *Trypanosoma brucei* F₁-ATPase requires the additional subunit p18

Manuscript in preparation: Gahura O, Šubrtová K, Váchová H, Panicucci B, Fearnley IM, Harbour ME, Walker JE, Zíková A.

The functionality of *Trypanosoma brucei* F₁-ATPase requires the additional subunit p18

Ondřej Gahura^{1,2}, Karolína Šubrtová¹, Hana Váchová¹, Brian Panicucci¹, Ian M. Fearnley², Michael E. Harbour², John E. Walker^{2#}, Alena Zíková^{1#}

¹Institute of Parasitology, Biology Centre CAS, Ceske Budejovice, Czech Republic

²The Medical Research Council Mitochondrial Biology Unit, Cambridge, United Kingdom

[#]Joint corresponding authors

Running title: *F₁-ATPase in Trypanosoma brucei*

To whom correspondence should be addressed: Alena Zíková, Institute of Parasitology, Biology Centre CAS, Branisovska 31, 37005, Ceske Budejovice, Czech Republic; Tel.: 0042038775482; Fax: 00420385310388; Email: azikova@paru.cas.cz

ABSTRACT

F₀F₁-ATP synthases are sophisticated membrane-bound molecular machines producing ATP in bacteria and eukaryotic organelles. The importance of ATP generation by this complex is underlined by an extraordinary conservancy of the catalytic F₁-ATPase moiety. We established a two-step chromatography procedure to isolate a highly pure and active F₁-ATPase from the procyclic form (PF) of the parasitic protist, *Trypanosoma brucei*. The purified complex contained all usual eukaryotic subunits (α , β , γ , δ , and ϵ) and their mitochondrial targeting sequences were identified by N-terminal sequencing and mass spectrometry (MS). Furthermore, *T. brucei* F₁-ATPase displays two unusual features. First, the subunit α is split into two fragments by *in vivo* occurring proteolytic cleavage. Using MS approach this cleavage site was mapped. Interestingly, the subunit α gets cleaved at two different sites resulting in the release of eight non-conserved residues. Second, an additional protein p18 co-purified with F₁-ATPase. This interaction withstood the chloroform-extraction conditions implying that p18 is a novel F₁-ATPase subunit. Moreover, RNAi mediated silencing of p18 affects the growth of both *T. brucei* life stages, PF

and the bloodstream form. The levels of F_1 and F_1F_0 monomeric/multimeric complexes are considerably reduced upon p18 down regulation, demonstrating its importance for the stability of F_1 -ATPase. The presence of additional subunit p18 and the subunit α cleavage are unique features of *T. brucei* F_1 -ATPase, which not only further increase the list of peculiarities of this pathogen, but also break the long-standing conception of the strict conservancy of the F_1 -ATPase complex in eukaryotes.

INTRODUCTION

The last protein complex of a five-component oxidative phosphorylation pathway, the mitochondrial F_0F_1 -ATP synthase or complex V, is a ubiquitous source of ATP in eukaryotes and as such plays a pivotal role in cellular energy production. It is a turbine-like assembly, which rotation is driven by the proton gradient across the inner mitochondrial membrane generated by the respiratory chain. The torque of this rotation is converted to high-energy covalent bonds of ATP.

The F_0F_1 -ATP synthases consist of two sectors, F_1 and F_0 (for review see (1-3)). The F_1 moiety protrudes from the inner mitochondrial membrane to the matrix and bears the catalytic activity. Besides ATP synthesis, it also is capable to conduct the reversed reaction, ATP hydrolysis, therefore is often called F_1 -ATPase. F_1 -ATPase is formed by a globular hexamer of alternating subunits α and β sitting on a central stalk consisting of largely helical subunit γ , and small subunits δ and ϵ . The F_0 subcomplex consists of a membrane segment (subunits a, c, A6L, and several accessory proteins), which houses the proton pore, and of a peripheral stalk (subunits b, d, OSCP, and F6), which serves as a stator immobilizing the $\alpha_3\beta_3$ headpiece. The proton channel is created on the interface of the subunit a and c. Multiple copies of subunit c form a rotary c-ring (4,5). Proton flow through the channel spins the c-ring together with the linked central stalk of F_1 (6). Clockwise rotation (as viewed from the membrane) of the asymmetric subunit γ induces conformational changes within the stationary $\alpha\beta$ hexamer leading to ADP phosphorylation on three catalytic sites situated on each of the subunits β . The resistance of $\alpha\beta$ hexamer to the torque of the central stalk is secured by the peripheral stalk. The peripheral stalk is an elongated structure positioned in parallel orientation to the F_1 moiety. It is anchored to the membrane via its subunit b, contacting the proton channel subunit a and some supernumerary

membrane-bound subunits (7). The interaction with F_1 is mediated mainly by OSCP, a protein localized on the top of peripheral stalk (8).

The composition of mitochondrial F_0F_1 -ATP synthases is believed to be highly conserved among eukaryotes. Differences are restricted only to the supernumerary F_0 subunits. For example, the mammalian enzyme contains supernumerary subunits A6L, e, f, g, DAPIT, and PL6.8 (9), while in yeast *Saccharomyces cerevisiae* the last two proteins are absent and additional two subunits i and k were identified (10,11). However, characterized F_0F_1 -ATPase composition is biased towards established model species, which predominantly belong to the super-group Opisthokonts, overlooking most of eukaryotic diversity (12).

Recently, unexpected features of mitochondrial F_0F_1 -ATP synthases such as missing and/or additional subunits or structural deviations were reported in representatives of eukaryotic super-groups Sar, Excavates, and Archaeplastida. All of them are phylogenetically distant from the traditional models (12). For example, in the free-living ciliate *Tetrahymena thermophila* and in the related apicomplexan parasite *Plasmodium falciparum*, comprehensive bioinformatic analyses failed to identify homologs of the proton channel subunit a and the peripheral stalk subunits b and F6 (13,14). At the same time, several novel components of *Tetrahymena* ATP synthase were identified by proteomic analysis. Strikingly, the subunit a was proposed to be replaced by a novel or extremely divergent mitochondrially encoded protein Ymf66 (15). However, the divergence in composition does not affect the function, as mitochondria from *Tetrahymena* (15) and *Plasmodium* (16) are capable to carry out oxidative phosphorylation. Similarly, the peripheral stalk subunits b, d, and A6L were not found in the green algae *Euglena gracilis* (Excavates; (17)) and in chlorophycean algae *Chlamydomonas* and *Polytomella* (Archaeplastida; (18,19)). Instead, several taxon-specific proteins called Asa1-9 (ATP synthase associated) associate with F_0F_1 -ATPase in these organisms (20). Together, these studies documented variability of ATP synthase composition across eukaryotes. Remarkably, none of the studies documented any alteration in the composition of the catalytic F_1 moiety.

Parasitic flagellate *Trypanosoma brucei* is a causative agent of sleeping sickness in humans and related diseases in domestic animals in Africa. Together with other pathogenic (e.g. *Leishmania* sp.) or free-living protists (*Bodo* sp.), *T. brucei* belongs to kinetoplastids, a highly divergent clade of Excavates (21). As an important pathogen, *T. brucei* experienced relatively long history of intensive research. Because

it can be cultivated *in vitro* and it is amenable to forward and reverse genetics approaches, it has become a universal model organism for kinetoplastids. Number of unprecedented biological processes has been discovered in trypanosomes. Some of them remained restricted only to closely related species (e. g. drastically reduced transcriptional regulation of gene expression, presence of single mitochondrion with unusual morphology), while others were later found also in phylogenetically distant organisms (e.g. RNA editing, GPI anchoring). In addition, some common eukaryotic machineries underwent divergent evolution and gained novel or modified functions in trypanosomes (e.g. Krebs cycle, trans-splicing).

Another striking example includes the mitochondrial F_0F_1 -ATP synthase/ATPase as the function of this enzyme is adapted to the environmental changes during the digenetic life cycle of the parasite. *T. brucei* alternates between the insect vector (tsetse fly) and a mammalian host. The insect procyclic form (PF) is characterized by fully active mitochondrion containing a conventional respiratory chain composed of complexes I, II, III and IV. In this stage the F_0F_1 -ATP synthase acts true to its name and synthesizes ATP by oxidative phosphorylation (22). In contrary, the bloodstream form (BF) relies on glycolysis for its ATP production and the mitochondrion is reduced in its size, function and activity, and lacks the typical cytochrome-mediated electron transport chain, which is coupled with proton translocation. Thus in this form, the essential (mitochondrial) mt membrane potential ($\Delta\psi_m$) is maintained by the reverse function of F_0F_1 -ATP synthase as this complex hydrolyses ATP and pumps protons from matrix across the mt inner membrane (23,24).

Structurally, the F_0F_1 -ATP synthase from *T. brucei* differs from other eukaryotes, missing all peripheral stalk and F_0 subunits except for OSCP, and subunit a and c. Nevertheless, the protein complexity of the F_0F_1 -ATP synthase complex is similar to the F-ATPases from other eukaryotes because it contains 14 kinetoplastid-specific proteins. These subunits are either novel or highly diverged F-ATPase subunits (25).

Here, we employed a biochemical purification to characterize the F_1 catalytic moiety from *T. brucei*. We describe two unique features of this enzyme: (i) it contains an additional stably associated protein p18 and (ii) the subunit α is split into two

fragments. None of these attributes has a parallel in any organism outside of Euglenozoa.

MATERIAL AND METHODS

Purification of F₁-ATPase

T. brucei PF Lister strain 427 was grown in SDM-79 media (Invitrogen) containing 10 % FBS to the late exponential phase ($2-3 \times 10^7$ cells/ml). Mitochondria were isolated by hypotonic lysis and percoll gradient centrifugation (26) and resuspended in buffer containing 50 mM Tris-HCl, pH 8.0, 250 mM sucrose, 5 mM benzamidine, and 5 mM ϵ -aminocaproic acid (ϵ -ACA) to final protein concentration of 16 mg/ml. Material was sonicated (6 x 15 s with one minute on ice between impulses) and disintegrated membranes were sedimented by ultracentrifugation (rotor Beckmann SW60Ti, 31,000 rpm, 5 hours, 4°C), and resuspended in the same buffer containing 1 mM ADP and a cocktail of protease inhibitors (pepstatin A, leupeptin, bestatin, diprotin A, and amastatin, 50 μ M each). F₁-ATPase was released by vigorous shaking (20 s) with 0.5 volume of chloroform saturated with 2 M Tris-HCl pH 8.5. The extracted sample was immediately spun (8,000 g, 5 min, 20°C). The top aqueous phase was cleared by centrifugation (2x30 min, 16,000 g, 20°C) and loaded on a HiTrap Q HP anion exchange chromatography column (GE Healthcare, United Kingdom) equilibrated in 20 mM Tris-HCl, pH 8.0, 1 mM ADP, 4 mM EDTA, 5 mM benzamidine, 5 mM ϵ -ACA. Elution was performed by a linear gradient of NaCl from 0 to 1 M in the same buffer in total volume of 25 ml. The fractions containing F₁-ATPase were pooled, concentrated (Vivaspin centrifugal concentrator, MWCO 100 kDa, Sartorius, Germany) to 200 - 500 μ l, and loaded on a gel-filtration column Superdex 200 10/300 GL (GE Healthcare, United Kingdom) washed by 20 mM Tris-HCl, pH 8.0, 200 mM NaCl, 1 mM ADP. The fractions containing F₁-ATPase were pooled and used for subsequent analyses.

ATPase activity measurements

The isolated F₁-ATPase was concentrated to >2 mg/ml, precipitated by one volume of saturated neutralized ammonium sulfate solution, and re-dissolved in 100 mM Tris-HCl pH 8.0, 4 mM EDTA, 50% glycerol. The activity of F₁-ATPase was measured by ATP regenerating assay (27). The hydrolysis of ATP is measured indirectly as a decrease of absorbance at 340 nm caused by decay of NADH in a

coupled reaction. The assay mixture contained 25 mM Tris, 25 mM MOPS, 50 mM KCl, 2 mM MgSO₄, adjusted to desired pH, 0.2 mM NADH, 2 mM ATP, 1 mM phosphoenolpyruvate (PEP), 10 µl/ml pyruvate kinase/lactic dehydrogenase from rabbit muscle (Sigma-Aldrich). All measurements were performed in 1 ml spectroscopic cuvettes with reaction mixture incubated at 37°C.

The inhibition of F₁-ATPase activity by resveratrol and sodium azide was assayed at pH 8.0. The inhibitors at different concentrations were added to the reaction mixture prior 0.7 µg of F₁-ATPase. The residual activities of the inhibited complex in equilibrium were measured. IC₅₀ values were calculated by fitting relative residual activities plotted against log inhibitor concentration into a sigmoidal dose-response curve with variable slope using GraphPad Prism 6 software.

ATPase activity in digitonin lysed mitochondria was measured with the Sumner assay, based on the release of phosphate when ATP is hydrolyzed by the enzyme (23,28). Briefly, crude mitochondria were extracted from 2x10⁸ cells with 0.015% digitonin, 0.6 M sorbitol, 2 mM EDTA, 20 mM Tris-HCl pH 7.5. Mitochondrial pellets were resuspended in an assay buffer (200 mM KCl, 2 mM MgCl₂, 10 mM Tris-HCl pH 8.0) and the 20 min reaction was initiated by the addition of neutralized ATP to a final concentration of 5 mM. Where indicated, samples were pre-treated with 2 mM sodium azide for 10 min at 27°C for lysates from PF and at 37°C for lysates from BF. The 100 µl reactions were stopped by the addition of 1.9 µl of 70% perchloric acid. After a 30 min incubation on ice, the samples were spun down (16,000 g, 10 min, 4°C) and 90 µl of the supernatant was incubated for 10 min with 0.5 ml of Sumner reagent (8.8% FeSO₄.7H₂O, 375 mM H₂SO₄, 6.6% (NH₄)Mo₇O₂₄.4H₂O) at room temperature (RT). 200 µl was transferred to a 96 well plate and the absorbance was measured at 610 nm using a plate reader (Infinite M200Pro, Tecan). To calibrate the assay, a standard curve was calculated from the absorbance values of inorganic phosphate samples (0– 2 mM).

Plasmid construction and *Trypanosoma* RNAi cell lines generation

To generate p18 RNAi construct, the 464 bp of p18 gene (Tb927.5.1710) was amplified by PCR from *T. brucei* strain 427 genomic DNA with the following oligonucleotides: FW-GCAGGATCCCTCGGCTACTGCATTCAACA, REV-GACAAGCTTACAGCATTACTACACGCCCC. The amplified fragment was digested with *Hind*III and *Bam*HI and inserted into the p2T7-177 vector, which is

targeted to the minichromosome 177 basepair repeat region (29). PF *T. brucei* strain 29-13 and BF single marker (SM) cells, both constitutively expressing the ectopic T7 RNA polymerase and tetracycline repressor, were transfected with *NotI* linearized p18 RNAi construct. The PF cells were grown at 27°C in SDM-79 media containing 10% FBS, 15 µg/ml of G418, 25 µg/ml hygromycin, and 2.5 µg/ml phleomycine, while the BF cells were grown in HMI-9 media containing 10% FBS, 2.5 µg/ml of G418, 5 µg/ml hygromycin, and 2.5 µg/ml phleomycine. The PF RNAi α cell line was described earlier (25).

The RNAi was induced by the addition of 1 µg/ml of tetracycline into the media. Cell densities were measured using the Z2 Cell Counter (Beckman Coulter Inc.). Throughout the analyses, cells were maintained in the exponential mid-log growth phase.

SDS-PAGE and Western blot

Protein samples were resolved on SDS-PAGE and stained by Coomassie Brilliant Blue dye or blotted onto a PVDF membrane. Membranes were probed with the appropriate primary antibody followed by incubation with a secondary HRP-conjugated goat anti-rabbit or anti-mouse antibody (1:2000, BioRad). Blots were developed using the ECL system (Pierce) and visualized on a ChemiDoc instrument (BioRad). When needed, membranes were stripped at 50°C for 30 min in a stripping buffer (62.5 mM Tris pH 6.8, 100 mM mercapthoethanol, 2% SDS) and re-probed. Primary antibodies used in this study were: mouse monoclonal antibody against mitochondrial Hsp70 (1:2000; (30)), rabbit polyclonal antibodies against ATPaseTb2 (1:1000), subunit β (1:2000), p18 (1:1000; all three in (31)), and α_{1-127} (1:1000; (32)).

Native protein gel electrophoresis

The protocol for high resolution clear native PAGE (hrCNE) was adapted from published studies (33,34). Briefly, crude mitochondrial vesicles obtained from $\sim 5 \times 10^8$ cells were resuspended in a lysis buffer (2 mM ϵ -ACA, 50 mM imidazole, 1 mM EDTA, 50 mM NaCl, pH 7.0) and lysed with 4 mg digitonin/1 mg protein for one hour on ice. The samples were spun down at 16,000 g for 30 min and the cleared lysates were mixed with a 5x loading dye (0.1% Ponceau-S, 50% glycerol) and

amount corresponding to 10 μg or 20 μg of protein for PF or BF, respectively, was loaded onto a 3%-12% native gradient gel. The resolved mitochondrial lysates were transferred onto a nitrocellulose membrane and probed with selected antibodies as described above.

Blue native PAGE (BN-PAGE) was carried out with Novex® NativePAGE™ Bis-Tris gel system (Life Technologies) using 3-12 % gradient gel according to the manufacturer's instructions.

Mitochondrial membrane potential measurement

The mitochondrial membrane potential ($\Delta\psi_m$) was determined utilizing the red-fluorescent stain Tetramethylrhodamine (TMRE). Cells in the exponential growth phase were stained with 60 nM of the dye for 30 min at 37°C for BF and 27°C for PF. Cells were pelleted (1,300 g, 10 min, RT), resuspended in 2 ml of PBS (pH 7.4) and immediately analyzed by flow cytometry (BD FACS Canto II Instrument). For each sample, 10,000 events were collected. Treatment with the uncoupler FCCP (20 μM) was used as a control for mt membrane depolarization. Data were evaluated using BD FACSDiva (BD Company) software.

Protein analyses by mass spectrometry (MS) and N-terminal sequencing

Protein bands from SDS-PAGE gel stained by Coomassie blue dye were digested by trypsin or chymotrypsin and identified by peptide mass fingerprinting and fragmentation in an ABI 4800 MALDI-TOF-TOF mass spectrometer (Applied Bioscience, USA) and Thermo Orbitrap XL spectrometer (Thermo Scientific, USA). The masses of peptides and their fragments were compared with the National Centre for Biotechnology Information non-redundant (NCBI nr) sequence database using MASCOT software (Matrix Science, UK). Total masses of proteins were determined by reverse phase liquid chromatography coupled MS (LC/MS) using positive ion electrospray ionization and a QTrap 4000 mass spectrometer (ABSciex).

For N-terminal sequencing, SDS-PAGE separated proteins were transferred to PVDF membrane and stained by Coomassie dye. The individual bands were excised and N-terminal sequences were determined by Edman degradation at the Protein and Nucleic Acid Chemistry Facility, Department of Biochemistry, University of Cambridge, UK.

Bioinformatic tools and sequence analyses

Sequence homology search was carried out with BLAST algorithms (35). Protein motifs were searched in Pfam (36), Prosite (37) and NCBI-CDD databases using Motif Search interface (www.genome.jp/tools/motif/). Structure homology search was performed with HHpred toolkit (38). Transmembrane domains were predicted with MEMSAT3 (39), TMHMM (40), TMPred (41), and TopPred 2 (42). Multiple sequence alignments were generated with MUSCLE iterative method (43) in Geneious software (Biomatters, New Zealand).

RESULTS

Purification of *T. brucei* F₁-ATPase

To isolate highly pure F₁-ATPase from PF cells of *T. brucei* we adopted and modified procedures previously used for F₁-ATPase purification from *B. taurus*, *S. cerevisiae* and other organisms (Fig. 1A) (44-46). Mitochondria purified from PF cells grown until the late exponential phase were used as a starting material. Upon mitochondria disintegration by sonication, F₁-ATPase was stripped from membranes by chloroform extraction. Contaminating proteins were removed by anion exchange chromatography followed by gel filtration. F₁-ATPase eluted as a single sharp peak, suggesting homogeneous population of purified complexes (Fig. 1B). The integrity of purified F₁-ATPase was confirmed by BN electrophoresis, wherein the complex migrates as a single band (Fig. 1C). The SDS-PAGE resolution of the band followed by Silver staining proved the presence of all subunits (data not shown). Typically, we obtained 2 mg of purified complex from $\sim 1.5 \times 10^{11}$ cells.

To prove that we purified an active complex we measured its ATPase activity. Maximal rate of ATP hydrolysis of 56.0 ± 4.9 $\mu\text{mol}/\text{min}/\text{mg}$ (56.0 μmol of hydrolyzed ATP per minute per mg of protein) occurred at pH 8.0. This value is similar to the activity of bovine F₁-ATPase measured at the same conditions (64.8 ± 4.3 $\mu\text{mol}/\text{min}/\text{mg}$). The complex remained active between pH 6.5 and 8.0, which likely represents physiologically relevant values. Out of this range the activity decreased rapidly (Fig. 1E). The activity was completely inhibited by 1mM sodium azide, a potent universal F₁-ATPase inhibitor, demonstrating the lack of any nonspecific ATP hydrolysis. However, *T. brucei* F₁-ATPase azide sensitivity is somewhat lower (IC₅₀ values of 59.5 μM) than the sensitivity of the bovine F₁-ATPase (IC₅₀ values of 15.9 μM). Similarly, resveratrol, a drug that efficiently inhibits bovine and yeast enzyme

affected trypanosome F₁-ATPase activity only at high concentrations, with IC₅₀ value of 144.4 μM (Tab. 1). The resveratrol IC₅₀ for bovine F₁-ATPase is 6.4 μM (47,48). Despite the specific activity is similar to the bovine enzyme, the different sensitivity to azide and resveratrol treatments suggest a possibility for parasite-specific features of F₁-ATPase.

Characterization of F₁-ATPase subunits

The purified F₁-ATPase was resolved on SDS-PAGE, the individual bands were excised, digested by trypsin, and proteins were identified by MALDI-TOF MS (Fig. 1D). The purified complex contains all conventional eukaryotic subunits of F₁-ATPase. The band intensities correspond to the expected stoichiometry $\alpha_3\beta_3\gamma_1\delta_1\varepsilon_1$. In contrast to any other known organism, the complex contains an additional subunit, which is referred to as p18, according to its molecular mass. Another extraordinary feature is that the subunit α is split into two fragments of apparent molecular masses of approximately 47 and 13 kDa (Fig.1D).

To characterize mature F₁-ATPase components, total masses of all subunits were measured by LC-MS and their N-termini were subjected to sequencing by Edman degradation. Together with the peptide fingerprinting data, these analyses enabled identification of mitochondrial targeting signals (MTS) and posttranslational modifications (PTM). The results are summarized in Tab. 2. N-terminal MTS were determined for all proteins with the exception of the subunit γ , for which only the removal of the first methionine was detected. This finding suggests that this subunit is imported via an internal MTS. Mt localization signals, which are placed within the protein sequence, are known from other organisms (49). Recently, such signal was also reported in *T. brucei* (50).

Expected masses of individual F₁-ATPase subunits (calculated from the relevant TriTrypDB entries; (51)) were compared with the measured total masses with the aim to identify potential post-translational modification (PTM). No PTMs were observed in the sequence of subunits α , ε and p18. The measured mass of the subunit δ suggests that its N-terminal glutamine is cyclized to pyroglutamate (pE). This data were supported by MALDI-TOF analysis, which provided a strong evidence for the N-terminal pE-containing peptide. The glutamine cyclization is catalyzed by glutaminyl cyclase (52), which homolog (Tb927.7.6940) is present in the *T. brucei* genome. Alternatively, pE can arise spontaneously at certain experimental conditions (53) and

therefore might be considered as an artifact. Distinguish between these two possibilities is difficult in our case, though spontaneous pE formation occurs with a low frequency and the lack of species with unmodified N-terminal glutamine in the purified complex supports the natural character of this PTM.

The subunit γ lacks the N-terminal MTS, exhibits cleavage of the N-terminal methionine and acetylation of the adjacent serine, a widespread PTM of eukaryotic proteins (54). In addition, we documented an alanine to valine substitution at position 65 (as numbered from the start methionine). Sequencing of genomic DNA of the strain used for the F₁-ATPase purification revealed heterogeneity in the codon of this residue, suggesting either population polymorphism or heterozygosity in the respective locus. In the case of subunit β , 14.5 Da difference was observed between calculated and measured total masses. We ruled out any amino acid substitution(s) by sequencing the corresponding genomic locus in the strain used for the F₁-ATPase preparation. Therefore, the observed discrepancy may reflect presence of an unknown PTM, possibly methylation.

In addition, the MS and sequencing analyses were used to map the exact position of the cleavage site in the subunit α and to precisely determine the identity of both resulting fragments, from now on referred to as α_{1-127} and $\alpha_{135-560}$ (Fig. 2A). The alignment of the subunit α amino acid sequences from species representing all main groups of eukaryotes and bacteria shows that the cleavage site occurs in a divergent part of the protein (Fig. 2B). The corresponding region of the bovine subunit α forms a loop that is exposed on the surface of F₁-ATPase (Fig. 2C). This loop is located between the N-terminal crown domain and the nucleotide-binding domain (55). In *T. brucei* and related *Leishmania* and *Euglena*, this region contains additional residues and thus the loop might be even further extended. Given its localization on the periphery of the F₁ headpiece, it is plausible to expect, that its cleavage would not affect the integrity and function of the complex, as the overall structural stability is achieved through multiple non-covalent interactions. In addition, the exposure of the cleavage site to the surface makes it a possible target for a putative specific protease.

Down-regulation of p18 results in loss of ATP synthase complexes.

To investigate the importance of p18 to F₀F₁-ATP synthase in *T. brucei*, we generated PF and BF cell lines, which enable tetracycline inducible down-regulation of the subunit p18 expression by RNA interference (PF p18^{RNAi} and BF p18^{RNAi}). The

growth of induced PF p18^{RNAi} cells was mildly affected after three days of RNAi induction and cells kept proliferating with an increased doubling time (Fig. 3A, left panel). The exact same growth response was observed after down-regulation of F₁-ATPase subunit α (PF α ^{RNAi} cell line, Fig. S1B) and the catalytic subunit β (56). The relatively weak growth phenotype is in agreement with the fact, that F₀F₁-ATP synthase is not the only source of ATP in the PF *T. brucei*. In this life stage, mitochondrial ATP is also generated by two different mt substrate phosphorylation reactions (57).

In contrast, the BF p18^{RNAi} cells exhibited growth arrest between day two and three after RNA induction (Fig. 3A, right panel). The partial recovery of the growth rate after day 4 is likely due to emergence of RNAi revertants, which is a common consequence of high selection pressure caused by silencing of essential genes in BF trypanosomes (58).

The RNAi efficiency was confirmed by western blot analysis using specific p18 antibody. The abundance of p18 declined dramatically two days after the RNAi induction in both PF and BF trypanosomes (Fig. 3B). The ablation of the subunit α led to decreased levels of the subunit β in PF (Fig. S1) and BF trypanosomes (23), suggesting that the core F₁ components are not stable without their binding partners. If p18 is an inherent F₁ constituent, its down regulation should also negatively impact total levels of other F₁-ATPase subunits. Indeed, the silencing of p18 resulted in decreased abundance of the subunit β in total lysates of both PF and BF cells (Fig. 3B), implying that F₁-ATPase is not being assembled and/or stable when p18 expression is attenuated. At the same time, the abundance of ATPaseTb2, a subunit of the fully assembled F₀F₁ complex, is also affected (Fig. 3B). This is in agreement with the fact that the rotor and peripheral stalk are not fully assembled in the absence of F₁ moiety and their components are susceptible to rapid degradation (or are down-regulated on the translational level) (59). Indeed, hrCN electrophoresis of crude mitochondrial lysates followed by immunostaining with anti- β and anti-ATPaseTb2 specific antibodies demonstrated, that the levels of F₁-ATPase and F₀F₁ complexes are significantly decreased in PF and BF p18^{RNAi} induced cells (Fig. 3C). We conclude that p18 is essential for F₁-ATPase structural integrity and stability in both life stages of *T. brucei*.

Disruption of F₁-ATPase enzymatic activities upon p18 silencing results in the $\Delta\psi_m$ perturbation.

To demonstrate that p18 is required for a proper function of F₁-ATPase, the total ATPase activity was measured in mt lysates from noninduced and RNAi induced PF p18^{RNAi} cells. Typically, the specific F₁-ATPase activity represents ~ 35-45% of total mt ATPase activity. Treatment with sodium azide was used as a positive control. Importantly, the total ATPase activity was significantly decreased after day 2 of RNAi induction. This decrease is comparable with a reduction of ATPase activity in noninduced cells upon sodium azide treatment (Fig. 4). Thus our results indicate that the enzymatic activity of F₁-ATPase is largely affected, likely due to the complex instability, when p18 subunit is silenced.

To assess a biological relevance of this finding, we measured the $\Delta\psi_m$ in both PF and BF RNAi^{p18} cell lines. Given the extraordinary behavior of the F₀F₁-ATP synthase/ATPase complex in two different life stages of the parasite, we expected to observe increase of the $\Delta\psi_m$ in PF and decrease of the $\Delta\psi_m$ in BF cells. Indeed, failure of F₁-ATPase activity in PF cells led to hyperpolarization of inner membrane reaching its maximum on day 3 and 4 (Fig. 5, left panel). The reason for this detected phenotype is a fact that F₀F₁-ATP synthase is important for proton movement back to the mt matrix. Once this complex is not present in the inner mt membrane, the proton pore is absent and the protons accumulate in the inner membrane space. In contrary, in BF cells a collapse of $\Delta\psi_m$ was observed on day 2 and 3 of p18 RNAi (Fig. 5, right panel). This observation is fully in the agreement with the literature as F₀F₁-ATPase complex generates the essential $\Delta\psi_m$ in this life stage (23,31).

DISCUSSION

In this work, we purified and characterized F₁-ATPase from pathogenic flagellate *T. brucei*. The purified F₁-ATPase was fully active and its specific activity was comparable with the activity of its bovine counterpart. However, in contrast to the bovine complex, trypanosome F₁-ATPase is less sensitive to typical F₁-ATPase inhibitors, azide and resveratrol (47,55). As the crystal structure of the bovine enzyme inhibited with the latter inhibitor is available, it is known that the resveratrol binding involves two α chains, one of three subunits β , and the central stalk subunit γ (47). Most of the residues important for the resveratrol binding are conserved in *T. brucei* with the exception of the γ subunit residues Ala²⁵⁶ and Lys²⁶⁰, which are

replaced in trypanosome γ protein sequence by a bulky phenylalanine and hydrophobic alanine, respectively. It is plausible to speculate that these substitutions may cause decreased sensitivity to this compound.

Interestingly, the purified F_1 -ATPase had a complex pattern of 7 different protein bands on SDS-PAGE stained with Coomassie. MS analysis showed that subunit α is cleaved into two fragments, α_{1-127} and $\alpha_{135-560}$. The cleavage of the subunit α can be either an intrinsic property of the trypanosome F_0F_1 complex or an unwanted consequence of the purification procedure. The predicted peripheral localization of the cleavage site on the surface of the F_1 -ATPase headpiece makes this region an easy target for specific proteolysis as well as for unspecific degradation. Nevertheless, several clues suggest that the cleavage is of natural rather than artificial character. Most importantly, the F_1 -ATPase exhibits ATP hydrolase activity in the presence of the cleaved subunit α . Furthermore, the cleavage was previously reported not only in *T. brucei* (25,32,60), but also in several other Kinetoplastid species (*Leishmania tarentolae*, (61); *Crithidia fasciculata*, (62)), and in *Euglena gracilis* (17). It is unlikely that different experimental strategies used in different species would generate the same artifact. The protein is cleaved at two positions after aminoacid Leu¹²⁷ and Leu¹³⁵ (Fig. 2A), suggesting involvement of a hypothetical leucyl endopeptidase. Such enzymatic activity has been so far identified only in spinach (*Spinacea oleracea*, (63)). Remarkably, comparison of α subunit protein sequences revealed that despite the overall conservancy, the Kinetoplastid subunit α significantly differs from any other main group of Eukaryotes. Moreover, the subunit α sequences of non-kinetoplastid eukaryotes are closer to the bacterial homologs than to the homologs in Kinetoplastids. This dissimilarity is obvious predominantly at the cleavage site and its proximity, at the C-terminal end of the protein (last ~70 residues), and in the crown domain (Fig. S2). The crown is situated at the top of F_1 moiety and is indispensable for binding of the catalytic segment to the peripheral stalk. This interaction is mediated by the contacts between the negatively charged N-terminal domain of OSCP and the N-terminal α -helix in one of the three subunits α (8,64). Interestingly, even though the helix is generally highly conserved in both prokaryotes and eukaryotes, the corresponding sequence is completely divergent in *T. brucei* and related species (see Fig. S2). It suggests that the F_1 -peripheral stalk interaction has undergone substantial changes in the lineage leading to Kinetoplastids. These changes could have involved

the split of the subunit α and also the employment of the novel subunit p18 (see below). In contrast to the subunit α , the subunit β is considerably less divergent in *T. brucei*. Its crown domain, which does not contact peripheral stalk, is much more conserved (Fig. S3). Nevertheless, also the sequences of subunit β in *T. brucei* and *Leishmania* are the most divergent among eukaryotes (15), documenting fast evolution of the F_1 -ATPase catalytic domain in Kinetoplastids.

The cleavage of subunit α explains the presence of one additional protein band in *T. brucei* F_1 -ATPase SDS-PAGE profile. The second unknown protein band was identified as p18, previously reported to be associated with F_0F_1 -ATP synthase in trypanosomatids (25,61,62). Based on its limited homology to subunit b of the peripheral stalk (62), this protein was used as a marker for the F_0 moiety. However, because the similarity was very poor, the homology was reconsidered as tentative only (25) and the direct relationship of p18 to F_1 -ATPase was speculated (65). The product of p18 gene is annotated as a ribonucleoprotein p18 in the TriTrypDB database (accession number Tb927.5.1710), as it was originally identified as a protein co-migrating with mitochondrial ribonucleoprotein complexes in native gels (66). Here we show that p18 co-purifies with F_1 -ATPase. Based on Coomassie (Fig 1C.) and Silver staining (data not shown) of the complex separated on SDS-PAGE the p18 subunit appears to be present in more than one copy per complex. This proposition is also supported by the observation that the F_0F_1 complexes purified with TAP-tagged p18 contained both tagged and non-tagged p18 species ((25) in this report p18 is referred to as subunit b). The exact stoichiometry of this subunit remains to be determined.

We propose that p18 is neither homolog nor functional analog of the subunit b based on following arguments. First of all, it remains associated with F_1 -ATPase throughout all the steps of isolation procedure. Especially, p18 persists after chloroform extraction that releases F_1 moiety from membrane proteins. Thus, it is unlikely that p18 is membrane-bound protein (contrary to subunit b), as there has been no example, wherein a membrane protein remained bound to F_1 -ATPase after its release by chloroform extraction.

Furthermore, we searched for possible transmembrane domains in p18 sequence employing five different prediction tools. Only one programme (MEMSAT) detected a hypothetical transmembrane helix (TMH) with very low probability. Moreover, the

detected TMH overlapped with a pentatricopeptide repeat (PPR) signature (see below), which is not a membrane motif. In addition, unlike the subunit b, which has its TMH at the very N-terminal end, the predicted TMH of p18 is localized in the C-terminal half of the protein. Therefore, based on *in silico* analyses p18 contains no TMH homologous to the subunit b and likely no transmembrane segments at all.

The observed decrease of F₁-ATPase abundance after p18 silencing (Fig. 3C) also supports the conclusion that p18 does not correspond to the subunit b. Inactivation of the subunit b (67) or other non-F₁ components (e.g. the subunit δ in *E. coli*, corresponding to eukaryotic OSCP; (68)) did not decrease levels of F₁ moiety. This is in agreement with the fact that F₁ is assembled as an independent unit independently from F₀ subunits. However, in the absence of F₀ components or their assembly factors, F₁-ATPase does not attach properly to the membrane, but remains intact and retains its ATPase activity (as demonstrated in *Saccharomyces cerevisiae*, (69,70), in *E. coli*, (68), and in *T. brucei*, (25)).

As mentioned above, p18 contains two PPR motifs and thus belongs to the PPR family (71). PPR proteins are abundant especially in plants, e.g. *Arabidopsis thaliana* genome contains approximately 450 PPR encoding genes (72). *T. brucei* and related species have over 30 PPR genes (71,73,74), that is more than any other non-plant eukaryote (humans and yeast have only six and five PPR proteins, respectively). Most described PPR proteins localize to mitochondria or chloroplasts and are implied in organellar RNA metabolism (for review see (75)). In trypanosomes, PPR proteins are components of mitochondrial ribosome (76,77), and involved in 3'end RNA processing (78). Only a handful of known PPR proteins possess a function independent of RNA binding and metabolism. Therefore, p18 is either a rare example of PPR protein unrelated to RNA function, or more interestingly, it represents a link between RNA processing and energy metabolism in *T. brucei*. Besides the two PPR motifs, no predicting tool we used, recognized any other motif in the p18 amino acid sequence. Similarly, no non-PPR signatures were predicted in any other PPR protein in *T. brucei* (74).

To identify p18 orthologs, we carried out primary and secondary structure similarity searches. BLAST tools found homologous proteins with high probability only within Kinetoplastids. All other hits had considerably lower probability scores and were usually related to plant PPR proteins. The HHpred toolkit that was designed to identify proteins with structural rather than sequential homology identified only

PPR, and TPR (tetratricopeptide) proteins. The TPR motif is very similar to PPR; TPR containing proteins have various functions and are ubiquitous in both prokaryotes and eukaryotes (79). Recently, p18 was also identified in *Euglena gracilis* (17), a member of Euglenids, which together with Kinetoplastids form Euglenozoa, a clade of Excavates (12). The comprehensive bioinformatics search in *E. gracilis* study using multiple approaches failed to identify p18 homologs in any organism outside Euglenozoa group.

AUTHOR CONTRIBUTIONS

Conceived and designed the experiments: OG AZ KS BP. Performed the experiments: OG KS HV. Analyzed the data: OG AZ KS BP. Wrote the paper: OG AZ BP.

ACKNOWLEDGMENTS

This work was funded by Ministry of Education ERC CZ grant LL1205 and the EMBO Installation grant 1965 (to AZ). We acknowledge the use of research infrastructure that has received funding from the European Union Seventh Framework Programme (FP7/2007-2013) under grant agreement no.316304.

FIGURE LEGENDS

Figure 1. Purification of F₁-ATPase from procyclic form of *T. brucei*.

A: Scheme of purification. Mt membrane fragments and submitochondrial particles were prepared by sonication from purified mitochondria. F₁-ATPase was released by chloroform extraction and purified by a two-step chromatography. For details see Material and Methods.

B: Final step of F₁-ATPase purification. The gel filtration elution profile was recorded by UV₂₈₀ radiation (lower panel). Fractions representing peaks 1 and 2 were resolved on SDS-PAGE (upper panel). The peak 3 corresponds to the signal from the excess of ADP. F₁-ATPase elutes in the peak 1. The dominant band in the peak 2 was identified as dihydrolipoyl dehydrogenase.

C: F₁-ATPase was resolved on 3-12% BN PAGE. The native marker sizes are depicted.

D: F₁-ATPase was resolved on SDS-PAGE, visualized with Coomassie staining and the individual bands were identified by MALDI-TOF MS.

E: ATPase activity of purified F₁-ATPase was measured by Pullmann assay in indicated pH values and normalized to the value at pH 8.0. Error bars represent standard deviations of three measurements.

Figure 2. The cleavage site of subunit α maps to the least conserved part of this protein and is located at the beginning of nucleotide binding domains.

A: Schematic depiction of subunit α in *T. brucei*. The black rectangle represents central nucleotide-binding domain. The two arrowheads indicate the position of two cleavage sites. The cleaved out sequence and the adjacent residues are shown.

B: Part of the alignment of subunit α sequences from different species covering all major groups of Bacteria and Eukaryotes. For the full protein alignment, see Fig. S2. The blue box highlights stretch of residues excised during the cleavage. The red box labels the residues of bovine subunit α that are depicted in Fig. 2C by red line. Bt – *Bos taurus*, Tb – *T. brucei*, Lm – *Leishmania major*, Eg – *Euglena gracilis*, Hs – *Homo sapiens*, Dm – *Drosophila melanogaster*, Ce – *Caenorhabditis elegans*, Sc – *Saccharomyces cerevisiae*, Pf – *Plasmodium falciparum*, Tt – *Tetrahymena thermophila*, At mt – *Arabidopsis thaliana*, the subunit α in mitochondria, At chl. – *Arabidopsis thaliana* – the subunit α in chloroplasts, Np – *Nostoc punctiforme*, Bs – *Bacillus subtilis*, Sp – *Streptococcus pneumoniae*, Sg – *Streptomyces griseus*, Rm – *Rhizobium melioidi*, Ec – *Escherichia coli*, St – *Salmonella enteritidis*, Bf – *Bacteroides fragilis*.

C. The cleavage sites in the subunit α in *T. brucei* align to a loop (red line) extending from the surface in the structure of bovine F₁-ATPase. Subunits α , β , γ , δ , and ϵ in the ground structure of bovine F₁-ATPase (80) are shown in yellow, green, blue, orange, and magenta, respectively. Left panel – view from top (matrix side). Right panel – view from side; only one of each α and β subunits (the pair in the empty conformation) is shown.

Figure 3. Silencing of p18 results in a decrease of F₁F₀-ATP synthase abundance in PF and BF trypanosomes.

A. Growth curve of induced and non-induced p18^{RNAi} PF (left panel) and BF (right panel) cells was measured for 8 days.

B. The steady state levels of p18, β , and ATPaseTb2 were determined in whole-cell lysates from non-induced and RNAi induced cells by Western blot. Antibody against Hsp70 was used as a loading control. This experiment was performed for both PF p18^{RNAi} (left panel) and BF p18^{RNAi} cells (right panel).

C. The stability of F₀F₁-ATP synthase/ATPase complexes upon p18 silencing was examined using hrCNE. Mitochondria from p18^{RNAi} PF (left panel) and p18^{RNAi} BF (right panel) RNAi non-induced cells (NON) and cells induced for 1 (IND1), 2 (IND2) and 3 (IND3) days were lysed by digitonin (4 mg/mg). Equal amounts of lysed mitochondrial proteins were fractionated on a 3%-12% hrCNE, blotted onto a nitrocellulose membrane and probed with the anti- β and anti-ATPaseTb2 antibodies. Positions of F₁-ATPase and monomeric (m) and dimeric (d) complexes are depicted by arrows. The sizes of a native marker (Invitrogen) are indicated. The same amount of lysates were resolved on SDS-PAGE, blotted, and probed with anti-Hsp70 antibody as a control (bottom panel).

Figure 4. The total ATPase activity is decreased upon p18 RNAi.

Employing the Sumner ATPase assay, the F₁-ATPase hydrolytic activity was measured in PF p18^{RNAi} cells either not induced (NON) or induced for 2 and 4 days (IND2, IND4). Crude mt vesicles were obtained by digitonin extraction and the ATPase activity was assayed by measuring the release of free phosphates. The specific F₁-ATPase inhibitor, azide (AZ, 4 μ M), was added as indicated. The total amount of free phosphate created from all ATPase enzymes present in the sample was set at 100%. The azide-sensitive activity representing the F₁-ATPase is depicted in dark grey. The results are means \pm s.d. (n = 2).

Figure 5. The $\Delta\psi_m$ is affected in PF and BF p18^{RNAi} cells.

The $\Delta\psi_m$ was measured in non-induced (NON) p18 RNAi cells and cells induced for 1, 2, 3 (PF and BF) and 4 (PF) days (IND1, IND2, IND3 and IND4) by flow cytometry using Mitotracker Red CMX-Ros. The results are means \pm s.d. (n = 3). *P < 0.05, Student's t-test. The results from PF p18^{RNAi} cell lines are presented in the left panel, while the results from BF p18^{RNAi} are in the right panel.

Figure S1. Silencing of the subunit α in PF cells results in mild growth phenotype and decrease of the subunit β abundance.

A. Growth curve of non-induced and induced α^{RNAi} cell line.

B. Levels of α_{1-127} and β in whole-cell lysates prepared from non-induced cells and from cells at indicated time points after α RNAi induction were monitored by Western blot. Antibody against Hsp70 was used as a loading control.

Figure S2. The alignment of F₁-ATPase subunit α sequences from different species including representatives of all major groups of Bacteria and Eukaryotes. Experimentally determined, predicted, or estimated mitochondrial targeting signals were excluded. Bt – *Bos taurus*, Tb – *T. brucei*, Lm – *Leishmania major*, Eg – *Euglena gracilis*, Hs – *Homo sapiens*, Dm – *Drosophila melanogaster*, Ce – *Caenorhabditis elegans*, Sc – *Saccharomyces cerevisiae*, Pf – *Plasmodium falciparum*, Tt – *Tetrahymena thermophila*, At mt – *Arabidopsis thaliana*, the subunit α in mitochondria, At chl. – *Arabidopsis thaliana* – the subunit α in chloroplasts, Np – *Nostoc punctiforme*, Bs – *Bacillus subtilis*, Sp – *Streptococcus pneumoniae*, Sg – *Streptomyces griseus*, Rm – *Rhizobium melioli*, Ec – *Escherichia coli*, St – *Salmonella enteritidis*, Bf – *Bacteroides fragilis*.

Figure S3. The alignment of F₁-ATPase subunit β sequences from different species including representatives of all major groups of Bacteria and Eukaryotes. The names of species are abbreviated as in Fig. S1.

Table 1. IC₅₀ values of inhibition of *T. brucei* and *B. taurus* F₁-ATPase by sodium azide and resveratrol.

Table 2. Observed and calculated masses, N-terminal sequences, and posttranslational modifications of intact mature F₁-ATPase subunits.

References

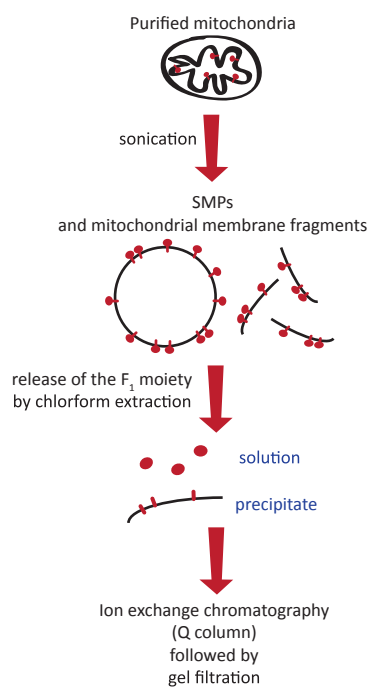
1. Walker, J. E. (2013) *Biochem Soc Trans* **41**, 1-16
2. Weber, J., and Senior, A. E. (2000) *Biochim Biophys Acta* **1458**, 300-309
3. Jonckheere, A. I., Smeitink, J. A., and Rodenburg, R. J. (2012) *J Inherit Metab Dis* **35**, 211-225
4. Junge, W. (1999) *Proc Natl Acad Sci U S A* **96**, 4735-4737
5. Hutcheon, M. L., Duncan, T. M., Ngai, H., and Cross, R. L. (2001) *Proc Natl Acad Sci U S A* **98**, 8519-8524
6. Stock, D., Leslie, A. G., and Walker, J. E. (1999) *Science* **286**, 1700-1705
7. Dickson, V. K., Silvester, J. A., Fearnley, I. M., Leslie, A. G., and Walker, J. E. (2006) *EMBO J* **25**, 2911-2918
8. Carbajo, R. J., Kellas, F. A., Yang, J. C., Runswick, M. J., Montgomery, M. G., Walker, J. E., and Neuhaus, D. (2007) *J Mol Biol* **368**, 310-318
9. Meyer, B., Wittig, I., Trifilieff, E., Karas, M., and Schagger, H. (2007) *Mol Cell Proteomics* **6**, 1690-1699
10. Arnold, I., Pfeiffer, K., Neupert, W., Stuart, R. A., and Schagger, H. (1999) *J Biol Chem* **274**, 36-40
11. Vaillier, J., Arselin, G., Graves, P. V., Camougrand, N., and Velours, J. (1999) *J Biol Chem* **274**, 543-548
12. Adl, S. M., Simpson, A. G., Lane, C. E., Lukes, J., Bass, D., Bowser, S. S., Brown, M. W., Burki, F., Dunthorn, M., Hampl, V., Heiss, A., Hoppenrath, M., Lara, E., Le Gall, L., Lynn, D. H., McManus, H., Mitchell, E. A., Mozley-Stanridge, S. E., Parfrey, L. W., Pawlowski, J., Rueckert, S., Shadwick, R. S., Schoch, C. L., Smirnov, A., and Spiegel, F. W. (2012) *J Eukaryot Microbiol* **59**, 429-493
13. Balabaskaran Nina, P., Morrisey, J. M., Ganesan, S. M., Ke, H., Pershing, A. M., Mather, M. W., and Vaidya, A. B. (2011) *J Biol Chem* **286**, 41312-41322
14. Vaidya, A. B., and Mather, M. W. (2009) *Annu Rev Microbiol* **63**, 249-267
15. Balabaskaran Nina, P., Dudkina, N. V., Kane, L. A., van Eyk, J. E., Boekema, E. J., Mather, M. W., and Vaidya, A. B. (2010) *PLoS Biol* **8**, e1000418
16. Uyemura, S. A., Luo, S., Vieira, M., Moreno, S. N., and Docampo, R. (2004) *J Biol Chem* **279**, 385-393
17. Perez, E., Lapaille, M., Degand, H., Cilibrasi, L., Villavicencio-Queijeiro, A., Morsomme, P., Gonzalez-Halphen, D., Field, M. C., Remacle, C., Baurain, D., and Cardol, P. (2014) *Mitochondrion*
18. Cardol, P., Gonzalez-Halphen, D., Reyes-Prieto, A., Baurain, D., Matagne, R. F., and Remacle, C. (2005) *Plant Physiol* **137**, 447-459
19. van Lis, R., Mendoza-Hernandez, G., Groth, G., and Atteia, A. (2007) *Plant Physiol* **144**, 1190-1199
20. Vazquez-Acevedo, M., Cardol, P., Cano-Estrada, A., Lapaille, M., Remacle, C., and Gonzalez-Halphen, D. (2006) *J Bioenerg Biomembr* **38**, 271-282
21. Stuart, K., Brun, R., Croft, S., Fairlamb, A., Gurtler, R. E., McKerrow, J., Reed, S., and Tarleton, R. (2008) *J Clin Invest* **118**, 1301-1310
22. Besteiro, S., Barrett, M. P., Riviere, L., and Bringaud, F. (2005) *Trends Parasitol* **21**, 185-191
23. Schnauffer, A., Clark-Walker, G. D., Steinberg, A. G., and Stuart, K. (2005) *EMBO J* **24**, 4029-4040
24. Brown, S. V., Hosking, P., Li, J., and Williams, N. (2006) *Eukaryot Cell* **5**, 45-53
25. Zikova, A., Schnauffer, A., Dalley, R. A., Panigrahi, A. K., and Stuart, K. D. (2009) *PLoS Pathog* **5**, e1000436
26. Schneider, A., Charriere, F., Pusnik, M., and Horn, E. K. (2007) *Methods Mol Biol* **372**, 67-80
27. Pullman, M. E., Penefsky, H. S., Datta, A., and Racker, E. (1960) *J Biol Chem* **235**, 3322-3329
28. Law, R. H., Manon, S., Devenish, R. J., and Nagley, P. (1995) *Methods Enzymol* **260**, 133-163
29. Wickstead, B., Ersfeld, K., and Gull, K. (2002) *Mol Biochem Parasitol* **125**, 211-216
30. Panigrahi, A. K., Zikova, A., Dalley, R. A., Acestor, N., Ogata, Y., Anupama, A., Myler, P. J., and Stuart, K. D. (2008) *Mol Cell Proteomics* **7**, 534-545
31. Subrtova, K., Panicucci, B., and Zikova, A. (2015) *PLoS Pathog* **11**, e1004660
32. Dean, S., Gould, M. K., Dewar, C. E., and Schnauffer, A. C. (2013) *Proc Natl Acad Sci U S A* **110**, 14741-14746
33. Wittig, I., Karas, M., and Schagger, H. (2007) *Mol Cell Proteomics* **6**, 1215-1225

34. Acestor, N., Zikova, A., Dalley, R. A., Anupama, A., Panigrahi, A. K., and Stuart, K. D. (2011) *Mol Cell Proteomics* **10**, M110 006908
35. Altschul, S. F., Gish, W., Miller, W., Myers, E. W., and Lipman, D. J. (1990) *J Mol Biol* **215**, 403-410
36. Finn, R. D., Bateman, A., Clements, J., Coggill, P., Eberhardt, R. Y., Eddy, S. R., Heger, A., Hetherington, K., Holm, L., Mistry, J., Sonnhammer, E. L., Tate, J., and Punta, M. (2014) *Nucleic Acids Res* **42**, D222-230
37. Sigrist, C. J., de Castro, E., Cerutti, L., Cuche, B. A., Hulo, N., Bridge, A., Bougueleret, L., and Xenarios, I. (2013) *Nucleic Acids Res* **41**, D344-347
38. Soding, J., Biegert, A., and Lupas, A. N. (2005) *Nucleic Acids Res* **33**, W244-248
39. Jones, D. T. (2007) *Bioinformatics* **23**, 538-544
40. Krogh, A., Larsson, B., von Heijne, G., and Sonnhammer, E. L. (2001) *J Mol Biol* **305**, 567-580
41. Hofmann, K., and Stoffel, W. (1992) *Computer applications in the biosciences : CABIOS* **8**, 331-337
42. Claros, M. G., and von Heijne, G. (1994) *Computer applications in the biosciences : CABIOS* **10**, 685-686
43. Edgar, R. C. (2004) *Nucleic Acids Res* **32**, 1792-1797
44. Beechey, R. B., Hubbard, S. A., Linnett, P. E., Mitchell, A. D., and Munn, E. A. (1975) *Biochem J* **148**, 533-537
45. Robinson, G. C., Bason, J. V., Montgomery, M. G., Fearnley, I. M., Mueller, D. M., Leslie, A. G., and Walker, J. E. (2013) *Open biology* **3**, 120164
46. Spitsberg, V. L., Pfeiffer, N. E., Partridge, B., Wylie, D. E., and Schuster, S. M. (1985) *Plant Physiol* **77**, 339-345
47. Gledhill, J. R., Montgomery, M. G., Leslie, A. G., and Walker, J. E. (2007) *Proc Natl Acad Sci U S A* **104**, 13632-13637
48. Gledhill, J. R., and Walker, J. E. (2005) *Biochem J* **386**, 591-598
49. Neupert, W., and Herrmann, J. M. (2007) *Annu Rev Biochem* **76**, 723-749
50. Hamilton, V., Singha, U. K., Smith, J. T., Weems, E., and Chaudhuri, M. (2014) *Eukaryot Cell* **13**, 539-547
51. Aslett, M., Aurrecochea, C., Berriman, M., Brestelli, J., Brunk, B. P., Carrington, M., Depledge, D. P., Fischer, S., Gajria, B., Gao, X., Gardner, M. J., Gingle, A., Grant, G., Harb, O. S., Heiges, M., Hertz-Fowler, C., Houston, R., Innamorato, F., Iodice, J., Kissinger, J. C., Kraemer, E., Li, W., Logan, F. J., Miller, J. A., Mitra, S., Myler, P. J., Nayak, V., Pennington, C., Phan, I., Pinney, D. F., Ramasamy, G., Rogers, M. B., Roos, D. S., Ross, C., Sivam, D., Smith, D. F., Srinivasamoorthy, G., Stoeckert, C. J., Jr., Subramanian, S., Thibodeau, R., Tivey, A., Treatman, C., Velarde, G., and Wang, H. (2010) *Nucleic Acids Res* **38**, D457-462
52. Schilling, S., Zeitschel, U., Hoffmann, T., Heiser, U., Francke, M., Kehlen, A., Holzer, M., Hutter-Paier, B., Prokesch, M., Windisch, M., Jagla, W., Schlenzig, D., Lindner, C., Rudolph, T., Reuter, G., Cynis, H., Montag, D., Demuth, H. U., and Rossner, S. (2008) *Nat Med* **14**, 1106-1111
53. Benedetti, C., Haynes, C. M., Yang, Y., Harding, H. P., and Ron, D. (2006) *Genetics* **174**, 229-239
54. Bayot, A., Gareil, M., Rogowska-Wrzesinska, A., Roepstorff, P., Friguet, B., and Bulteau, A. L. (2010) *J Biol Chem* **285**, 11445-11457
55. Bowler, M. W., Montgomery, M. G., Leslie, A. G., and Walker, J. E. (2006) *Proc Natl Acad Sci U S A* **103**, 8646-8649
56. Millerioux, Y., Morand, P., Biran, M., Mazet, M., Moreau, P., Wagnies, M., Ebikeme, C., Deramchia, K., Gales, L., Portais, J. C., Boshart, M., Franconi, J. M., and Bringaud, F. (2012) *J Biol Chem* **287**, 17186-17197
57. Bochud-Allemann, N., and Schneider, A. (2002) *J Biol Chem* **277**, 32849-32854
58. Chen, Y., Hung, C. H., Burderer, T., and Lee, G. S. (2003) *Mol Biochem Parasitol* **126**, 275-279
59. Rak, M., Zeng, X., Briere, J. J., and Tzagoloff, A. (2009) *Biochim Biophys Acta* **1793**, 108-116
60. Brown, B. S., Stanislawski, A., Perry, Q. L., and Williams, N. (2001) *Mol Biochem Parasitol* **113**, 289-301
61. Kang, X., Falick, A. M., Nelson, R. E., Gao, G., Rogers, K., Aphasizhev, R., and Simpson, L. (2004) *J Biol Chem* **279**, 3893-3899

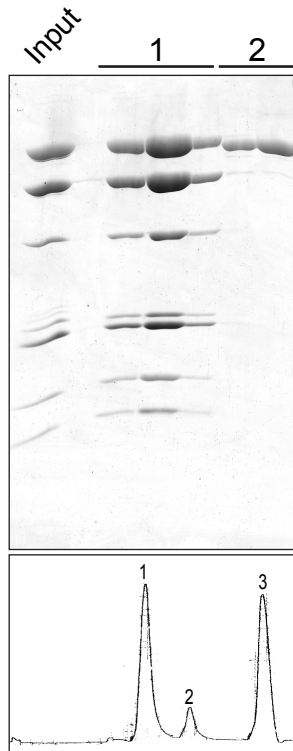
62. Speijer, D., Breek, C. K., Muijsers, A. O., Hartog, A. F., Berden, J. A., Albracht, S. P., Samyn, B., Van Beeumen, J., and Benne, R. (1997) *Mol Biochem Parasitol* **85**, 171-186
63. Aducci, P., Ascenzi, P., Pierini, M., and Ballio, A. (1986) *Plant Physiol* **81**, 812-816
64. Rees, D. M., Leslie, A. G., and Walker, J. E. (2009) *Proc Natl Acad Sci U S A* **106**, 21597-21601
65. Hashimi, H., Benkovicova, V., Cermakova, P., Lai, D. H., Horvath, A., and Lukes, J. (2010) *Int J Parasitol* **40**, 45-54
66. Bringaud, F., Peris, M., Zen, K. H., and Simpson, L. (1995) *Mol Biochem Parasitol* **71**, 65-79
67. Paul, M. F., Velours, J., Arselin de Chateaubodeau, G., Aigle, M., and Guerin, B. (1989) *Eur J Biochem* **185**, 163-171
68. Hilbers, F., Eggers, R., Pradela, K., Friedrich, K., Herkenhoff-Hesselmann, B., Becker, E., and Deckers-Hebestreit, G. (2013) *J Biol Chem* **288**, 25880-25894
69. Helfenbein, K. G., Ellis, T. P., Dieckmann, C. L., and Tzagoloff, A. (2003) *J Biol Chem* **278**, 19751-19756
70. Lytovchenko, O., Naumenko, N., Oeljeklaus, S., Schmidt, B., von der Malsburg, K., Deckers, M., Warscheid, B., van der Laan, M., and Rehling, P. (2014) *EMBO J* **33**, 1624-1638
71. Pusnik, M., Small, I., Read, L. K., Fabbro, T., and Schneider, A. (2007) *Mol Cell Biol* **27**, 6876-6888
72. Lurin, C., Andres, C., Aubourg, S., Bellaoui, M., Bitton, F., Bruyere, C., Caboche, M., Debast, C., Gualberto, J., Hoffmann, B., Lecharny, A., Le Ret, M., Martin-Magniette, M. L., Mireau, H., Peeters, N., Renou, J. P., Szurek, B., Taconnat, L., and Small, I. (2004) *Plant Cell* **16**, 2089-2103
73. Mingler, M. K., Hingst, A. M., Clement, S. L., Yu, L. E., Reifur, L., and Koslowsky, D. J. (2006) *Mol Biochem Parasitol* **150**, 37-45
74. Aphasizhev, R., and Aphasizheva, I. (2013) *RNA Biol* **10**, 1495-1500
75. Barkan, A., and Small, I. (2014) *Annu Rev Plant Biol* **65**, 415-442
76. Zikova, A., Panigrahi, A. K., Dalley, R. A., Acestor, N., Anupama, A., Ogata, Y., Myler, P. J., and Stuart, K. (2008) *Mol Cell Proteomics* **7**, 1286-1296
77. Ridlon, L., Skodova, I., Pan, S., Lukes, J., and Maslov, D. A. (2013) *J Biol Chem* **288**, 32963-32978
78. Aphasizheva, I., Maslov, D., Wang, X., Huang, L., and Aphasizhev, R. (2011) *Mol Cell* **42**, 106-117
79. Allan, R. K., and Ratajczak, T. (2011) *Cell Stress Chaperones* **16**, 353-367
80. Bowler, M. W., Montgomery, M. G., Leslie, A. G., and Walker, J. E. (2007) *J Biol Chem* **282**, 14238-14242

Fig. 1

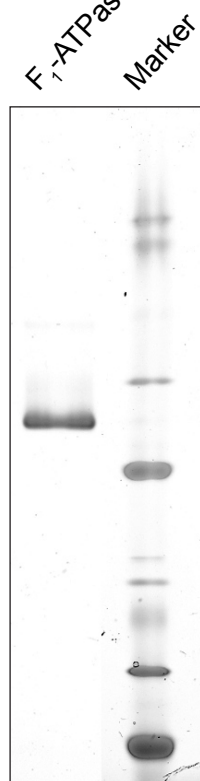
A



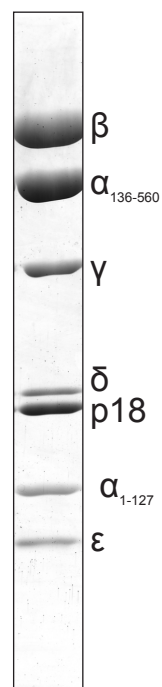
B



C



D



E

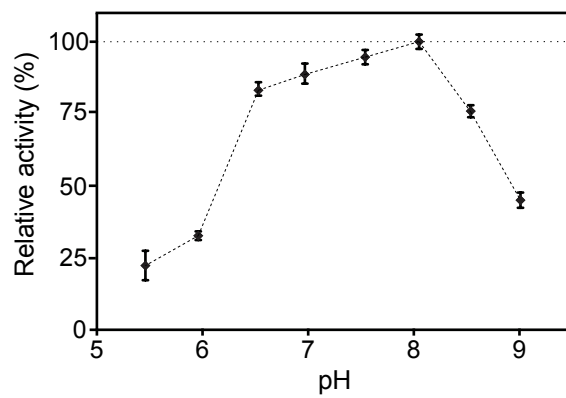
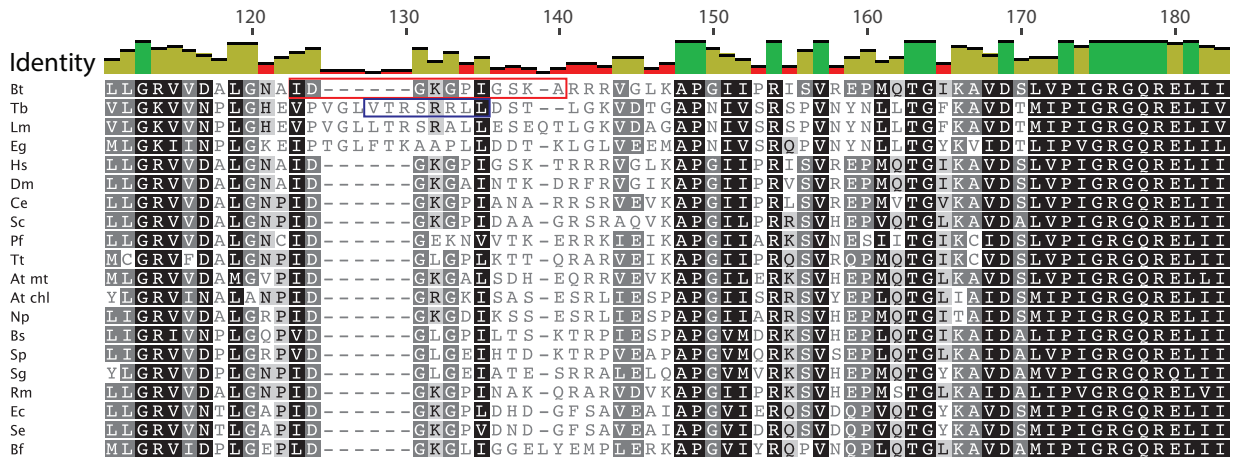


Fig. 2

A



B



C

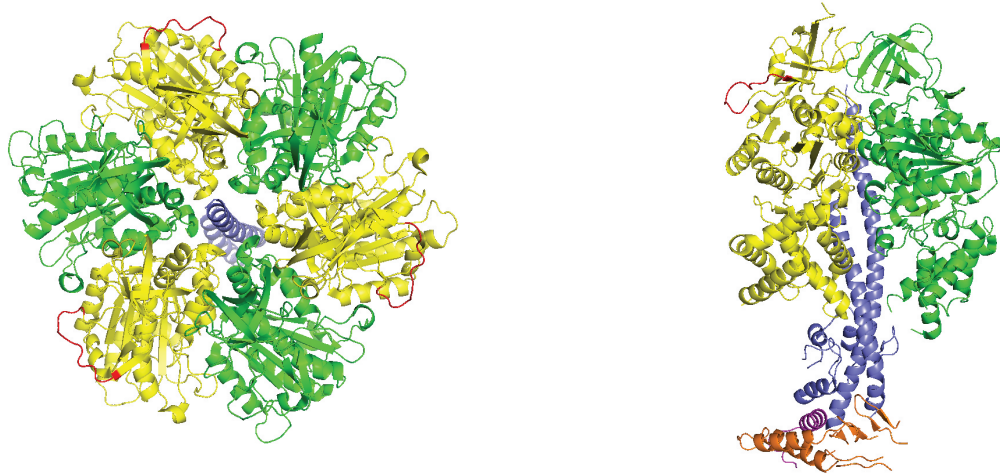


Fig. 3

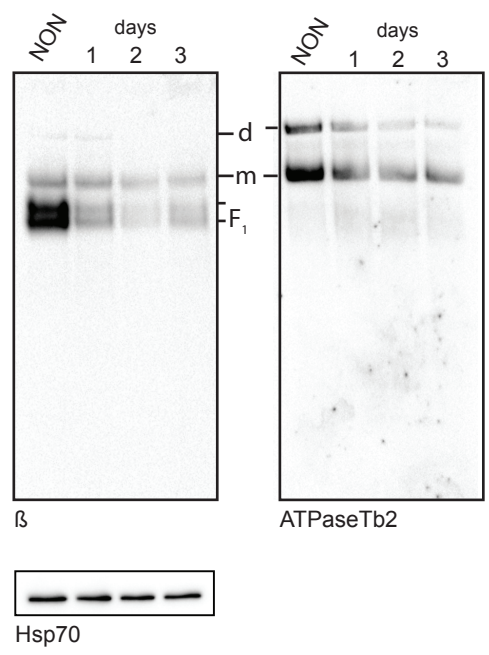
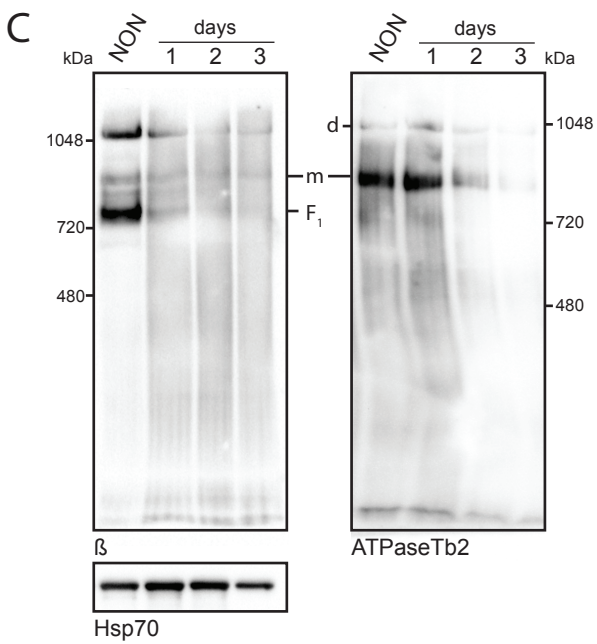
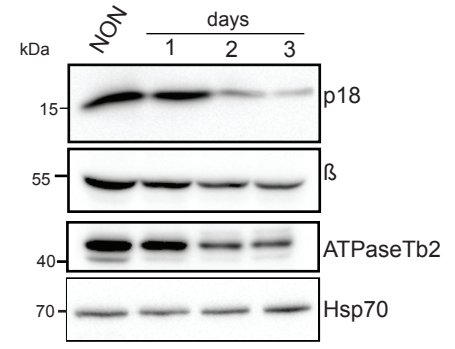
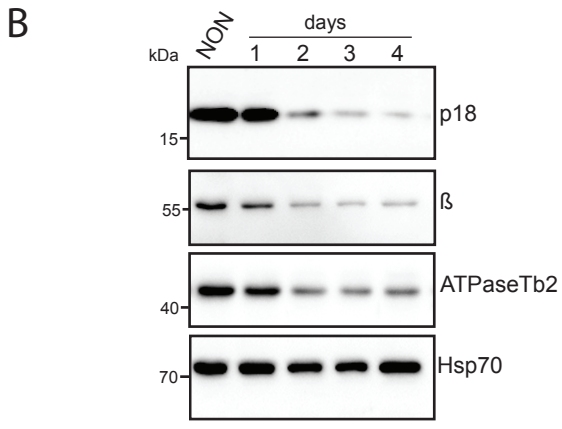
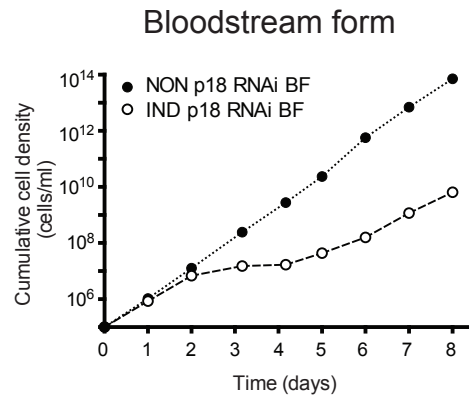
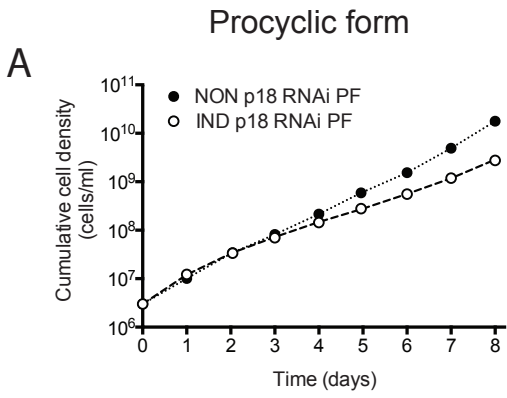


Fig. 4

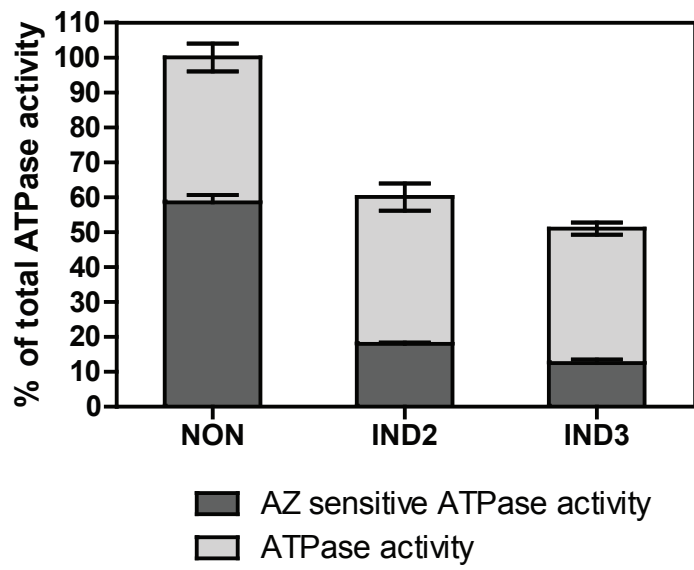
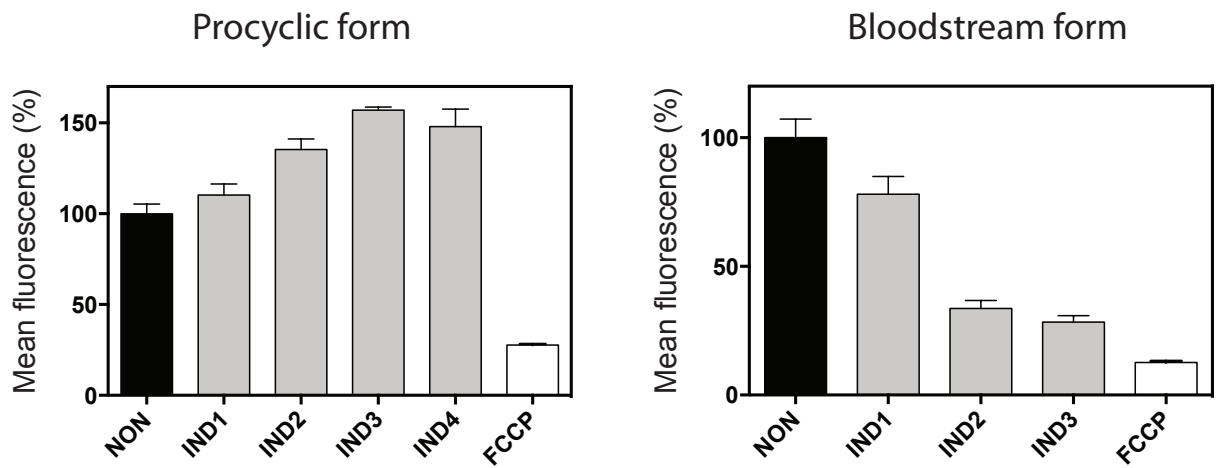


Fig. 5



Tab. 1

	<i>T. brucei</i> F ₁ -ATPase		Bovine F ₁ -ATPase	
	IC ₅₀ (μ M)	95 % confidence interval (μ M)	IC ₅₀ (μ M)	95 % confidence interval (μ M)
Azide	59.5	47.8-74.0	15.9	10.4-24.2
Resveratrol	144	135-154	6.4*	-

*Gledhill et al., 2007

Tab. 2

Subunit	Accession number ^a	Mass (Da)		Mass difference (Da)	Modification	N-terminal sequence ^b	Length (residues) ^c
		Observed	Calculated				
α_{1-127}	Tb427.07.7420	12956	12956.9	< 1	none	AATAP	127
$\alpha_{136-560}$		47108	47098.6	+9.4	none	DSTLG	425
β	Tb427.03.1380	53575	53560.5	+14.5		ASTAP	498
γ	Tb427.10.180	34340	34428.3 ^d	-88.3	-Met1+ α N-acetyl	SGKLR	304
δ	Tb427.06.4990	18138	18154.5	-16.5	Gln1 cyclized to pE	QSAPH	165
ϵ	Tb427.10.5050	7646	7646.5	< 1	none	SSSWR	66
p18	Tb427.05.1710	19168	19168.7	< 1	none	AATSA	170

^aTriTrypDB

^bFirst five residues in the mature protein

^cTotal length of the mature protein in amino acids

^dV65 in mature amino acid sequence

Fig. S1

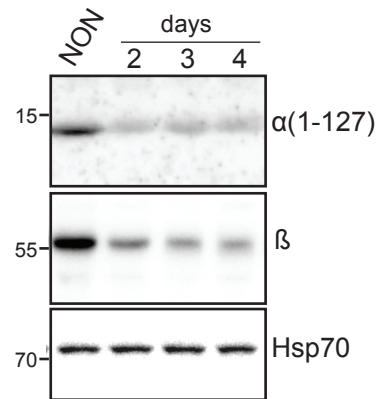
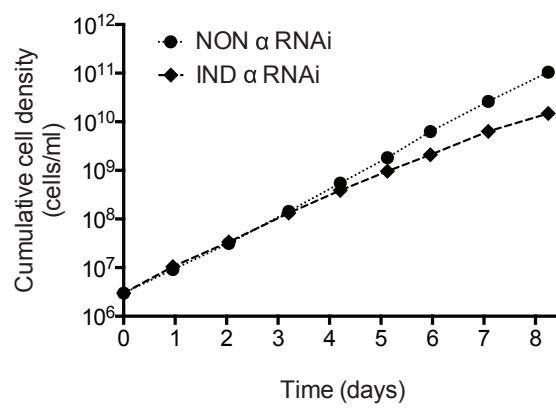


Fig. S2

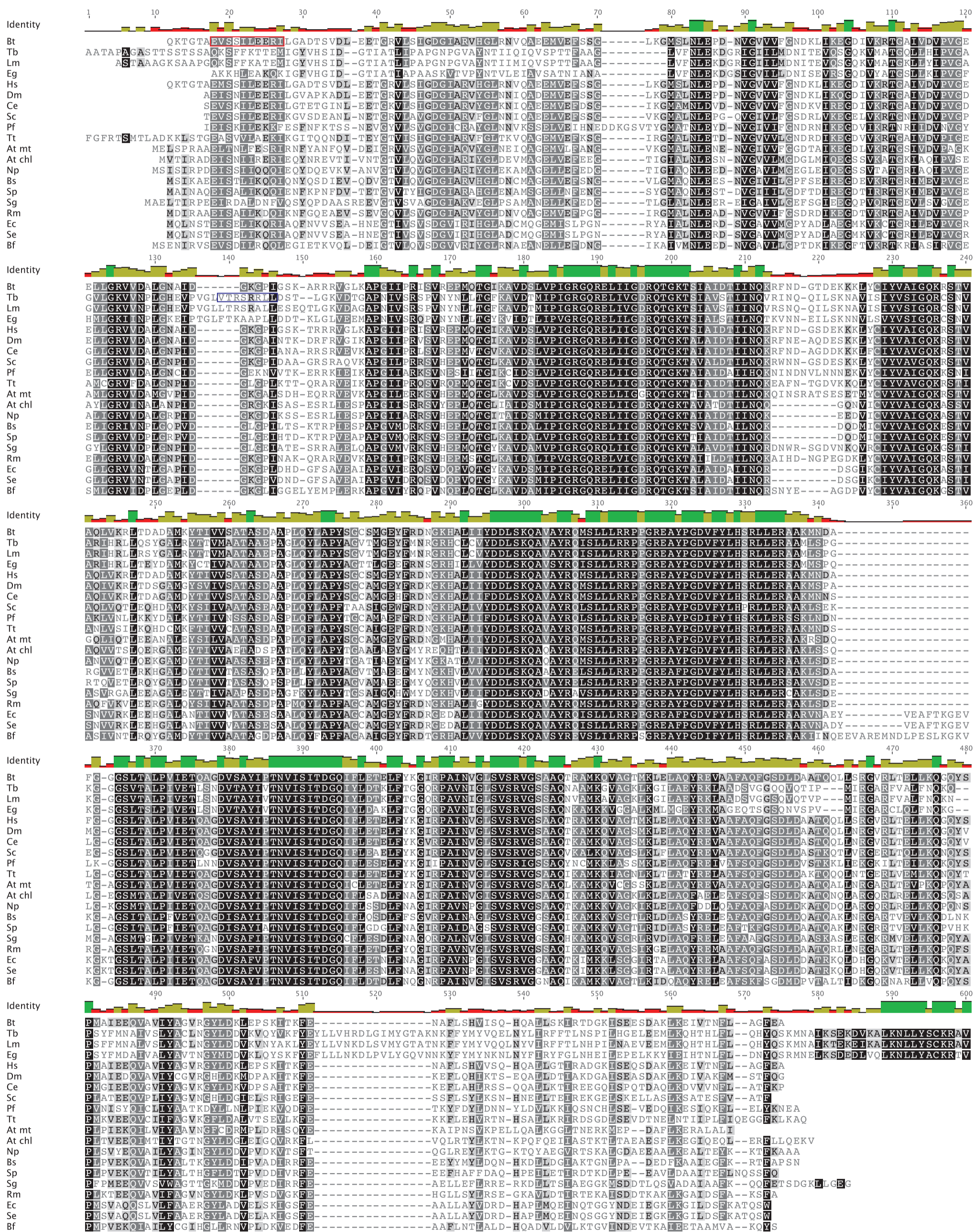
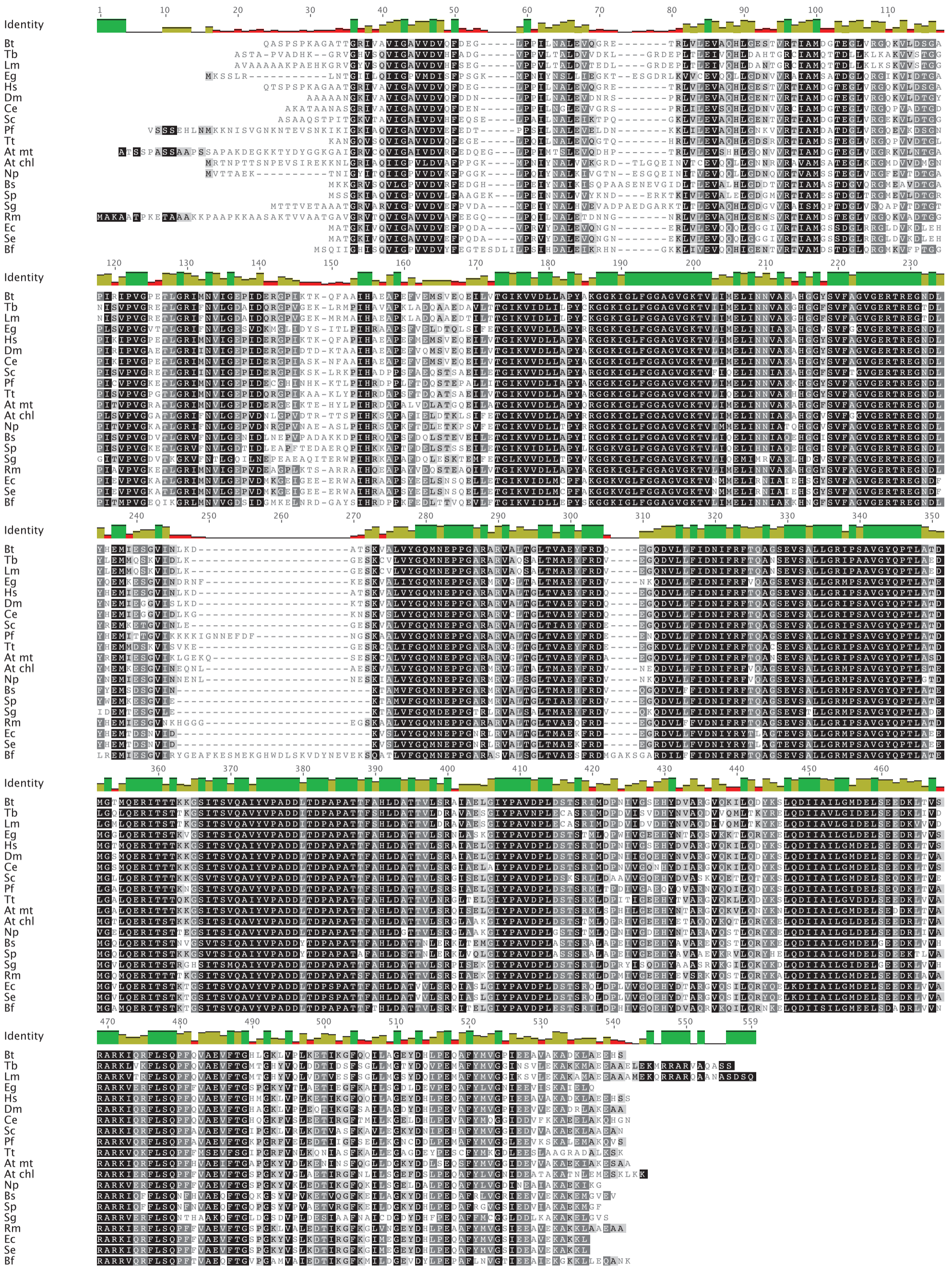


Fig. S3



3.2.2. Functional analysis of ATPaseTb1, a novel and essential subunit of the F_oF₁-ATP synthase in *T. brucei*

In preparation: Šubrtová K, Gnipová A, Panicucci B, Zíková A.

3.2.2. Functional analysis of ATPaseTb1, a novel and essential subunit of the F₀F₁-ATP synthase in *T. brucei*

Karolína Šubrtová^{1,2}, Anna Gnipová^{2,*}, Brian Panicucci², Alena Zíková^{1,2}

¹ Faculty of Science, University of South Bohemia, Branišovská 31, 370 05 České Budějovice, Czech Republic

² Laboratory of Functional Genomics of Protists, Department of Molecular Parasitology, Institute of Parasitology, Biology Centre, ASCR, v.v.i. , Branišovská 31, 370 05 České Budějovice, Czech Republic

* current address: Plant molecular biology, Central European Institute of Technology, Masaryk University, Kamenice 753/5, 625 00, Brno-Bohunice, Czech Republic

Rationale and background:

The composition of *T. brucei* F₀F₁-ATP synthase/ATPase was determined using a combination of methods (tandem-affinity chromatography, glycerol gradient fractionation and immunoprecipitation) followed by mass spectrometry or western blot analysis (Zikova et al. 2009; Šubrtová et al. 2015). It was shown, that this complex contains up to 14 novel subunits of unknown function. The largest (47kDa) subunit, ATPaseTb1 (Tb927.10.520), appears to be specific for Euglenozoa, as a bioinformatics analysis using BLASTp did not recognize any obvious homolog of this protein outside of this group, and a homolog of ATPaseTb1 was detected in a proteomic analysis of *Euglena gracilis* F₀F₁-ATP synthase complex (Zikova et al. 2009; Perez et al. 2014). Importantly, ATPaseTb1 silencing inhibited growth of procyclic *T. brucei*, reduced mt ATP production by oxidative phosphorylation, and affected the structural integrity of F₀F₁-monomers and oligomers (Zikova et al. 2009). In this study, we aim to gain a greater understanding of the specific function of ATPaseTb1 in PF and BF trypanosomes.

Results:

ATPaseTb1 is expressed in PF427, BF427, Dk164 *T. brucei* and *T. b. evansi* cells and it is a mt membrane-bound protein.

The activity of the F₀F₁-ATP synthase complex as well as the steady-state abundance of its subunits differs between various trypanosome cell types (Chi et al. 1998; Schnauffer et al. 2005; Šubrtová et al. 2015). Thus, we investigated the abundance of ATPaseTb1 in four different cell types using western blot analysis. Immunoblot with specific antibody against ATPaseTb1 revealed differences in expression of this protein between PF, BF and Dk cells. Compared to PF cells, the level of ATPaseTb1 was decreased in BF cells, and further reduced in both, the laboratory induced Dk164 and naturally occurring Dk *T. b. evansi*, strains. The lowest abundance of ATPaseTb1 was observed in Dk164 sample, where the specific corresponding band was barely detected. In summary, the steady-state levels of ATPaseTb1

between PF, BF, and Dk cells are consistent with the published studies showing reduction of the mitochondria size, function and activity in different forms of trypanosomes (Schnauffer et al. 2005; Vertommen et al. 2008; Urbaniak et al. 2012).

As ATPaseTb1 protein sequence included a predicted transmembrane domain (Supp. Fig.2), we decided to explore its localization within the trypanosome cell. The subcellular localization of ATPaseTb1 was determined using the BF ATPaseTb1_v5 cell line from which mitochondria were purified by hypotonic lysis and subsequently treated with Na₂CO₃. The Western blot analyses using cytosolic marker enolase proved the purity of the extracted mitochondrial fraction as the enolase signal was missing from the mt fraction. Western blot with antibody against the matrix-localized guide RNA binding protein (MRP1) revealed that the membrane fraction was contaminated with matrix proteins. Nevertheless, the mt inner membrane carrier protein (TbAAC) was detected exclusively within its respective compartment, demonstrating purity of the mt membrane fraction. ATPaseTb1 was detected only in the mt membrane fraction, implying that this protein is embedded in the inner mt membrane.

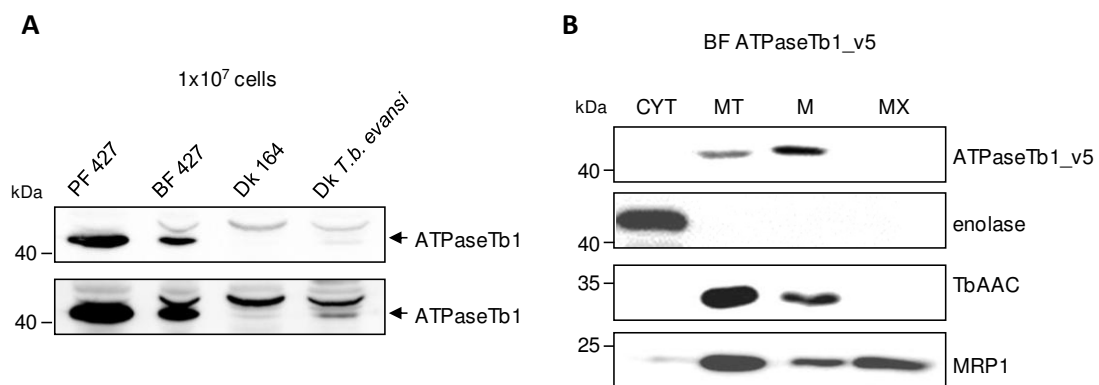


Fig. 1A. ATPaseTb1 expression was investigated in different cell types of Trypanosomes.

The steady-state abundance of ATPaseTb1 (two different exposure times) was determined by western blot analysis of whole cell lysates from 1x10⁷ cells resolved on SDS-PAGE gels. Specific band corresponding to ATPaseTb1 is indicated by arrow. The relevant sizes of the protein marker are indicated on the left.

Fig. 1B. Subcellular localization of ATPaseTb1 was determined using BF cells expressing V5-tagged ATPaseTb1.

The ATPaseTb1 coding sequence was PCR amplified from *T. brucei* 427 gDNA (oligonucleotides:FW—ACAAAGCTTATGCAGGGCAGTTGG, REV-ACAGGATCCAGCTGTGTGTCGGCC). Using the HindIII and BamHI restriction sites inherent in the primers (underlined), the fragment was cloned into the pT7_v5 vector, the construct was linearized and transfected into BF427 SM cell line as previously described (Wirtz et al. 1999). The induction of ectopically expressed ATPaseTb1 fused with a C-terminal 3xv5 tag was triggered by the addition of 1 µg/ml of tet into the media. Cytosolic (CYT) and mitochondrial (MT) fractions were obtained from ATPaseTb1_v5 tagged expressing cells by hypotonic lysis. Mitochondrial pellets were treated with Na₂CO₃ and centrifuged at a high-speed spin to obtain mt membrane (M) and matrix (MX) fractions. The method was performed as described (Šubrtová et al. 2015). Purified fractions were analyzed by western blot with the following antibodies: anti-v5 (ATPaseTb1_v5), anti-enolase (cytosol), anti-TbAAC (mt inner membrane), and anti-MRP1 (mt matrix). The relevant sizes of the protein marker are indicated on the left.

**ATPaseTb1 is a part of the monomeric
and oligomeric F₀F₁-ATP synthase/ATPase complexes.**

The hrCNE profile and GG sedimentation pattern of F₀F₁-ATP synthase complex were previously reported (Zikova et al. 2009; Šubrtová et al. 2015). In agreement with the literature, the hrCNE followed by western blot analysis with the antibody against F₁ subunit p18 revealed four bands in both PF427 and BF427 samples. The lowest two bands presumably represent the F₁-ATPase (subunits α , β , γ , δ , ϵ) and F₁-ATPase with a c-ring (Meyer et al. 2007). The higher bands likely correspond to F₀F₁- monomers and higher oligomers. Importantly, antibody against ATPaseTb1 visualized only the two higher bands, which correspond to the F₀F₁-monomers and -multimers.

The presence of ATPaseTb1 only within the fully assembled F₀F₁ complexes was confirmed by sedimentation in glycerol gradient followed by western analyses of resolved fractions. In agreement with the literature, anti-p18 antibody depicted two distinct regions in the fractionated complex, which are defined as 10S (F₁) (fractions 6–8), and 40S ((F₀F₁)_n)(fractions 14–22). The specific antibody against ATPaseTb1 immunodecorated only the 40S complexes, which represent F₀F₁ –monomeric and - multimeric complexes. In summary, our results indicate that the ATPaseTb1 is a component of the fully assembled F₀F₁-ATP synthase complex.

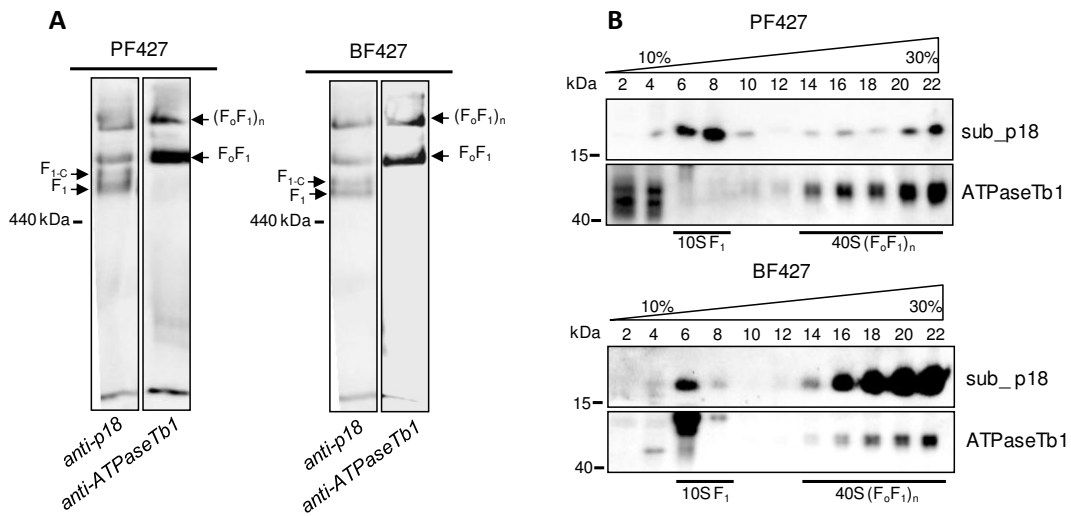


Fig. 2A. The F_oF_1 -ATP synthase/ATPase complex was examined by hRCNE followed by western blot analysis. The technique was performed as reported (Šubrtová et al. 2015). Briefly, purified mitochondria from PF427 and BF427 cells were lysed with digitonin (4 mg/mg), fractionated on a 3%-12% hRCNE and blotted onto a nitrocellulose membrane. The F_1 -ATPase (F_1), the F_1 -ATPase bound with the c-ring (F_1+c), and the monomeric F_oF_1 /multimeric ($(F_oF_1)_n$) complexes were visualized using specific polyclonal antibodies against either subunit p18 or ATPaseTb1. The size of ferritin from the equine spleen (440 kDa) is indicated on the left.

Fig. 2B. The sedimentation profile of F_1 - and F_oF_1 -ATP synthase/ATPase complex was determined using glycerol gradient (GG) sedimentation. Hypotonically purified mitochondria from PF427 and BF427 cells were lysed with 1% Triton X-100 and fractionated on a 10–30% GG as described (Zikova et al. 2009; Šubrtová et al. 2015). The GG fractions were collected, fractionated by SDS-PAGE and analyzed by western blots. Western analyzes with an anti-p18 antibody depicted the sedimentation profile of the F_1 -ATPase and monomeric/multimeric F_oF_1 -ATP synthase/ATPase complexes, whereas the anti-ATPaseTb1 antibody only immunodecorated this subunit within the monomeric/multimeric F_oF_1 -ATP synthase/ATPase. The sedimentation pattern of two structural forms of the F_oF_1 -ATP synthase complexes (10S and 40S) were determined according to published study (Zikova et al. 2009) and are underlined. The GG fractions and the sizes of the protein marker are indicated.

**Silencing of ATPaseTb1 inhibits growth of PF *T. brucei*
and disrupts the F₀F₁-ATP synthase complexes.**

To investigate the specific function of ATPaseTb1, we employed PF ATPaseTb1 RNAi cell line which was generated previously (Zikova et al. 2009). In agreement with the previous study, the down-regulation of ATPaseTb1 inhibited cell growth. The growth phenotype was first detected on day 4 of RNAi induction. The targeted KD of ATPaseTb1 was confirmed by western blot analysis of whole cell lysates harvested from an equivalent number of cells for induced and noninduced cells. Western blot analysis using the specific antibody against ATPaseTb1 revealed a 75% reduction of the targeted protein on day 2 of RNAi induction. The ATPaseTb1 protein was almost completely diminished (only 3-2% of the signal left) at day 4 and day 6 after RNAi induction.

Effect of ATPaseTb1 depletion on structural integrity of F₀F₁-ATP synthase was examined by hrCNE and western blot analyses with anti-β (F₁-ATPase subunit) and anti-ATPaseTb2 (F₀ subunit) antibodies. This approach demonstrated that levels of the F₀F₁ complexes were substantially decreased in ATPaseTb1 KD cells already at day 2 of RNAi induction. Simultaneously, the levels of F₁-ATPase were increased, suggesting that the F₁ moiety is not incorporated into the fully assembled complex. This reduction of F₀F₁-ATP synthase complexes preceded the growth inhibition. In agreement with the published data (Zikova et al. 2009), ATPaseTb1 subunit appears to be essential for the structural integrity of the assembled PF F₀F₁-ATP synthase.

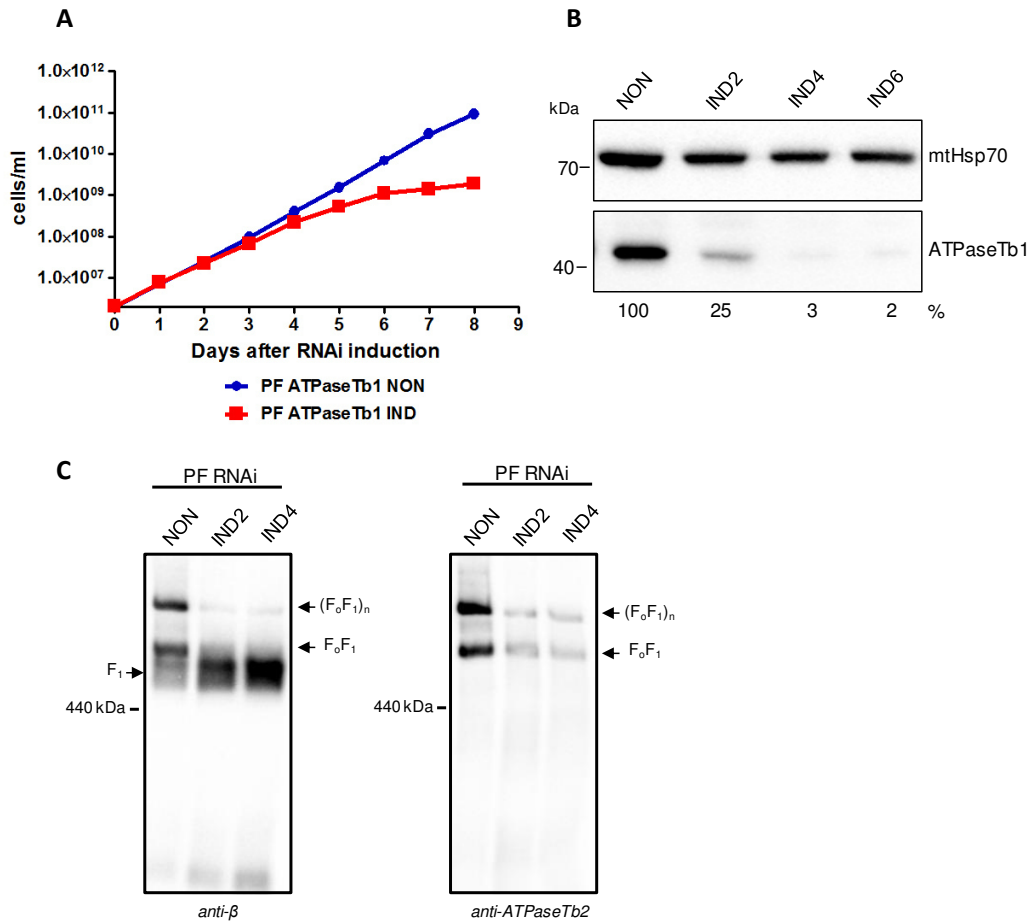


Fig. 3A. The *in vitro* growth of the PF ATPaseTb1 knock-down cells was inspected for eight days. The pZJM vector for the tet inducible RNAi of ATPaseTb1 and the generation of PF ATPaseTb1 RNAi cell line were described in detail earlier (Zikova et al. 2009). The induction of RNAi was triggered by addition of 1 μ g/ml of tet into the media. Growth curves of the noninduced (NON) and induced (IND) ATPaseTb1 RNAi PF *T. brucei* cell lines were measured for 8 days. Cells were maintained in the exponential growth phase (between 10^6 and 10^7 cells/ml) and the cumulative cell number represents the cell density adjusted by the daily dilution factor. The figure is representative of at least three independent RNAi-inductions.

Fig. 3B. The steady-state abundance of ATPaseTb1 was investigated in RNAi induced and noninduced PF cells. The expression levels of ATPaseTb1 in noninduced (NON) RNAi cells and in cells induced with tet for 2, 4 and 6 days (IND2, IND4, IND6) was determined by western blot analysis using a specific ATPaseTb1 antibody, and antibody against matrix protein mtHsp70. The bands immunodetected with anti-mtHsp70 served as a loading control. The numbers beneath the blots represent the abundance of immunodetected ATPaseTb1 (expressed as a percentage of NON sample after normalizing to the loading control). The relevant sizes of the protein marker are indicated on the left. The figure is a representative western blot from at least three independent RNAi-inductions.

Fig. 3C. The stability of native F_0F_1 -ATP synthase complexes upon ATPaseTb1 silencing was examined using hrCNE. The equal amounts of digitonin lysed mitochondria from RNAi non-induced cells (NON) and cells induced for 2 (IND2) and 4 (IND4) days were fractionated on a 3%- 12% hrCNE, blotted onto a nitrocellulose membrane, and probed with the anti-beta and anti-ATPaseTb2 antibodies. Details of this method were reported in (Šubrtová et al. 2015). Positions of F_1 -ATPase and monomeric and dimeric F_0F_1 -ATP synthases are depicted by arrows. The size of ferritin from equine spleen (440 kDa) is indicated.

Loss of ATPaseTb1 does not affect the oligomycin sensitivity of PF *T. brucei*.

To explore the importance of the remaining F_0F_1 -ATP synthase complexes detected in Fig.3C, we measured the sensitivity of PF ATPaseTb1 KD cell line to oligomycin, an inhibitor of the coupled F_0F_1 -ATP synthase. Sensitivity to this inhibitor was examined by Alamar blue assay and expressed as EC_{50} values. Comparison of the EC_{50} value of each sample revealed differences between two experiments (NON+IND3 and NON+IND4). This discrepancy may be attributed to the different starting cell densities, or to an inherent variability of the Alamar blue assay. These measurements will have to be repeated to obtain more accurate EC_{50} values \pm SE. Nevertheless, the EC_{50} values did not differ between NON and IND3/IND4 samples, suggesting that OM sensitivity of PF cells is not affected upon ATPaseTb1 silencing. This result may appear surprising, as it was shown that at the same time the structural integrity of the coupled F_0F_1 -ATP synthase complexes was strongly affected (Fig. 3C). Therefore, we expected an increase of EC_{50} values in RNAi induced samples as the cells are producing much less ATP by oxidative phosphorylation. However, this result suggests that the residual levels of F_0F_1 -ATP synthase complexes after ATPaseTb1 depletion may be sufficient to contribute to ATP production.

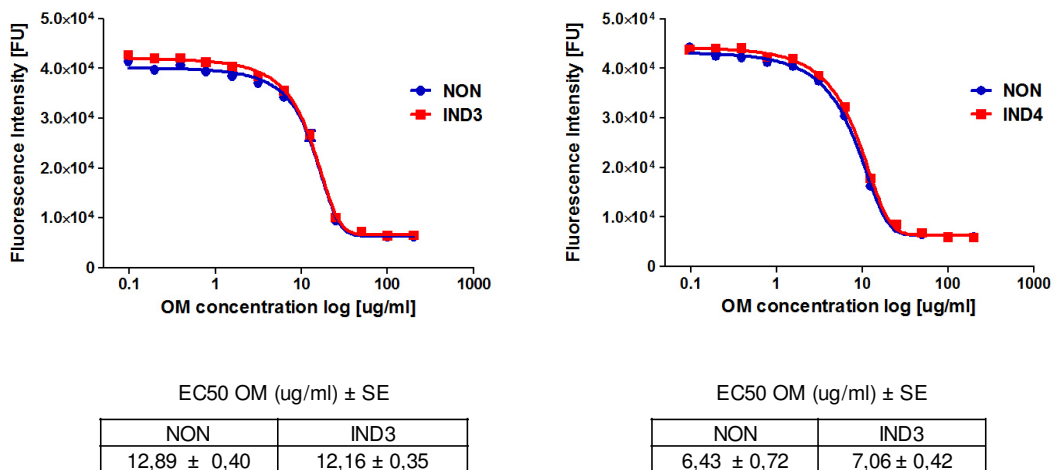


Fig. 4. The oligomycin (om) sensitivity of PF ATPaseTb1 RNAi cells was investigated using a Alamar blue dose-response assay. The experiment was performed with non-induced (NON) cells and cells RNAi induced for 3 (IND3) and 4 (IND4) days. This fluorimetric/colorimetric assay was carried out according to published studies (Ráz et al. 1997; Dean et al. 2013) with minor modifications. Briefly, om stock solution was serially diluted in 100ul of SDM in a 96-well plate to reach final concentrations ranging from 200 to 0,1 μ g/ml. An equal volume of medium containing NON or IND PF cells was added to the wells to achieve a final number 1×10^5 (NON and IND4) or 2×10^5 (NON and IND3) cells/well. The plate was incubated at 27 °C for 48 or 72 h, after which resazurin sodium salt in PBS was added to each well (final concentration 12,5 μ g/ml). The plate was incubated for another 24 h. Fluorescence was measured in a microplate reader with excitation and emission filters of 560 and 590 nm, respectively. Data were analyzed by using GraphPad Prism software. Depicted graphs are showing dose-response curves of NON and IND cells (each point represents a mean \pm standard error (SE) of a technical triplicate), y- axis shows artificial fluorescence units (FU), x-axis indicates oligomycin concentration in logarithmic scale. The 50% effective concentrations (EC_{50}) were derived from a variable slope nonlinear regression.

ATPaseTb1 depletion increases the $\Delta\psi_m$ in PF cells.

Because the F_0F_1 -ATP synthase utilizes the proton motive force to synthesize ATP, we investigated if the $\Delta\psi_m$ is affected upon ATPaseTb1 silencing. FACS analysis revealed a significant increase of the $\Delta\psi_m$ in the PF ATPaseTb1 KD cell population, starting on day 2 after RNAi induction. This change precedes the growth phenotype (Fig.3A) and therefore it appears to be a specific effect of ATPaseTb1 down-regulation, rather than a result of decreased cell viability. Importantly, the $\Delta\psi_m$ was increased up to 60%, with the highest values detected at day 4 post induction. This result indirectly confirms the disappearance of F_0F_1 complexes, which contain the proton pore. Therefore, the protons accumulate in the mt inner membrane space, and this accumulation is followed by hyperpolarization of the inner mt membrane. It is plausible to speculate, that the increase of $\Delta\psi_m$ is followed by an elevated production of reactive oxygen species (ROS), which might be the cause of the observed growth phenotype.

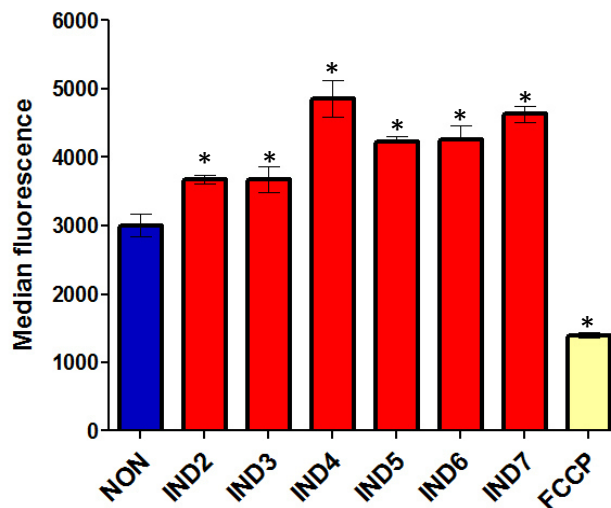


Fig. 5. The $\Delta\psi_m$ was measured *in vivo* by flow cytometry using Mitotracker Red. The technique was carried out exactly as described (Šubrtová et al. 2015). Cells were harvested from non-induced (NON) ATPaseTb1 RNAi cultures and cell cultures induced for 2-4 and 7 days (IND2-4 and IND7). For each sample, 10,000 events were collected. Treatment with the protonophore FCCP (20 μ M) was used as a control for mt membrane depolarization. Data were evaluated using BD FACSDiva (BD Company) and GraphPad Prism software. The median fluorescence for each sample is depicted on the y-axis of the column graph. The results are means \pm SD (standard deviation) from three independent RNAi inductions. * $P < 0.05$, Student's t-test.

Loss of ATPaseTb1 impairs the editing and/or stability of the F_0 subunit a transcript.

Our results indicated that the down-regulation of ATPaseTb1 impairs the membrane-bound F_0 moiety. The composition of the F_0 proton pore is extremely conserved amongst eukaryotes, as it always comprises homologues of two highly hydrophobic subunits c and a (Walker 2013). The *T. brucei* F_0 proton pore consists of the nuclear encoded subunit c, and the kDNA encoded pan-edited subunit a. As antibodies against neither of these subunits are available in our laboratory, we attempted to validate our previous data by investigating the

effect of ATPaseTb1 KD on mRNA levels of subunit a using RT-qPCR. This analysis revealed a decrease of edited sub a mRNA 2 days post-induction. Compared to non-induced samples, the levels of edited mRNA were decreased by ~30 to 45%. Quantification of pre-edited sub a mRNAs revealed less consistent result as the relative mRNA levels in the induced cells fluctuated between a ~10% decrease and ~20% increase, dependently on the housekeeping standard. Nevertheless, the data indicate that the editing and/or stability of subunit a transcript is affected shortly after ATPaseTb1 silencing. It has to be noted that this experiment was performed only once and more repeats are needed to obtain a larger data set for statistical analysis.

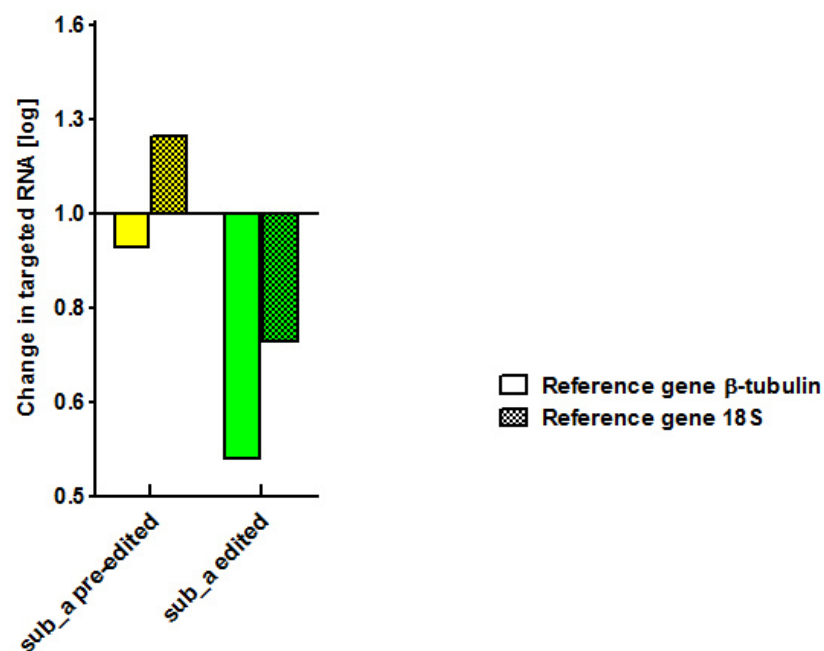


Fig. 6. Real time quantitative PCR (RT-qPCR) analysis was used to determine mRNA levels for pre-edited and edited transcripts of subunit a (sub_a). RT-qPCR was performed as described (Carnes et al. 2005). Relative amounts of RNA template in the samples were calculated using the $\Delta\Delta C_t$ method according to (Ballester et al. 2004). RNA was isolated from non-induced and RNAi induced cells (2 days after tet-induction). RNAs were quantified by qRT-PCR using primer sets specific for pre-edited and edited subunit a mRNAs (Aphasizheva et al. 2011). Relative RNA abundance depicted in column graph indicates RNA levels in RNAi induced cells compared to those determined in non-induced cells. RNA levels were standardized to the housekeeping genes β -tubulin and 18S RNAs (oligonucleotides: β -tubulin FW: GCAGAGTCCAACATGAACGA, β -tubulin RV: CGTCCGCTCTAGTATTGCT, 18S RNAs FW: GCGAAACGCCAAGCTAATAC, 18S RNAs RV: AGCCGCGACATAGAAAAAGA).

ATPaseTb1 silencing in BF trypanosomes causes rapid growth inhibition.

In contrast to PF cells, the bloodstream stage is completely dependent on the F_0F_1 -ATPase activity, as it generates the indispensable $\Delta\psi_m$ (Nolan & Voorheis 1992; Schnauffer et al. 2005; Brown et al. 2006). The BF ATPaseTb1 RNAi cell line was generated to gain more insight into the specific function of this subunit in the infective stage of *T. brucei*. Analysis of growth of BF ATPaseTb1 RNAi cell line revealed a severe growth phenotype emerging after 9 hours upon RNAi induction. A subpopulation of cells became irresponsive to RNAi induction at day 2, resulting in a partial growth recovery. This development of RNAi revertants is well documented (Chen et al. 2003). A specific decrease of ATPaseTb1 mRNA transcript levels was verified by RT-qPCR analysis. The RNA was isolated from cells RNAi induced for 6 hours. This time point was selected to verify the efficiency of the ATPaseTb1 RNAi before the observed growth inhibition. Our results showed that the mRNA abundance was decreased by $\sim 40\%$ in RNAi induced cells. The targeted down-regulation of ATPaseTb1 was also confirmed by western blot analysis of whole cell lysates using the specific antibody against ATPaseTb1. Quantification of volume intensities of the specific bands demonstrated a reduction of the targeted protein by ~ 40 and $\sim 30\%$ in IND1 and IND3 samples, respectively. In conclusion, our data suggests that ATPaseTb1 is essential for viability of BF cell grown *in vitro*.

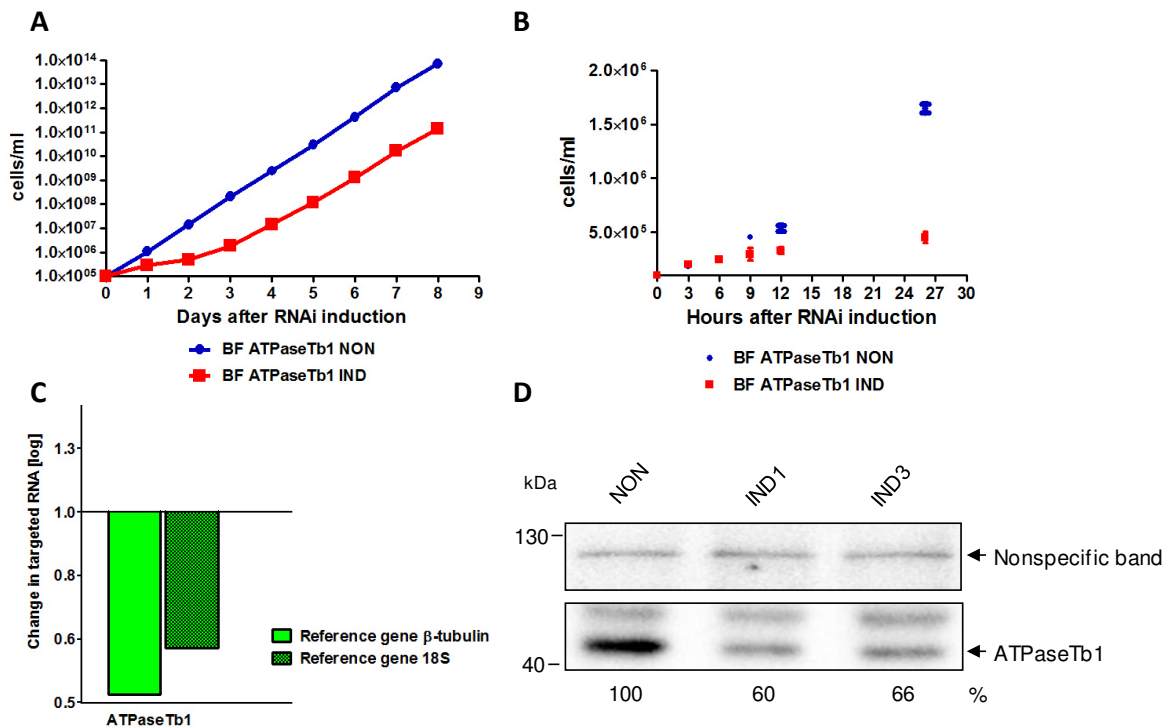


Fig. 7A. Growth curves of the non-induced (NON) and RNAi induced (IND) ATPaseTb1 RNAi BF *T. brucei* cell lines were measured for eight days. The ATPaseTb1 RNAi construct includes a 637 bp fragment that was PCR amplified from *T. brucei* 427 gDNA with the following oligonucleotides: FW-CACAAGCTTGGAAGCTCAGGACC, REV- CACCTCGAGGCAGAAACGCATC. Utilizing the HindIII and XhoI restriction sites inherent in the primers (underlined), this fragment was cloned into the p2T7-TA blue plasmid (Alibu et al. 2005). The construct was linearized with *NotI* and transfected into BF427 SM cell line as previously described (Wirtz et al. 1999). The induction of dsRNA expression was triggered by the addition of 1 μ g/ml of tet into the media. During the growth curve analysis, cells were maintained in the exponential growth phase (between 10^5 and 10^6 cells/ml). Cumulative cell number represents the normalization of cell density by multiplication with the dilution factor. The figure is representative of three independent RNAi-inductions.

Fig. 7B. The growth of BF ATPase Tb1 RNAi non-induced (NON) and induced (IND) cells was investigated during the first 26 hours after RNAi induction. Cells were diluted to starting density 1×10^5 cells/ml, and counted at 3,6,9,12 and 26 hours after tet-induction. The graph shows means \pm SD from three independent RNAi inductions.

Fig. 7C. RT-qPCR analysis was used to determine the efficacy of ATPaseTb1 RNAi. The method was performed as in Fig. 6B. RNA was isolated from non-induced and RNAi induced cells (6h after tet-induction). RNAs were quantified by qRT-PCR using primer sets specific for ATPaseTb1 mRNAs (FW: CAACAGACGCAAGAGGCATA, RV: CGCTCTGCTCAACGAAGTCT). RNA levels in RNAi induced cells were compared to those in non-induced cells. RNA levels were standardized to β -tubulin and 18S RNAs.

Fig. 7D. The steady-state abundance of ATPaseTb1 in non-induced (NON) and cells 1 and 3 days post RNAi induction (IND1 and IND3) was determined by western blot analysis using specific ATPaseTb1 antibody. The non-specific band detected on the same membrane served as a loading control. The numbers beneath the blots represent the abundance of ATPaseTb1 (expressed as a percentage of NON sample after normalizing to the loading control). The relevant sizes of the protein marker are indicated on the left. The figure is a representative western blot from at least three independent RNAi inductions.

ATPaseTb1 knock-down alters morphology of BF cells and mitochondria.

The rapid beginning of growth inhibition in ATPaseTb1 silenced cells prompted us to investigate an overall appearance of the cell and its mitochondrion. The immunofluorescent analysis (IFA) of non-induced and RNAi induced cells revealed that ATPaseTb1 down-regulation caused severe defects in both cellular and mitochondrial morphology. Staining with a DNA-specific dye DAPI and anti-mtHsp70 antibody demonstrated that RNAi induced cells exhibit an aberrant number of nuclei (N) and kinetoplasts (K), in addition to alterations in mitochondrial shape. The predominantly observed aberrancies in N/K ratio included anuclear cells (0N \times K) and large "monster" cells with multiple nuclei and kinetoplasts (xN \times K), suggesting a severe disruption of the process of cell division. The ATPaseTb1 KD cells also exhibited fragmented mitochondria, indicating that shape and structure of this organelle are impaired. These alterations were observed already at day 1 of RNAi induction. Furthermore, the number of abnormal cells appeared to be increased on day 2 post-induction; however these changes remain to be quantified.

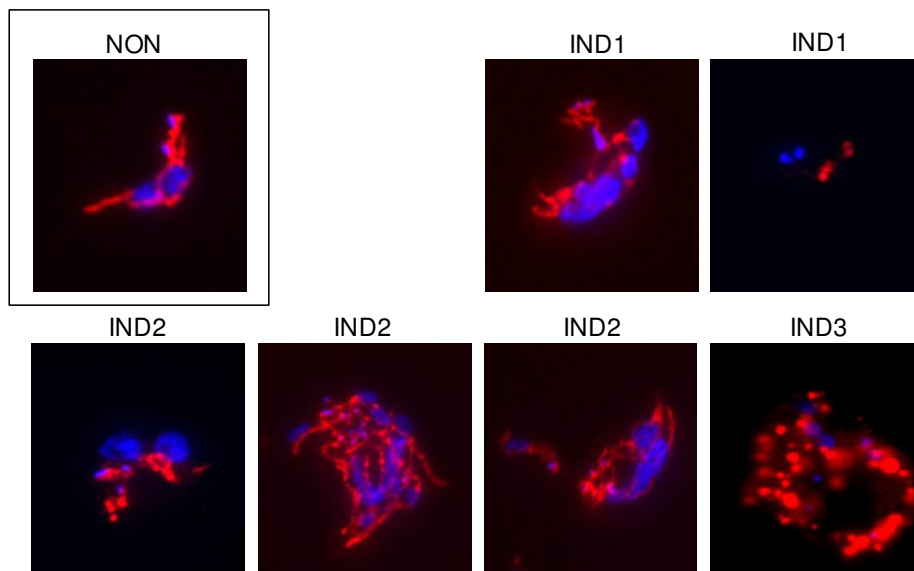


Fig. 8A. Mitochondrial morphology was investigated by indirect immunofluorescence in BF ATPaseTb1 KD cells. BF ATPaseTb1 RNAi non-induced (NON) cells and cells 1-3 days after RNAi induction (IND1 - IND3) were fixed, permeabilized and visualized by fluorescence microscopy according to published protocols (Zikova et al. 2008; Gnipová et al. 2015). Nuclei and kinetoplasts were stained by DAPI (blue). Mitochondria were immunolabeled using primary monoclonal antibody against mtHsp70 and secondary anti-mouse IgG antibody Texas-Red conjugate (red). Displayed pictures represent merged microphotographs from both channels. Representative images of normal (NON) and aberrant cells (IND1 - IND3) are shown.

**Effect of ATPaseTb1 knock-down on the stability of F₀F₁-ATPase complexes
in BF *T. brucei* cells.**

Functional characterization of PF ATPaseTb1 RNAi cells suggested that ATPaseTb1 is involved in the stability of the membrane bound F₀F₁ complexes. Thus, we investigated if ATPaseTb1 possesses the same function in BF cells, and the loss of F₀F₁ complexes is the reason for the observed early growth inhibition. The structural integrity of the F₀F₁-ATPase was examined using hrCNE followed by western blot analyses. In agreement with the published data (Šubrtová et al. 2015), western blot analysis of RNAi non-induced sample using the anti-β and anti-p18 antibodies revealed three major bands (on the anti-β immunoblot, the individual bands were not well resolved due to overloading and the blot overexposure) representing the F₁-ATPase and F₀F₁ complexes. Importantly, the bands corresponding to the F₁-ATPase and F₀F₁ complexes were not affected at day 1 after RNAi induction. The expected impairment of F₀F₁-monomer and F₀F₁-oligomer was detected at day 2 after tet addition.

The structural integrity of the F₀F₁-ATP synthase complex was also inspected by the sedimentation in glycerol gradient and western analyses of resolved fractions. The sedimentation profile of the fractionated F₀F₁-ATPase from RNAi non-induced cells revealed two distinct regions. Antibody against subunit β immunodetected both 10S (fractions 4–6) and 40S ((F₀F₁)_n) (fractions 10–22) regions, while the anti-ATPaseTb2 detected only the 40S complexes. When the same western analyses were performed on fractions obtained from 1 day tet induced sample, no shifts of sedimentation values were observed. This result correlates with hrCNE data, as no changes in F₀F₁-ATPase integrity were detected at day 1 after RNAi induction. In conclusion, the structural integrity of the BF F₀F₁-ATPase complex remains intact until day 2 of ATPaseTb1 RNAi. Thus, the observed early onset of growth inhibition is not caused by the complex instability.

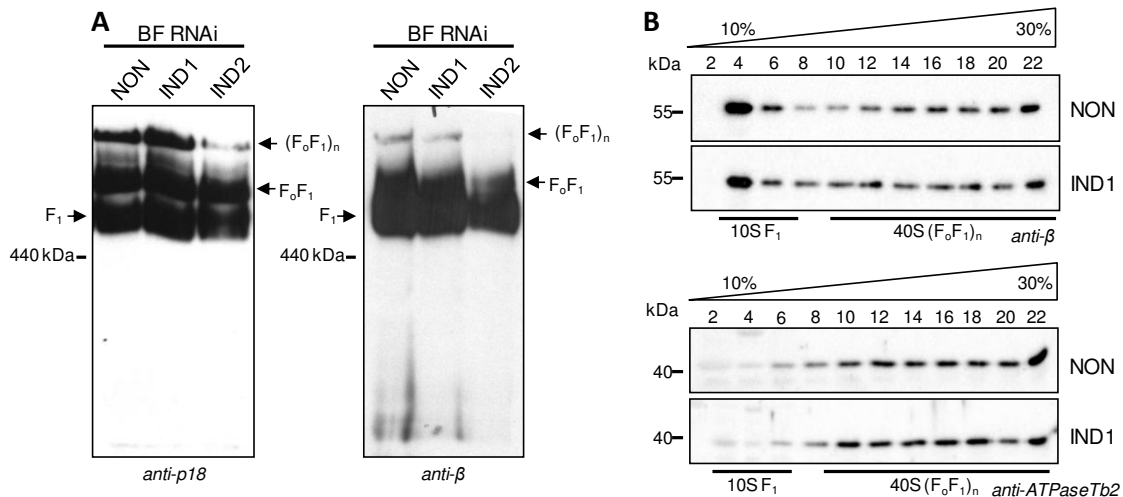


Fig. 9A. The stability of F_oF₁-ATPase complexes upon ATPaseTb1 ablation was examined using hrCNE.

Mitochondria from RNAi non-induced cells (NON) and cells induced for 1 (IND1) and 2 (IND2) days were lysed by digitonin (4mg/mg). The equal amounts of lysed mitochondria were fractionated on a 3%-12% hrCNE, blotted onto nitrocellulose membrane and probed with anti-p18 and anti-β antibodies. For details of this method see (Šubrtová et al. 2015). Positions of F₁-ATPase and monomeric and dimeric F_oF₁ - ATPases are depicted by arrows. The size of ferritin from equine spleen (440 kDa) is indicated.

Fig. 9B. The sedimentation profile of F_oF₁-ATPase complexes was examined using western blot analysis of GG fractions.

Mitochondria from RNAi non-induced cells (NON) and cells induced for 1 day (IND1) were lysed with 1% Triton X-100 and equal amount of the cleared lysed samples was loaded on a 10-30% glycerol gradient according to published protocols (Zikova et al. 2009; Šubrtová et al. 2015). Western analyses with antibodies against F₁-ATPase subunits (β, p18) and F_o subunit (ATPaseTb2) depicted the sedimentation profile of the F_oF₁-ATPase complexes. The numbers of glycerol gradient fractions (labelled from top to bottom) and sizes of the protein marker are indicated.

Effect of ATPaseTb1 silencing on the F₁-ATPase activity in BF ATPaseTb1 RNAi cells.

As the structural integrity of the complex was unaffected shortly after RNAi induction, the early growth phenotype may be explained by an impairment of the complex function. The F₁-ATPase hydrolytic activity was investigated by two different methods. The first approach, Sumner assay, is based on the colorimetric detection of the release of free phosphate. Mitochondrial lysates were isolated from non-induced cells and cells tet induced for 1 day. Treatment with azide, an inhibitor of the F₁-ATPase, demonstrated that the specific F₁-ATPase activity represented ~30% of the total mt ATPase activity. The comparison of NON and IND1 samples indicated that neither the total ATPase nor the azide-sensitive activities were significantly altered between these two samples. This result implies that the total, as well as the specific F₁-ATPase activities are not changed after 1 day of ATPaseTb1 down-regulation. Thus, the impairment of the hydrolytic F₁-ATPase activity cannot be the reason for the early growth phenotype manifestation. Second method for qualitative determination of the F₁- and F_oF₁-ATPase activities is BN gel fractionation followed by in-gel

histochemical staining. This technique revealed three major bands in RNAi non-induced cells, representing the ATPase activities of F_1 -ATPase, F_0F_1 - monomer and -oligomer. Importantly, the higher two bands were reduced in samples from cells RNAi induced for 1 and 3 days. Furthermore, the staining intensity of the band corresponding to the F_1 -ATPase was increased. As the F_1 -ATPase activity is not affected in RNAi induced samples, it is unlikely that the decreased intensity of the F_0F_1 bands is due to F_1 activity impairment. Presumably, it is rather due to the instability of these higher F_0F_1 complexes. Generally, this result is in agreement with the hrCNE analysis showing that ATPaseTb1 silencing causes instability of F_0F_1 complexes. However, there is a discrepancy, as the in-gel histochemical staining revealed this reduction at day 1, whereas the hrCNE analysis did not reveal any change until day 2 of RNAi induction. Therefore, these experiments will have to be repeated.

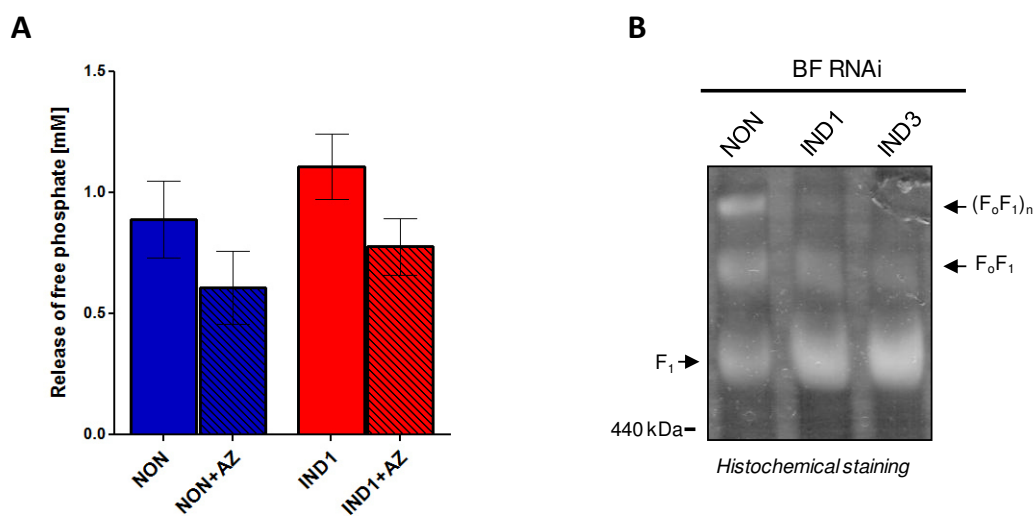


Fig. 10A. The F_1 -ATPase hydrolytic activity was measured in RNAi non-induced (NON) and cells induced for 1 day (IND1) using Sumner reagent. The method was performed as described (Šubrtová et al. 2015). Crude mt vesicles were obtained by digitonin extraction and ATPase activity was assayed by measuring release of free phosphate. F_1 -ATPase inhibitor, sodium azide (AZ, 2 mM), was added as indicated. Means \pm SD from three independent assays (RNAi inductions) are shown.

Fig. 10B. The F_0F_1 -ATPase hydrolytic activity upon ATPaseTb1 knock-down was investigated on Blue native (BN) gel followed by activity staining. This technique was described in detail earlier (Šubrtová et al. 2015). Mitochondria from RNAi non-induced cells (NON) and cells induced for 1 (IND1) and 3 (IND3) days were lysed with 2% DDM. The equal amounts of lysed mitochondria were fractionated on a 2%-12% BNE and the F_0F_1 -ATPase activity was visualized by in-gel histochemical staining. Positions of F_1 -ATPase and monomeric F_0F_1 -ATPase are depicted by arrows. The size of ferritin from equine spleen (440 kDa) is indicated.

Silencing of ATPaseTb1 results in a decreased $\Delta\psi_m$ of BF *T. brucei*.

To test whether ATPaseTb1 is essential for $\Delta\psi_m$ generation, we monitored $\Delta\psi_m$ in BF ATPaseTb1 KD cell line using two different methods. *In vivo* analysis using flow cytometry with Mitotracker Red revealed a decrease of $\Delta\psi_m$ in cells RNAi induced for 6, 9 and 12 hours (IND6h, IND9h, and IND12h). The $\Delta\psi_m$ was reduced by ~20% at 6 hours post-induction, and further decreased by ~40% in IND9h and IND12h samples. The $\Delta\psi_m$ was also measured *in situ* in digitonin-permeabilized BF cells using Safranin O. This spectrofluorometric analysis demonstrated a substantial decrease of $\Delta\psi_m$ at day 1 after RNAi induction. Addition of oligomycin induced depolarization of $\Delta\psi_m$ in both NON and IND1 samples, indicating a residual presence and activity of F_0F_1 complexes in RNAi induced cells. Further addition of FCCP, a proton uncoupler, collapsed the $\Delta\psi_m$ completely.

It has to be noted that presented experiments were performed only once and thus they have to be repeated to obtain larger data set. However, it is plausible to speculate that the decrease of the $\Delta\psi_m$ shortly after RNAi induction is due to an impairment of the proper function of the proton pore and not because of instability of the whole complex.

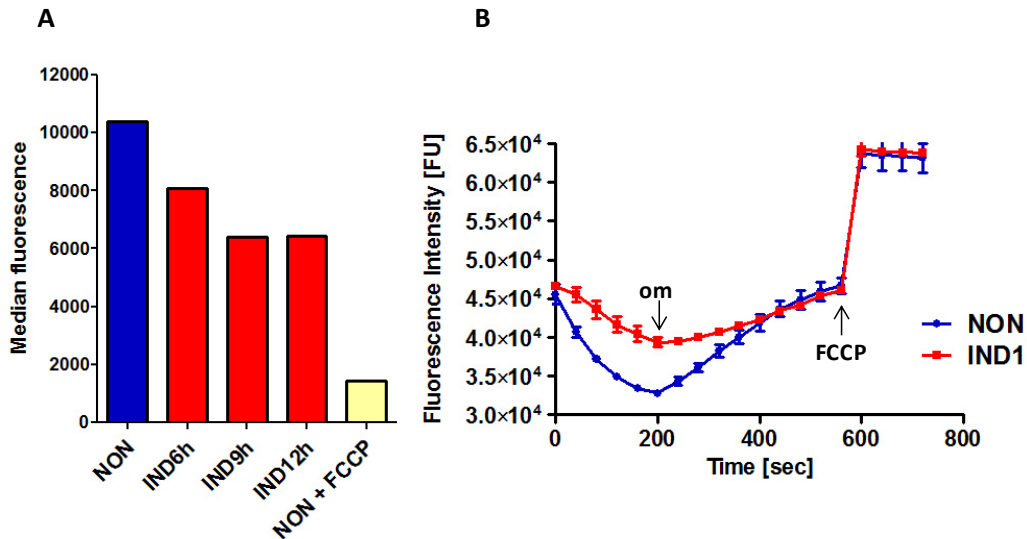


Fig. 11A. The $\Delta\psi_m$ was measured *in vivo* by flow cytometry. The technique was performed as described in Fig. 6A using Mitotracker Red. For more details see (Šubrtová et al. 2015). Mitochondrial membrane potential was investigated in non-induced (NON) and cells induced for 6, 9, 12 hours (IND6h, IND9h, IND12h). The median fluorescence for each sample is depicted on the y-axis of the column graph. The results were obtained from one RNAi induction.

Fig. 11B. Analysis of $\Delta\psi_m$ *in situ* using a fluorescent probe Safranin O. The $\Delta\psi_m$ was investigated in non-induced cells (NON) and cells 1 day post RNAi induction (IND1). The experiment was conducted exactly as reported earlier (Huang et al. 2013). Briefly, BF cells were harvested, washed, resuspended in a reaction buffer containing Safranin O (12,5 μ M) and ATP (1mM) (detailed composition in (Huang et al. 2013)), and permeabilized with digitonin (40 μ M). Fluorescence quenching of Safranin O was monitored in a microplate spectrofluorometer (excitation 496 nm and emission 586 nm). Time- dependent mt membrane potential curves of NON and IND1 cells are shown, each point represents a mean \pm SD of technical triplicate, y- axis shows artificial fluorescence units (FU). The inhibitor oligomycin (om, 2,5 μ g/ml) and protonophore FCCP (10uM) were added as indicated. The experiment was performed with cells from one RNAi induction.

Loss of ATPaseTb1 decreases cytosolic ATP levels in BF. *T. brucei*.

The level of cellular ATP is an important marker for cell viability. It is possible that the strong growth phenotype and the morphological changes in BF ATPaseTb1 RNAi induced cells were caused by ATP level imbalance. To explore this possibility, we generated BF ATPaseTb1 cLUC cell line and measured levels of cytosolic ATP *in vivo*. The luciferase expression and its cytosolic localization was determined by western blot analyses of cellular samples processed by digitonine fractionation. Immunoblots with anti-enolase, anti-mtHsp70, and anti-hexokinase antibodies established the purity of the extracted cytosolic and organellar fractions as the respective markers were confined within their corresponding subcellular compartments. The antibody against the firefly luciferase immunodetected several bands, however the major band was observed in the cytosolic fraction, indicating that this protein is indeed targeted to the cytosol.

The *in vivo* cytosolic ATP level was monitored by luciferase bioluminescence in RNAi non-induced cells and cells induced for 1 and 2 days. The down-regulation of ATPaseTb1 decreased the level of cytosolic ATP by ~40% in IND1 and by ~30% in IND2. In conclusion, the cytosolic ATP is reduced after ATPaseTb1 silencing.

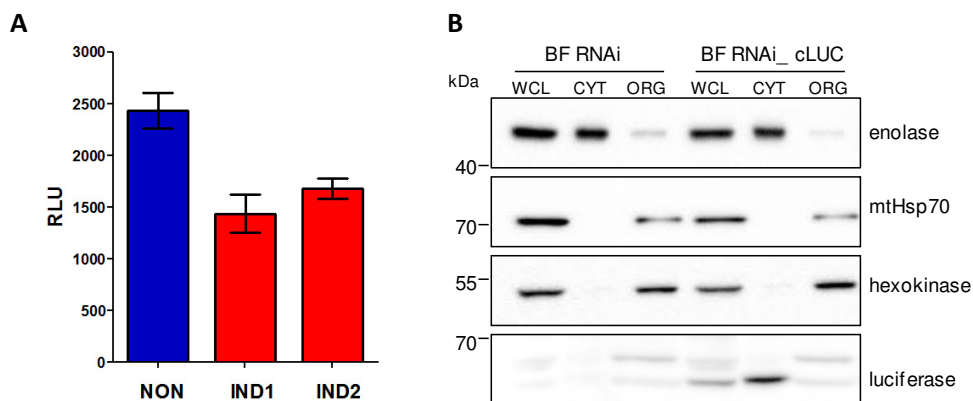
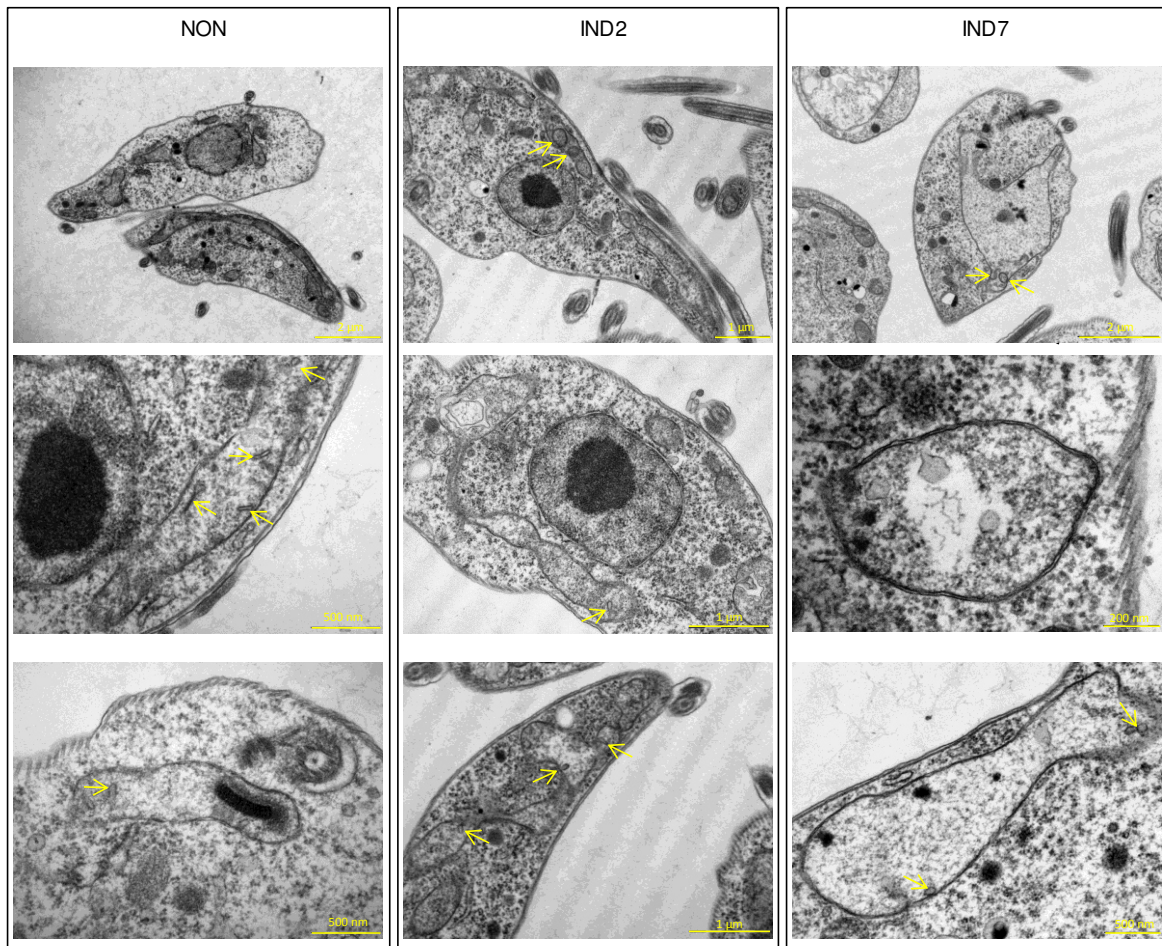


Fig. 12A. Cytosolic ATP was measured *in vivo* using ATP-dependent luciferase bioluminescence. Level of cytosolic ATP was determined in BF RNAi ATPaseTb1 cell line expressing cytosolic firefly luciferase reporter (cLUC). The pHD1344tub vector for the constitutive expression of cLUC was described earlier (Gnipová et al. 2015). The construct was linearized and transfected into BF ATPaseTb1 RNAi cell line as reported (Wirtz et al. 1999). The bioluminescence of cLUC was measured according to (Gnipová et al. 2015). Briefly, an equivalent number of non-induced (NON) and cells 1 and 2 days post RNAi induction (IND1, IND2) was harvested, and luciferase luminiscence was measured *in vivo* upon addition of D-luciferin. Column graph shows means of luminiscence \pm SD obtained from three independent RNAi experiments. The y-axis represents the relative light units (RLU).

Fig. 12B. The subcellular localization of expressed firefly luciferase was investigated using digitonin fractionation. Equal quantities of cells from the parental BF RNAi ATPaseTb1 cell line and BF RNAi ATPaseTb1 expressing cLUC reporter were harvested and fractionated using SoTe/0,015% digitonin buffer according to (Charrière et al. 2006; Paris et al. 2011). Obtained whole cell lysate (WCL), crude cytosolic (CYT) and organellar (ORG) fractions were analyzed using western blot with following antibodies: anti-enolase (cytosol), anti-mtHsp70 (mitochondrion), anti-hexokinase (glycosome) and antibody against firefly luciferase. The sizes of the protein marker are indicated on the left.

ATPaseTb1 depletion causes a mild mitochondrial swelling in PF *T. brucei*.

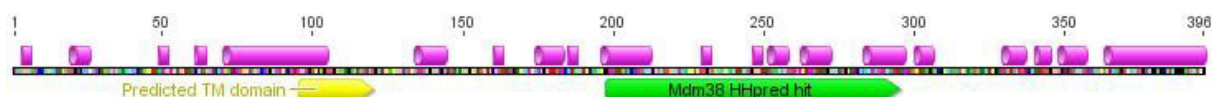
The images of electron micrographs from ultrathin sections of PF ATPaseTb1 KD cells revealed a swollen mitochondria in RNAi induced cells. The organelles were identified by the presence of double membrane, cristae and kinetoplast. Compared to NON samples, the mitochondria of IND2 cells were only mildly affected, while IND7 mitochondria displayed more profound swelling. Discoidal cristae, which are characteristic for PF *T. brucei* (Adl et al. 2012), remained present in the swollen organelle upon ATPaseTb1 knock-down.



Supplementary Fig. 1. The ultrastructure of mitochondria was inspected by transmission electron microscopy (TEM). The samples and ultrathin sections for TEM were prepared and processed as described (Yurchenko et al. 2006) from RNAi non-induced (NON) cells, and cells harvested 2 (IND2) or 7 (IND7) days post RNAi induction. Representative images of transmission electron micrographs are shown, scale bars are designated in yellow, and mt cristae are indicated by arrows.

ATPaseTb1 possesses a putative transmembrane domain and a region homologous to the yeast protein Mdm38.

Bioinformatic analysis of ATPaseTb1 revealed a putative TM domain (AA 96–120) with a prediction score 1,78. This predicted TM is in agreement with the experimental data which demonstrated that ATPaseTb1 is a membrane-bound protein. The *in silico* analysis of ATPaseTb1 AA sequence using the HHpred toolkit revealed a region (AA 198–295) homologous to yeast protein Mdm38. A probability of this hit was 87,3 and a P-value was $5,1E^{-05}$.



Supplementary Fig.2. In silico analysis of ATPaseTb1 amino acid (AA) sequence. A schematic representation of the ATPaseTb1 protein is shown. A putative transmembrane (TM) domain (indicated in yellow) was predicted by MEMSAT-SVM software (<http://bioinf.cs.ucl.ac.uk/psipred/>) (Nugent & Jones 2009). The search based on HMM-HMM comparison was done using the HHpred toolkit (<http://toolkit.tuebingen.mpg.de/>) (Biegert et al. 2006). A positive hit is depicted in green. The regions of alpha-helices were predicted by software from EMBOSS garnier, indicated in magenta and depicted on the AA sequence line.

Discussion:

ATPaseTb1, the largest novel subunit of the *T. brucei* F_0F_1 -ATP synthase complex, was functionally characterized in PF and BF trypanosomes. Previously, it was demonstrated that this protein is essential for maintaining the normal growth rate of the insect *T. brucei* stage and for the integrity of membrane bound F_0F_1 complexes (Zikova et al. 2009). To expand the published data, we exploited the generated PF ATPaseTb1 RNAi cell line to further characterize ATPaseTb1 function. Using specific polyclonal antibodies against ATPaseTb1 we were able to verify the RNAi efficiency in PF RNAi ATPaseTb1 cell line. The immunoblot confirmed specific and efficient ATPaseTb1 silencing. In agreement with the published results, ATPaseTb1 silencing caused inhibition of cell growth. Furthermore, the amounts of F_0F_1 - monomers and - oligomers were significantly decreased upon ATPaseTb1 knock-down. Notably, the severe decrease of ATPaseTb1 protein level and the reduction of F_0F_1 -ATP synthase complexes were detected 2 days before the beginning of the growth phenotype. Thus, it seems that the instability of F_0F_1 -ATP synthase is not the primary reason for the observed reduced growth. This observation raised an question, what other biological consequences of the F_0F_1 -ATP synthase impairment are responsible for the reduced growth.

In PF cells, the function of F_0F_1 -ATP synthase complex is to synthesize ATP, although ATP molecules are also produced by two substrate phosphorylation pathways during the conversion of succinyl-CoA to succinate, and acetyl-CoA to acetate (Bochud-Allemann &

Schneider 2002) (see Section 2, Figure 4, step 6 and 21). In contrast to other aerobic eukaryotes, PF *T. brucei* cells do not fully depend on the ATP produced by oxidative phosphorylation if they are grown in the presence of glucose (Lamour et al. 2005; Coustou et al. 2008). This observation is further supported by our data showing that RNAi induced ATPaseTb1 cells exhibit the same oligomycin sensitivity as non-induced cells. Therefore, the residual levels of the F_oF₁ complexes, detected at day 2 and 4 upon ATPaseTb1 silencing, are sufficient for the ATP production by OxPhos pathway. It would be interesting to examine the levels of F_oF₁ complexes later in RNAi experiment, when the growth phenotype is fully developed, to see if the F_oF₁ complexes are completely diminished or still present at low levels.

The ATP synthesis is coupled with the protons movement down their concentration gradient through the membrane bound F_o moiety. Structure of this proton pore is strictly conserved amongst eukaryotes. A proposed model for H⁺ translocation is generally accepted and specific residues of subunits a and c, which participate in this process are well characterized (Walker 2013). The apparent loss of the F_oF₁ complexes in ATPaseTb1 KD cells prompted us to investigate an effect of ATPaseTb1 silencing on $\Delta\psi_m$. The depletion of this subunit caused an increase of $\Delta\psi_m$, first observed already 2 days after RNAi induction. This hyperpolarization of the inner membrane might be explained by an impairment of the F_o pore followed by an accumulation of protons in inner membrane space. In other eukaryotes, it was reported that an increase of $\Delta\psi_m$ leads to elevated levels of free oxygen radicals (ROS) (Korshunov et al. 1997; Kucharczyk et al. 2009). In PF ATPaseTb1 KD cells, the highest levels of $\Delta\psi_m$ were detected between days 4 and 7 of RNAi-induction, coinciding with the start and progress of the growth inhibition. This observation may suggest that an elevated ROS production may indeed be responsible for the observed growth phenotype. To elaborate this working hypothesis, the mt ROS levels will be analysed in a near future.

Interestingly, it was also reported that raised levels of ROS induced mitochondria swelling in rat cells (Galindo et al. 2003). As indicated in Supp.Fig.1, a mild mt swelling was also detected in PF ATPaseTb1 KD cells. Mitochondrion swelling is an often observed phenotype when mt ion homeostasis is disrupted (Nowikovsky et al. 2009). In trypanosomes one such example involves RNAi silencing of Letm1, a vital mt protein maintaining K⁺/H⁺ homeostasis (Hashimi et al. 2013). Letm1 KD resulted in K⁺ accumulation in the mt matrix followed by osmotic stress (Hashimi et al. 2013). However, in contrast to Letm1 KD, ATPaseTb1 depletion caused milder swelling phenotype observed in later time points during the RNAi induction. This result indicates that the mitochondrion swelling in PF ATPaseTb1 RNAi cell line is not caused by an osmotic imbalance, but most likely it is a secondary effect of a mitochondria dysfunction (for example elevated ROS production).

Obtained results prompted us to investigate the F_o moiety impairment in more detail. Because the organization of the F_o pore is extremely conserved, it is unlikely that ATPaseTb1 would be directly involved in H⁺ translocation. However, this protein might be involved in the assembly of this pore and thus ensures its proper function. Biogenesis of F_o moiety in model organisms requires several proteins, which are involved in i) mRNA stability and/or

translation of F_o subunits, ii) post-translational processing of subunit a precursor, iii) assembly of the c-ring, iv) assembly of the subunit a with the c-ring (Ackerman & Tzagoloff 2005; Rak et al. 2009). One such factor is mt inner membrane protein, Mdm38, which is required for the incorporation of subunit a to the inner mt membrane of *S. cerevisiae* (Frazier et al. 2006). Mdm38 deletion mutants (*mdm38Δ*) have unaltered steady state levels of the F_oF_1 -ATP synthase complex and its subunits (Frazier et al. 2006; Bauerschmitt et al. 2010). However, a proportion of subunit a is not being assembled into the complex and is accumulating as a free protein in *mdm38Δ* mitochondria (Frazier et al. 2006). Interestingly, a bioinformatics search based on Hidden Markov models revealed a region within ATPaseTb1 protein sequence, which has a strong homology to Mdm38 (Supp. Fig.2). Therefore, it might be speculated that *T. brucei* ATPaseTb1 functions similarly to Mdm38 and helps to assemble subunit a into the F_o moiety. The contradicting fact is that Mdm38 was not found to interact with any mature F_oF_1 -ATP synthase subunit (Frazier et al. 2006), whereas ATPaseTb1 is a stable subunit of F_o moiety (Zikova et al. 2009; Šubrtová et al. 2015; this study).

As there were no available antibodies against trypanosome F_o pore subunits, we decided to explore the effect of ATPaseTb1 silencing on the F_o pore stability/assembly by quantifying the pre-edited and edited mRNA transcripts of subunit a by RT-qPCR. Preliminary data from this analysis indicated that the loss of ATPaseTb1 impaired the RNA editing process and/or the stability of sub a mRNA, as the levels of edited mRNAs were reduced in RNAi induced cells. Intriguingly, the similar trend was observed in BF cells with mutation in subunit γ (Dean et al. 2013), which uncouples the F_oF_1 -ATPase complex (C. Dewar, personal communication). These cells prevent the production of fully edited mature mRNA of subunit a to avoid a proton leak through an uncoupled F_oF_1 -ATPase complex, because the free movement of protons across the IM would cause $\Delta\psi_m$ dissipation, which would be detrimental for the cells.

As just mentioned, the proton translocation by F_oF_1 -ATPase is crucial for BF cells viability. To gain additional insight into the specific function of ATPaseTb1, the BF RNAi cell line was created. The targeted down-regulation of ATPaseTb1 resulted in rapid and severe growth inhibition observed already 9 hours post-induction. After 24 hours of RNAi induction the cell density was decreased 3.5 times, even though the ATPaseTb1 steady-state level was reduced only by 40%. To our knowledge, such a quick onset of a severe growth phenotype triggered by a mild reduction of the targeted protein was not described for any other studied subunit of the BF F_oF_1 -ATPase (Schnauffer et al. 2005; Šubrtová et al. 2015; Gahura et al. manuscript in preparation).

Furthermore, the ATPaseTb1 silenced cells displayed an impaired mt morphology with altered nucleus/kinetoplast (N/K) ratios. These changes might represent a secondary effect of ATPaseTb1 silencing due to a reduction of $\Delta\psi_m$. When the $\Delta\psi_m$ decreases, import of metabolites and proteins into the BF mitochondria would become inefficient (Nolan & Voorheis 1992), and likely this would be followed by changes in mt morphology and disruption of the cell division.

Another interesting phenotype observed upon ATPaseTb1 down-regulation is the decreased level of cytosolic ATP. The cytosolic ATP was reduced by ~40 % at day 1 upon RNAi induction. At this time point, the structural integrity of the F_0F_1 complexes appears to be unaffected. Thus, it is unlikely that this observed ATP reduction is caused by a wasteful hydrolysis of unassembled free F_1 -ATPase. The decreased levels of cytosolic ATP might be explained by the decrease of $\Delta\psi_m$. Notably, oligomycin treatment of BF cells reduces the oxygen consumption, pyruvate production, and also cellular ATP levels (Miller & Klein 1980; Nolan & Voorheis 1992). This indicates that the loss of $\Delta\psi_m$ affects the Gly-3-P/DHAP shuttle including mt Gly-3-P oxidase, that passes electrons to ubiquinone and finally to TAO. Why the BF respiration is sensitive to changes in the $\Delta\psi_m$ is unclear (Nolan & Voorheis 1992) and the mechanism underlying this effect is under investigation. Moreover, the ATP levels and pyruvate production were also reduced when respiration through TAO was compromised either by RNAi of this enzyme or by SHAM inhibition (Opperdoes et al. 1976; Nolan & Voorheis 1992; Helfert et al. 2001). Indeed, during glycolysis under anaerobic conditions, BF trypanosomes produce equimolar amounts of pyruvate and glycerol (see Section 2, Figure 2, step 9), and thus the net production of ATP is decreased by half (Hannaert et al. 2003). BF cells grown in anaerobic conditions or in the presence of SHAM die within 24 hours (Helfert et al. 2001). It might be speculated, that the decrease of $\Delta\psi_m$ detected early after RNA induction is truly the primary effect of ATPaseTb1 silencing. The loss of $\Delta\psi_m$ would be followed by a reduction of cytosolic ATP and death of the parasite. Similarly as in PF cells, data imply that ATPaseTb1 is involved in a proper functioning of the F_0 pore. The instability of F_0F_1 complexes observed later in the RNAi could be explained by a secondary effect of the proton pore impairment as the cells would attempt to avoid H^+ leak.

Compiling all the data from PF and BF ATPaseTb1 RNAi cell lines, we propose that ATPaseTb1 may function as an assembly factor of the F_0 pore, or it might be responsible for the stability of the highly hydrophobic subunit a. However, we acknowledge that typical F_0F_1 assembly factors are not stably interacting with the complex, and thus this hypothesis needs to be supported by more experiments.

References:

- Ackerman, S.H. & Tzagoloff, A., 2005. Function, structure, and biogenesis of mitochondrial ATP synthase. *Progress in nucleic acid research and molecular biology*, 80, pp.95–133.
- Adl, S.M. et al., 2012. The revised classification of eukaryotes. *The Journal of eukaryotic microbiology*, 59(5), pp.429–93.
- Alibu, V.P. et al., 2005. A doubly inducible system for RNA interference and rapid RNAi plasmid construction in *Trypanosoma brucei*. *Molecular and biochemical parasitology*, 139(1), pp.75–82.
- Aphasizheva, I. et al., 2011. Pentatricopeptide repeat proteins stimulate mRNA adenylation/uridylation to activate mitochondrial translation in trypanosomes. *Molecular cell*, 42(1), pp.106–17.
- Ballester, M. et al., 2004. Real-time quantitative PCR-based system for determining transgene copy number in transgenic animals. *BioTechniques*, 37(4), pp.610–3.
- Bauerschmitt, H. et al., 2010. Ribosome-binding proteins Mdm38 and Mba1 display overlapping functions for regulation of mitochondrial translation. *Molecular biology of the cell*, 21(12), pp.1937–44.
- Biegert, A. et al., 2006. The MPI Bioinformatics Toolkit for protein sequence analysis. *Nucleic acids research*, 34(Web Server issue), pp.W335–9.
- Bochud-Allemann, N. & Schneider, A., 2002. Mitochondrial substrate level phosphorylation is essential for growth of procyclic *Trypanosoma brucei*. *The Journal of biological chemistry*, 277(36), pp.32849–54.
- Brown, S. V et al., 2006. ATP Synthase Is Responsible for Maintaining Mitochondrial Membrane Potential in Bloodstream Form *Trypanosoma brucei*. *Eukaryotic cell*, 5(1), pp.45–53.
- Carnes, J. et al., 2005. An essential RNase III insertion editing endonuclease in *Trypanosoma brucei*. *Proceedings of the National Academy of Sciences of the United States of America*, 102(46), pp.16614–9.
- Coustou, V. et al., 2008. Glucose-induced remodeling of intermediary and energy metabolism in procyclic *Trypanosoma brucei*. *The Journal of biological chemistry*, 283(24), pp.16342–54.
- Dean, S. et al., 2013. Single point mutations in ATP synthase compensate for mitochondrial genome loss in trypanosomes. *Proceedings of the National Academy of Sciences of the United States of America*, 110(36), pp.14741–6.
- Frazier, A.E. et al., 2006. Mdm38 interacts with ribosomes and is a component of the mitochondrial protein export machinery. *The Journal of cell biology*, 172(4), pp.553–64.
- Galindo, M.F. et al., 2003. Reactive oxygen species induce swelling and cytochrome c release but not transmembrane depolarization in isolated rat brain mitochondria. *British journal of pharmacology*, 139(4), pp.797–804.
- Gnipová, A. et al., 2015. The ADP/ATP carrier and its relationship to OXPHOS in an ancestral protist, *Trypanosoma brucei*. *Eukaryotic cell*, 14(3), pp.297–310.
- Hannaert, V. et al., 2003. Evolution of energy metabolism and its compartmentation in Kinetoplastida. *Kinetoplastid Biology and Disease*, 2(11), pp.1–30.
- Hashimi, H. et al., 2013. Trypanosome Letm1 protein is essential for mitochondrial potassium homeostasis. *The Journal of biological chemistry*, 288(37), pp.26914–25.
- Helfert, S. et al., 2001. Roles of triosephosphate isomerase and aerobic metabolism in *Trypanosoma brucei*. *The Biochemical journal*, 357(Pt 1), pp.117–25.
- Huang, G., Vercesi, A.E. & Docampo, R., 2013. Essential regulation of cell bioenergetics in *Trypanosoma brucei* by the mitochondrial calcium uniporter. *Nature communications*, 4, p.2865.
- Charrière, F. et al., 2006. Dual targeting of a single tRNA(Trp) requires two different tryptophanyl-tRNA synthetases in *Trypanosoma brucei*. *Proceedings of the National Academy of Sciences of the United States of America*, 103(18), pp.6847–52.
- Chen, Y. et al., 2003. Development of RNA interference revertants in *Trypanosoma brucei* cell lines generated with a double stranded RNA expression construct driven by two opposing promoters. *Molecular and biochemical parasitology*, 126(2), pp.275–9.
- Chi, T.B., Brown B, S. V & Williams, N., 1998. Subunit 9 of the mitochondrial ATP synthase of *Trypanosoma brucei* is nuclearly encoded and developmentally regulated. *Molecular and biochemical parasitology*, 92(1), pp.29–38.
- Korshunov, S.S., Skulachev, V.P. & Starkov, A.A., 1997. High protonic potential actuates a mechanism of production of reactive oxygen species in mitochondria. *FEBS letters*, 416(1), pp.15–8.
- Kucharczyk, R. et al., 2009. Mitochondrial ATP synthase disorders: molecular mechanisms and the quest for curative therapeutic approaches. *Biochimica et biophysica acta*, 1793(1), pp.186–99.
- Lamour, N. et al., 2005. Proline metabolism in procyclic *Trypanosoma brucei* is down-regulated in the presence of glucose. *The Journal of biological chemistry*, 280(12), pp.11902–10.

- Meyer, B. et al., 2007. Identification of two proteins associated with mammalian ATP synthase. *Molecular & cellular proteomics : MCP*, 6(10), pp.1690–9.
- Miller, P.G. & Klein, R.A., 1980. Effects of oligomycin on glucose utilization and calcium transport in African trypanosomes. *Journal of general microbiology*, 116(2), pp.391–6.
- Nolan, D.P. & Voorheis, H.P., 1992. The mitochondrion in bloodstream forms of *Trypanosoma brucei* is energized by the electrogenic pumping of protons catalysed by the F1F0-ATPase. *European journal of biochemistry / FEBS*, 209(1), pp.207–16.
- Nowikovsky, K., Schweyen, R.J. & Bernardi, P., 2009. Pathophysiology of mitochondrial volume homeostasis: potassium transport and permeability transition. *Biochimica et biophysica acta*, 1787(5), pp.345–50.
- Nugent, T. & Jones, D.T., 2009. Transmembrane protein topology prediction using support vector machines. *BMC bioinformatics*, 10, p.159.
- Opperdoes, F.R., Borst, P. & Fonck, K., 1976. The potential use of inhibitors of glycerol-3-phosphate oxidase for chemotherapy of African trypanosomiasis. *FEBS letters*, 62(2), pp.169–72.
- Paris, Z. et al., 2011. Futile import of tRNAs and proteins into the mitochondrion of *Trypanosoma brucei evansi*. *Molecular and biochemical parasitology*, 176(2), pp.116–20.
- Perez, E. et al., 2014. The mitochondrial respiratory chain of the secondary green alga *Euglena gracilis* shares many additional subunits with parasitic Trypanosomatidae. *Mitochondrion*, pp.1–12.
- Rak, M. et al., 2009. Assembly of F0 in *Saccharomyces cerevisiae*. *Biochimica et biophysica acta*, 1793(1), pp.108–16.
- Räz, B. et al., 1997. The Alamar Blue assay to determine drug sensitivity of African trypanosomes (*T.b. rhodesiense* and *T.b. gambiense*) in vitro. *Acta tropica*, 68(2), pp.139–47.
- Schnauffer, A. et al., 2005. The F1-ATP synthase complex in bloodstream stage trypanosomes has an unusual and essential function. *The EMBO journal*, 24(23), pp.4029–40.
- Šubrťová, K., Panicucci, B. & Ziková, A., 2015. ATPaseTb2, a Unique Membrane-bound FoF1-ATPase Component, Is Essential in Bloodstream and Dyskinetoplasmic Trypanosomes. *PLoS pathogens*, 11(2), p.e1004660.
- Urbaniak, M.D., Guther, M.L.S. & Ferguson, M.A.J., 2012. Comparative SILAC proteomic analysis of *Trypanosoma brucei* bloodstream and procyclic lifecycle stages. *PLoS one*, 7(5), p.e36619.
- Vertommen, D. et al., 2008. Differential expression of glycosomal and mitochondrial proteins in the two major life-cycle stages of *Trypanosoma brucei*. *Molecular and biochemical parasitology*, 158(2), pp.189–201.
- Walker, J.E., 2013. The ATP synthase: the understood, the uncertain and the unknown. *Biochemical Society transactions*, 41(1), pp.1–16.
- Wirtz, E. et al., 1999. A tightly regulated inducible expression system for conditional gene knock-outs and dominant-negative genetics in *Trypanosoma brucei*. *Molecular and biochemical parasitology*, 99(1), pp.89–101.
- Yurchenko, V. et al., 2006. An integrated morphological and molecular approach to a new species description in the Trypanosomatidae: the case of *Leptomonas podlipaevi* n. sp., a parasite of *Boisea rubrolineata* (Hemiptera: Rhopalidae). *The Journal of eukaryotic microbiology*, 53(2), pp.103–11.
- Zikova, A. et al., 2009. The F(0)F(1)-ATP synthase complex contains novel subunits and is essential for procyclic *Trypanosoma brucei*. *PLoS pathogens*, 5(5), p.e1000436.
- Zikova, A. et al., 2008. *Trypanosoma brucei* mitochondrial ribosomes. *Molecular & Cellular Proteomics*, 7(7), pp.1286–1296.

CHAPTER 4

CONCLUSIONS

4.1. Conclusions and future perspectives

Elucidating the structure and function of the F_0F_1 -ATP synthase in parasitic trypanosomes represents intriguing research topics, for the following reasons:

- i) The *T. brucei* F_0F_1 -ATP synthase has diverged significantly from homologous complexes of other eukaryotic lineages, as it contains up to 14 novel subunits with no homology outside Kinetoplastida or the Euglenozoa group (Zikova et al. 2009; Perez et al. 2014).
- ii) The activity of *T. brucei* F_0F_1 -ATP synthase differs between the bloodstream and procyclic stages of the parasite, as it synthesizes ATP during the PF stage and then reverses its function as it hydrolyzes ATP to maintain the $\Delta\psi_m$ in BF cells (Nolan & Voorheis 1992; Schnauffer et al. 2005; Brown et al. 2006). The mechanism of this regulation is unknown.
- iii) The F_0F_1 -ATPase has a unique function in dyskinetoplastic trypanosomes, which lack the F_0 subunit a. Dk trypanosomes employ their F_1 -ATPase hydrolytic activity coupled with AAC transport to generate their $\Delta\psi_m$ by the electrogenic ADP^{3-}/ATP^{4-} exchange. This mechanism is independent of proton pumping, and requires key compensatory mutations in the F_1 subunit γ (Schnauffer et al. 2005; Dean et al. 2013).

The work presented in this thesis mainly addressed the function of three unique subunits of the *T. brucei* F_0F_1 -ATP synthase complex: ATPaseTb1, ATPaseTb2, and p18. Notably, the ATPaseTb2 studies provided new insight into the structure and function of the F_0F_1 -ATPase complex in Dk trypanosomes (Šubrtová et al. 2015). The composition of the *T. brucei* F_1 -ATPase was also investigated (Gahura et al. manuscript in preparation). Furthermore, we explored the function of the ADP/ATP carrier and inspected its physical association with the OxPhos complexes (Gnipová et al. 2015).

The major focus of my thesis concerned the function of the Kinetoplastida-specific ATPaseTb2 (Šubrtová et al. 2015), which proved to be very intriguing. Results demonstrated that this F_0 subunit is essential for maintaining the $\Delta\psi_m$ and the normal growth rate of Dk trypanosomes, despite the previous assumption that Dk cells generate their mt membrane potential exclusively via activity of the F_1 -ATPase and TbAAC. Importantly, it was demonstrated that the membrane bound F_0F_1 complexes are present in Dk mitochondrion and that ATPaseTb2 is part of these F_0F_1 -ATPase complexes. Combining all of the bioinformatic and experimental data lead us to hypothesize that ATPaseTb2 might be a component of the peripheral stalk (Šubrtová et al. 2015). Furthermore, we speculate that the peripheral stalk subunits in Dk cells help to anchor the F_1 -ATPase to the mt inner membrane, keeping it within the close vicinity of the TbAAC. This arrangement may increase the efficiency of generating the $\Delta\psi_m$ in a mitochondrion with poorly defined cristae. To

support this hypothesis, it would be beneficial to down-regulate another component of the peripheral stalk in this cell type. However, due to the very low homology of the trypanosome F_0F_1 -ATPase subunits to their eukaryotic and prokaryotic counterparts, the only identified subunit of the *T. brucei* peripheral stalk is OSCP (Zikova et al. 2009). Unfortunately, this subunit is not an ideal candidate as the N-terminal region of the subunit α , which contains the binding site for OSCP, is absent in *T. b. evansi* (Dean et al. 2013). Thus, it is conceivable that OSCP has a divergent function in Dk cells. It is likely that the overall composition of the peripheral stalk in trypanosomes will profoundly differ from the yeast and mammalian stalks, as it may contain novel and unique subunits. It may resemble the atypical stalk described from chlorophycean algae (Cano-Estrada et al. 2010). Indeed, preliminary data from RNAi studies in Dk *T. b. evansi* and BF *T. brucei* revealed that OSCP is essential neither for cell viability nor for maintaining the $\Delta\psi_m$ (data not shown). However, as the achieved levels of OSCP knock-down in these cell lines can always be argued to be insufficient for phenotypical analysis, the function of OSCP and the peripheral stalk, is still under active investigation. Results of the functional study concerning the euglenozoa-specific subunit ATPaseTb1 (Results 3.2.2.) demonstrated that this protein is part of the F_0 moiety in both BF and PF *T. brucei*. Moreover, the entirety of the data collected to this point suggests that ATPaseTb1 might play a role in the assembly or stability of the proton pore in *T. brucei*, however additional experiments are required to establish this conclusion.

Another Euglenozoa-specific subunit, p18, was detected previously in various F_0F_1 -ATP synthase preparations (Speijer et al. 1997; Nelson et al. 2004; Zikova et al. 2009; Perez et al. 2014). This protein was previously misidentified as the homolog of the peripheral stalk subunit b, and therefore assigned to the F_0 moiety (Speijer et al. 1997). Nevertheless, the direct association of p18 with the F_1 moiety was considered (Hashimi et al. 2010) and finally experimentally proven in this work (Gahura et al. manuscript in preparation). This result was unexpected because the composition of F_1 -ATPases from other organisms is highly conserved and involves only five subunits (α , β , γ , δ , ϵ). Our functional analyses revealed that p18 is essential for the stability and activity of F_1 -ATPase and thus its down-regulation disrupts the $\Delta\psi_m$. Ongoing investigations in the laboratory are addressing the stoichiometry of p18 within the F_1 -ATPase and identifying the F_1 subunits that interact with p18.

The major aim of the F_1 -ATPase study (Gahura et al. manuscript in preparation) was to characterize the composition and activity of the *T. brucei* F_1 moiety in detail. The catalytic F_1 -ATPase was purified by ion exchange chromatography followed by gel filtration. The specific ATPase activities of the F_1 -enzyme were measured and individual F_1 subunits were identified by mass spectrometry (MS). The MS analyses revealed that this highly pure complex contains homologs of eukaryotic subunits α , β , γ , δ , and ϵ ; and Euglenozoa-specific subunit p18. Mitochondrial targeting sequences of individual subunits, and precise cleavage sites in the subunit α , were determined using MS approaches and N-terminal sequencing. As previously mentioned, the *in vivo* proteolytic cleavage of subunit α appears to be specific for the Euglenozoa group (Speijer et al. 1997; Nelson et al. 2004; Zikova et al. 2009; Perez et al. 2014), but the biological significance of this cleavage is unclear.

The work presented so far is centered on the composition of the *T. brucei* F₀F₁-ATPase, trying to determine the organization of the unique subunits and their role within this essential complex. Aim of our current research is to resolve the structure of F₁-ATPase by X-ray crystallography, and thus gain better insight into the role of p18 and elucidate specific interactions of individual subunits. In addition, the high resolution structure of the enzyme in the complex with its natural inhibitor TbIF1 could be exploited in structure-based drug design. Another approach has also been established to purify the fully assembled F₀F₁-ATP synthase complex. This technique is based on the binding of F₁-ATPase to a tagged TbIF1 and subsequent affinity chromatography purification of bound complexes. These highly purified complexes will undergo structural studies using high-resolution cryo-EM to solve topography of the F₀ moiety and the peripheral stalk.

In the meantime, a comprehensive yeast two-hybrid analysis is being performed, to determine interaction partners for Euglenozoa-specific subunits, hopefully providing a framework for the architecture of the F₀F₁-ATP synthase complex. Furthermore, powerful *in vivo* imaging techniques can also be applied to further verify potential interaction partners as well as the overall state of the complexes in trypanosoma cells. These methods include using APEX (ascorbate peroxidase) an engineered enzyme that functions as an EM-tag (Martell et al. 2012; Lam et al. 2014); or FRET (Förster resonance energy transfer) (Pollok 1999). All of these methods should provide greater insight into the molecular structure of the F₀F₁-ATP synthase, and thus resolve key questions regarding the precise location of subunit p18 and the structure of the peripheral stalk.

Another study presented in this thesis concerned ADP/ATP carrier of PF trypanosomes (Gnipová et al. 2015). *T. brucei* possesses two AAC homologues, but only TbAAC (TbMCP5) was postulated to be the principal ADP/ATP carrier in PF mitochondrion (Peña-Diaz et al. 2012; Gnipová et al. 2015). Our TbAAC study confirmed that this carrier is indeed essential for PF trypanosomes, although the data suggest that another carrier may be able to contribute to the mitochondrial import of ATP. Obtained results further implied that TbAAC is most likely not a stable component of any supramolecular assembly in PF trypanosomes (Gnipová et al. 2015). It would be intriguing to assess the structure and functional interactome of TbAAC within BF and Dk trypanosomes, where the poorly developed cristae might promote a supramolecular association between TbAAC, PiC, and F₀F₁-ATPase (F₀F₁-ATP hydrolasome) to create a more efficient microenvironment. While it is reasonable to expect that TbAAC will be indispensable for both these cell types, as they need to provide substrate for the F₁-ATPase hydrolytic activity (Schnauffer et al. 2005; Dean et al. 2013), it is interesting that BF cells are more tolerant to the AAC inhibitor bongkreikic acid than Dk cells (Dean et al. 2013).

Future research may also address the potential supramolecular organisation of F₀F₁-ATP synthase oligomers in the mt inner membrane of *T. brucei*. Macromolecular organization of this complex was explored in a phylogenetically distant organism using cryo-electron tomography (cryo-ET). Three-dimensional reconstructions of cryo-ET images revealed long rows of F₀F₁-ATP synthase dimers on tightly curved cristae tips (Strauss et al.

2008; Davies et al. 2011; Daum et al. 2013). Another study investigating the mitochondria of *Podospora anserina* revealed that the supramolecular organisation of the F_0F_1 -ATP synthase complex is remodelled throughout the fungal aging process. With increasing age, the F_0F_1 -dimers were disassociating into F_0F_1 -monomers, causing mt cristae to disappear (Daum et al. 2013). It would be interesting to assess the arrangement of F_0F_1 -ATP synthase/ATPase complex in Dk trypanosomes as well as in different stages of *T. brucei*, as the mt structure and folding of the inner membrane are profoundly different in these cell types (Priest & Hajduk 1994; Brun et al. 1998).

In conclusion, further investigation of the F_0F_1 -ATP synthase complex in trypanosomes will contribute to the evidence from other non-model eukaryotes that the composition and architecture of this functionally conserved complex, is significantly higher than previously assumed.

References:

- Brown, S. V et al., 2006. ATP Synthase Is Responsible for Maintaining Mitochondrial Membrane Potential in Bloodstream Form *Trypanosoma brucei*. *Eukaryotic cell*, 5(1), pp.45–53.
- Brun, R., Hecker, H. & Lun, Z.R., 1998. *Trypanosoma evansi* and *T. equiperdum*: distribution, biology, treatment and phylogenetic relationship (a review). *Veterinary parasitology*, 79(2), pp.95–107.
- Cano-Estrada, A. et al., 2010. Subunit-subunit interactions and overall topology of the dimeric mitochondrial ATP synthase of *Polytomella* sp. *Biochimica et biophysica acta*, 1797(8), pp.1439–48.
- Daum, B. et al., 2013. Age-dependent dissociation of ATP synthase dimers and loss of inner-membrane cristae in mitochondria. *Proceedings of the National Academy of Sciences of the United States of America*, 110(38), pp.15301–6.
- Davies, K.M. et al., 2011. Macromolecular organization of ATP synthase and complex I in whole mitochondria. *Proceedings of the National Academy of Sciences of the United States of America*, 108(34), pp.14121–6.
- Dean, S. et al., 2013. Single point mutations in ATP synthase compensate for mitochondrial genome loss in trypanosomes. *Proceedings of the National Academy of Sciences of the United States of America*, 110(36), pp.14741–6.
- Gnipová, A. et al., 2015. The ADP/ATP carrier and its relationship to OXPHOS in an ancestral protist, *Trypanosoma brucei*. *Eukaryotic cell*, 14(3), pp.297–310.
- Hashimi, H. et al., 2010. The assembly of F(1)F(O)-ATP synthase is disrupted upon interference of RNA editing in *Trypanosoma brucei*. *International journal for parasitology*, 40(1), pp.45–54.
- Lam, S.S. et al., 2014. Directed evolution of APEX2 for electron microscopy and proximity labeling. *Nature Methods*, 12(1), pp.51–4.
- Martell, J.D. et al., 2012. Engineered ascorbate peroxidase as a genetically encoded reporter for electron microscopy. *Nature biotechnology*, 30(11), pp.1143–8.
- Nelson, R.E. et al., 2004. The I-complex in *Leishmania tarentolae* is a uniquely-structured F-1-ATPase. *Molecular and Biochemical Parasitology*, 135(2), pp.219–222.
- Nolan, D.P. & Voorheis, H.P., 1992. The mitochondrion in bloodstream forms of *Trypanosoma brucei* is energized by the electrogenic pumping of protons catalysed by the F1F0-ATPase. *European journal of biochemistry / FEBS*, 209(1), pp.207–16.
- Peña-Díaz, P. et al., 2012. Functional characterization of TbMCP5, a conserved and essential ADP/ATP carrier present in the mitochondrion of the human pathogen *Trypanosoma brucei*. *The Journal of biological chemistry*, 287(50), pp.41861–74.
- Perez, E. et al., 2014. The mitochondrial respiratory chain of the secondary green alga *Euglena gracilis* shares many additional subunits with parasitic Trypanosomatidae. *Mitochondrion*, pp.1–12.
- Pollok, B., 1999. Using GFP in FRET-based applications. *Trends in Cell Biology*, 9(2), pp.57–60.
- Priest, J.W. & Hajduk, S.L., 1994. Developmental regulation of mitochondrial biogenesis in *Trypanosoma brucei*. *Journal of bioenergetics and biomembranes*, 26(2), pp.179–91.
- Schnauffer, A. et al., 2005. The F1-ATP synthase complex in bloodstream stage trypanosomes has an unusual and essential function. *The EMBO journal*, 24(23), pp.4029–40.
- Speijer, D. et al., 1997. Characterization of the respiratory chain from cultured *Crithidia fasciculata*. *Molecular and Biochemical Parasitology*, 85, pp.171–186.
- Strauss, M. et al., 2008. Dimer ribbons of ATP synthase shape the inner mitochondrial membrane. *The EMBO journal*, 27(7), pp.1154–60.
- Šubrtová, K., Panicucci, B. & Ziková, A., 2015. ATPaseTb2, a Unique Membrane-bound FoF1-ATPase Component, Is Essential in Bloodstream and Dyskinetoplasmic Trypanosomes. *PLoS pathogens*, 11(2), p.e1004660.
- Zikova, A. et al., 2009. The F(0)F(1)-ATP synthase complex contains novel subunits and is essential for procyclic *Trypanosoma brucei*. *PLoS pathogens*, 5(5), p.e1000436.

© for non-published parts Karolína Šubrtová
karolinasubrtova@yahoo.com

F₀F₁-ATP synthase/ATPase in the parasitic protist, *Trypanosoma brucei*. Ph.D. Thesis, 2015

All rights reserved
For non-commercial use only

Printed in the Czech Republic

University of South Bohemia in České Budějovice
Faculty of Science
Branišovská 1760
CZ-37005 České Budějovice, Czech Republic

Phone: +420 387 776 201
www.prf.jcu.cz, e-mail: sekret-fpr@prf.jcu.cz